# RETROVIRAL CAPSID RECOGNITION BY THE HOST RESTRICTION FACTOR TRIM5ALPHA

by

Viswanathan Chandrasekaran

A dissertation submitted to the faculty of
The University of Utah
in partial fulfillment of the requirements for the degree of

Doctor of Philosophy

Department of Biochemistry

The University of Utah

May 2015

**The University of Utah Graduate School**

# STATEMENT OF DISSERTATION APPROVAL

The dissertation of **Viswanathan Chandrasekaran**

has been approved by the following supervisory committee members:

| | | |
|---|---|---|
| **Wesley I. Sundquist** | , Chair | **01/26/2015** Date Approved |
| **Sherwood R. Casjens** | , Member | **01/26/2015** Date Approved |
| **Christopher P. Hill** | , Member | **01/26/2015** Date Approved |
| **Michael S. Kay** | , Member | **01/26/2015** Date Approved |
| **Martin C. Rechsteiner** | , Member | **10/31/2014** Date Approved |

and by **Wesley I. Sundquist** , Chair/Dean of

the Department/College/School of **Biochemistry**

and by David B. Kieda, Dean of The Graduate School.

# ABSTRACT

Mammalian hosts have evolved protein "restriction factors" to combat retroviruses. TRIM5α and the related TRIMCyp protein (collectively TRIM5), are restriction factors that can potently restrict retroviruses, including HIV-1, by binding their capsids and blocking reverse transcription. Previous studies have shown that the C-terminal SPRY/CypA domains of TRIM5 proteins bind the capsids of susceptible retroviruses and that higher-order oligomerization of TRIM5 proteins apparently also contributes to capsid binding. However, the biochemical and structural details of these interactions are not fully understood. To study how TRIM5 proteins recognize capsids, we have developed new methods for expressing and purifying recombinant TRIM5 proteins. Here, we report biochemical, electron microscopic and X-ray crystallographic studies of pure recombinant TRIM5 proteins and their complexes with authentic HIV-1 core particles and *in vitro*-assembled mimics of the HIV-1 capsid surface.

In Chapter 2, we report the expression, purification and electron crystallographic studies of a restrictive, but non-native chimeric rhesus TRIM5 protein (TRIM5-21R), and show that TRIM5-21R can spontaneously self-assemble into paracrystalline hexagonal lattices comprising 6-sided rings. Moreover, ring assembly is promoted by TRIM5-21R binding to hexagonal HIV-1 CA assemblies. In Chapter 3, we report the first crystal structure of a TRIM coiled-coil domain (from human TRIM25) as well as supporting analytical ultracentrifugation and disulfide crosslinking experiments showing that other

TRIM coiled-coils, including TRIM5, also form antiparallel dimers that are ~170 Å long. In Chapter 4, we describe the expression and purification of 11 different mammalian TRIM5 alleles. We demonstrate that TRIM5 hexagonal assembly is a conserved property and report electron microscopic and biochemical studies showing that TRIM5 proteins form a ~35 nm-spaced, flexible hexagonal "net" on the surface of decorated HIV-1 cores and other capsid mimics. In Chapter 5, I present my ongoing attempts to crystallize and determine the structure of the TRIM5α core domains in the assembled state.

Taken together, my work supports a "pattern recognition" model for capsid recognition in which TRIM5 proteins have evolved to restrict a variety of different retroviruses by cooperatively assembling flexible hexagonal nets that can bind avidly and adapt to the symmetry, hexagonal spacing and curvature of retroviral capsids.

To my parents, Usha and Chandrasekaran

CONTENTS

LIST OF TABLES

LIST OF FIGURES

# CHAPTER 1

## INTRODUCTION

The human immunodeficiency virus / acquired immune deficiency syndrome (HIV/AIDS) pandemic infects an estimated 35.3 million people, with 2.3 million new infections each year (1). Although highly active antiretroviral therapy (HAART) has contributed to a measurable decline in the number of AIDS deaths, from 2.3 million in 2005 to 1.6 million in 2012, significant challenges nonetheless prevent disease eradication. The high cost and limited availability of HAART in the developing world, the rapid emergence of drug resistance and HIV's ability to escape sterilizing immunity by establishing latent reservoirs in patients necessitate continued HIV research (2).

An exciting new direction that has gained prominence in retrovirology, and microbiology in general, is the discovery and characterization of mammalian intrinsic immune pathways that counteract viral replication (3). Antiviral molecules that mediate such pathways are collectively termed "restriction factors" and their study could, in principle, lead to new therapeutic strategies against HIV type 1 (HIV-1) (4-6). Here, I describe our biochemical and structural studies of one such restriction factor, TRIM5α.

## 1.1 Structure of HIV-1 and its mature capsid

HIV-1 is an enveloped virus of the *Lentivirus* genus in the *Retroviridae* family. Its positive-sense single-stranded RNA genome encodes 3 major polyproteins: Gag, Gag-Pol and Env; and 6 accessory or regulatory proteins: Tat, Rev, Nef, Vpr, Vif and Vpu (7). Together, these viral proteins organize the virion and orchestrate the different steps of viral replication. HIV-1 virions exist in two forms – a noninfectious immature form that is initially released from producer cells and a mature form that is generated by subsequent proteolytic processing of Gag and Gag-Pol and rearrangement of the processed proteins (reviewed in (8)). Autoproteolysis by the PR domain of Pol releases the Pol-derived viral enzymes, reverse transcriptase (RT), integrase (IN) and protease (PR), and the Gag-derived structural proteins, MA, CA, NC, as well as three smaller spacer peptides, SP1, SP2 and p6. The Golgi-resident host enzyme furin cleaves Env into gp120 (SU) and gp41 (TM). The uncleaved Gag polyprotein organizes the immature virion and also coordinates viral assembly and egress from producer cells (9). The processed MA, CA and NC proteins then dramatically reorganize to form the mature virion.

Figure 1.1A shows an electron micrograph (left) and a more detailed schematic (right) of a mature HIV-1 virion. Immature virions vary in size, but are typically ~110-120 nm in diameter. The HIV-1 limiting membrane is derived from the host lipid bilayer and is rich in cholesterol and acidic phospholipids (10). Approximately 7-14 trimeric Env "spikes" (comprising gp120 and gp41) decorate the outer surface of the viral membrane (11) and myristoylated MA trimers form a "matrix" layer against the inner bilayer (12-14). The central electron-dense, conical ribonucleoprotein assembly is known as the viral core. The core contains two NC-bound viral RNA genomes (this assembly is called the

Figure 1.1 Structure of the mature HIV-1 virion. (A) Electron micrograph of a mature HIV-1 virion (left) and a cartoon schematic of its major components (right).

(B) Structure of the mature HIV-1 capsid. Cartoon representation of a HIV-1 CA monomer showing the N-terminal (NTD, orange) and C-terminal (CTD, blue) domains (left), surface representation of a CA hexamer surrounded by 6 neighboring CA hexamers in cartoon representations (middle) and a model of a HIV-1 fullerene cone (right), with insets highlighting CA pentamers (top; yellow/blue) and hexamers (bottom; orange/blue).

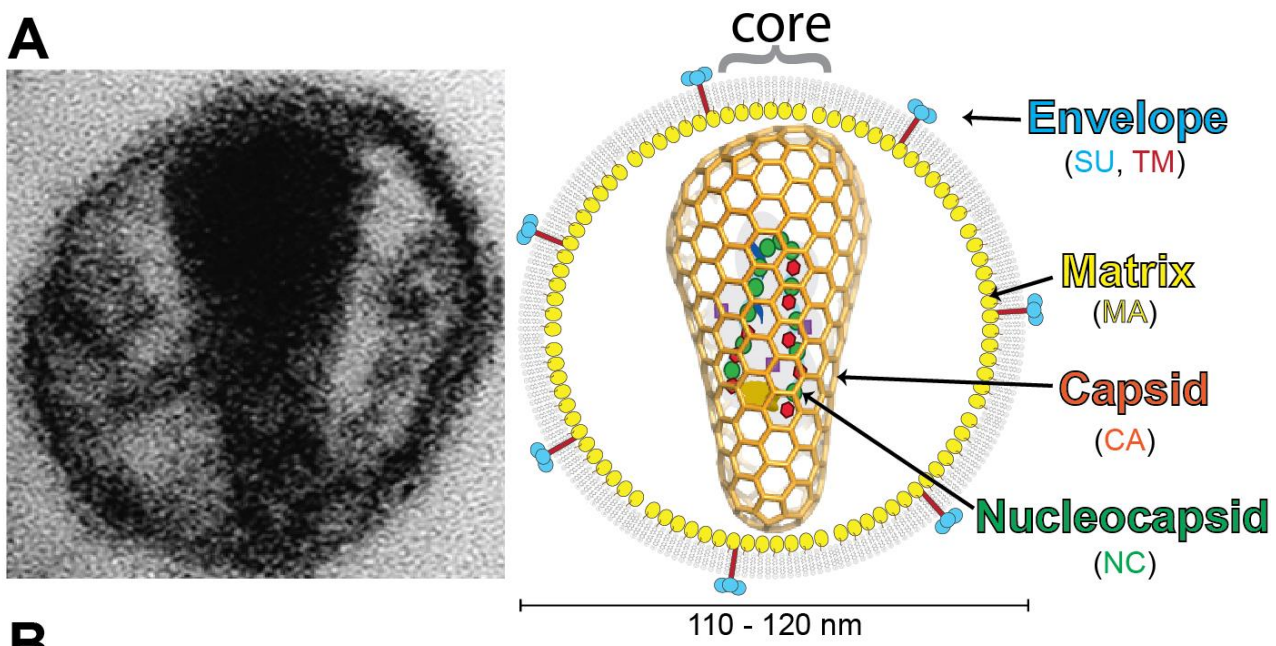
A
core
Envelope
(SU, TM)
Matrix
(MA)
Capsid
(CA)
Nucleocapsid
(NC)
110 - 120 nm
B
NTD
N
C
CTD

"nucleocapsid") as well as the viral proteins IN, RT and Vpr, within an outer CA protein shell (called the "capsid").

Structural studies have led to an atomic-level understanding of the mature HIV-1 capsid structure (15-27). CA monomers comprise α-helical N-terminal (NTD; orange) and C-terminal (CTD; blue) domains, which are connected by a flexible linker (Figure 1.1B, left). The exact process by which ~1500 CA copies nucleate and grow into a mature capsid is not fully understood, but the structural contributions of the CA protein domains are clear (9). The NTD mediates CA hexamerization and the six outward-facing CTDs contact the CTDs of neighboring hexamers to form a hexagonal lattice, which is further stabilized by NTD-CTD interactions (Figure 1.1B, middle) (22). Lattice curvature is accommodated by changes in the "bite" angle between the NTD and CTD of individual CA monomers. The constituent CA subunits of the capsid are never identical to one another, because the capsid lacks global symmetry and curvature abolishes the perfect six-fold symmetry observed in crystal structures of the CA hexamer (21, 22, 27). The surface lattice therefore exhibits only local or "pseudo" six-fold symmetry about the axis of each hexamer (Figure 1.1B, right). Euler's polyhedron theorem dictates that convex polyhedra assembled from hexameric building blocks can enclose space only if they also include (exactly) 12 pentamers. Gratifyingly, CA also forms quasi-equivalent pentamers (Figure 1.1B, right, top inset) (23, 26), and their inclusion produces a conical capsid that is a "fullerene cone" (17, 23).

The CA hexamer/pentamer model also accounts for the spherical and cylindrical capsids formed by other retroviral genera (17). Despite sharing <10% sequence identity, all retroviral CA proteins have identical tertiary structures and assemble hexamers and

pentamers (20, 27, 28). Global variations in capsid morphology can, therefore, arise simply from differences in hexamer numbers and pentamer positions (29, 30). For example, the narrow and broad ends of the lentiviral fullerene cone shown in Figure 1.1B (right) have 5 and 7 pentamers, respectively (a "P = 5,7" cone (17)), whereas pseudosymmetric distributions of 6 pentamers on either end would yield cylindrical capsids (which predominate in D-type retroviruses). Near-uniform pentamer distributions create roughly spherical capsids (present in C-type retroviruses), and finally, perfectly symmetrical distribution of the pentamers generates an icosahedral capsid. Although the majority of HIV-1 capsids belong to the P = 5,7 class, ~50% of HIV-1 core particles display wider cone angles, irregular or cylindrical shapes, and in those cases the capsids contain atypical pentamer distributions (Chapter 4 and refs. (17, 31-33)). Unlike regular, crystallizable capsids of icosahedral viruses, individual retroviral capsids differ from one another even within a morphological class (such as HIV-1 P = 5,7 cones) (34, 35). Thus, although retroviral capsids are highly organized, they are nevertheless asymmetric and highly pleomorphic. These properties have important implications for capsid recognition by host restriction factors such as TRIM5α (Section 1.6, Chapter 2, (36)).

## 1.2 Overview of the HIV-1 lifecycle

HIV-1 initially binds at the plasma membrane of target cells via interactions between the gp120 subunit of the viral Env glycoprotein and cell surface CD4 receptors. Receptor binding exposes additional binding sites for either of two chemokine co-receptors, CCR5 or CXCR4. Coreceptor binding activates the transmembrane gp41 glycoprotein to fuse the viral and cellular membranes, which releases the viral core into the cytoplasm (37, 38).

There is some debate as to whether fusion occurs directly at the plasma membrane or from endosomes, following endocytosis (39, 40).

Once the core is in the cytoplasm, three steps transform the core particle into a preintegration complex (PIC) (Figure 1.2A): (a) A "reverse transcription initiation complex" comprising RT, a $tRNA^{Lys,3}$ primer and the two RNA copies (inset) initiates reverse transcription of the viral RNA into a complementary double-stranded DNA (cDNA), (b) the capsid "uncoats", releasing CA subunits and (c) the PIC is actively transported across the cytoplasm and imported into the nucleus. The timing, order and sites of these steps are still controversial (represented in Figure 1.2A as a gray cloud).

Proper capsid uncoating appears to be critical for efficient reverse transcription (and *vice versa*), because CA mutations that reduce capsid stability typically inhibit cDNA synthesis *in vivo* and conversely, reverse transcriptase inhibitors and mutations can alter the kinetics of capsid uncoating (41, 42). Early models of early events postulated that reverse transcription and uncoating occur immediately after cytoplasmic entry and that the newly formed PIC containing viral cDNA, IN and other viral and host factors is transported across the cytoplasm and imported into the nucleus. Exciting new findings, however, suggest a more direct role for the mature capsid lattice in nuclear targeting and import:

(a) CA sequences dictate the ability of lentiviruses, including HIV-1, to infect non-dividing cells that contain intact nuclear envelopes (43). (b) CA hijacks a nuclear transport factor, transportin 3 (TNPO3), by binding to its cellular substrate, cleavage and polyadenylation specificity factor subunit 6 (CPSF6), via a pocket located at the NTD-CTD hexameric lattice interface. This observation implies that CA hexamers must be intact when the TNPO3/CPSF6 complex is engaged (44). (c) CA also directly binds nuclear pore

Figure 1.2 HIV-1 lifecycle.

(A) Early events in the HIV-1 lifecycle. Entry: The viral membrane fuses with the plasma or endosomal membrane and the core particle enters the cytoplasm. Reverse Transcription: RT initiates and completes reverse transcription of the viral RNA. Uncoating: The capsid disassembles into low molecular weight forms of CA. Nuclear Import: The preintegration complex (PIC) is delivered into the nucleus. Integration: IN mediates integration of the viral cDNA into the host chromosome. Maroon dashed ellipses highlight the early-stage restriction factors Fv1, TRIM5α, TRIMCyp, SAMHD1, APOBEC3G, MxB.

(B) Late events in the HIV-1 lifecycle. Transcription, Splicing, Nuclear Export: HIV-1 proviral DNA is transcribed, spliced (in some cases) and exported out of the nucleus. Assembly: HIV-1 proteins are translated in the cytoplasm and on the ER (Env), and transported to the plasma membrane, where they assemble into nascent particles. Budding: The ESCRT machinery aids HIV-1 budding. Maturation: The released virus is processed by PR. Maroon dashed ellipses highlight the late stage restriction factors TRIM28, Schlafen11, ZAP, Tetherin. This figure was made in collaboration with Yen-Li Li.

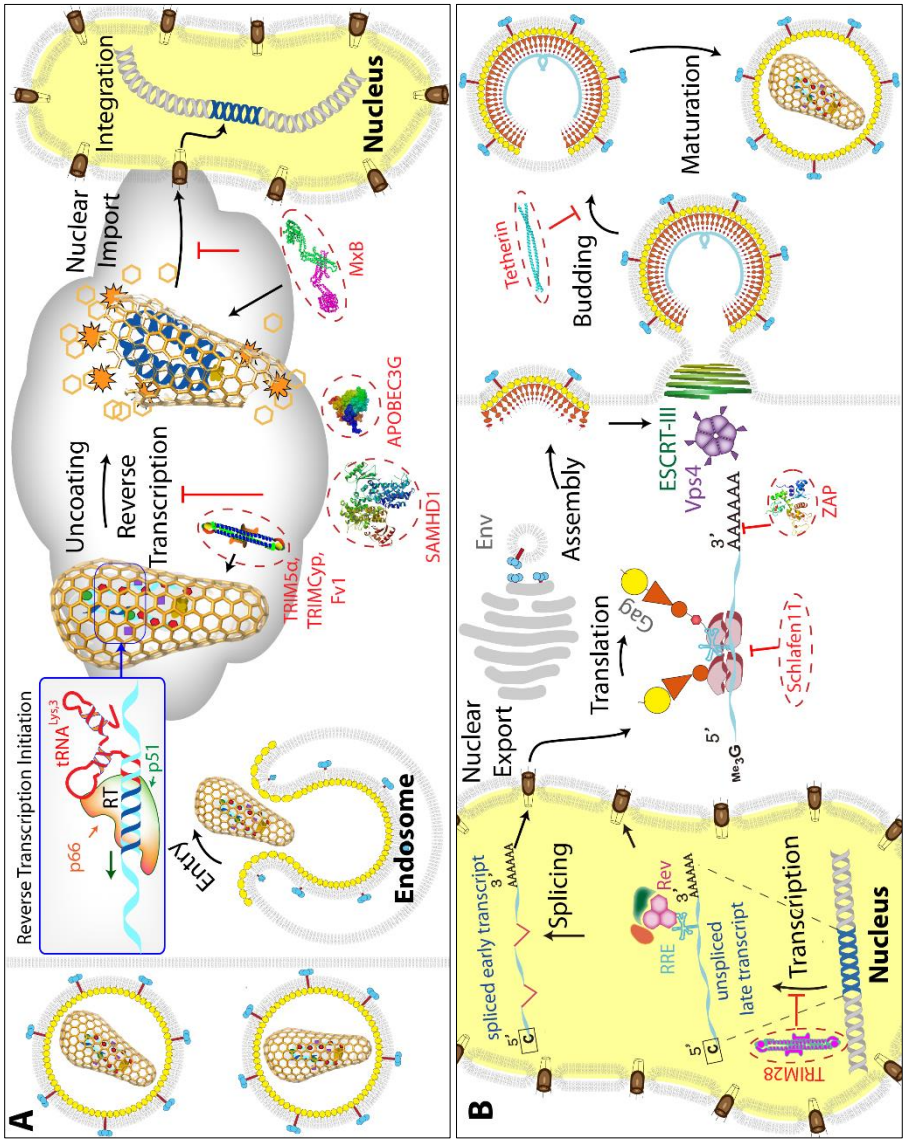
A
Reverse Transcription Initiation
tRNA Lys3
p66
RT
p51
Entry
Endosome
Uncoating
Reverse Transcription
Nuclear Import
Integration
Nucleus
TRIM5α, TRIMCyp, Fv1
APOBEC3G
SAMHD1
MxB
B
Nuclear Export
spliced early transcript
Splicing
Translation
Gag
Env
Assembly
Budding
Tetherin
Maturation
ESCRT-III
Vps4
ZAP
Schlafen11
Rev
RRE
unspliced late transcript
Transcription
TRIM28
Nucleus

complex (NPC) components, NUP153 (using the same NTD-CTD pocket) and NUP358, a cyclophilin domain-containing protein (using the cyclophilin binding loop on the CA NTD). These observations imply that CA hexamers are also associated with PICs at this stage (45, 46). Finally, (d) mutations in CA (N74D, P90A) or competitive inhibitors (e.g., PF-74, BI-1, BI-2, cyclosporine) that disrupt these interactions affect uncoating and nuclear import, and also render the viral genome susceptible to restriction, suggesting that these host factors help uncoat the capsid *just prior* to PIC nuclear entry, thus shielding viral reverse transcripts from host restriction (44, 47-51). Collectively, these observations suggest that the intact capsid may deliver the PIC to the nuclear pore, or perhaps even through it (52).

Once the PIC enters the nucleus, the dsDNA viral genome must be integrated into the host chromosomes. The process of integration is becoming better understood, owing especially to recent atomic resolution crystal structures that capture different steps in this process (53, 54). Integration is mediated by the intasome, a complex of tetrameric IN subunits that bind to the viral cDNA ends. Assisted by host factors such as lens epithelium-derived growth factor, LEDGF, IN associates preferentially with highly-transcribed, non-chromatin regions of the host chromosome, engages both strands of the target DNA in a ternary "target capture complex" and catalyzes concerted strand transfer of the viral cDNA ends in the chromosomal DNA (reviewed in (55, 56)). Host DNA repair machinery subsequently repairs the insertion wound (57). In summary, the early steps of entry, reverse transcription, uncoating, nuclear import and integration collectively create a DNA copy of the HIV-1 genome (the "provirus") that is covalently integrated into the host chromosome.

HIV-1 proviruses can lie dormant in small populations of resting $CD4^+$ memory T cells and in other infected cells within patient tissues, where they remain unaffected by HAART therapy (58, 59). These latently infected $CD4^+$ memory T cells turn over with a half-life of years, but can be reactivated at any time, providing an enormous challenge for viral eradication. Except for these so-called "latent reservoirs", the majority of infected cells transcribe their integrated DNA proviruses into mRNA, which launches the late events in HIV-1 replication.

During the late stage steps in HIV-1 replication, RNA transcription is stimulated by the viral factor, Tat, which increases the processivity of host RNA Pol II complexes. Longer, unspliced RNAs are exported into the cytoplasm by the action of the viral Rev protein. Once in the cytoplasm, these RNAs can either serve as positive-strand genomes, or can code for regulatory proteins and structural proteins that assemble progeny virions (Figure 1.2B). As copies of the genomic RNA and viral proteins accumulate, Gag orchestrates their trafficking, assembly and egress from the plasma membrane as nascent virions (reviewed in (8, 9)). The host endosomal sorting complexes required for transport (ESCRTs) facilitate HIV-1 budding and catalyze the final step of membrane fission, thus releasing immature virions and their newly acquired lipid membranes from the cell (60). Finally, PR cleaves the structural polyproteins, and the subunits then rearrange to produce mature infectious virions.

## 1.3 Retroviral restriction factors

In mammalian hosts, the innate immune system provides rapid, nonadaptive responses to foreign intrusions and the adaptive (or acquired) immune system mounts a slower, but

more specific response to viral (and other pathogenic) antigens. These two lines of defense, together with modern antiretroviral drugs, are the three most important defenses against the establishment and expansion of retroviral infections. It is desirable, however, to forestall retroviral infection and prevent viral spread to uninfected cells *before* proviruses (and latency) can be established. Unfortunately, prophylactic vaccines have so far only displayed modest (if any) success against HIV-1 (61, 62). Owing to the strong selective pressure of retroviral infections, mammals have evolved constitutively-expressed cellular genes, termed restriction factors, which can rapidly detect and block retroviral replication in cells (63). Restriction factors lack immunological memory to repeated infections, are highly specific towards particular pathogens and are typically induced by interferon signaling pathways that indicate the presence of foreign pathogens (3). Restriction factors function in concert with one other and with antiviral signaling pathways. Restriction factor expression is typically upregulated by interferon-α (IFN-α), IRF3, IRF7, AP-1 and NF-κB pathways, and conversely, can themselves trigger the release of IFN-α and other cytokines upon sensing retrovirus-associated patterns (such as viral RNA or capsids) (64-66). Such systemic responses to infection, although poorly understood, limit viral spread by coordinating multiple lines of defense and establishing an "antiviral state".

Existing clinical AIDS therapies target several different steps of the viral lifecycle. In fact, only combination therapies that target several different replication steps *simultaneously* can effectively lower HIV-1 titers in patients, owing to HIV-1's astonishing ability to acquire drug resistance. Analogous selection pressures also dictate the evolution of antiretroviral restriction factors, which can again block nearly every step in the viral lifecycle using diverse strategies (see Figure 1.2 A, B; restriction factors are highlighted in

maroon dashed ellipses). The well-studied restriction factors that mediate early, postentry blocks to retroviral replication are: Fv1, TRIM5α and TRIMCyp, APOBEC3G, SAMHD1 and Mx2, and the known restriction factors that block late events are: TRIM28, ZAP, Schlafen 11 and Tetherin (for reviews, see refs. (5, 63, 67)).

Discoveries of restriction factors often resulted from observations that certain species (or cell types) support retroviral replication less well than others (Table 1.1). A related approach exploited the observations that normally permissive cells become non-permissive when infected with HIV-1 or SIV strains lacking accessory genes such as Vpu, Vif and Vpx (which antagonize Tetherin, APOBEC3G and SAMHD1, respectively). Diverse methods were used to identify the restricting protein, such as: comparative transcriptional profiling (as in the case of Tetherin and Mx2), biochemical and mass spectrometric analyses (SAMHD1, TRIM28), positional cloning (Fv1), reverse transcriptase PCR (RT-PCR; TRIMCyp), cDNA subtraction assays (APOBEC3G) and cDNA library screens (TRIM5α) (for references, see Table 1.1). Future strategies will likely mimic current approaches, but may also include evolutionary and large-scale genomics techniques (68). A detailed summary of HIV-1 restriction factors is presented in Table 1.1.

Restriction factors are specialized immune molecules that have typically evolved from proteins that serve other purposes but now function solely to combat HIV-1 (or other specific pathogens) and can therefore undergo extensive duplication, copy number variation and genetic drift to diversify their pathogen range and restriction mechanisms. This feature distinguishes them from host cell factors that *aid* HIV-1 replication, such as the ESCRT machinery, which are also under evolutionary pressure to escape usurpation, but cannot endlessly undergo positive selection without jeopardizing their cellular

Table 1.1 Retroviral restriction factors

| Restriction Factor | Replication Step Blocked or Altered | Type of protein | Mechanism Of Action | Viral Evasion Strategy | Method Of Discovery | Historical Notes | References |
|---|---|---|---|---|---|---|---|
| **Fv1** Friend virus susceptibility 1 | Uncoating (prior to reverse transcription) | Retroviral Gag-like | Unknown | CA mutations | Positional cloning | First discovery of a heritable trait that governed mouse susceptibility to leukemia | (69-71) |
| **TRIM5α** Tripartite motif containing 5; alpha isoform | Uncoating (prior to reverse transcription) | Capsid-binding E3 ubiquitin ligase | Accelerated capsid dissociation, blocked RT and nuclear entry | CA mutations | Ectopic expression of a rhesus cDNA library in otherwise permissive HeLa cells infected with a reporter HIV-1 strain | The molecular basis for the long-sought Lv1 and Ref1 activities that limited HIV-1 and N-MLV tropism | (72-75) |
| **TRIMCyp** Tripartite motif containing 5-cyclophilin A fusion protein | Uncoating (prior to reverse transcription) | Capsid binding E3 ubiquitin ligase | Accelerated capsid dissociation, blocked RT and nuclear entry | CA mutations | Search for additional RNAi targets to CypA-specific siRNAs | Its discovery explained why owl monkeys are the only new world monkeys that restrict HIV-1 | (76-82) |
| **APOBEC3G** (and other APOBEC family members) Apolipoprotein B mRNA-editing, enzyme-catalytic, polypeptide-like 3G | Reverse transcription | Cytidine deaminase | Converts C to U in minus strand DNA during reverse transcription | Vif-mediated proteasomal degradation of APOBEC3G | PCR-based cDNA subtraction screen comparing expression profiles in permissive and restrictive cell types | APOBEC3G discovery explained the cell-type dependence of Vif requirement for HIV-1 replication | (83) |
| **SAMHD1** Sterile alpha motif and histidine-aspartate domain-containing protein 1 | Reverse transcription | Deoxynucleotide triphosphate (dNTP) hydrolase | Reduces intracellular dNTP levels below that needed for reverse transcription | Vpx (or Vpr/Nef) - mediated proteasomal degradation (or downregulation) of SAMHD1 | Mass spectrometric identification of Vpx-associated factors | The dendritic- and myeloid cell factor that is counteracted by Vpx of HIV-2 and Vpr of SIV | (84-86) |

Table 1.1 continued

| Restriction Factor | Replication Step Blocked or Altered | Type of protein | Mechanism Of Action | Viral Evasion Strategy | Method Of Discovery | Historical Notes | References |
|---|---|---|---|---|---|---|---|
| **Mx2 (MxB)** Myxovirus resistance 2 (B) | Nuclear import | Dynamin-like GTPase | ? | CypA-escape mutations on CA | Transcriptional profiling of interferon-α-upregulated factors in monocytoid cells | Explains the cell-type dependence of INF-α stimulation of HIV-1 inhibition | (87-89) |
| **TRIM28** Tripartite motif containing 28 | Transcription | Transcriptional corepressor | Targeted transcriptional silencing of proviruses | ? | Mass spectrometric identification of protein complexes of PBS DNA | The factor in mouse embryonic stem cells and carcinomas that silences M-MLV transcription | (90, 91) |
| **ZAP** Zinc-finger antiviral protein | Viral mRNA synthesis | CCCH zinc finger motif RNA binding protein | Exosomal degradation of viral mRNAs | ? | Mammalian cDNA library screen for dominant antiretroviral genes | - | (92-94) |
| **Schlafen 11** | Viral translation | Putative DNA/RNA helicase | Codon-bias discrimination | HIV-1 Vpu | | - | (95) |
| **Tetherin** Bone marrow stromal antigen 2 | Viral release | type II single-pass transmembrane protein | Physically tethers budded virions to cell membranes | AP1-dependent mistrafficking and lysosomal degradation of tetherin by Vpu. Viral Env and Nef proteins perform analogous functions in other primate retroviruses. | Comparative transcriptional (microarray) profiling of interferon α upregulated, Vpu-sensitive factors | Explains the accumulation of HIV-1 particles on infected cell surfaces in the absence of Vpu | (96-98) |

functions (99). Members of the APOBEC family of restriction factors (AID, APOBEC1, APOBEC3A-G, etc.), for instance, mediate varied immune functions, including antibody gene diversification and restriction of nonretroviruses (e.g., hepatitis B virus) (100). Another important example is the tripartite motif-containing (TRIM) family of restriction factors, which has expanded dramatically in humans to contain related but distinct genes, including TRIM5 (Section 1.4).

Many restriction factors are evolving rapidly across primates, as evidenced by a non-synonymous to synonymous mutation ratio (dN/dS), >1 in their pathogen interaction domains, which indicates that the region is under positive selection (99, 101-106). Positive selection is a consequence of an arms race for survival, the so-called "Red Queen" effect, in which hosts evolve new restriction factors and retroviruses counter-evolve escape strategies *ad infinitum* (68, 107) (a reference to Lewis Carroll's Red Queen's observation that "It takes all the running one can do, just to stay in the same place".) Both modern-day retroviruses and their hosts bear evolutionary imprints of this arms race. For example, the host factor APOBEC3G blocks retroviral replication by deaminating cytidine to uracil in nascent, minus-strand DNA during reverse transcription and as a consequence the genomes of extant lentiviruses are AU-rich (108). Similarly, simian immunodeficiency virus (SIV) Nef and Vpr can downregulate tetherin (from non-human primates), a cell surface restriction factor that tethers escaping virions (109, 110), but human tetherin has evolved to lack five residues that determine Nef susceptibility (103). Remarkably, this adaptation in humans drove the emergence of HIV-1 Vpu, which efficiently triggers the lysosomal degradation of tetherin (111).

At first glance, retroviruses may appear to have won the battle against host restriction systems for they continue to colonize mammals, as the AIDS pandemic attests. Restriction factors do, however, protect modern hosts against cross-species transmissions of infections (i.e., zoonotic spread) and limit retroviral species tropism (3). Indeed, paleovirological studies have uncovered several examples of ancient retroviruses that have evolved dramatically or have gone extinct owing to selection pressure from restriction factors (112-114).

There are indications that an understanding of HIV-1 restriction factors could result in novel AIDS therapies, even though none currently exist in the market (reviewed in (4, 115-117)). High-throughput screening studies have identified small molecule lead compounds (RN-18, IMB-26, IMB-35, VEC-5, MM-1 and MM-2) that prevent Vif-induced proteasomal degradation of human APOBEC3G (118-121). Another promising strategy is to inhibit human APOBEC3G itself (122), because adaptive evolutionary diversity in HIV-1 strains arises partly from APOBEC3G-induced viral hypermutation (123, 124). Possible therapeutic strategies for augmenting TRIM5α and TRIMCyp, the restriction factors that are the focus of this dissertation, are discussed in Section 1.7.

## 1.4 The TRIM protein family

The Tripartite Motif (TRIM) family of proteins is present in both invertebrates and vertebrates and comprises over 100 genes in humans (125-132). Some TRIMs (called group 1 TRIM genes (133)) perform varied, evolutionarily-ancient roles during cellular proliferation, differentiation, development, apoptosis, as well as other functions, but many

others (group 2) are species-specific, positively-selected genes that are upregulated during viral infection and are, therefore, *bona fide* antiviral restriction factors (65, 134).

By definition, the tripartite motif comprises an ordered arrangement of a RING (really interesting new gene) domain, one or two B-box domains (B-box 1 and B-box 2) and a coiled-coil (abbreviated as RBCC), depicted schematically in Figure 1.3. Individual TRIM proteins can sometimes lack one or more of these domains, but even in those cases, the remaining domains strictly follow this order. TRIM proteins differ from one another in the varied domain(s) that follows the RBCC domains, and the family itself is more extensively classified into 11 subfamilies (C-I to C-XI) based on these C-terminal domains (135, 136). For more detailed representations of the RBCC and C-terminal domains of individual TRIMs, see refs. (66, 67, 136).

TRIM restriction factors have so far been identified using diverse methods such as viral restriction screens, interferon induction profiling, functional genomics and evolutionary approaches, but the task is nevertheless difficult and each method suffers from specific shortcomings (65, 137-140). One difficulty arises from the fact that many TRIM genes undergo alternative splicing to produce as many as 11 different isoforms, not all of which possess restriction ability (137). Another challenge is that the species- and virus-specific nature of restriction implies that even broad-based functional approaches cannot uncover every antiviral TRIM (139, 141). Finally, although some TRIM restriction factors can be identified by dN/dS analyses, several other genes that are essential for restriction nevertheless do not display signs of positive selection (137). A case in point is murine TRIM28, which is essential for retroviral transcriptional silencing in the germline (Table 1.1), but does not contain regions of positive selection since it only interacts indirectly with

Figure 1.3 Domain architectures of TRIM family proteins

## TRIM Protein Domain Architecture (General)


RBCC domains

| | | |
|---|---|---|
| ARF | MATH | Fibronectin type 3 |
| COS | BROMO | Plant homeodomain |
| MID | PRYSPRY | Transmembrane domain |
| PML | NHL repeat | Filamin-type immunoglobulin |
| | Cyclophilin A | |

### TRIM5α


### TRIMCyp

proviral DNA (via the bridging zinc finger protein ZFP809 (142)). For these reasons, many TRIM family members remain poorly characterized, although there are a few well-studied members.

### 1.4.1 TRIM5α and TRIMCyp

The search for suitable primate models for AIDS in the 1990s led to the interesting observation that many non-human primate cells resist HIV-1 infection (73, 143). The phenotype was labeled "lentivirus-susceptibility 1" (Lv1) and a similar N-MLV restriction activity in human cells was referred to as Ref1. In 2004, Stremlau, Sodroski and colleagues identified the alpha-isoform of TRIM5 as the restriction factor that blocks HIV-1 replication in rhesus macaque cells (Table 1.1) (72). Subsequently, they and several other groups demonstrated that TRIM5α is responsible for the previously documented Lv1 and Ref1 activities (74, 75, 144). TRIM5α mediates an early, postentry block to retroviral replication prior to reverse transcription. The protein comprises RING, B-box 2 and coiled-coil domains followed by a C-terminal PRYSPRY (B30.2) domain that binds directly to retroviral capsids (Figure 1.3) (145). Owing to its importance in retroviral restriction, TRIM5α has become one of the best-studied members of the TRIM protein family.

A notable TRIM5 variant, TRIMCyp, has evolved independently in the *Aotus* (owl monkey) and *Macaca* (macaques) genera of new world and old world monkeys, respectively. TRIMCyp contains a capsid-binding cyclophilin A (CypA) domain in place of the PRYSPRY domain of TRIM5α (see Figure 1.4) (76-81). In most cell types, CypA is an essential co-factor for HIV-1 replication that participates in capsid uncoating and/or nuclear entry (45, 146, 147). Retrotransposition of the c*ypA* gene into the *TRIM5* locus has

Figure 1.4 General steps in TRIM5 protein restriction of HIV-1. Capsid Recognition: Soluble cytoplasmic TRIM5 dimers must recognize mature retroviral capsids. Ubiquitylation: The RING domains dimerize and recruit the Ubc13/Uev1A heterodimeric E2 complex to catalyze the synthesis of K63-linked polyubiquitin chains. Signaling and Restriction: TAB2/TAB3 ubiquitin adapters recruit the TAK1 kinase complex and initiate NF-κB and AP-1 signaling. The proteasome somehow accelerates capsid disassembly and leads to a block in reverse transcription. In addition, TRIM5 can also target CA for degradation via p62-, and Beclin1-mediated selective autophagy.

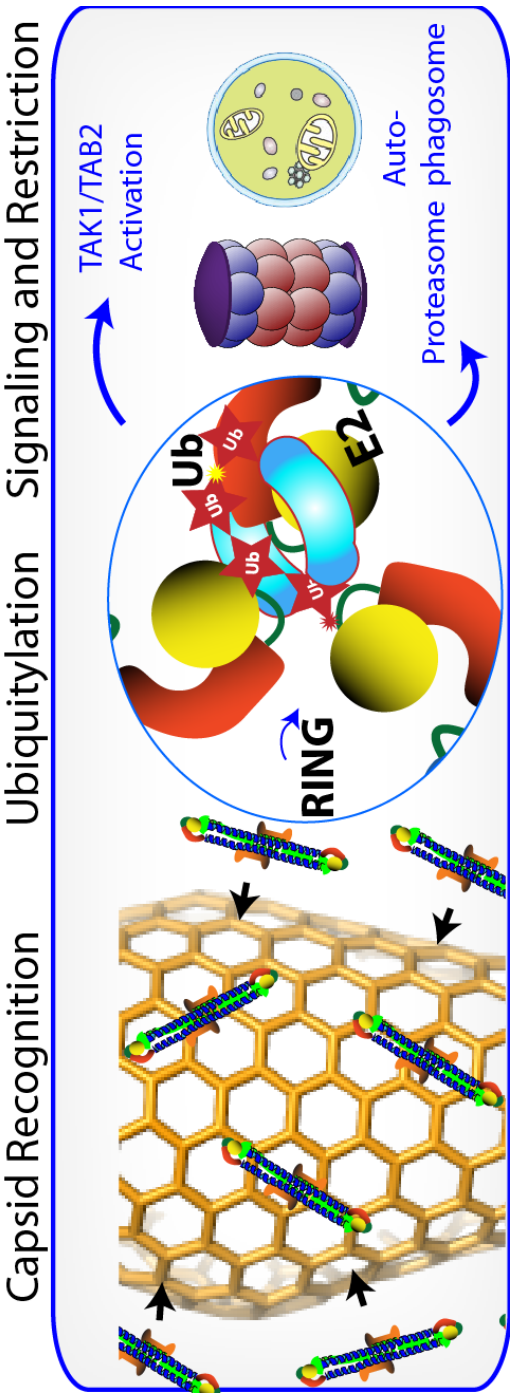
Capsid Recognition
Ubiquitylation
Signaling and Restriction
RING
E2
Ub
TAK1/TAB2
Activation
Auto-
Proteasome phagosome

thus conferred owl monkeys and macaques with a potent restriction factor from which the virus cannot easily evade by evolving CypA-binding escape mutations.

## 1.5 Structures of TRIM protein domains

TRIM proteins are constitutive coiled-coil domain-mediated oligomers (148). Although initial reports incorrectly characterized some TRIM proteins as trimeric (149, 150), we and others have demonstrated that the elongated, ~17 nm long coiled-coil domain forms an antiparallel dimer (Figure 1.5). The chemically-crosslinked, elongated dimer migrates anomalously slowly by SDS-PAGE, however, explaining the initial trimeric assignment (see Appendix, Chapter 2, 3, (151, 152)). To date, only TRIM5 and TRIM25 have been formally shown to be dimeric (151-154), but identical 'knobs-into-holes' patterns of hydrophobic coiled-coil residues are conserved among many family members, indicating that all TRIM proteins form dimers. Most TRIM proteins appear to homodimerize preferentially, although heterodimers of closely related TRIMs are also possible (148)).

The coiled-coil also forms a "platform" that orients the TRIM binding domains (e.g., the PRYSPRY domain in the case of TRIM5α) and can recruit TRIM binding partners. In at least some cases, members of the melanoma antigen (MAGE) family of ~60 human proteins bind specifically to TRIM coiled-coil domains. The MAGE proteins appear to provide an 'E4' activity that somehow enhances TRIM E3 function (155).

TRIM proteins constitute the largest family of human RING-containing proteins, and have been shown to act as E3 Ub ligases, and/or in several instances (156), as E3 SUMO ligases. RING domains bind two zinc ions in a $Cys_3HisCys_4$ cross-brace arrangement

Figure 1.5 Representative 3-dimensional structures of TRIM domains. RING (yellow): Overlay of RING domain structures from human TRIM5α (2ECV), TRIM34 (2EGP), TRIM30 (2ECW), TRIM32 (2CT2), TRIM39 (2ECJ), TRIM31 (2YSL) and the TRIM37 RING dimer (3LRQ), which is stabilized by a 4-helix bundle. The second RING monomer is shown in black and the Zn ions are shown as purple spheres.

B-box 2 (red): Overlay of B-box 2 structures from human TRIM5α (2YRG), TRIM29 (2CSV), TRIM54 (3Q1D), TRIM63 (3DDT) and the tandem B-box 1 (purple) - Box 2 structure from TRIM18 (2JUN). The TRIM63 B-box 2 crystallized as a homodimer and the second monomer is shown in black. Zn ions are shown as purple spheres.

Coiled-coil (blue): Structures of the TRIM5α B-box 2-coiled-coil (4TN3) and the TRIM25 (4LTB) and TRIM69 (4NQJ) coiled-coils. Note the conserved antiparallel fold-back configuration of the coiled-coil-L2 linker region as well as variations in the overall curvature.

PRYSPRY (orange): Structures of the rhesus TRIM5α PRYSPRY domain (2LM3, 3UV9, 4B3N). The v1 hypervariable loop is disordered/deleted in the crystal structures and undefined in the NMR structure.

CypA (green): Overlay of owl monkey TRIMCyp CypA domains in complex with HIV-1 CA constructs (2X83, 4DGA).

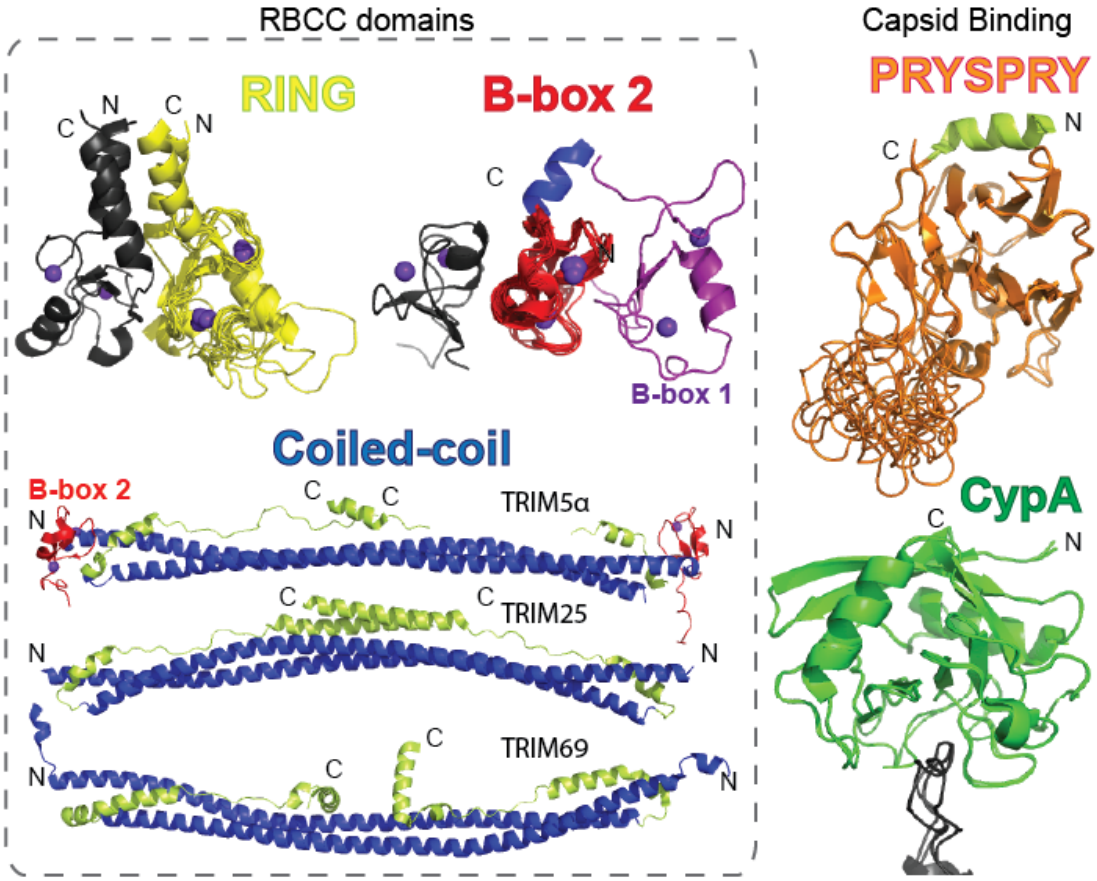
RBCC domains
RING
B-box 2
B-box 1
Coiled-coil
B-box 2
TRIM5α
TRIM25
TRIM69
Capsid Binding
PRYSPRY
CypA

(157). RING domains often dimerize to function (158), including the TRIM37 and TRIM5α RINGs (PDB IDs: 3LRQ and 4TKP). These dimers are stabilized by a four-helix bundle formed by two helices that flank the zinc-binding core, reminiscent of the BRCA1-BARD1 RING heterodimer (159) (and Dmitri Ivanov, personal communication). As discussed further in Chapter 5, TRIM5 RING dimerization likely regulates its E3 ubiquitin ligase activity, and could, in turn, be regulated by B-box 2-dependent and capsid-dependent TRIM5 assembly (64). B-box domains are exclusive to the TRIM family and resemble RING domains structurally (160). B-box 2 domains can occur alone in TRIM proteins, but B-box 1 domains, when present, are always followed by B-box 2 domains. The tandem B-box 1-B-box 2 structure is reminiscent of RING-RING heterodimers (161), but the roles of these tandem domains are unclear. The B-box 1 domain could regulate RING activation, or conceivably even possess E3 ligase activity, though there is no biochemical evidence for this activity. In the case of TRIM5, and perhaps in other self-assembling TRIM proteins, the B-box 2 mediates intermolecular interactions between TRIM dimers to form higher-order oligomers (Section 1.6, Chapter 2 and (162, 163)). Other TRIM B-box 2 domains have been crystallized as dimers and the dimer interface involves the equivalent surface patch seen in TRIM5, but it is not yet known whether these isolated B-box 2 dimers are relevant for TRIM higher-order assembly or merely a crystallographic artifact (see Chapter 5).

PRYSPRY (B30.2) domains have canonical immunoglobulin folds, comprising two sandwiched β-sheets that present target binding loops at their edges. In the case of TRIM5α, these ‘hypervariable’ loops are positively-selected to bind retroviral capsids, including HIV-1 (106, 164, 165). The atomic details of the interaction are still unknown, but the

broad specificity of individual TRIM5α alleles suggests that these loops, especially the flexible v1 loop (Figure 1.5), may adopt different conformations to bind different capsids. Similar conformational heterogeneity has already been observed in crystal structures of the CypA domain of owl monkey TRIMCyp in complex with several CA constructs (166-168). HIV-1 CA is not recognized by the PRYSPRY domain of human TRIM5α, but interestingly, binding and restriction can be rescued by the deletion or Pro substitution of the v1 loop Arg332 residue (169, 170).

## 1.6 TRIM5 protein assembly

Mammalian host cells can be invaded by divergent retroviruses with highly variable capsid morphologies and dissimilar CA sequences, yet individual TRIM5α alleles can often recognize and restrict multiple different retroviruses (171). When a retroviral core is released into the cytoplasm of a cell that expresses a restrictive TRIM5α allele, the PRYSPRY domain of TRIM5α binds directly to the capsid surface, although the precise binding epitopes are only known for the TRIMCyp variant. The broad reactivity of TRIM5 proteins reflects cooperative capsid binding. Evidence in support of this idea includes: (a) The affinity of the PRYSPRY domain for free HIV-1 CA dimers is undetectably weak in solution (172), suggesting that the RBCC domains can somehow augment capsid binding strength. (b) Fluorescence microscopy images of YFP-TRIM5α-expressing cells infected with mCherry-Vpr-labeled HIV-1 viruses reveal that multiple TRIM5 molecules coat invading viral cores. (c) Many TRIM family members, including TRIM5α, can assemble/aggregate into cytoplasmic and nuclear “TRIM bodies” ((148, 173); also see the Appendix).

These observations and our understanding of the capsid structure suggest that higher-order TRIM5 multimers may assemble on viral cores, thereby creating avidity effects and facilitating PRYSPRY-recognition of repeating patterns on the capsid surface. Indeed, TRIM5α multimerization appears to be mediated by a hydrophobic patch on the TRIM5α B-box 2 surface, and this surface is required for HIV-1 restriction (162, 163). Our studies provide the first electron microscopic image of these TRIM5α self-assemblies (Chapters 2 and 4 and ref. (154)).

CypA-CA interactions are well-characterized (174), and unlike the PRYSPRY domain of TRIM5α, the CypA domain of TRIMCyp binds to cyclophilin-binding loops on monomeric CA proteins with measurable $K_d$ values of 48-130 μM (166). As might be expected, B-box 2-mediated higher-order self-assembly is therefore less critical for TRIMCyp binding and restriction of HIV-1 (175, 176). Nevertheless, TRIMCyp self-assembly may buffer against CA mutations that lower CypA affinities and also facilitate RING domain activation and downstream signaling, as described in the following sections (64, 166). The bigger question of how TRIM5 self-assemblies interact with the assembled capsid surface is still unsolved, but our progress so far is presented in Chapters 4 and 5.

## 1.7 TRIM5 restriction mechanisms

TRIM5α induces dissociation of susceptible capsids and also blocks reverse transcription (145), perhaps because reverse transcription requires proper capsid stability and uncoating (177). TRIM5-induced capsid disassembly requires both the RING E3 ubiquitin ligase activity as well as proteasome function, and mutations in the RING domain or treatment with proteasomal inhibitors blocks capsid disassembly and allows reverse

transcription to proceed (Figure 1.4) (173, 178). The virus remains restricted under these experimental conditions, however, perhaps because the TRIM5-bound core is 'trapped' in TRIM5 cytoplasmic bodies and prevented from delivering the PIC into the nucleus (173). This explanation is supported by the observations that artificial multimers of CypA can potently block HIV-1 replication prior to nuclear import (179, 180).

Posttranslational protein ubiquitylation mediates a series of important cellular events. In this process, the Ub C-terminus is activated by a Ub-activating (E1) enzyme and transferred to a ubiquitin-conjugating (E2) enzyme. Ubiquitin ligase (E3) enzymes like TRIM5α then help transfer the Ub either to the N-terminus or to a side chain Lys or Cys residue of a protein substrate. Substrates can either be different proteins, or Ub itself, which has 7 Lys residues (e.g., Lys63). Ub-Ub coupling results in the formation of poly-Ub chains, and the chain linkage typically dictates the biological readout (reviewed in (181, 182)).

In one current model for TRIM5 restriction (Figure 1.4), capsid binding activates the RING domain of TRIM5α to bind the heterodimeric E2 ubiquitin conjugating enzyme, Ubc13/Uev1A (also known as Ube2N/Ube2V1), and catalyze the synthesis of K63-linked poly-Ub chains that are *not anchored* to any substrate (64). These free Ub chains can be sensed by the Ub-specific adapters, TAB2 and TAB3, which in turn activates the TAK1 kinase complex. TAK1 helps to establish an antiviral state by activating the NF-κB and AP-1 response pathways. Ubc13 and TAK1 are essential for TRIM5α-mediated block to reverse transcription (and for proteasome-dependent capsid disassembly), suggesting that these signaling events may somehow recruit the proteasome to the TRIM5-bound capsid. Conceivably, the ATP-dependent unfolding/chaperone activity of the 19S subunit of the

26A proteasome could remove CA subunits and thereby induce capsid dissociation. It is unclear, however, how free K63-linked poly-Ub chains could recruit the proteasome to the TRIM5-bound capsid, because (a) they are unanchored and therefore free to diffuse away from the site of restriction; and (b) canonical proteasome recruitment occurs in cells via K48-linked (rather than K63-linked) poly-Ub chains.

A recent study has also indicated a role for directed autophagy in TRIM5-mediated capsid degradation (183). According to this study, TRIM5α binds p62/Sequestosome-1 (SQSTM-1) and Beclin-1, which in turn recruit autophagosomes to degrade capsids in lysosomes. Indeed, p62 can bind and co-localize with TRIM5α in cells (184), and in other contexts, can serve as an adaptor that targets substrates to nascent autophagosomes as well as proteasomes (185, 186). It is presently unclear whether proteasome-mediated capsid dissociation and autophagosomal capsid degradation are mutually exclusive processes or complementary.

Mechanistic insight into TRIM5 restriction could, in principle, be harnessed to design novel AIDS therapies. TRIM5 proteins likely block reverse transcription in a fashion analogous to capsid-weakening CA mutations, which trigger premature capsid dissociation (177). Human TRIM5α only weakly restricts HIV-1, if at all (72, 165, 170, 187). Therapies to introduce functional TRIM5 alleles have been demonstrated in cats and proposed in humans (188, 189), but gene therapy is expensive as well as inherently dangerous. An alternative approach would be to identify small molecules that modulate capsid stability in either direction ((51), and references therein). Indeed, such compounds (PF74, BI-1, BI-2) have already been identified, even if they do not precisely mimic TRIM5 proteins to function (50, 190). Finally, small-molecule agonists could, in principle, augment the low

affinity of human TRIM5α for HIV-1 capsids by acting as a 'molecular glue' at the TRIM5α-capsid interface, akin to auxin hormones in plants (191).

Several outstanding issues remain in the TRIM field: (a) the conserved arrangement and strict ordering suggests that the RBCC motif functions as a single structural unit rather than as independently functioning modules. What is the the structural basis for this concerted action? (b) Most TRIM proteins can assemble into higher order cytoplasmic or nuclear structures called "TRIM bodies" (148). Similarly, TRIM5 proteins can assemble on incoming retroviral capsids, and these assemblies appear to be the functional form of the protein. What are the compositions, structures and functions of higher order TRIM assemblies? (c) What are the substrates and cognate E2 enzymes for TRIM-mediated ubiquitylation and SUMOylation, and how is TRIM E3 activity regulated? (d) What are the biological consequences of TRIM ubiquitylation? In the case of TRIM5 proteins, ubiquitylation somehow regulates innate immune signaling pathways such as type I and II interferon responses, activation of NF-κB, AP-2, IRF3 and IRF7 (65, 192, 193), yet the precise stepwise pathways are not known. (e) Finally, why do several autoimmune and hereditary disease phenotypes map to TRIM proteins, often in their C-terminal domains (136)?

Structural and biochemical analyses that could, in principle, address many of these questions are challenging because TRIM proteins are difficult to purify and readily partition into insoluble self-assemblies when over-expressed or concentrated. In this dissertation, I describe how I have overcome these technical hurdles, studied the biochemical and assembly properties of TRIM5α, and proposed and validated a model for TRIM5 assembly and retroviral capsid recognition.

## 1.8 Overview of chapters

The overall aim of my research was to determine how TRIM5 proteins recognize retroviral capsids. This goal has required me to: (a) develop methods to express and purify recombinant TRIM5 proteins, (b) study how they self-assemble and co-assemble on hexagonal CA lattices that mimic the surface of the HIV-1 capsid (in collaboration with Mark Yeager's group), (c) image HIV-1 capsids decorated with TRIM5α using electron cryotomography (in collaboration with Yen-Li Li and Grant Jensen's group) and (d) crystallize and attempt to determine the crystal structure of TRIM5 proteins, both alone and in complex with hexameric CA assemblies (in collaboration with Chris Hill's and Owen Pornillos's groups).

The Appendix reports the first expression, purification and biochemical characterization of a recombinant TRIM5 protein, a restrictive variant of rhesus TRIM5α called "TRIM5-21R". In this construct, the native rhesus TRIM5α RING domain was replaced with the RING domain of human TRIM21. This substitution increases the half-life of the protein in mammalian and insect cells (194), and facilitates protein expression and purification in quantities sufficient for biochemical and EM studies. This study revealed that TRIM5-21R is a dimeric E3 Ub ligase that binds authentic equine infectious anemia virus (EIAV) capsids, as well as helical tubes of HIV-1 CA formed *in vitro*.

Chapter 2 reports the discovery that TRIM5-21R dimers can spontaneously self-assemble and co-assemble with 2D crystals of HIV-1 CA to form hexagonal lattices comprising open rings of TRIM5-21R. We proposed a model in which TRIM5 proteins recognize the "pattern" of the capsid surface by assembling hexagonal lattices that complement the symmetry and conserved ~90-100 Å hexameric spacings of retroviral

capsids. Such assemblies could position repeating PRYSPRY domains over their capsid surface epitopes, thus augmenting the weak intrinsic capsid affinities of TRIM5 PRYSPRY (and CypA) domains through avidity effects.

The crystal structure of the TRIM25 coiled-coil/L2 linker domain is reported in Chapter 3. (The X-ray crystallography was performed by the Pornillos lab.) I performed supporting biochemical experiments that revealed that this region of most TRIMs, including TRIM5α, form analogous antiparallel dimers.

In the work reported in Chapter 4, we validated our "pattern recognition" model by directly visualizing hexagonal TRIM5α assemblies on the surfaces of purified HIV-1 core particles using cryoelectron tomography. To achieve this, I developed methods for expressing and purifying multimilligram quantities of several different primate TRIM5α proteins.

In Chapter 5, I report my (unpublished) attempts to crystallize and determine the X-ray structure of assembled TRIM5α, and outline my future plans to crystallize TRIM5-CA complexes.

## 1.9 References

1. **UNAIDS.** 2013. 2013 UNAIDS Report on the global AIDS epidemic. UNAIDS.

2. **Geeraert L, Kraus G, Pomerantz RJ.** 2008. Hide-and-seek: the challenge of viral persistence in HIV-1 infection. Annual review of medicine **59:**487-501.

3. **Bieniasz PD.** 2004. Intrinsic immunity: a front-line defense against viral attack. Nat Immunol **5:**1109-1115.

4. **Santa-Marta M, de Brito PM, Godinho-Santos A, Goncalves J.** 2013. Host Factors and HIV-1 Replication: Clinical Evidence and Potential Therapeutic Approaches. Frontiers in immunology **4:**343.

5. **Bieniasz PD.** 2003. Restriction factors: a defense against retroviral infection. Trends in microbiology **11:**286-291.

6. **Hartley JW, Rowe WP, Huebner RJ.** 1970. Host-range restrictions of murine leukemia viruses in mouse embryo cell cultures. J Virol **5:**221-225.

7. **Frankel AD, Young JA.** 1998. HIV-1: fifteen proteins and an RNA. Annual review of biochemistry **67:**1-25.

8. **Sundquist WI, Krausslich HG.** 2012. HIV-1 assembly, budding, and maturation. Cold Spring Harbor perspectives in medicine **2:**a006924.

9. **Ganser-Pornillos BK, Yeager M, Sundquist WI.** 2008. The structural biology of HIV assembly. Curr Opin Struct Biol **18:**203-217.

10. **Waheed AA, Freed EO.** 2009. Lipids and membrane microdomains in HIV-1 replication. Virus research **143:**162-176.

11. **Chertova E, Bess JW, Jr., Crise BJ, Sowder IR, Schaden TM, Hilburn JM, Hoxie JA, Benveniste RE, Lifson JD, Henderson LE, Arthur LO.** 2002. Envelope glycoprotein incorporation, not shedding of surface envelope glycoprotein (gp120/SU), Is the primary determinant of SU content of purified human immunodeficiency virus type 1 and simian immunodeficiency virus. J Virol **76:**5315-5325.

12. **Tedbury PR, Ablan SD, Freed EO.** 2013. Global rescue of defects in HIV-1 envelope glycoprotein incorporation: implications for matrix structure. PLoS Pathog **9:**e1003739.

13. **Rao Z, Belyaev AS, Fry E, Roy P, Jones IM, Stuart DI.** 1995. Crystal structure of SIV matrix antigen and implications for virus assembly. Nature **378:**743-747.

14. **Hill CP, Worthylake D, Bancroft DP, Christensen AM, Sundquist WI.** 1996. Crystal structures of the trimeric human immunodeficiency virus type 1 matrix protein: implications for membrane association and assembly. Proc Natl Acad Sci U S A **93:**3099-3104.

15. **Gitti RK, Lee BM, Walker J, Summers MF, Yoo S, Sundquist WI.** 1996. Structure of the amino-terminal core domain of the HIV-1 capsid protein. Science **273:**231-235.

16. **Gamble TR, Yoo S, Vajdos FF, von Schwedler UK, Worthylake DK, Wang H, McCutcheon JP, Sundquist WI, Hill CP.** 1997. Structure of the carboxyl-terminal dimerization domain of the HIV-1 capsid protein. Science **278:**849-853.

17. **Ganser BK, Li S, Klishko VY, Finch JT, Sundquist WI.** 1999. Assembly and analysis of conical models for the HIV-1 core. Science **283:**80-83.

18. **Worthylake DK, Wang H, Yoo S, Sundquist WI, Hill CP.** 1999. Structures of the HIV-1 capsid protein dimerization domain at 2.6 A resolution. Acta crystallographica. Section D, Biological crystallography **55:**85-92.

19. **Li S, Hill CP, Sundquist WI, Finch JT.** 2000. Image reconstructions of helical assemblies of the HIV-1 CA protein. Nature **407:**409-413.

20. **Ganser BK, Cheng A, Sundquist WI, Yeager M.** 2003. Three-dimensional structure of the M-MuLV CA protein on a lipid monolayer: a general model for retroviral capsid assembly. EMBO J **22:**2886-2892.

21. **Ganser-Pornillos BK, Cheng A, Yeager M.** 2007. Structure of full-length HIV-1 CA: a model for the mature capsid lattice. Cell **131:**70-79.

22. **Pornillos O, Ganser-Pornillos BK, Kelly BN, Hua Y, Whitby FG, Stout CD, Sundquist WI, Hill CP, Yeager M.** 2009. X-Ray Structures of the Hexameric Building Block of the HIV Capsid. Cell.

23. **Pornillos O, Ganser-Pornillos BK, Yeager M.** 2011. Atomic-level modelling of the HIV capsid. Nature **469:**424-427.

24. **Zhao G, Perilla JR, Yufenyuy EL, Meng X, Chen B, Ning J, Ahn J, Gronenborn AM, Schulten K, Aiken C, Zhang P.** 2013. Mature HIV-1 capsid structure by cryo-electron microscopy and all-atom molecular dynamics. Nature **497:**643-646.

25. **Byeon IJ, Meng X, Jung J, Zhao G, Yang R, Ahn J, Shi J, Concel J, Aiken C, Zhang P, Gronenborn AM.** 2009. Structural convergence between Cryo-EM and NMR reveals intersubunit interactions critical for HIV-1 capsid function. Cell **139:**780-790.

26. **Cardone G, Purdy JG, Cheng N, Craven RC, Steven AC.** 2009. Visualization of a missing link in retrovirus capsid assembly. Nature **457:**694-698.

27. **Mortuza GB, Haire LF, Stevens A, Smerdon SJ, Stoye JP, Taylor IA.** 2004. High-resolution structure of a retroviral capsid hexameric amino-terminal domain. Nature **431:**481-485.

28. **Campos-Olivas R, Newman JL, Summers MF.** 2000. Solution structure and dynamics of the Rous sarcoma virus capsid protein and comparison with capsid proteins of other retroviruses. J Mol Biol **296:**633-649.

29. **Ganser-Pornillos BK, von Schwedler UK, Stray KM, Aiken C, Sundquist WI.** 2004. Assembly properties of the human immunodeficiency virus type 1 CA protein. J Virol **78:**2545-2552.

30. **Heymann JB, Butan C, Winkler DC, Craven RC, Steven AC.** 2008. Irregular and Semi-Regular Polyhedral Models for Rous Sarcoma Virus Cores. Computational and mathematical methods in medicine **9:**197-210.

31. **Benjamin J, Ganser-Pornillos BK, Tivol WF, Sundquist WI, Jensen GJ.** 2005. Three-dimensional structure of HIV-1 virus-like particles by electron cryotomography. J Mol Biol **346:**577-588.

32. **Briggs JA, Grunewald K, Glass B, Forster F, Krausslich HG, Fuller SD.** 2006. The mechanism of HIV-1 core assembly: insights from three-dimensional reconstructions of authentic virions. Structure **14:**15-20.

33. **Briggs JA, Wilk T, Welker R, Krausslich HG, Fuller SD.** 2003. Structural organization of authentic, mature HIV-1 virions and cores. EMBO J **22:**1707-1715.

34. **Rossmann MG.** 2013. Structure of viruses: a short history. Quarterly reviews of biophysics **46:**133-180.

35. **Fry EE, Grimes J, Stuart DI.** 1999. Virus crystallography. Molecular biotechnology **12:**13-23.

36. **Goldstone DC, Walker PA, Calder LJ, Coombs PJ, Kirkpatrick J, Ball NJ, Hilditch L, Yap MW, Rosenthal PB, Stoye JP, Taylor IA.** 2014. Structural studies of postentry restriction factors reveal antiparallel dimers that enable avid binding to the HIV-1 capsid lattice. Proc Natl Acad Sci U S A **111:**9609-9614.

37. **Berger EA, Murphy PM, Farber JM.** 1999. Chemokine receptors as HIV-1 coreceptors: roles in viral entry, tropism, and disease. Annual review of immunology **17:**657-700.

38. **Eckert DM, Kim PS.** 2001. Mechanisms of viral membrane fusion and its inhibition. Annual review of biochemistry **70:**777-810.

39. **Miyauchi K, Kim Y, Latinovic O, Morozov V, Melikyan GB.** 2009. HIV enters cells via endocytosis and dynamin-dependent fusion with endosomes. Cell **137:**433-444.

40. **Marsh M, Helenius A.** 2006. Virus entry: open sesame. Cell **124:**729-740.

41. **Hulme AE, Perez O, Hope TJ.** 2011. Complementary assays reveal a relationship between HIV-1 uncoating and reverse transcription. Proc Natl Acad Sci U S A **108:**9975-9980.

42. **Yang Y, Fricke T, Diaz-Griffero F.** 2013. Inhibition of reverse transcriptase activity increases stability of the HIV-1 core. J Virol **87:**683-687.

43. **Yamashita M, Perez O, Hope TJ, Emerman M.** 2007. Evidence for direct involvement of the capsid protein in HIV infection of nondividing cells. PLoS Pathog **3:**1502-1510.

44. **Lee K, Ambrose Z, Martin TD, Oztop I, Mulky A, Julias JG, Vandegraaff N, Baumann JG, Wang R, Yuen W, Takemura T, Shelton K, Taniuchi I, Li Y, Sodroski J, Littman DR, Coffin JM, Hughes SH, Unutmaz D, Engelman A, KewalRamani VN.** 2010. Flexible use of nuclear import pathways by HIV-1. Cell host & microbe **7:**221-233.

45. **Schaller T, Ocwieja KE, Rasaiyaah J, Price AJ, Brady TL, Roth SL, Hue S, Fletcher AJ, Lee K, KewalRamani VN, Noursadeghi M, Jenner RG, James LC, Bushman FD, Towers GJ.** 2011. HIV-1 capsid-cyclophilin interactions determine nuclear import pathway, integration targeting and replication efficiency. PLoS Pathog **7:**e1002439.

46. **Bichel K, Price AJ, Schaller T, Towers GJ, Freund SM, James LC.** 2013. HIV-1 capsid undergoes coupled binding and isomerization by the nuclear pore protein NUP358. Retrovirology **10:**81.

47. **Rasaiyaah J, Tan CP, Fletcher AJ, Price AJ, Blondeau C, Hilditch L, Jacques DA, Selwood DL, James LC, Noursadeghi M, Towers GJ.** 2013. HIV-1 evades innate immune recognition through specific cofactor recruitment. Nature **503:**402-405.

48. **Ambrose Z, Lee K, Ndjomou J, Xu H, Oztop I, Matous J, Takemura T, Unutmaz D, Engelman A, Hughes SH, KewalRamani VN.** 2012. Human immunodeficiency virus type 1 capsid mutation N74D alters cyclophilin A dependence and impairs macrophage infection. J Virol **86:**4708-4714.

49. **Matreyek KA, Yucel SS, Li X, Engelman A.** 2013. Nucleoporin NUP153 phenylalanine-glycine motifs engage a common binding pocket within the HIV-1 capsid protein to mediate lentiviral infectivity. PLoS Pathog **9:**e1003693.

50. **Lamorte L, Titolo S, Lemke CT, Goudreau N, Mercier JF, Wardrop E, Shah VB, von Schwedler UK, Langelier C, Banik SS, Aiken C, Sundquist WI, Mason SW.** 2013. Discovery of novel small-molecule HIV-1 replication inhibitors that stabilize capsid complexes. Antimicrob Agents Chemother **57:**4622-4631.

51. **Blair WS, Pickford C, Irving SL, Brown DG, Anderson M, Bazin R, Cao J, Ciaramella G, Isaacson J, Jackson L, Hunt R, Kjerrstrom A, Nieman JA, Patick AK, Perros M, Scott AD, Whitby K, Wu H, Butler SL.** 2010. HIV capsid

is a tractable target for small molecule therapeutic intervention. PLoS Pathog **6:**e1001220.

52. **Arhel NJ, Souquere-Besse S, Munier S, Souque P, Guadagnini S, Rutherford S, Prevost MC, Allen TD, Charneau P.** 2007. HIV-1 DNA Flap formation promotes uncoating of the pre-integration complex at the nuclear pore. EMBO J **26:**3025-3037.

53. **Maertens GN, Hare S, Cherepanov P.** 2010. The mechanism of retroviral integration from X-ray structures of its key intermediates. Nature **468:**326-329.

54. **Hare S, Gupta SS, Valkov E, Engelman A, Cherepanov P.** 2010. Retroviral intasome assembly and inhibition of DNA strand transfer. Nature **464:**232-236.

55. **Li X, Krishnan L, Cherepanov P, Engelman A.** 2011. Structural biology of retroviral DNA integration. Virology **411:**194-205.

56. **Krishnan L, Engelman A.** 2012. Retroviral integrase proteins and HIV-1 DNA integration. J Biol Chem **287:**40858-40866.

57. **Li L, Olvera JM, Yoder KE, Mitchell RS, Butler SL, Lieber M, Martin SL, Bushman FD.** 2001. Role of the non-homologous DNA end joining pathway in the early steps of retroviral infection. EMBO J **20:**3272-3281.

58. **Ruelas DS, Greene WC.** 2013. An integrated overview of HIV-1 latency. Cell **155:**519-529.

59. **Blankson JN, Persaud D, Siliciano RF.** 2002. The challenge of viral reservoirs in HIV-1 infection. Annual review of medicine **53:**557-593.

60. **McCullough J, Colf LA, Sundquist WI.** 2013. Membrane fission reactions of the mammalian ESCRT pathway. Annual review of biochemistry **82:**663-692.

61. **West AP, Jr., Scharf L, Scheid JF, Klein F, Bjorkman PJ, Nussenzweig MC.** 2014. Structural insights on the role of antibodies in HIV-1 vaccine and therapy. Cell **156:**633-648.

62. **Schiffner T, Sattentau QJ, Dorrell L.** 2013. Development of prophylactic vaccines against HIV-1. Retrovirology **10:**72.

63. **Harris RS, Hultquist JF, Evans DT.** 2012. The restriction factors of human immunodeficiency virus. J Biol Chem **287:**40875-40883.

64. **Pertel T, Hausmann S, Morger D, Zuger S, Guerra J, Lascano J, Reinhard C, Santoni FA, Uchil PD, Chatel L, Bisiaux A, Albert ML, Strambio-De-Castillia**

**C, Mothes W, Pizzato M, Grutter MG, Luban J.** 2011. TRIM5 is an innate immune sensor for the retrovirus capsid lattice. Nature **472:**361-365.

65. **Versteeg GA, Rajsbaum R, Sanchez-Aparicio MT, Maestre AM, Valdiviezo J, Shi M, Inn KS, Fernandez-Sesma A, Jung J, Garcia-Sastre A.** 2013. The E3-ligase TRIM family of proteins regulates signaling pathways triggered by innate immune pattern-recognition receptors. Immunity **38:**384-398.

66. **Kawai T, Akira S.** 2011. Regulation of innate immune signalling pathways by the tripartite motif (TRIM) family proteins. EMBO molecular medicine **3:**513-527.

67. **Nisole S, Stoye JP, Saib A.** 2005. TRIM family proteins: retroviral restriction and antiviral defence. Nat Rev Microbiol **3:**799-808.

68. **Daugherty MD, Malik HS.** 2012. Rules of engagement: molecular insights from host-virus arms races. Annual review of genetics **46:**677-700.

69. **Best S, Le Tissier P, Towers G, Stoye JP.** 1996. Positional cloning of the mouse retrovirus restriction gene Fv1. Nature **382:**826-829.

70. **Lilly F.** 1967. Susceptibility to two strains of Friend leukemia virus in mice. Science **155:**461-462.

71. **Pincus T, Rowe WP, Lilly F.** 1971. A major genetic locus affecting resistance to infection with murine leukemia viruses. II. Apparent identity to a major locus described for resistance to friend murine leukemia virus. The Journal of experimental medicine **133:**1234-1241.

72. **Stremlau M, Owens CM, Perron MJ, Kiessling M, Autissier P, Sodroski J.** 2004. The cytoplasmic body component TRIM5alpha restricts HIV-1 infection in Old World monkeys. Nature **427:**848-853.

73. **Cowan S, Hatziioannou T, Cunningham T, Muesing MA, Gottlinger HG, Bieniasz PD.** 2002. Cellular inhibitors with Fv1-like activity restrict human and simian immunodeficiency virus tropism. Proc Natl Acad Sci U S A **99:**11914-11919.

74. **Hatziioannou T, Perez-Caballero D, Yang A, Cowan S, Bieniasz PD.** 2004. Retrovirus resistance factors Ref1 and Lv1 are species-specific variants of TRIM5alpha. Proc Natl Acad Sci U S A **101:**10774-10779.

75. **Keckesova Z, Ylinen LM, Towers GJ.** 2004. The human and African green monkey TRIM5alpha genes encode Ref1 and Lv1 retroviral restriction factor activities. Proc Natl Acad Sci U S A **101:**10780-10785.

76. **Sayah DM, Sokolskaja E, Berthoux L, Luban J.** 2004. Cyclophilin A retrotransposition into TRIM5 explains owl monkey resistance to HIV-1. Nature **430:**569-573.

77. **Newman RM, Hall L, Kirmaier A, Pozzi LA, Pery E, Farzan M, O'Neil SP, Johnson W.** 2008. Evolution of a TRIM5-CypA splice isoform in old world monkeys. PLoS Pathog **4:**e1000003.

78. **Virgen CA, Kratovac Z, Bieniasz PD, Hatziioannou T.** 2008. Independent genesis of chimeric TRIM5-cyclophilin proteins in two primate species. Proc Natl Acad Sci U S A **105:**3563-3568.

79. **Wilson SJ, Webb BL, Ylinen LM, Verschoor E, Heeney JL, Towers GJ.** 2008. Independent evolution of an antiviral TRIMCyp in rhesus macaques. Proc Natl Acad Sci U S A **105:**3557-3562.

80. **Brennan G, Kozyrev Y, Hu SL.** 2008. TRIMCyp expression in Old World primates Macaca nemestrina and Macaca fascicularis. Proc Natl Acad Sci U S A **105:**3569-3574.

81. **Nisole S, Lynch C, Stoye JP, Yap MW.** 2004. A Trim5-cyclophilin A fusion protein found in owl monkey kidney cells can restrict HIV-1. Proc Natl Acad Sci U S A **101:**13324-13328.

82. **Hofmann W, Schubert D, LaBonte J, Munson L, Gibson S, Scammell J, Ferrigno P, Sodroski J.** 1999. Species-specific, postentry barriers to primate immunodeficiency virus infection. J Virol **73:**10020-10028.

83. **Sheehy AM, Gaddis NC, Choi JD, Malim MH.** 2002. Isolation of a human gene that inhibits HIV-1 infection and is suppressed by the viral Vif protein. Nature **418:**646-650.

84. **Laguette N, Sobhian B, Casartelli N, Ringeard M, Chable-Bessia C, Segeral E, Yatim A, Emiliani S, Schwartz O, Benkirane M.** 2011. SAMHD1 is the dendritic- and myeloid-cell-specific HIV-1 restriction factor counteracted by Vpx. Nature **474:**654-657.

85. **Hrecka K, Hao C, Gierszewska M, Swanson SK, Kesik-Brodacka M, Srivastava S, Florens L, Washburn MP, Skowronski J.** 2011. Vpx relieves inhibition of HIV-1 infection of macrophages mediated by the SAMHD1 protein. Nature **474:**658-661.

86. **Goldstone DC, Ennis-Adeniran V, Hedden JJ, Groom HC, Rice GI, Christodoulou E, Walker PA, Kelly G, Haire LF, Yap MW, de Carvalho LP, Stoye JP, Crow YJ, Taylor IA, Webb M.** 2011. HIV-1 restriction factor

SAMHD1 is a deoxynucleoside triphosphate triphosphohydrolase. Nature **480:**379-382.

87. **Goujon C, Moncorge O, Bauby H, Doyle T, Ward CC, Schaller T, Hue S, Barclay WS, Schulz R, Malim MH.** 2013. Human MX2 is an interferon-induced post-entry inhibitor of HIV-1 infection. Nature **502:**559-562.

88. **Liu Z, Pan Q, Ding S, Qian J, Xu F, Zhou J, Cen S, Guo F, Liang C.** 2013. The interferon-inducible MxB protein inhibits HIV-1 infection. Cell host & microbe **14:**398-410.

89. **Kane M, Yadav SS, Bitzegeio J, Kutluay SB, Zang T, Wilson SJ, Schoggins JW, Rice CM, Yamashita M, Hatziioannou T, Bieniasz PD.** 2013. MX2 is an interferon-induced inhibitor of HIV-1 infection. Nature **502:**563-566.

90. **Teich NM, Weiss RA, Martin GR, Lowy DR.** 1977. Virus infection of murine teratocarcinoma stem cell lines. Cell **12:**973-982.

91. **Wolf D, Goff SP.** 2007. TRIM28 mediates primer binding site-targeted silencing of murine leukemia virus in embryonic cells. Cell **131:**46-57.

92. **Gao G, Guo X, Goff SP.** 2002. Inhibition of retroviral RNA production by ZAP, a CCCH-type zinc finger protein. Science **297:**1703-1706.

93. **Guo X, Ma J, Sun J, Gao G.** 2007. The zinc-finger antiviral protein recruits the RNA processing exosome to degrade the target mRNA. Proc Natl Acad Sci U S A **104:**151-156.

94. **Guo X, Carroll JW, Macdonald MR, Goff SP, Gao G.** 2004. The zinc finger antiviral protein directly binds to specific viral mRNAs through the CCCH zinc finger motifs. J Virol **78:**12781-12787.

95. **Li M, Kao E, Gao X, Sandig H, Limmer K, Pavon-Eternod M, Jones TE, Landry S, Pan T, Weitzman MD, David M.** 2012. Codon-usage-based inhibition of HIV protein synthesis by human schlafen 11. Nature **491:**125-128.

96. **Neil SJ, Zang T, Bieniasz PD.** 2008. Tetherin inhibits retrovirus release and is antagonized by HIV-1 Vpu. Nature **451:**425-430.

97. **Van Damme N, Goff D, Katsura C, Jorgenson RL, Mitchell R, Johnson MC, Stephens EB, Guatelli J.** 2008. The interferon-induced protein BST-2 restricts HIV-1 release and is downregulated from the cell surface by the viral Vpu protein. Cell host & microbe **3:**245-252.

98. **Neil SJ, Sandrin V, Sundquist WI, Bieniasz PD.** 2007. An interferon-alpha-induced tethering mechanism inhibits HIV-1 and Ebola virus particle release but is counteracted by the HIV-1 Vpu protein. Cell host & microbe **2:**193-203.

99. **Meyerson NR, Rowley PA, Swan CH, Le DT, Wilkerson GK, Sawyer SL.** 2014. Positive selection of primate genes that promote HIV-1 replication. Virology **454-455:**291-298.

100. **Desimmie BA, Delviks-Frankenberrry KA, Burdick RC, Qi D, Izumi T, Pathak VK.** 2014. Multiple APOBEC3 restriction factors for HIV-1 and one Vif to rule them all. J Mol Biol **426:**1220-1245.

101. **Compton AA, Hirsch VM, Emerman M.** 2012. The host restriction factor APOBEC3G and retroviral Vif protein coevolve due to ongoing genetic conflict. Cell host & microbe **11:**91-98.

102. **Laguette N, Rahm N, Sobhian B, Chable-Bessia C, Munch J, Snoeck J, Sauter D, Switzer WM, Heneine W, Kirchhoff F, Delsuc F, Telenti A, Benkirane M.** 2012. Evolutionary and functional analyses of the interaction between the myeloid restriction factor SAMHD1 and the lentiviral Vpx protein. Cell host & microbe **11:**205-217.

103. **Lim ES, Malik HS, Emerman M.** 2010. Ancient adaptive evolution of tetherin shaped the functions of Vpu and Nef in human immunodeficiency virus and primate lentiviruses. J Virol **84:**7124-7134.

104. **Lim ES, Fregoso OI, McCoy CO, Matsen FA, Malik HS, Emerman M.** 2012. The ability of primate lentiviruses to degrade the monocyte restriction factor SAMHD1 preceded the birth of the viral accessory protein Vpx. Cell host & microbe **11:**194-204.

105. **Sawyer SL, Emerman M, Malik HS.** 2004. Ancient adaptive evolution of the primate antiviral DNA-editing enzyme APOBEC3G. PLoS biology **2:**E275.

106. **Sawyer SL, Wu LI, Emerman M, Malik HS.** 2005. Positive selection of primate TRIM5alpha identifies a critical species-specific retroviral restriction domain. Proc Natl Acad Sci U S A **102:**2832-2837.

107. **Huthoff H, Towers GJ.** 2008. Restriction of retroviral replication by APOBEC3G/F and TRIM5alpha. Trends in microbiology **16:**612-619.

108. **Bishop KN, Holmes RK, Sheehy AM, Davidson NO, Cho SJ, Malim MH.** 2004. Cytidine deamination of retroviral DNA by diverse APOBEC proteins. Current biology : CB **14:**1392-1396.

109. **Zhang F, Wilson SJ, Landford WC, Virgen B, Gregory D, Johnson MC, Munch J, Kirchhoff F, Bieniasz PD, Hatziioannou T.** 2009. Nef proteins from simian immunodeficiency viruses are tetherin antagonists. Cell host & microbe **6:**54-67.

110. **Nikovics K, Dazza MC, Ekwalanga M, Mammano F, Clavel F, Saragosti S.** 2012. Counteraction of tetherin antiviral activity by two closely related SIVs differing by the presence of a Vpu gene. PloS one **7:**e35411.

111. **Sauter D, Schindler M, Specht A, Landford WN, Munch J, Kim KA, Votteler J, Schubert U, Bibollet-Ruche F, Keele BF, Takehisa J, Ogando Y, Ochsenbauer C, Kappes JC, Ayouba A, Peeters M, Learn GH, Shaw G, Sharp PM, Bieniasz P, Hahn BH, Hatziioannou T, Kirchhoff F.** 2009. Tetherin-driven adaptation of Vpu and Nef function and the evolution of pandemic and nonpandemic HIV-1 strains. Cell host & microbe **6:**409-421.

112. **Perez-Caballero D, Soll SJ, Bieniasz PD.** 2008. Evidence for restriction of ancient primate gammaretroviruses by APOBEC3 but not TRIM5alpha proteins. PLoS Pathog **4:**e1000181.

113. **Lee YN, Bieniasz PD.** 2007. Reconstitution of an infectious human endogenous retrovirus. PLoS Pathog **3:**e10.

114. **Kaiser SM, Malik HS, Emerman M.** 2007. Restriction of an extinct retrovirus by the human TRIM5alpha antiviral protein. Science **316:**1756-1758.

115. **Sloan RD, Wainberg MA.** 2013. Harnessing the therapeutic potential of host antiviral restriction factors that target HIV. Expert review of anti-infective therapy **11:**1-4.

116. **Shankar EM, Velu V, Vignesh R, Vijayaraghavalu S, Rukumani DV, Sabet NS.** 2012. Recent advances targeting innate immunity-mediated therapies against HIV-1 infection. Microbiology and immunology **56:**497-505.

117. **Ellegard R, Shankar EM, Larsson M.** 2011. Targeting HIV-1 innate immune responses therapeutically. Curr Opin HIV AIDS **6:**435-443.

118. **Zuo T, Liu D, Lv W, Wang X, Wang J, Lv M, Huang W, Wu J, Zhang H, Jin H, Zhang L, Kong W, Yu X.** 2012. Small-molecule inhibition of human immunodeficiency virus type 1 replication by targeting the interaction between Vif and ElonginC. J Virol **86:**5497-5507.

119. **Nathans R, Cao H, Sharova N, Ali A, Sharkey M, Stranska R, Stevenson M, Rana TM.** 2008. Small-molecule inhibition of HIV-1 Vif. Nature biotechnology **26:**1187-1192.

120. **Matsui M, Shindo K, Izumi T, Io K, Shinohara M, Komano J, Kobayashi M, Kadowaki N, Harris RS, Takaori-Kondo A.** 2014. Small molecules that inhibit Vif-induced degradation of APOBEC3G. Virology journal **11:**122.

121. **Cen S, Peng ZG, Li XY, Li ZR, Ma J, Wang YM, Fan B, You XF, Wang YP, Liu F, Shao RG, Zhao LX, Yu L, Jiang JD.** 2010. Small molecular compounds inhibit HIV-1 replication through specifically stabilizing APOBEC3G. J Biol Chem **285:**16546-16552.

122. **Li M, Shandilya SM, Carpenter MA, Rathore A, Brown WL, Perkins AL, Harki DA, Solberg J, Hook DJ, Pandey KK, Parniak MA, Johnson JR, Krogan NJ, Somasundaran M, Ali A, Schiffer CA, Harris RS.** 2012. First-in-class small molecule inhibitors of the single-strand DNA cytosine deaminase APOBEC3G. ACS chemical biology **7:**506-517.

123. **Sadler HA, Stenglein MD, Harris RS, Mansky LM.** 2010. APOBEC3G contributes to HIV-1 variation through sublethal mutagenesis. J Virol **84:**7396-7404.

124. **Berkhout B, de Ronde A.** 2004. APOBEC3G versus reverse transcriptase in the generation of HIV-1 drug-resistance mutations. Aids **18:**1861-1863.

125. **van der Aa LM, Levraud JP, Yahmi M, Lauret E, Briolat V, Herbomel P, Benmansour A, Boudinot P.** 2009. A large new subset of TRIM genes highly diversified by duplication and positive selection in teleost fish. BMC biology **7:**7.

126. **Tareen SU, Sawyer SL, Malik HS, Emerman M.** 2009. An expanded clade of rodent Trim5 genes. Virology **385:**473-483.

127. **Si Z, Vandegraaff N, O'Huigin C, Song B, Yuan W, Xu C, Perron M, Li X, Marasco WA, Engelman A, Dean M, Sodroski J.** 2006. Evolution of a cytoplasmic tripartite motif (TRIM) protein in cows that restricts retroviral infection. Proc Natl Acad Sci U S A **103:**7454-7459.

128. **Schaller T, Hue S, Towers GJ.** 2007. An active TRIM5 protein in rabbits indicates a common antiviral ancestor for mammalian TRIM5 proteins. J Virol **81:**11713-11721.

129. **Sawyer SL, Emerman M, Malik HS.** 2007. Discordant evolution of the adjacent antiretroviral genes TRIM22 and TRIM5 in mammals. PLoS Pathog **3:**e197.

130. **Johnson WE, Sawyer SL.** 2009. Molecular evolution of the antiretroviral TRIM5 gene. Immunogenetics **61:**163-176.

131. **Han K, Lou DI, Sawyer SL.** 2011. Identification of a genomic reservoir for new TRIM genes in primate genomes. PLoS genetics **7:**e1002388.

132. **Boudinot P, van der Aa LM, Jouneau L, Du Pasquier L, Pontarotti P, Briolat V, Benmansour A, Levraud JP.** 2011. Origin and evolution of TRIM proteins: new insights from the complete TRIM repertoire of zebrafish and pufferfish. PloS one **6:**e22022.

133. **Sardiello M, Cairo S, Fontanella B, Ballabio A, Meroni G.** 2008. Genomic analysis of the TRIM family reveals two groups of genes with distinct evolutionary properties. BMC evolutionary biology **8:**225.

134. **Rahm N, Telenti A.** 2012. The role of tripartite motif family members in mediating susceptibility to HIV-1 infection. Curr Opin HIV AIDS **7:**180-186.

135. **Short KM, Cox TC.** 2006. Subclassification of the RBCC/TRIM superfamily reveals a novel motif necessary for microtubule binding. J Biol Chem **281:**8970-8980.

136. **Ozato K, Shin DM, Chang TH, Morse HC, 3rd.** 2008. TRIM family proteins and their emerging roles in innate immunity. Nature reviews. Immunology **8:**849-860.

137. **Malfavon-Borja R, Sawyer SL, Wu LI, Emerman M, Malik HS.** 2013. An evolutionary screen highlights canonical and noncanonical candidate antiviral genes within the primate TRIM gene family. Genome biology and evolution **5:**2141-2154.

138. **Carthagena L, Bergamaschi A, Luna JM, David A, Uchil PD, Margottin-Goguet F, Mothes W, Hazan U, Transy C, Pancino G, Nisole S.** 2009. Human TRIM gene expression in response to interferons. PloS one **4:**e4894.

139. **Uchil PD, Quinlan BD, Chan WT, Luna JM, Mothes W.** 2008. TRIM E3 ligases interfere with early and late stages of the retroviral life cycle. PLoS Pathog **4:**e16.

140. **Uchil PD, Hinz A, Siegel S, Coenen-Stass A, Pertel T, Luban J, Mothes W.** 2013. TRIM protein-mediated regulation of inflammatory and innate immune signaling and its association with antiretroviral activity. J Virol **87:**257-272.

141. **Fletcher AJ, Towers GJ.** 2013. Inhibition of retroviral replication by members of the TRIM protein family. Current topics in microbiology and immunology **371:**29-66.

142. **Wolf D, Goff SP.** 2009. Embryonic stem cells use ZFP809 to silence retroviral DNAs. Nature **458:**1201-1204.

143. **Besnier C, Takeuchi Y, Towers G.** 2002. Restriction of lentivirus in monkeys. Proc Natl Acad Sci U S A **99:**11920-11925.

144. **Perron MJ, Stremlau M, Song B, Ulm W, Mulligan RC, Sodroski J.** 2004. TRIM5alpha mediates the postentry block to N-tropic murine leukemia viruses in human cells. Proc Natl Acad Sci U S A **101:**11827-11832.

145. **Stremlau M, Perron M, Lee M, Li Y, Song B, Javanbakht H, Diaz-Griffero F, Anderson DJ, Sundquist WI, Sodroski J.** 2006. Specific recognition and accelerated uncoating of retroviral capsids by the TRIM5alpha restriction factor. Proc Natl Acad Sci U S A **103:**5514-5519.

146. **Li Y, Kar AK, Sodroski J.** 2009. Target cell type-dependent modulation of human immunodeficiency virus type 1 capsid disassembly by cyclophilin A. J Virol **83:**10951-10962.

147. **Di Nunzio F, Danckaert A, Fricke T, Perez P, Fernandez J, Perret E, Roux P, Shorte S, Charneau P, Diaz-Griffero F, Arhel NJ.** 2012. Human nucleoporins promote HIV-1 docking at the nuclear pore, nuclear import and integration. PloS one **7:**e46037.

148. **Reymond A, Meroni G, Fantozzi A, Merla G, Cairo S, Luzi L, Riganelli D, Zanaria E, Messali S, Cainarca S, Guffanti A, Minucci S, Pelicci PG, Ballabio A.** 2001. The tripartite motif family identifies cell compartments. EMBO J **20:**2140-2151.

149. **Mische CC, Javanbakht H, Song B, Diaz-Griffero F, Stremlau M, Strack B, Si Z, Sodroski J.** 2005. Retroviral restriction factor TRIM5alpha is a trimer. J Virol **79:**14446-14450.

150. **Rhodes DA, Trowsdale J.** 2007. TRIM21 is a trimeric protein that binds IgG Fc via the B30.2 domain. Molecular immunology **44:**2406-2414.

151. **Kar AK, Diaz-Griffero F, Li Y, Li X, Sodroski J.** 2008. Biochemical and Biophysical Characterization of a Chimeric TRIM21-TRIM5alpha Protein. J Virol.

152. **Langelier CR, Sandrin V, Eckert DM, Christensen DE, Chandrasekaran V, Alam SL, Aiken C, Olsen JC, Kar AK, Sodroski JG, Sundquist WI.** 2008. Biochemical characterization of a recombinant TRIM5alpha protein that restricts human immunodeficiency virus type 1 replication. J Virol **82:**11682-11694.

153. **Sanchez JG, Okreglicka K, Chandrasekaran V, Welker JM, Sundquist WI, Pornillos O.** 2014. The tripartite motif coiled-coil is an elongated antiparallel hairpin dimer. Proc Natl Acad Sci U S A **111:**2494-2499.

154. **Ganser-Pornillos BK, Chandrasekaran V, Pornillos O, Sodroski JG, Sundquist WI, Yeager M.** 2011. Hexagonal assembly of a restricting TRIM5alpha protein. Proc Natl Acad Sci U S A **108:**534-539.

155. **Doyle JM, Gao J, Wang J, Yang M, Potts PR.** 2010. MAGE-RING protein complexes comprise a family of E3 ubiquitin ligases. Molecular cell **39:**963-974.

156. **Chu Y, Yang X.** 2011. SUMO E3 ligase activity of TRIM proteins. Oncogene **30:**1108-1116.

157. **Borden KL, Freemont PS.** 1996. The RING finger domain: a recent example of a sequence-structure family. Curr Opin Struct Biol **6:**395-401.

158. **Liew CW, Sun H, Hunter T, Day CL.** 2010. RING domain dimerization is essential for RNF4 function. The Biochemical journal **431:**23-29.

159. **Brzovic PS, Rajagopal P, Hoyt DW, King MC, Klevit RE.** 2001. Structure of a BRCA1-BARD1 heterodimeric RING-RING complex. Nat Struct Biol **8:**833-837.

160. **Borden KL.** 1998. RING fingers and B-boxes: zinc-binding protein-protein interaction domains. Biochemistry and cell biology = Biochimie et biologie cellulaire **76:**351-358.

161. **Tao H, Simmons BN, Singireddy S, Jakkidi M, Short KM, Cox TC, Massiah MA.** 2008. Structure of the MID1 tandem B-boxes reveals an interaction reminiscent of intermolecular ring heterodimers. Biochemistry **47:**2450-2457.

162. **Li X, Sodroski J.** 2008. The TRIM5{alpha} B-box 2 Domain Promotes Cooperative Binding to the Retroviral Capsid by Mediating Higher-order Self-association. J Virol.

163. **Diaz-Griffero F, Qin XR, Hayashi F, Kigawa T, Finzi A, Sarnak Z, Lienlaf M, Yokoyama S, Sodroski J.** 2009. A B-box 2 surface patch important for TRIM5alpha self-association, capsid binding avidity, and retrovirus restriction. J Virol **83:**10737-10751.

164. **Perez-Caballero D, Hatziioannou T, Yang A, Cowan S, Bieniasz PD.** 2005. Human tripartite motif 5alpha domains responsible for retrovirus restriction activity and specificity. J Virol **79:**8969-8978.

165. **Stremlau M, Perron M, Welikala S, Sodroski J.** 2005. Species-specific variation in the B30.2(SPRY) domain of TRIM5alpha determines the potency of human immunodeficiency virus restriction. J Virol **79:**3139-3145.

166. **Caines ME, Bichel K, Price AJ, McEwan WA, Towers GJ, Willett BJ, Freund SM, James LC.** 2012. Diverse HIV viruses are targeted by a conformationally dynamic antiviral. Nature structural & molecular biology **19:**411-416.

167. **Ylinen LM, Price AJ, Rasaiyaah J, Hue S, Rose NJ, Marzetta F, James LC, Towers GJ.** 2010. Conformational adaptation of Asian macaque TRIMCyp directs lineage specific antiviral activity. PLoS Pathog **6:**e1001062.

168. **Price AJ, Marzetta F, Lammers M, Ylinen LM, Schaller T, Wilson SJ, Towers GJ, James LC.** 2009. Active site remodeling switches HIV specificity of antiretroviral TRIMCyp. Nature structural & molecular biology **16:**1036-1042.

169. **Yap MW, Nisole S, Stoye JP.** 2005. A single amino acid change in the SPRY domain of human Trim5alpha leads to HIV-1 restriction. Current biology : CB **15:**73-78.

170. **Li Y, Li X, Stremlau M, Lee M, Sodroski J.** 2006. Removal of arginine 332 allows human TRIM5alpha to bind human immunodeficiency virus capsids and to restrict infection. J Virol **80:**6738-6744.

171. **Hatziioannou T, Cowan S, Goff SP, Bieniasz PD, Towers GJ.** 2003. Restriction of multiple divergent retroviruses by Lv1 and Ref1. EMBO J **22:**385-394.

172. **Sebastian S, Luban J.** 2005. TRIM5alpha selectively binds a restriction-sensitive retroviral capsid. Retrovirology **2:**40.

173. **Campbell EM, Perez O, Anderson JL, Hope TJ.** 2008. Visualization of a proteasome-independent intermediate during restriction of HIV-1 by rhesus TRIM5alpha. J Cell Biol **180:**549-561.

174. **Yoo S, Myszka DG, Yeh C, McMurray M, Hill CP, Sundquist WI.** 1997. Molecular recognition in the HIV-1 capsid/cyclophilin A complex. J Mol Biol **269:**780-795.

175. **Diaz-Griffero F, Kar A, Lee M, Stremlau M, Poeschla E, Sodroski J.** 2007. Comparative requirements for the restriction of retrovirus infection by TRIM5alpha and TRIMCyp. Virology **369:**400-410.

176. **Li X, Song B, Xiang SH, Sodroski J.** 2007. Functional interplay between the B-box 2 and the B30.2(SPRY) domains of TRIM5alpha. Virology **366:**234-244.

177. **Forshey BM, von Schwedler U, Sundquist WI, Aiken C.** 2002. Formation of a human immunodeficiency virus type 1 core of optimal stability is crucial for viral replication. J Virol **76:**5667-5677.

178. **Roa A, Hayashi F, Yang Y, Lienlaf M, Zhou J, Shi J, Watanabe S, Kigawa T, Yokoyama S, Aiken C, Diaz-Griffero F.** 2012. RING domain mutations uncouple TRIM5alpha restriction of HIV-1 from inhibition of reverse transcription and acceleration of uncoating. J Virol **86:**1717-1727.

179. **Javanbakht H, Diaz-Griffero F, Yuan W, Yeung DF, Li X, Song B, Sodroski J.** 2007. The ability of multimerized cyclophilin A to restrict retrovirus infection. Virology **367:**19-29.

180. **Yap MW, Mortuza GB, Taylor IA, Stoye JP.** 2007. The design of artificial retroviral restriction factors. Virology **365:**302-314.

181. **Fang S, Weissman AM.** 2004. A field guide to ubiquitylation. Cellular and molecular life sciences : CMLS **61:**1546-1561.

182. **VanDemark AP, Hill CP.** 2002. Structural basis of ubiquitylation. Curr Opin Struct Biol **12:**822-830.

183. **Mandell MA, Jain A, Arko-Mensah J, Chauhan S, Kimura T, Dinkins C, Silvestri G, Munch J, Kirchhoff F, Simonsen A, Wei Y, Levine B, Johansen T, Deretic V.** 2014. TRIM Proteins Regulate Autophagy and Can Target Autophagic Substrates by Direct Recognition. Developmental cell **30:**394-409.

184. **O'Connor C, Pertel T, Gray S, Robia SL, Bakowska JC, Luban J, Campbell EM.** 2010. p62/sequestosome-1 associates with and sustains the expression of retroviral restriction factor TRIM5alpha. J Virol **84:**5997-6006.

185. **Moscat J, Diaz-Meco MT, Wooten MW.** 2009. Of the atypical PKCs, Par-4 and p62: recent understandings of the biology and pathology of a PB1-dominated complex. Cell death and differentiation **16:**1426-1437.

186. **Seibenhener ML, Babu JR, Geetha T, Wong HC, Krishna NR, Wooten MW.** 2004. Sequestosome 1/p62 is a polyubiquitin chain binding protein involved in ubiquitin proteasome degradation. Molecular and cellular biology **24:**8055-8068.

187. **Zhang F, Hatziioannou T, Perez-Caballero D, Derse D, Bieniasz PD.** 2006. Antiretroviral potential of human tripartite motif-5 and related proteins. Virology **353:**396-409.

188. **Chan E, Towers GJ, Qasim W.** 2014. Gene therapy strategies to exploit TRIM derived restriction factors against HIV-1. Viruses **6:**243-263.

189. **Wongsrikeao P, Saenz D, Rinkoski T, Otoi T, Poeschla E.** 2011. Antiviral restriction factor transgenesis in the domestic cat. Nature methods **8:**853-859.

190. **Shi J, Zhou J, Shah VB, Aiken C, Whitby K.** 2011. Small-molecule inhibition of human immunodeficiency virus type 1 infection by virus capsid destabilization. J Virol **85:**542-549.

191. **Tan X, Calderon-Villalobos LI, Sharon M, Zheng C, Robinson CV, Estelle M, Zheng N.** 2007. Mechanism of auxin perception by the TIR1 ubiquitin ligase. Nature **446:**640-645.

192. **Rajsbaum R, Garcia-Sastre A, Versteeg GA.** 2014. TRIMmunity: the roles of the TRIM E3-ubiquitin ligase family in innate antiviral immunity. J Mol Biol **426:**1265-1284.

193. **Grutter MG, Luban J.** 2012. TRIM5 structure, HIV-1 capsid recognition, and innate immune signaling. Current opinion in virology **2:**142-150.

194. **Diaz-Griffero F, Li X, Javanbakht H, Song B, Welikala S, Stremlau M, Sodroski J.** 2006. Rapid turnover and polyubiquitylation of the retroviral restriction factor TRIM5. Virology **349:**300-315.

# CHAPTER 2

# HEXAGONAL ASSEMBLY OF A RESTRICTING TRIM5ALPHA PROTEIN

Barbie K. Ganser-Pornillos, Viswanathan Chandrasekaran, Owen Pornillos, Joseph G. Sodroski, Wesley I. Sundquist, and Mark Yeager

Reprinted with permission from PNAS 108(2), 534-539.

# Hexagonal assembly of a restricting TRIM5α protein

Barbie K. Ganser-Pornillos[a,b,1], Viswanathan Chandrasekaran[c,1], Owen Pornillos[a,b], Joseph G. Sodroski[d], Wesley I. Sundquist[c,2], and Mark Yeager[a,b,e,2]

[a]Department of Molecular Physiology and Biological Physics, University of Virginia School of Medicine, Charlottesville, VA 22908; [b]Department of Cell Biology, The Scripps Research Institute, La Jolla, CA 92037; [e]Division of Cardiovascular Medicine, Department of Medicine, University of Virginia Health System, Charlottesville, VA 22908; [c]Department of Biochemistry, University of Utah, Salt Lake City, UT 84112; and [d]Department of Cancer Immunology and AIDS, Dana-Farber Cancer Institute, and Division of AIDS, Harvard Medical School, Boston, MA 02115

Edited by Stephen P. Goff, Columbia University College of Physicians and Surgeons, New York, NY, and approved November 23, 2010 (received for review September 9, 2010)

**TRIM5α proteins are restriction factors that protect mammalian cells from retroviral infections by binding incoming viral capsids, accelerating their dissociation, and preventing reverse transcription of the viral genome. Individual TRIM5 isoforms can often protect cells against a broad range of retroviruses, as exemplified by rhesus monkey TRIM5α and its variant, TRIM5-21R, which recognize HIV-1 as well as several distantly related retroviruses. Although capsid recognition is not yet fully understood, previous work has shown that the C-terminal SPRY/B30.2 domain of dimeric TRIM5α binds directly to viral capsids, and that higher-order TRIM5α oligomerization appears to contribute to the efficiency of capsid recognition. Here, we report that recombinant TRIM5-21R spontaneously assembled into two-dimensional paracrystalline hexagonal lattices comprising open, six-sided rings. TRIM5-21R assembly did not require the C-terminal SPRY domain, but did require both protein dimerization and a B-box 2 residue (Arg121) previously implicated in TRIM5α restriction and higher-order assembly. Furthermore, TRIM5-21R assembly was promoted by binding to hexagonal arrays of the HIV-1 CA protein that mimic the surface of the viral capsid. We therefore propose that TRIM5α proteins have evolved to restrict a range of different retroviruses by assembling a deformable hexagonal scaffold that positions the capsid-binding domains to match the symmetry and spacing of the capsid surface lattice. Capsid recognition therefore involves a synergistic combination of direct binding interactions, avidity effects, templated assembly, and lattice complementarity.**

electron microscopy | HIV-1 capsid | lattice complementarity | retroviral restriction | two-dimensional crystal

The susceptibility of mammals to retroviral infections is restricted by innate immunity factors that protect the host and limit retroviral tropism. One such restriction factor, TRIM5α, can block replication of HIV-1 and other retroviruses at the postentry stage and prevent accumulation of viral reverse transcripts (1–4). As illustrated in Fig. 1, TRIM5α proteins comprise four domains: an N-terminal RING domain that functions as a ubiquitin E3 ligase (5 kDa), a B-box 2 domain required for restriction and higher-order assembly (5 kDa), a dimerization region predicted to form a coiled-coil(s) (13 kDa), and a C-terminal SPRY/B30.2 domain that contacts retroviral capsids (22 kDa). The RING/B-box 2 and coiled-coil/SPRY domains are separated by linker regions, termed L1 and L2, respectively.

Retroviral capsids can vary in shape, but in all cases comprise CA protein hexamers and pentamers, with a conserved interhexamer lattice spacing of ~90 Å [reviewed in (5)]. For example, HIV-1 capsids are closed fullerene cones composed of ~250 CA hexamers and 12 pentamers (6, 7), whereas other retroviral capsids form cylinders, spheres, or polyhedra (8, 9). In addition to variations in capsid morphology, CA proteins can also vary substantially in primary sequence. Nevertheless, individual TRIM5α proteins can often recognize and restrict a variety of different retroviruses (3, 10–12 and references therein), as exemplified by rhesus monkey TRIM5α, which restricts HIV-1, as well as several distantly related retroviruses. These observations raise the question of how a diverse collection of retroviral capsids can be recognized by a single protein. This issue is of particular importance for understanding viral tropism because the ability of different TRIM5α alleles to restrict specific retroviruses is typically dictated at the level of capsid recognition.

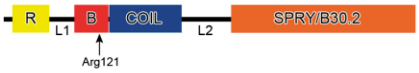


**Fig. 1.** Schematic representation of the rhesus monkey TRIM5α protein. The four principal domains are illustrated as colored boxes: R, RING domain, yellow; B, B-box 2 domain, red; COIL, predicted coiled-coil domain, blue; SPRY/B30.2 domain, orange. The L1 and L2 linker regions are also labeled. The position of residue Arg121 within the B-box 2 domain is indicated by the arrow. In the TRIM5-21R construct used in this study, the RING domain of rhesus TRIM5α was replaced with the RING domain from human TRIM21.

Perhaps surprisingly, TRIM5α proteins bind individual CA subunits very weakly, if at all (4). Instead, robust binding is only observed when CA is assembled into hexagonal lattices that mimic the surfaces of retroviral capsids (2, 13–16), indicating that TRIM5α recognizes epitopes that are formed when CA assembles and/or that TRIM5α recognizes a repeating pattern of epitopes on the capsid surface. Consistent with the latter model, there are several reports that oligomerization of TRIM5α contributes to the efficiency of capsid recognition, implying that avidity effects probably play an important role in TRIM5α/capsid interactions. In cells, both TRIM5α dimerization and higher-order oligomerization are important for retroviral capsid binding and restriction (14, 15, 17–21). Dimerization of TRIM5α enhances binding to capsid mimics in vitro (15) and requires the putative coiled-coil domain (18, 22–24). Higher-order oligomerization is dependent on a hydrophobic patch on the surface of the B-box 2 domain (21, 25) and a region located immediately downstream of the predicted coiled-coil domain (residues 263–278) (26). How these elements contribute to capsid binding has not yet been examined in vitro.

To learn how TRIM5 restriction factors form higher-order assemblies, we examined a recombinant TRIM5α construct, designated TRIM5-21R, in which the N-terminal RING domain of rhesus TRIM5α was replaced by the homologous RING domain from the related human TRIM21 protein. This construct was selected for study because it potently restricts HIV-1 replica-

Author contributions: B.K.G.-P., V.C., O.P., W.I.S., and M.Y. designed research; B.K.G.-P., V.C., and O.P. performed research; B.K.G.-P., V.C., O.P., J.G.S., W.I.S., and M.Y. contributed new reagents/analytic tools; B.K.G.-P., V.C., O.P., W.I.S., and M.Y. analyzed data; and B.K.G.-P., V.C., O.P., J.G.S., W.I.S., and M.Y. wrote the paper.

The authors declare no conflict of interest.

This article is a PNAS Direct Submission.

[1]B.K.G.-P. and V.C. contributed equally to this work.

[2]To whom correspondence may be addressed. E-mail: wes@biochem.utah.edu or yeager@virginia.edu.

This article contains supporting information online at www.pnas.org/lookup/suppl/doi:10.1073/pnas.1013426108/-/DCSupplemental.

tion in culture (10, 11) and can be expressed and purified more readily than wild-type TRIM5α (14, 15). Electron microscopy (EM) and biochemical studies revealed that recombinant TRIM5-21R spontaneously forms two-dimensional hexagonal arrays that are complementary in symmetry and dimensions to retroviral capsids. Moreover, assembly of TRIM5-21R was promoted by preformed two-dimensional crystals of the HIV-1 CA protein, suggesting that TRIM5α proteins employ "pattern recognition" to bind the hexagonal CA arrays found in all retroviral capsids.

## Results

**TRIM5-21R Spontaneously Assembles into Two-Dimensional Paracrystalline Hexagonal Lattices.** Negative-stain EM was used to examine TRIM5-21R assemblies formed under a range of different conditions. These experiments revealed that purified TRIM5-21R dimers spontaneously formed two-dimensional paracrystalline hexagonal arrays when incubated at low protein concentrations (~10 μM), and under moderate ionic strength conditions [20 mM Tris, pH 8, 25 mM NaCl, 1 mM tris(2-carboxyethyl)phosphine (TCEP)] (Fig. 2*A*). This hexagonal TRIM5-21R lattice was also observed in unstained samples preserved in vitreous ice (Fig. 2*B*). Although the TRIM5-21R crystals did not exhibit long-range order, image processing without imposed symmetry confirmed that the protein formed a lattice composed of six-sided rings, with inter-ring spacings of 315–355 Å (Fig. 2*A*, inset) and p3 or p6 plane-group symmetry (Table 1). Within each ring, regions of high density at the threefold and twofold symmetry axes were connected by thinner regions of weaker density (Fig. 2*C*).

**TRIM5-21R Lattice Formation Does Not Require the Capsid-Binding SPRY Domain.** Although the C-terminal SPRY/B30.2 domain of TRIM5α is required for capsid binding (2), this domain was not necessary for TRIM5-21R assembly in vitro because a truncated construct that lacked the SPRY domain (TRIM5-21R$_{1-276}$) could still form hexagonal arrays (Fig. S1). These crystals closely resembled those formed by wild-type TRIM5-21R, although the efficiency of TRIM5-21R$_{1-276}$ assembly was somewhat lower (see *Materials and Methods* for details). Thus, the RING, B-box 2, and coiled-coil domains are sufficient to form a hexagonal scaffold that displays different capsid-binding domains, including the SPRY/B30.2 of TRIM5α, as well as the cyclophilin A domains of the related TRIMCyp family of restriction factors (27–34). Notably, these three N-terminal domains are conserved across the entire TRIM/RBCC (Tripartite Motif/RING, B-box, Coiled-Coil) family of proteins. It is therefore possible that analogous scaffolds display the different recognition domains found in other TRIM family members. Indeed, higher-order assemblies have even been reported for other RING domain proteins outside of the TRIM family (35–38).

**TRIM5-21R Lattice Formation and Capsid Recognition Exhibit Similar Requirements for Coiled-Coil and B-box 2 Oligomerization.** To evaluate the biological relevance of the hexagonal TRIM5-21R assemblies, we tested whether there were common requirements for efficient TRIM5α restriction in vivo, retroviral capsid binding within cells, binding to pure recombinant HIV-1 CA, and hexagonal lattice formation. These experiments built on the observations that efficient retroviral restriction in cells requires both: (*i*) TRIM5α dimerization mediated by the putative coiled-coil motif (14, 15, 17–20), and (*ii*) higher-order assembly mediated by a hydrophobic patch in the B-box 2 domain and a key exposed arginine residue (Arg121) (21, 25). We previously used cosedimentation binding assays to show that TRIM5-21R dimerization enhances TRIM5-21R binding to helical tubes of HIV-1 CA hexamers (15). Here, we employed a similar binding assay to analyze the effect of the B-box 2 R121E mutation on TRIM5-21R binding to CA tubes in vitro. As shown in Fig. 3, pure dimeric TRIM5-21R alone did not pellet through a 70% sucrose cushion, but the protein did copellet through the cushion when bound to assembled HIV-1 CA tubes (positive control, compare lanes 1 and 4 or lanes 7 and 10). In contrast, a TRIM5-21R construct that lacked the SPRY domain failed to copellet with CA tubes, consistent with

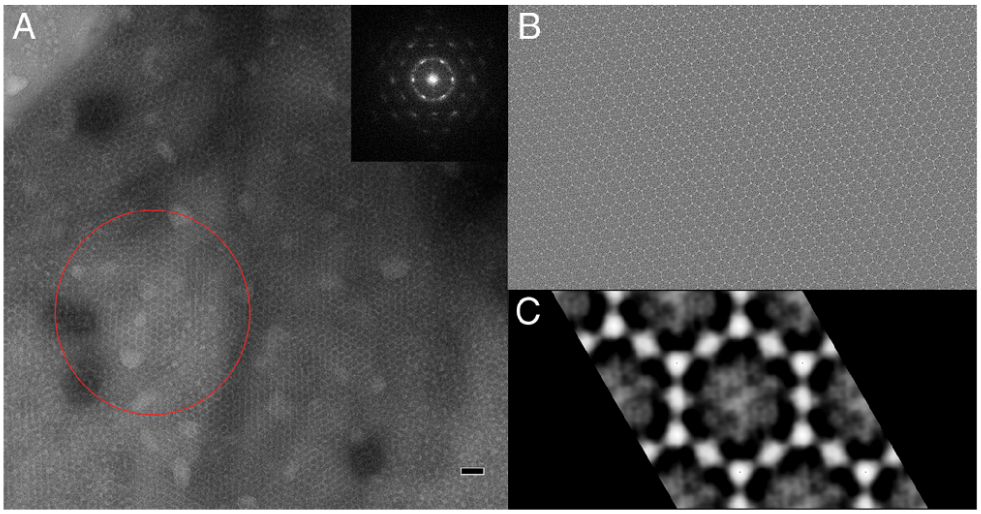


**Fig. 2.** Hexagonal assemblies of TRIM5-21R. (*A*) Representative negatively-stained EM image of a hexagonal array formed spontaneously by dimeric TRIM5-21R upon incubation on a carbon-coated grid. (Scale bar,100 nm). The red circle demarcates a region with clear hexagonal order, as shown in the computed Fourier transform (inset). (*B*) Fourier-filtered image of a TRIM5-21R array preserved in vitreous ice. (*C*) Projection density map of (*B*) shown in gray scale (with no imposed symmetry), illustrating that the hexagonal lattice is composed of six-sided rings. The unit cell parameters for the crystals are: (*A*) *a* 347 Å, *b* 335 Å, $\gamma$ 119.3°; (*B*) and (*C*) *a* 348 Å, *b* 346 Å, and $\gamma$ 120.5°.

**Table 1. Analyses of the TRIM5-21R lattices**

I. Unit cell parameters from images of 10 negatively-stained crystals

| | |
|---|---|
| *a* – *b*, Å (average/range) | 334 ± 12/310 – 353 |
| γ, ° (average) | 119.0 ± 1.4 |

II. ALLSPACE (50) analysis of the TRIM5-21R lattice shown in Fig. 2 *B* and *C*

| Candidate plane group | Residual | Target residual |
|---|---|---|
| p1 | 14.9 | |
| p2 | 14.9* | 21.2 |
| p3 | 9.4* | 14.9 |
| p312 | 10.1* | 15.2 |
| p321 | 9.4* | 15.1 |
| p6 | 10.5* | 16.2 |
| p622 | 10.3* | 15.5 |

*Most probable.

the known requirement for the SPRY domain in capsid binding (negative control, compare lanes 4 and 6 or lanes 10 and 12). In the actual experiment, the TRIM5-21R$_{R121E}$ mutant did not bind detectably to CA tubes when the binding reactions were performed at low protein concentrations (0.5 μM TRIM5-21R proteins and 3 μM CA subunits, compare lanes 4 and 5). However, attenuated capsid binding by TRIM5-21R$_{R121E}$ was detected when the binding reaction was performed at higher protein concentrations (1 μM TRIM5-21R proteins and 6 μM CA subunits, compare lanes 10 and 11). Thus, TRIM5-21R$_{R121E}$ retained some CA binding activity, presumably because the B-box 2 mutation did not affect the integrity of the SPRY binding domain, but the mutation reduced binding efficiency. These observations are consistent with the idea that higher-order TRIM5-21R assembly contributes to the avidity of capsid binding.

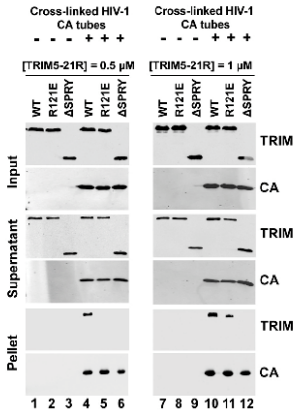


**Fig. 3.** TRIM5-21R binding to helical tubes of cysteine-crosslinked HIV-1 CA hexamers requires the SPRY domain and is enhanced by B-box 2 domain interactions. TRIM5-21R proteins were incubated in the absence of CA (lanes 1–3 and 7–9) or in the presence of a 6-fold molar excess of CA subunits assembled into helical tubes that mimic the hexagonal capsid lattice (lanes 4–6 and 10–12). Binding experiments were performed at two different TRIM5-21R protein concentrations (0.5 μM, lanes 1–6 or 1 μM, lanes 7–12) using either wild-type, full-length TRIM5-21R proteins (WT, lanes 1, 4, 7, and 10), TRIM5-21R proteins with the R121E mutation (R121E, lanes 2, 5, 8, and 11), or truncated TRIM5-21R proteins that lacked the SPRY domain (ΔSPRY, lanes 3, 6, 9, and 12). Pelletable CA and associated TRIM5-21R proteins (Pellet, 4% of total), were separated from unassembled and soluble CA proteins and unbound TRIM5-21R (Supernatant, 1% of total) by centrifugation, and analyzed by Western blotting, with the input levels of both proteins shown for reference (Input, 1% of total).

We also tested whether TRIM5-21R dimerization and higher-order assembly were required for hexagonal lattice formation in vitro. We previously reported that recombinant TRIM5-21R expressed in insect cells can be isolated in both monomeric and dimeric forms that do not interconvert rapidly (15). Two-dimensional crystallization trials with the kinetically trapped TRIM5-21R monomer revealed that this species was impaired in lattice formation (see *Materials and Methods* for details). This result suggested that the TRIM5-21R dimer, which is the predominant species in mammalian cells (15), is the likely building block of the hexagonal lattice. Furthermore, a TRIM5-21R construct that contained the R121E mutation failed to form hexagonal crystals, even at concentrations that were 30-fold higher than those required for assembly of the wild-type protein. Sedimentation equilibrium experiments showed that this mutant protein remained dimeric in solution (Fig. S2), implying that the R121E mutation disrupted an interface that mediates lattice formation. Thus, the hydrophobic surface patch on the B-box 2 domain that is required for restriction and for efficient retroviral capsid binding in cells was also required for efficient CA binding and for assembly of the TRIM5-21R hexagonal lattice in vitro.

**Hexagonal Arrays of HIV-1 CA That Mimic the Capsid Surface Act as a Template for Assembly of TRIM5-21R Arrays.** Given that TRIM5 protein assembly enhances capsid binding, we reasoned that two-dimensional hexagonal crystals of HIV-1 CA that mimic the capsid lattice might also promote TRIM5-21R assembly. To test this idea, we first had to develop a stable HIV-1 CA lattice that could withstand extended incubation with TRIM5-21R, which was necessary because the TRIM5-21R and CA crystals are stabilized by different buffer conditions and because TRIM5-21R binding destabilizes CA lattices (2, 15–17). The successful construct was an HIV-1 CA fusion protein, termed CA-NC$_{A14C/E45C/W184A}$, that: (*i*) spanned the CA and NC domains of HIV-1 Gag, (*ii*) contained A14C and E45C mutations within the CA N-terminal domain that allowed disulfide crosslinking to stabilize the CA hexamers (39, 40), and (*iii*) contained a W184A mutation in the C-terminal domain of CA that promoted planar sheet formation (40). The two-dimensional hexagonal crystals formed by this protein were stabilized by both the engineered disulfide bonds (39, 40) and by interactions between the NC domains and a 25-mer repeating TG oligodeoxynucleotide (25-TG) (41). It was also necessary to identify suitable incubation conditions that minimized spontaneous assembly of TRIM5-21R, which was achieved by performing the incubations under more basic conditions than those used in the untemplated assembly reactions (pH 9.0 vs. 8.0).

TRIM5-21R dimers were incubated in solution with the preassembled CA-NC crystals, and aliquots of the reaction mixtures were applied to carbon-coated grids and examined by negative-stain EM (Fig. 4*A*). At incubation times >6 h, the surfaces of the CA-NC crystals were decorated with TRIM5-21R (compare Fig. 4*B* with Fig. 4*C*). In contrast, spontaneous assembly of TRIM5-21R crystals was rarely observed in the absence of added CA-NC crystals. Fourier transforms of the decorated crystals revealed well defined reflections that corresponded to the CA lattice, as well as more diffuse peaks corresponding to the first-order reflections of the TRIM5-21R lattice (Fig. 4*D*). The boundaries of ordered TRIM5-21R and CA lattices typically coincided almost exactly (Fig. 4*A*), and regions directly adjacent to the crystals lacked both CA and TRIM5-21R diffraction. Furthermore, the CA-NC crystals did not serve as a template for assembly of TRIM5-21R constructs that carried the R121E mutation or lacked the SPRY domain. Thus, the hexagonal CA lattice promoted assembly of the TRIM5-21R lattice, and templated assembly required both the capsid-binding activity of the SPRY domain, as well as higher-order interactions mediated by the B-box 2 domain.

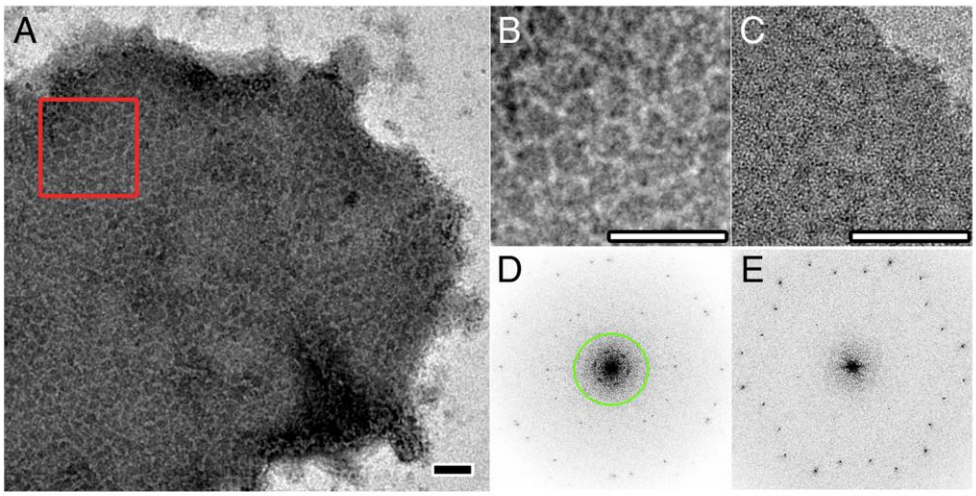


**Fig. 4.** TRIM5-21R assembly is promoted by preformed, stabilized two-dimensional CA-NC$_{A14C/E45C/W184A}$ crystals that mimic the surface of the HIV-1 capsid. (*A*) Representative EM image of a CA-NC/TRIM5-21R cocrystal (1:1 molar protein ratio, 24 h incubation). (*B*) Expanded view of the region boxed in red in (*A*). The contrast was stretched using Adobe Photoshop to enhance the clarity of the TRIM5-21R hexagons. (*C*) EM image of CA-NC alone at the same magnification as (*B*), shown for comparison. Scale bars, 100 nm. (*D*) and (*E*) Computed Fourier transforms of the crystals shown in (*B*) and (*C*), respectively. In (*D*), diffraction from the TRIM5-21R lattice is evident (circled in green). Note that in this case, there are at least two stacked TRIM lattices (the first-order reflections of each correspond to a hexagonal lattice with ~350 Å spacing), and at least three stacked CA lattices ($a = 93.1$ Å, $b = 93.1$ Å, and $\gamma = 119.0°$; $a = 92.5$ Å, $b = 94.2$ Å, and $\gamma = 118.9°$; $a = 93.1$ Å, $b = 92.6$ Å, and $\gamma = 118.8°$). The TRIM and CA diffraction patterns do not overlap in spatial frequency owing to the size of the TRIM lattice and its lack of long-range order. As expected, TRIM diffraction is absent in the transform of CA-NC alone, which shows two CA lattices (*E*).

## Discussion

We have shown that TRIM5-21R, a variant of TRIM5α that potently restricts HIV-1 replication in culture, assembles in vitro into two-dimensional arrays comprising hexagonal rings. Hexagonal lattice formation is an intrinsic property of the protein, because it occurred spontaneously under standard buffer conditions, in the absence of added precipitant. We note that TRIM5α and its variants can also spontaneously assemble in cells, particularly when the protein is expressed at high levels or when proteasome function is inhibited (10, 22, 42–45). We speculate that these "TRIM bodies" may contain hexagonal arrays of TRIM5 proteins, although other cellular proteins are clearly also associated with the bodies (10, 46). More importantly, we found that a preassembled mimic of the HIV-1 capsid surface promoted formation of the hexagonal TRIM5-21R lattice in vitro, suggesting that incoming retroviral capsids can serve as templates for TRIM5 assembly, even under conditions where assembly would otherwise be disfavored.

Similarities between the requirements for retroviral restriction and TRIM5-21R assembly in vitro suggest that the hexagonal TRIM5-21R arrays described here are functionally relevant. Specifically, we observed that kinetically trapped, monomeric TRIM5-21R proteins were deficient in assembly, suggesting that the basic assembly unit is the TRIM5-21R dimer. TRIM5-21R dimerization is also essential for retroviral restriction in cells (17, 18). Similarly, the R121E mutation inhibited TRIM5-21R assembly in vitro, and this mutation also inhibits retroviral restriction and blocks formation of capsid-associated, higher-order TRIM5 assemblies in cells (21, 25).

Our results support a model in which TRIM5α proteins recognize retroviral capsids through a number of cooperative interactions that include: (*i*) direct, but weak binding of the SPRY domain to the capsid surface, (*ii*) TRIM5α dimerization, (*iii*) assembly of a hexagonal lattice of TRIM5α dimers, and (*iv*) complementarity between the symmetries and spacings of the TRIM5α and capsid lattices, which would reinforce TRIM5α assembly and create powerful avidity effects. In essence, we suggest that TRIM5α proteins employ "pattern recognition" to bind the hexagonal CA lattices found in all retroviral capsids (4). Although this cooperative mode of binding does not alleviate the requirement for direct capsid binding, it does reduce the affinity required for isolated TRIM5/CA interactions, thereby making it easier for individual TRIM5α proteins to restrict a variety of highly divergent retroviruses and also buffering the system against CA mutations that diminish binding affinity. Additional mechanisms that could regulate cooperative TRIM5α binding and restriction include auto-inhibition of unassembled TRIM5α subunits, TRIM5α phosphorylation (15, 47), TRIM5α ubiquitylation (10, 15, 48, 49), and the coupling of lattice formation to TRIM5α ubiquitin E3 ligase activity via conformational changes and/or proximity effects.

As illustrated in Fig. 5, idealized TRIM5-21R arrays with unit cell spacings of 315–355 Å could overlay on retroviral capsid lattices with unit cell spacings of 90–100 Å in at least three ways, which differ slightly in the matching of spacings and symmetry elements. Unfortunately, the EM images of the TRIM5-21R/CA cocrystals typically revealed multiple, stacked CA and TRIM layers (e.g., at least three distinct CA lattices and two TRIM lattices can be observed in the power spectrum shown in Fig. 4*D*). This overlap precluded us from identifying the interacting TRIM and CA lattices and determining their exact spatial relationship. In any case, the TRIM lattice must presumably be distorted from ideal geometries in order to accommodate the irregularly curved surfaces of retroviral capsids. This requirement may explain why the TRIM5-21R lattice appears to be mosaic and flexible, and may also limit the range over which the two lattices can interact. Indeed, slight mismatches between the interacting lattices will tend to create discontinuities in the extended CA lattice that

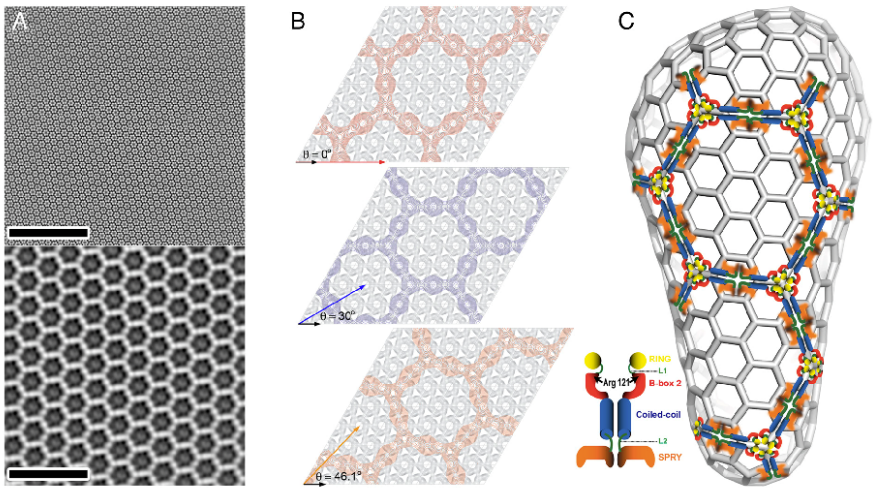


**Fig. 5.** Possible modes of interaction between the TRIM5-21R and CA lattices. (*A*) Fourier-filtered images of CA-NC$_{A14C/E45C/W184A}$ crystals alone (*top*) and TRIM5-21R crystals alone (*bottom*) illustrate the dramatic difference in unit cell size of the two lattices. (Scale bars, 100 nm). (*B*) Assuming rigid, planar lattices, we can envision at least three different binding modes between the larger TRIM5-21R hexagonal lattice (colored) and the smaller CA lattice (gray). In these different binding modes, the TRIM5-21R lattice vectors (colored arrows) are rotated by either 0° (*top*), 30° (*center*), or 46.1° (*bottom*) relative to the CA lattice vectors (black arrows), and the interactions require TRIM5-21R lattice spacings of 360–400 Å, 312–346 Å, or 324–361 Å, respectively (given CA lattice spacings of 90–100 Å). The experimentally observed range of lattice spacings in our TRIM5-21R arrays is shown in Table 1. (*C*) Schematic model of an HIV-1 fullerene cone illustrating how TRIM5α could recognize the capsid lattice. Notice that only a small number of TRIM5α hexameric rings are required to create high avidity and that the lattice-matching geometry must be able to accommodate a greater radius of curvature in the outer TRIM5α lattice as compared to the inner CA lattice. Although the reconstructions do not allow us to position the different domains unambiguously, we modeled the coiled-coil domains within the narrowest density along each edge of the TRIM5α hexagon because the coiled-coil is expected to be the thinnest of the TRIM5α domains. The length of each hexagon edge (~17 nm), together with the apparent twofold symmetry, suggests that each edge may be composed of two TRIM5α dimers, with coiled-coil elements linking L2/SPRY and RING/B-box 2 domains that occupy the regions of high local density at the midpoint and ends of each edge. We tentatively positioned six RING/B-box 2 domains at each threefold symmetry axis and four SPRY domains about the midpoint of each ring edge. Other models are possible, however, and higher resolution reconstructions will be required to define the TRIM lattice architecture unambiguously.

could contribute to the accelerated capsid dissociation that accompanies restriction (2, 15–17).

In summary, we propose that retroviral capsid binding and higher-order TRIM5 assembly are coupled because the hexagonal TRIM5 lattice can align multiple SPRY domains over repeating binding sites on the hexagonal CA lattice. Implicit in our model is the idea that retroviruses could evade TRIM5α recognition *either* by evolving surface mutations that eliminate SPRY domain recognition *or* by altering the regularity of capsid subunit conformations and lattice spacings. These selective pressures will tend to favor plasticity in both the TRIM5α and capsid lattices, consistent with the extensive shape polymorphism exhibited by retroviral capsids.

## Materials and Methods

**Construction, Expression, and Purification of Recombinant Proteins.** TRIM5-21R and HIV-1 CA proteins were expressed and purified as described in *SI Text*.

**Binding Assays.** TRIM5-21R binding to disulfide-stabilized HIV-1 CA tubes was measured by using a published cosedimentation assay (2). Experimental details are described in *SI Text*.

**TRIM5-21R Assembly.** Aliquots (~5 μL) of freshly concentrated TRIM5-21R protein solutions (0.7–1.2 mg/mL) were incubated on carbon-coated EM grids for 5–30 min. Grids were then moved directly onto a 40-μL drop of 0.1 M KCl for 3 min, blotted, placed on a 20-μL drop of 2% uranyl acetate for 2 min, blotted, and air dried. Alternatively, TRIM5-21R (>0.7 mg/mL) was stored for 3–5 d at 4 °C in 20 mM Tris, pH 8, 25 mM NaCl, 1 mM TCEP, whereupon the protein assembled into large hexagonal sheets that precipitated from solution and could be analyzed by EM. Thus, hexagonal sheet assembly is an intrinsic property of TRIM5-21R.

Spontaneous assembly of TRIM5-21R dimers was observed in 20/22 independent protein preparations, but there was substantial variability in assembly efficiencies across the different preparations. This variability precluded quantitative assessment of the relative assembly efficiencies of wild-type and mutant proteins. However, clear trends were observed. Specifically, the R121E mutant failed to assemble under all conditions tested. The SPRY domain deletion mutant, TRIM5-21R$_{1-276}$, spontaneously assembled in 2/2 independent preparations. However, these crystals were sparse, and were generally smaller and less well ordered than assemblies formed by wild-type TRIM5-21R dimers. To assess the assembly efficiencies of monomeric and dimeric TRIM5-21R, we compared matched samples that were separated by ion exchange chromatography. In three independent experiments, hexagonal arrays were observed for the dimeric TRIM5-21R fraction but not for the monomeric fraction. In a fourth trial, assemblies were observed in the monomeric TRIM5-21R incubation, but were ~4-fold less frequent than in the dimer incubation.

**Templated Assembly of TRIM5-21R on Hexagonal Arrays of HIV-1 CA-NC.** To form stable two-dimensional crystals that mimicked the surface of the viral capsid, HIV-1 CA-NC$_{A14C/E45C/W184A}$ (232 μM) was incubated with 25-TG (143 μM) in 50 mM Tris, pH 8, 250 mM NaCl, 50 mM β-mercaptoethanol (βME) for 90 min at 37 °C. EM analyses confirmed that the CA-NC arrays assembled into the same hexagonal arrays as wild-type HIV-1 CA, with unit cell spacings of ~90 Å in both cases (Fig. 5*A*). Following assembly reactions, the CA-NC crystals were diluted 25-fold into 50 mM Tris, pH 8, 300 mM NaCl, and incubated for an additional 10 min at room temperature to promote disulfide bond formation. TRIM5-21R proteins were then added in 1- to 10-fold molar excess, and the pH was immediately adjusted to 9.0 by addition of Tris buffer to a final concentration of 100 mM. Samples were incubated for 1–60 h,

applied to carbon-coated EM grids, washed and stained as described above, and visualized by EM.

**Electron Microscopy and Image Analysis.** Sample and EM grid preparation are described above. For cryoEM, samples were applied to carbon-coated molybdenum grids, washed with 0.1 M KCl, blotted to near dryness, and plunged into a slurry of liquid ethane. Images were recorded at a magnification of 11,000–30,000× under low electron-dose conditions (~20 $e^-/Å^2$) using a 2k × 2k CCD camera (Gatan) fitted to a Tecnai T12 transmission electron microscope (Phillips/FEI) or a 4k × 4k camera fitted to a Tecnai F20. For processing, images were converted to MRC format (50). Manual indexing, unbending (to correct for lattice distortions), and corrections for the contrast transfer function were performed with the program 2dx (51). Fourier-filtered images were created after one or two rounds of unbending, and a 1-pixel hole was used to mask diffraction spots.

**ACKNOWLEDGMENTS.** We thank Debbie Eckert for assistance with analytical ultracentrifugation experiments. This work was funded by the National Institutes of Health (NIH) through Grants R01-AI63987 (J.G.S), R37 AI-45405-06 (W.I.S.), P50-GM082545 (to W.I.S. and M.Y.), and R01-GM066087 (M.Y.). Electron microscopy experiments were conducted at the National Resource for Automated Molecular Microscopy, which is supported by the NIH through the National Center for Research Resources' P41 program (RR17573) and at the University of Virginia Molecular Electron Microscopy Core facility (1S10RR025067 and 1G20RR031199).

1. Stremlau M, et al. (2004) The cytoplasmic body component TRIM5α restricts HIV-1 infection in Old World monkeys. *Nature* 427:848–853.
2. Stremlau M, et al. (2006) Specific recognition and accelerated uncoating of retroviral capsids by the TRIM5α restriction factor. *Proc Natl Acad Sci USA* 103:5514–5519.
3. Huthoff H, Towers GJ (2008) Restriction of retroviral replication by APOBEC3G/F and TRIM5α. *Trends Microbiol* 16:612–619.
4. Luban J (2007) Cyclophilin A TRIM5, and resistance to human immunodeficiency virus type 1 infection. *J Virol* 81:1054–1061.
5. Ganser-Pornillos BK, Yeager M, Sundquist WI (2008) The structural biology of HIV assembly. *Curr Opin Struct Biol* 18:203–217.
6. Ganser BK, Li S, Klishko VY, Finch JT, Sundquist WI (1999) Assembly and analysis of conical models for the HIV-1 core. *Science* 283:80–83.
7. Li S, Hill CP, Sundquist WI, Finch JT (2000) Image reconstructions of helical assemblies of the HIV-1 CA protein. *Nature* 407:409–413.
8. Ganser-Pornillos BK, von Schwedler UK, Stray KM, Aiken C, Sundquist WI (2004) Assembly properties of the human immunodeficiency virus type 1 CA protein. *J Virol* 78:2545–2552.
9. Heymann JB, Butan C, Winkler DC, Craven RC, Steven AC (2008) Irregular and semi-regular polyhedral models for Rous sarcoma virus cores. *Comput Math Method M* 9:197–210.
10. Diaz-Griffero F, et al. (2006) Rapid turnover and polyubiquitylation of the retroviral restriction factor TRIM5. *Virology* 349:300–315.
11. Li X, et al. (2006) Functional replacement of the RING, B-box 2, and coiled-coil domains of tripartite motif 5α (TRIM5α) by heterologous TRIM domains. *J Virol* 80:6198–6206.
12. Hatziioannou T, Cowan S, Goff SP, Bieniasz PD, Towers GJ (2003) Restriction of multiple divergent retroviruses by Lv1 and Ref1. *EMBO J* 22:385–394.
13. Sebastian S, Luban J (2005) TRIM5α selectively binds a restriction-sensitive retroviral capsid. *Retrovirology* 2:40.
14. Kar AK, Diaz-Griffero F, Li Y, Li X, Sodroski J (2008) Biochemical and biophysical characterization of a chimeric TRIM21- TRIM5α protein. *J Virol* 82:11669–11681.
15. Langelier CR, et al. (2008) Biochemical characterization of a recombinant TRIM5α protein that restricts human immunodeficiency virus type 1 replication. *J Virol* 82:11682–11694.
16. Black LR, Aiken C (2010) TRIM5α disrupts the structure of assembled HIV-1 capsid complexes in vitro. *J Virol* 84:6564–6569.
17. Perron MJ, et al. (2007) The human TRIM5α restriction factor mediates accelerated uncoating of the N-tropic murine leukemia virus capsid. *J Virol* 81:2138–2148.
18. Javanbakht H, et al. (2006) Characterization of TRIM5α trimerization and its contribution to human immunodeficiency virus capsid binding. *Virology* 353:234–246.
19. Yap MW, Mortuza GB, Taylor IA, Stoye JP (2007) The design of artificial retroviral restriction factors. *Virology* 365:302–314.
20. Javanbakht H, et al. (2007) The ability of multimerized cyclophilin A to restrict retrovirus infection. *Virology* 367:19–29.
21. Diaz-Griffero F, et al. (2009) A B-box 2 surface patch important for TRIM5α self-association, capsid binding avidity, and retrovirus restriction. *J Virol* 83:10737–10751.
22. Reymond A, et al. (2001) The tripartite motif family identifies cell compartments. *EMBO J* 20:2140–2151.
23. Mische CC, et al. (2005) Retroviral restriction factor TRIM5α is a trimer. *J Virol* 79:14446–14450.
24. Perez-Caballero D, Hatziioannou T, Yang A, Cowan S, Bieniasz PD (2005) Human tripartite motif 5α domains responsible for retrovirus restriction activity and specificity. *J Virol* 79:8969–8978.
25. Li X, Sodroski J (2008) The TRIM5α B-box 2 domain promotes cooperative binding to the retroviral capsid by mediating higher-order self-association. *J Virol* 82:11495–11502.
26. Sastri J, et al. (2010) Identification of residues within the L2 region of rhesus TRIM5α that are required for retroviral restriction and cytoplasmic body localization. *Virology* 405:259–266.
27. Sayah DM, Sokolskaja E, Berthoux L, Luban J (2004) Cyclophilin A retrotransposition into TRIM5 explains owl monkey resistance to HIV-1. *Nature* 430:569–573.
28. Gamble TR, et al. (1996) Crystal structure of human cyclophilin A bound to the amino-terminal domain of HIV-1 capsid. *Cell* 87:1285–1294.
29. Brennan G, Kozyrev Y, Hu SL (2008) TRIMCyp expression in Old World primates *Macaca nemestrina* and *Macaca fascicularis*. *Proc Natl Acad Sci USA* 105:3569–3574.
30. Virgen CA, Kratovac Z, Bieniasz PD, Hatziioannou T (2008) Independent genesis of chimeric TRIM5-cyclophilin proteins in two primate species. *Proc Natl Acad Sci USA* 105:3563–3568.
31. Wilson SJ, et al. (2008) Independent evolution of an antiviral TRIMCyp in rhesus macaques. *Proc Natl Acad Sci USA* 105:3557–3562.
32. Newman RM, et al. (2008) Evolution of a TRIM5-CypA splice isoform in old world monkeys. *PLoS Pathog* 4:e1000003.
33. Yap MW, Dodding MP, Stoye JP (2006) Trim-cyclophilin A fusion proteins can restrict human immunodeficiency virus type 1 infection at two distinct phases in the viral life cycle. *J Virol* 80:4061–4067.
34. Nisole S, Lynch C, Stoye JP, Yap MW (2004) A Trim5-cyclophilin A fusion protein found in owl monkey kidney cells can restrict HIV-1. *Proc Natl Acad Sci USA* 101:13324–13328.
35. Saurin AJ, Borden KL, Boddy MN, Freemont PS (1996) Does this have a familiar RING? *Trends Biochem Sci* 21:208–214.
36. Kentsis A, Gordon RE, Borden KL (2002) Control of biochemical reactions through supramolecular RING domain self-assembly. *Proc Natl Acad Sci USA* 99:15404–15409.
37. Yin Q, et al. (2009) E2 interaction and dimerization in the crystal structure of TRAF6. *Nat Struct Mol Biol* 16:658–666.
38. Mace PD, et al. (2008) Structures of the cIAP2 RING domain reveal conformational changes associated with ubiquitin-conjugating enzyme (E2) recruitment. *J Biol Chem* 283:31633–31640.
39. Pornillos O, et al. (2009) X-ray structures of the hexameric building block of the HIV capsid. *Cell* 137:1282–1292.
40. Pornillos O, Ganser-Pornillos BK, Banumathi S, Hua Y, Yeager M (2010) Disulfide bond stabilization of the hexameric capsomer of human immunodeficiency virus. *J Mol Biol* 401:985–995.
41. Campbell S, Rein A (1999) In vitro assembly properties of human immunodeficiency virus type 1 Gag protein lacking the p6 domain. *J Virol* 73:2270–2279.
42. Song B, et al. (2005) TRIM5α association with cytoplasmic bodies is not required for antiretroviral activity. *Virology* 343:201–211.
43. Wu X, Anderson JL, Campbell EM, Joseph AM, Hope TJ (2006) Proteasome inhibitors uncouple rhesus TRIM5α restriction of HIV-1 reverse transcription and infection. *Proc Natl Acad Sci USA* 103:7465–7470.
44. Perez-Caballero D, Hatziioannou T, Zhang F, Cowan S, Bieniasz PD (2005) Restriction of human immunodeficiency virus type 1 by TRIM-CypA occurs with rapid kinetics and independently of cytoplasmic bodies, ubiquitin, and proteasome activity. *J Virol* 79:15567–15572.
45. Campbell EM, Perez O, Anderson JL, Hope TJ (2008) Visualization of a proteasome-independent intermediate during restriction of HIV-1 by rhesus TRIM5α. *J Cell Biol* 180:549–561.
46. O'Connor C, et al. (2010) p62/sequestosome-1 associates with and sustains the expression of retroviral restriction factor TRIM5α. *J Virol* 84:5997–6006.
47. Daub H, et al. (2008) Kinase-selective enrichment enables quantitative phosphoproteomics of the kinome across the cell cycle. *Mol Cell* 31:438–448.
48. Yamauchi K, Wada K, Tanji K, Tanaka M, Kamitani T (2008) Ubiquitination of E3 ubiquitin ligase TRIM5α and its potential role. *FEBS J* 275:1540–1555.
49. Javanbakht H, Diaz-Griffero F, Stremlau M, Si Z, Sodroski J (2005) The contribution of RING and B-box 2 domains to retroviral restriction mediated by monkey TRIM5α. *J Biol Chem* 280:26933–26940.
50. Crowther RA, Henderson R, Smith JM (1996) MRC image processing programs. *J Struct Biol* 116:9–16.
51. Gipson B, Zeng X, Zhang ZY, Stahlberg H (2007) 2dx—user-friendly image processing for 2D crystals. *J Struct Biol* 157:64–72.

# Supporting Information

Ganser-Pornillos et al. 10.1073/pnas.1013426108

## SI Materials and Methods

**Construction, Expression, and Purification of TRIM5-21R Proteins.** Baculovirus expression vectors for One-STrEP-FLAG (OSF)-tagged TRIM5-21R proteins were based on the previously reported Gateway (Invitrogen) donor vector, pDONR221/OSFT-TRIM5-21R (WISP-08-177) (1). We first created a new vector that encoded full-length, wild-type TRIM5-21R (pDONR221/OSFP-TRIM5-21R, WISP-10-430), but had a PreScission protease site (LEVLFQGP) in place of the TEV protease site of WISP-08-177 and lacked an artifactual C-terminal Gly-Gly extension. Quikchange site-directed mutagenesis (Stratagene) was used to introduce the R121E mutation (rhesus TRIM5α numbering) into the B-box 2 domain (pDONR221/OSFP-TRIM5-21R$_{R121E}$, WISP-10-431) or to introduce a premature stop codon after residue 276 (pDONR221/OSFP-TRIM5-21R$_{1-276}$, WISP-10-432, encoding the ΔSPRY construct used for in vitro assembly). These constructs were incorporated into baculovirus expression vectors using the BaculoDirect system (Invitrogen) in SF21 cells. The recombinant baculovirus that encoded the ΔSPRY construct (OSFT-TRIM5-21R$_{1-232}$) used for the binding experiments illustrated in Fig. 3 was described previously (1).

Expression and purification methods for the new OSF-tagged PreScission-cleavable TRIM5-21R constructs were adapted from protocols described previously (1). SF21 cells (6 L at 2× $10^6$ cells/mL in SF-900 II serum-free media, Invitrogen) were infected with recombinant baculovirus at a multiplicity of infection of 4, and harvested by centrifugation 48 h later. All protein purification steps were performed at 4 °C. Cells were resuspended in lysis buffer [50 mM Tris, pH 8, 50 mM NaCl, 1 mM tris(2-carboxyethyl)phosphine (TCEP)] supplemented with 1.5% (w/v) Triton X-100 and 0.007 volume of protease inhibitor cocktail (Sigma), and lysed in a 100-mL Dounce homogenizer (15 strokes). The lysate was clarified by ultracentrifugation (184,000 × *g* for 50 min), filtered (0.45 μm), and loaded onto a 5-mL StrepTrap HP column (GE Lifesciences). The column was washed with 50 mL of lysis buffer and eluted in the same buffer supplemented with 2.5 mM D-desthiobiotin. The eluate was loaded onto two 5-mL HiTrap HP Q-Sepharose columns (GE Lifesciences) connected in series, and the protein was eluted with a 100-mL linear NaCl gradient (0.05–0.5 M). The TRIM5-21R monomers and dimers eluted as distinct peaks (1) that were collected separately and dialyzed into size-exclusion buffer (12 h, 20 mM Tris, pH 8, 25 mM NaCl, 1 mM TCEP). For in vitro assembly experiments (but not for CA binding assays), the affinity tag was removed during this dialysis step by the addition of 100 units of PreScission protease (GE Lifesciences) per mg of substrate. Proteins were then purified to homogeneity by size-exclusion chromatography in dialysis buffer (Superdex 200 16/60 column, GE Lifesciences), and concentrated using a Vivaspin 20 concentrator (30 kDa cutoff, Sartorius Stedim). At this stage, we noticed that there was an inverse relationship between protein solubility (assessed by the appearance of aggregates that induced light scattering at 340 nm) and assembly competence. For example, the assembly-competent wild-type TRIM5-21R dimer could be concentrated to only ~1.5 mg/mL in size-exclusion buffer (pH 8), whereas the assembly-incompetent R121E mutant could be concentrated to ~30 mg/mL in the same buffer. The TRIM5-21R$_{1-276}$ ΔSPRY construct and wild-type TRIM5-21R monomer had intermediate solubilities (~2 mg/mL and ~10 mg/mL, respectively).

The following modifications to the protocol were made for TRIM5-21R proteins used in the HIV-1 CA-NC cocrystallization experiments: (*i*) buffers contained 20 mM N-cyclohexyl-2-aminoethanesulfonic acid (CHES), pH 10 instead of Tris, (*ii*) NaCl was omitted, except during the gradient elution step of anion-exchange chromatography, and (*iii*) PreScission protease cleavage was performed in the anion-exchange eluate *prior* to dialysis into size-exclusion buffer. These modifications prevented premature protein assembly and also improved protein solubility slightly.

The masses of all purified TRIM5-21R proteins were within 2 Da of the expected values (assuming loss of N-terminal methionines and N-terminal acetylation), as determined by electrospray ionization mass spectrometry. Typical yields of TRIM5-21R dimers were ~0.5 mg/L culture for the wild-type and TRIM5-21R$_{1-276}$ proteins, and ~5 mg/L for TRIM5-21R$_{R121E}$. Yields of the monomeric proteins were typically ~5-fold lower than the dimeric proteins.

**Construction, Expression, and Purification of HIV-1 CA Proteins.** The HIV-1 CA$_{A14C/E45C}$ protein used for binding experiments was expressed and purified as described previously (2, 3). The HIV-1 CA-NC$_{A14C/E45C/W184A}$ expression construct was created by Quikchange site-directed mutagenesis of WISP-96-18 (4), and the protein was expressed and purified as described (4), except that β-mercaptoethanol (βME) was added at a concentration of 100 mM to the lysis buffer, and maintained at 20 mM in all subsequent steps. The unusually high concentration of βME in the lysis buffer was empirically determined to improve yield, presumably by disrupting preassembled and/or aggregated protein (2, 3).

**Binding Assays.** Disulfide-stabilized HIV-1 CA tubes were assembled by stepwise dialysis of 1 mg/mL HIV-1 CA$_{A14C/E45C}$ as described previously (2). Purified OSF-tagged wild-type, R121E, and ΔSPRY TRIM5-21R proteins were incubated in the presence or absence of the disulfide-stabilized CA tubes for 1 h at 25 °C in binding buffer (20 mM Tris, pH 8, 25 mM NaCl, 1 mM TCEP), with CA subunits present in a 6-fold molar excess over TRIM5-21R subunits. Unbound TRIM and unassembled soluble CA proteins were separated from assembled and bound complexes by centrifugation through a 70% (w/v) sucrose cushion (in binding buffer lacking TCEP). At these low protein concentrations, unbound TRIM5-21R proteins did not assemble appreciably, and therefore remained in the supernatant fraction. Aliquots (200 μL) of the binding reactions were layered onto cushions (4 mL) and subjected to centrifugation at 108,000 × *g* for 30 min at 4 °C. Input and supernatant fractions were sampled directly. The protein pellet was dissolved in 200 μL of binding buffer, concentrated by precipitation with 5% (vol/vol) trichloroacetic acid, and resuspended in 10 μL of SDS-PAGE sample buffer supplemented with 2 μL of 2 M urea, 2 M Tris, pH 12.

Proteins were separated by SDS-PAGE, electrotransferred onto nitrocellulose membranes, and visualized by Western blotting with a rabbit anti-HIV-1 CA (made in-house, 1:5,000 dilution) or a mouse anti-FLAG antibody (Sigma,1:3,000 dilution) to detect OSF-tagged TRIM5-21R constructs. Secondary antibodies (1:20,000 Alexa 680-nm, Molecular Probes; or 1:10,000 IRDye 800-nm, Rockland) were detected using an Odyssey infrared imaging system (Li-Cor, Inc.).

1. Langelier CR, et al. (2008) Biochemical characterization of a recombinant TRIM5α protein that restricts human immunodeficiency virus type 1 replication. *J Virol* 82:11682–11694.
2. Pornillos O, et al. (2009) X-ray structures of the hexameric building block of the HIV capsid. *Cell* 137:1282–1292.
3. Pornillos O, Ganser-Pornillos BK, Banumathi S, Hua Y, Yeager M (2010) Disulfide bond stabilization of the hexameric capsomer of human immunodeficiency virus. *J Mol Biol* 481:985–995.
4. Ganser BK, Li S, Klishko VY, Finch JT, Sundquist WI (1999) Assembly and analysis of conical models for the HIV-1 core. *Science* 283:80–83.

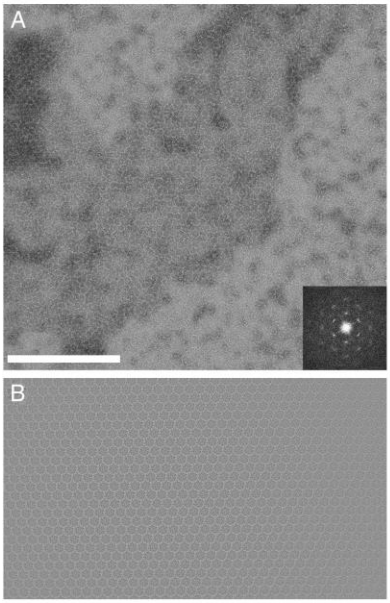


**Fig. S1.** Analysis of the hexagonal lattice formed by the truncated TRIM5-21R$_{1\text{-}276}$ (ΔSPRY) protein. (*A*) Image of the negatively-stained assemblies, with the computed Fourier transform of the central section (inset). (Scale bar,500 nm). (*B*) Fourier filtered image of the crystal shown in part (*A*).

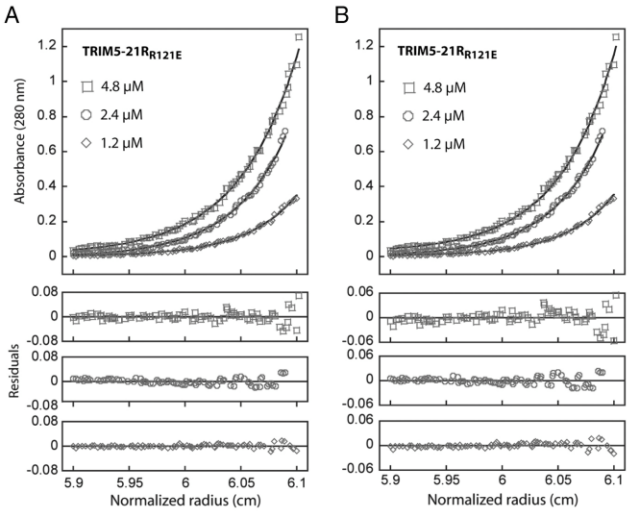


**Fig. S2.** Equilibrium sedimentation distributions of purified OSF-tagged TRIM5-21R$_{R121E}$. Centrifugation experiments were performed at 4 °C in 20 mM Tris, pH 8, 25 mM NaCl, 1 mM TCEP, using an Optima XL-I centrifuge and An-60 Ti rotor (Beckman). The data points (open symbols) and the best-fit curves (solid lines) are shown at the top, and residual differences between the data and two different single-species models are shown at the bottom. The data shown are for initial protein concentrations of 1.2, 2.4, and 4.8 μM at a rotor speed of 14,000 rpm. Data sets were also collected at 16,000 rpm, and all of the data were globally fitted to: (*A*) a model in which the molecular weight was not constrained during the refinement ($MW_{calc}$ = 62,253 Da, $MW_{obs}$ = 119,017 Da, $MW_{obs}/MW_{calc}$ = 1.91) or (*B*) a model in which the molecular weight was fixed to that of a dimer (124,506 Da). Nonlinear least-squares data fitting was performed using the Heteroanalysis software (1). Solvent density and protein partial specific volume were calculated with the program SEDNTERP (2).

1 Cole JL (2004) Analysis of heterogeneous interactions. *Methods Enzymol* 384:212–232.
2 Laue TM, Shah BD, Ridgeway TM, Pelletier SL (1992) Computer-aided interpretation of analytical sedimentation data for proteins. *Ultracentrifugation in Biochemistry and Polymer Science*, eds Harding SE, Rowe AJ, Horton JC (Royal Society of Chemistry, Cambridge, England), 90–125.

# CHAPTER 3

# THE TRIPARTITE MOTIF COILED-COIL IS AN ELONGATED ANTIPARALLEL HAIRPIN DIMER

Jacint G. Sanchez, Katarzyna Okreglicka, Viswanathan Chandrasekaran, Jordan M. Welker, Wesley I. Sundquist, and Owen Pornillos

Reprinted with permission from PNAS 111(7), 2494-2499.

# The tripartite motif coiled-coil is an elongated antiparallel hairpin dimer

Jacint G. Sanchez[a,1], Katarzyna Okreglicka[a,1], Viswanathan Chandrasekaran[b], Jordan M. Welker[a], Wesley I. Sundquist[b], and Owen Pornillos[a,2]

[a]Department of Molecular Physiology and Biological Physics and The Myles H. Thaler Center for AIDS and Human Retrovirus Research, University of Virginia, Charlottesville, VA 22908; and [b]Department of Biochemistry, University of Utah, Salt Lake City, UT 84112

Edited by Alfonso Mondragon, Northwestern University, Evanston, IL, and accepted by the Editorial Board January 8, 2014 (received for review October 8, 2013)

**Tripartite motif (TRIM) proteins make up a large family of coiled-coil-containing RING E3 ligases that function in many cellular processes, particularly innate antiviral response pathways. Both dimerization and higher-order assembly are important elements of TRIM protein function, but the atomic details of TRIM tertiary and quaternary structure have not been fully understood. Here, we present crystallographic and biochemical analyses of the TRIM coiled-coil and show that TRIM proteins dimerize by forming interdigitating antiparallel helical hairpins that position the N-terminal catalytic RING domains at opposite ends of the dimer and the C-terminal substrate-binding domains at the center. The dimer core comprises an antiparallel coiled-coil with a distinctive, symmetric pattern of flanking heptad and central hendecad repeats that appear to be conserved across the entire TRIM family. Our studies reveal how the coiled-coil organizes TRIM25 to polyubiquitylate the RIG-I/viral RNA recognition complex and how dimers of the TRIM5α protein are arranged within hexagonal arrays that recognize the HIV-1 capsid lattice and restrict retroviral replication.**

antiparallel dimer | disulfide crosslinking | X-ray crystallography

Tripartite motif (TRIM) proteins make up the largest superfamily of RING E3 ubiquitin ligases, with more than 100 members in the human proteome (1, 2). TRIM proteins function in a variety of cellular pathways, and many regulate innate immunity and/or mediate antiviral responses. Antiviral TRIMs include TRIM25, which regulates the IFN response to RNA viruses (3, 4), and TRIM5α, which senses and inhibits early stages of retroviral replication (5, 6).

TRIM proteins share a common N-terminal domain organization, termed the tripartite or RBCC (RING, B-box, coiled-coil) motif, followed by variable C-terminal protein recognition domains (Fig. 1*A* and *B*). "Linker" segments of unknown structure typically separate both the RING and B-box domains (L1) and the coiled-coil and terminal effector domains (L2). The coiled-coil region mediates oligomerization, and both homooligomeric and heterooligomeric TRIMs have been described (7–13). Furthermore, many TRIM proteins form higher-order assemblies in vitro and form punctate or fibrous structures in cells (14–16). For example, TRIM5α assembly allows the protein to function as a cytosolic pattern-recognition receptor that can intercept the incoming capsids of diverse retroviruses, including HIV-1 (6). This results in species-specific "restriction" of viral replication (5), capsid dissociation (5, 6), and induction of innate immune responses (17). Retroviral capsids are recognized through a remarkable mechanism of multivalent pattern recognition. TRIM5α forms a homodimer (10, 11, 18), which can further assemble into a 2D lattice of linked hexagons (18). The hexagonal TRIM5α net matches the symmetry and spacing of the retroviral capsid surface lattice, thereby positioning multiple C-terminal B30.2/SPRY domains to interact with their repeating binding epitopes on the capsid.

Structures of isolated RING, B-box, and C-terminal domains of several TRIM proteins have been described, but the molecular details of TRIM oligomerization and high-order assembly have yet to be defined. Here, we report biochemical and crystallographic characterization of a coiled-coil-containing fragment of TRIM25. The crystallized construct forms a stable dimer in solution, and the structure reveals an elongated dimer composed of interdigitating hairpin-shaped subunits. We also present evidence that this dimer architecture is conserved across other TRIM family members, including TRIM5α. Finally, our studies allow us to assign the domain organization in the low-resolution EM reconstruction of the TRIM5α lattice (18) and thereby gain new insights into the mechanism of retroviral capsid pattern recognition.

## Results

**$TRIM25_{189–379}$ Forms an Elongated, Antiparallel Dimer.** We chose human TRIM25 for analysis because it lacks the propensity of TRIM5α to form high-order assemblies and is therefore more tractable biochemically. In initial experiments, we found that a series of coiled-coil-containing TRIM25 constructs, including the full tripartite motif and the full-length protein, behaved as single species during purification. All of these constructs eluted rapidly on gel filtration chromatographs, indicating they had elongated shapes and/or were oligomers. The shortest well-behaved construct spanned residues 189–379, which includes the entire coiled-coil region as well as the N-terminal half of the L2 linker region that connects the coiled-coil to the B30.2/SPRY domain (Fig. 1*A*). Analytical ultracentrifugation experiments revealed that this construct is a stable dimer (Fig. 1*C*; Fig. S1 *A–C*), implying that the full-length protein is also probably dimeric.

### Significance

Tripartite motif or TRIM proteins make up the largest superfamily of RING-domain E3 ubiquitin ligases. These enzymes function in a wide variety of important cellular processes, particularly innate antiviral response mechanisms. Dimerization is critical for the function of many TRIM proteins. Here we show how TRIM25 dimerizes and demonstrate that this dimerization mode is apparently conserved across the entire TRIM protein family. Our results reveal how the dimerization domain positions the other TRIM effector domains to recognize and ubiquitylate substrates and how the TRIM5 family can form higher-order hexagonal assemblies that increase the avidity of substrate recognition.

Author contributions: W.I.S. and O.P. designed research; J.G.S., K.O., V.C., J.M.W., and O.P. performed research; J.G.S., K.O., V.C., J.M.W., W.I.S., and O.P. analyzed data; and J.G.S., K.O., V.C., W.I.S., and O.P. wrote the paper.

The authors declare no conflict of interest.

This article is a PNAS Direct Submission. A.M. is a guest editor invited by the Editorial Board.

Data deposition: The atomic coordinates and structure factors have been deposited in the Protein Data Bank, www.pdb.org (PDB ID code 4LTB).

[1]J.G.S. and K.O. contributed equally to this work.

[2]To whom correspondence should be addressed. E-mail: opornillos@virginia.edu.

This article contains supporting information online at www.pnas.org/lookup/suppl/doi:10.1073/pnas.1318962111/-/DCSupplemental.

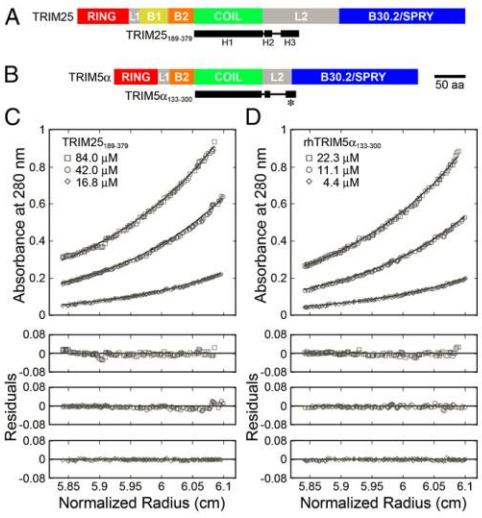


**Fig. 1.** Domain organization and dimerization of TRIM proteins. (*A*) Schematic of the domain structure of TRIM25. The principal domains and linker regions are RING (red), L1 (gray), B-box 1 (yellow), B-box 2 (orange), coiled-coil (green), L2 (gray), and B30.2/SPRY (blue). The TRIM25$_{189-379}$ construct used in this study is shown beneath (black), with the secondary structure derived from the crystal structure (rectangles represent helices). (*B*) Analogous schematic of the domain structure of TRIM5α. TRIM5α does not contain a B-box 1 domain and has a shorter L2. The TRIM5α$_{133-300}$ construct used in this study is shown beneath (black). The asterisk denotes a predicted helix (H3) that crosses from L2 into the B30.2 domain. (*C*) TRIM25$_{189-379}$ is a stable dimer in solution. Equilibrium sedimentation distributions of the indicated protein concentrations are shown for the rotor speed of 12,000 rpm. (*Upper*) Absorbance measurements (open symbols; 280 nm) and best-fit curves (solid lines). (*Lower*) Residual differences. Equilibrium distributions were also measured at rotor speeds of 17,000 and 23,000 rpm (not shown for clarity), and all of the data were globally fit to a single-species model in which the molecular weight ($M_{obs}$) was allowed to float ($M_{obs}$ = 41,674 Da; $M_{calc}$ = 21,835 Da; $M_{obs}/M_{calc}$ = 1.91). Fits in which the molecular weight was fixed to that of a dimer are shown in Fig. S1*A*. (*D*) TRIM5α$_{133-300}$ is also a stable dimer in solution ($M_{obs}$ = 43,505 Da; $M_{calc}$ = 23,038 Da; $M_{obs}/M_{calc}$ = 1.89). See Fig. S1*D* for fits to a single-species model with a fixed dimer molecular weight.

To determine the molecular basis for TRIM25 dimerization, we crystallized TRIM25$_{189\ 379}$ and determined its structure to 2.6 Å resolution (Fig. S2; Table S1; *Materials and Methods*). The asymmetric unit comprises a single, elongated dimer ~17 nm in length (Fig. 2). Each subunit in the symmetrical dimer folds back into a hairpin configuration with long and short arms. The elements annotated as the coiled-coil and L2 linker are structurally distinct, with the coiled-coil residues forming the long arm of each subunit (helix H1, colored green in Fig. 2*A*) and the L2 residues forming the short arm that folds back and packs against H1 (helices H2, H3, and an irregular but well-ordered intervening segment, colored gray). The two subunits dimerize intimately in an antiparallel orientation, similar to two interdigitated bobby pins (Fig. 2*B*). Almost all hydrophobic side-chains are involved in packing interactions, which occur along the entire length of each hairpin and bury a total surface area of 5,102 Å$^2$. Polar and charged side-chains also form numerous hydrogen bonding and salt bridge interactions.

TRIM proteins have been predicted to contain two distinct coiled-coil segments separated by a helical, but noncoil, segment (19, 20). The TRIM25 structure reveals that these segments actually make up a single contiguous coil, helix H1, which forms the long arm of each subunit. The dimeric H1–H1′ interaction is mediated by classic "knobs-into-holes" packing of both heptad repeats (wherein amino acid residue positions in each repeat are denoted by the letters *abcdefg*) and hendecad repeats (*abcdefghijk*) (Fig. 3; Fig. S2 *C* and *D*). Residues in the *h* positions of the hendecads also form "knobs-to-knobs" interactions (21). The repeats are arranged in a symmetric 7-7-7-7-11-11-11-11-7-7-7-7 pattern, which produces a supercoil that is canonically left-handed at the ends but is underwound and slightly right-handed in the middle. This unusual configuration likely explains why sequence analysis programs failed to predict H1 as a single, contiguous coil. The hendecads mediate interactions at the center of the coiled-coil, and superhelical underwinding allows H1 and H1′ to sit side by side and form an amphipathic platform. Here, the terminal H3 helices from the short arm of each hairpin pack against one side of the platform to form a 4-helix bundle. Thus, the structure indicates that both ensuing C-terminal B30.2 domains will be centrally located on the same side of the dimer.

**TRIM25 Dimerization Requires Hydrophobic Residues at the Center of the Coiled-Coil.** The central region of the coiled-coil platform (boxed in Fig. 3*A*, expanded in Fig. 3*B*) has a particularly high density of intermolecular interactions because of tight packing of the H1 helices against one another and against the H3 helices (Fig. 2). Key H1–H1′ interactions in this region include the Leu252 side-chain, which packs against Tyr245′, Met248′, Lys249′, and the symmetry equivalent Leu252′ in the apposing helix (Fig. 3*B*). This segment is further stabilized by salt bridges between the Lys249 and Asp253 side-chains and is flanked on either end by a buried hydrogen bond network (indicated by square brackets in Fig. 3*B*) involving the Tyr245 side-chain hydroxyl, a buried water molecule (orange sphere), Ser255 (H1′), Glu256 (H1′), Ser259 (H1′), Thr341 (H3′), and Gln356 (H3, not shown for clarity). This region therefore appears to be particularly important for dimer stability.

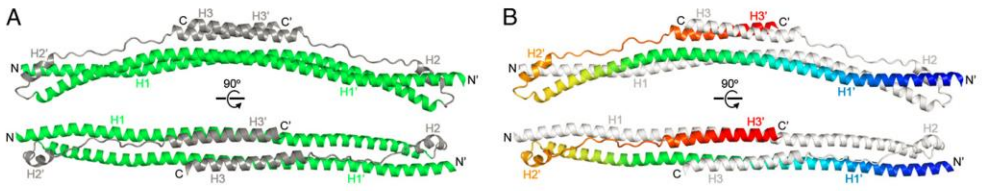


**Fig. 2.** Structure of the TRIM25$_{189-379}$ dimer. (*A*) Orthogonal views of the dimer in ribbons representation, with the coiled-coil and L2 segments colored in green and gray, respectively (matching the color scheme of Fig. 1). (*B*) Orthogonal views of the dimer with one subunit colored in rainbow gradient, with blue at the N terminus and red at the C terminus, and the other subunit in white.

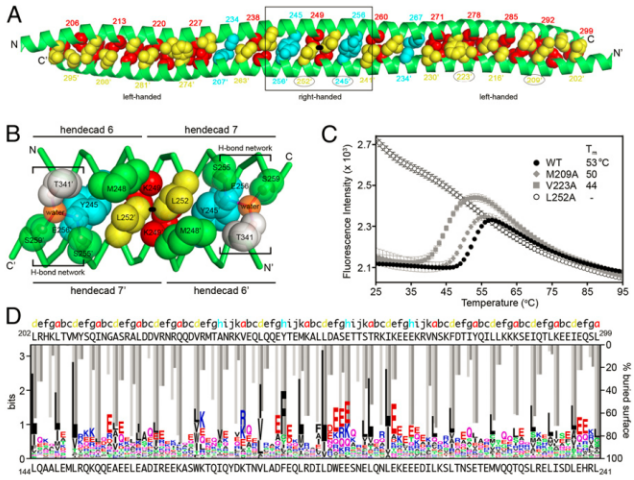


**Fig. 3.** Dimeric packing of TRIM coiled-coil helices. (*A*) Coiled-coil formed by the H1 and H1′ helices in the TRIM25$_{189–379}$ structure. Side-chains that mediate interhelix packing interactions are numbered and shown as spheres, with the *a*, *d*, and *h* positions colored in red, yellow, and cyan, respectively. Circled numbers indicate mutation sites analyzed in *C*. The dimer symmetry axis (black oval) runs perpendicular to the page. (*B*) Expanded view of the central region boxed in *A*. Side-chains that mediate important packing interactions are shown as spheres, colored as in *A* and labeled, as are buried water molecules (orange). (*C*) Thermofluor melting curves of wild-type (filled circles), L252A (open circles), M209A (filled diamonds), and V223A (filled squares). The high fluorescence signal for L252A at 25 °C indicates that the hydrophobic residues of this mutant are already exposed. Error bars represent the SDs from 4 replicates performed in parallel. (*D*) Structure-to-sequence alignment. The graph shows a multiple sequence alignment of 54 different human TRIM coiled-coil/L2 sequences displayed in logo format (see Fig. S4 for full alignment). The sequence alignment is overlaid with percentage buried surface area plots calculated using the entire TRIM25$_{189–379}$ structure (light gray bars) or the H1/H1′ helices only (dark gray bars). Heptad/hendecad residue assignments are color coded as in *A*. The TRIM25 sequence is shown at the top and the aligned TRIM5α sequence at the bottom, with the first and last residue numbers indicated.

Coiled-coils represent a special case of protein folding in which formation of the hydrophobic core is coupled to oligomerization (dimerization in this case). We therefore used differential scanning fluorescence thermal melting assays to examine the coupled folding/dimerization transition. In this assay, the signal comes from a dye that fluoresces on binding hydrophobic side-chains that become exposed as the protein unfolds with increasing temperature (22). As shown in Fig. 3*C* (filled circles), wild-type TRIM25$_{189\ 397}$ displayed a typical coiled-coil differential scanning fluorescence profile with a single transition and an apparent melting temperature ($T_m$) of 53 °C. Consistent with the structure, the L252A mutant was difficult to purify and did not display a sigmoidal melting curve, indicating it was already unfolded (or misfolded), even at 25 °C (Fig. 3*C*, open circles). The Y245A mutant was also apparently misfolded and could not even be purified. In contrast, two control proteins with alanine substitutions for completely buried residues elsewhere in H1 (M209A and V223A) were properly folded, albeit with reduced stability (Fig. 3*C*, gray symbols). These results confirm that the center of the coiled-coil helix is critical for proper folding of the TRIM25 dimer, perhaps making up the "trigger site" that directs coiled-coil formation (23–25).

This central region of TRIM25 is also where the terminal H3 helices pack to form the 4-helix bundle and contribute hydrophobic residues to the compact core. Unlike H1 mutants, however, alanine substitutions in buried hydrophobic H3 residues (T341A, L344A, and L348A) did not prevent TRIM25$_{189\ 379}$ coiled-coil formation (Fig. S3*A*). These results are consistent with the observation that TRIM5 protein dimerization requires only the coiled-coil domain and that both upstream (RING and B-boxes) and downstream (L2 equivalents and beyond) elements are dispensable (8, 19, 26, 27). Thus, even though the coiled-coil and L2 regions appear to form an integrated "domain" in our structure, the L2 segment is apparently not critical for dimerization and may be dynamic. Consistent with this idea, the average temperature factor for the short arm was 15% higher than the long arm in the native structure. In the selenomethionine crystal, one of the L2 arms had extremely poor density, likely because it had dissociated from the coiled-coil (Fig. S3*B*).

**The H1 Coiled-Coil Heptad/Hendecad Pattern Is Conserved in the TRIM Family.** The TRIM25 coiled-coil sequence diverges significantly from other human TRIM proteins (e.g., TRIM25 and TRIM5α share only ~10% sequence identity in this region). Nevertheless, our analysis of the human TRIM family using the secondary structure prediction program JPRED (28) indicated that the putative coiled-coil regions of most TRIM proteins are embedded within a contiguous helix of about 110 amino acids, consistent with the TRIM25 structure. To align these regions, we performed a structure-to-sequence comparison by first generating a multiple sequence alignment (MSA) of the coiled-coil regions of 54 different human TRIM family members (Fig. S4). The alignment revealed a pattern of conserved hydrophobic amino acids, with leucine being the most highly represented residue. We next calculated and plotted the percentage buried surface area (BSA) for each residue in the H1/H1′ portion of the TRIM25 structure (i.e., not including the L2 arms) and aligned this plot with the MSA. As shown in Fig. 3*D*, there is excellent correspondence between the pattern of conserved hydrophobic positions in the MSA plot and the *a*, *d*, and *h* positions that mediate formation of the H1/H1′ dimer (dark gray bars; see also Fig. S4). These results indicate that the unusual pattern

of heptad and hendecad repeats is conserved across the TRIM protein family and that the structures of other dimeric TRIM coiled-coils likely resemble the TRIM25 structure.

We also calculated a BSA plot for the entire structure (Fig. 3*D*, light gray bars). Comparison of the two BSA plots revealed that packing of the long and short arms of the TRIM25 subunits is mediated by H1 residues in the *c*, *g*, and *k* positions. Importantly, these residues are also conserved in the MSA, particularly at the center of the dimer (e.g., Glu244, Met248, Leu251). These results indicate that the hairpin configuration of the subunits and the central 4-helix bundle are also likely to be conserved.

**TRIM5α and TRIM25 Have Similar Dimer Architectures.** The 17-nm length of the $TRIM25_{189\ 379}$ dimer corresponds almost exactly to the length of each edge of the assembled TRIM5α hexagon (18), suggesting that the TRIM25 structure can also inform our understanding of the TRIM5α hexagonal lattice. Intermolecular disulfide bond formation was used to probe and compare the structures of the TRIM25 and TRIM5α dimers in solution. The $TRIM25_{189\ 379}$ crystal structure was analyzed using a disulfide prediction program (29) to identify three pairs of residues that are in close proximity in the dimer and are predicted to form intermolecular disulfides when mutated into cysteines (Fig. 4*A*). Two of the designed disulfides, A216C/K285C and A234C/E267C, probe for packing and phase of the H1/H1′ helices (i.e., antiparallel coiled-coil formation), and the third, S195C/L308C, probes for packing of H1 in one subunit against H2 in the other subunit (i.e., the fold-back configuration). These disulfide bonds collectively sample the entire length of the dimer (Fig. 4*A*).

As shown in Fig. 4*B*, all three double-cysteine mutant $TRIM25_{189\ 379}$ proteins behaved as designed. Each formed intermolecular disulfide crosslinks very efficiently under nonreducing conditions and migrated exclusively as crosslinked dimers on a denaturing polyacrylamide gel (lanes 7, 9, and 11). In contrast, three negative controls that contained scrambled pairs of cysteines migrated almost exclusively as monomers under the same conditions (Fig. 4*B*, even-numbered lanes). Thus, disulfide crosslinking can be used as a sensitive probe of the dimeric conformation of TRIM25.

Analogous disulfide crosslinking experiments were performed on rhesus $TRIM5\alpha_{133\ 300}$ to test whether the TRIM5α protein also adopts a similar dimeric structure. Equilibrium sedimentation distributions of the wild-type $TRIM5\alpha_{133\ 300}$ fit well to a single-species dimer model, confirming that this region was sufficient for dimerization (Fig. 1*D*; Fig. S1 *D–F*). Three pairs of $TRIM5\alpha_{133\ 300}$ cysteine mutants were then created in positions that were equivalent to the three crosslinking pairs of $TRIM25_{189\ 379}$ (colored dots in Fig. S4). As shown in Fig. 4*C*, these $TRIM5\alpha_{133\ 300}$ Cys pairs also formed intermolecular disulfides efficiently (lanes 7, 9, and 11), although the A137C/L249C disulfide crosslink formed somewhat less efficiently than did the A158C/T227C and I176C/E209C crosslinks, suggesting that H2 may not reside in precisely the same position in TRIM25 and TRIM5α. The crosslinks were judged to be stable because the proteins migrated almost exclusively as dimers, even after extended incubation under mildly reducing conditions (2 mM β-mercaptoethanol), consistent with the favorable disulfide geometries predicted by the homology model. We therefore conclude that TRIM5α and TRIM25 form dimers of similar structure.

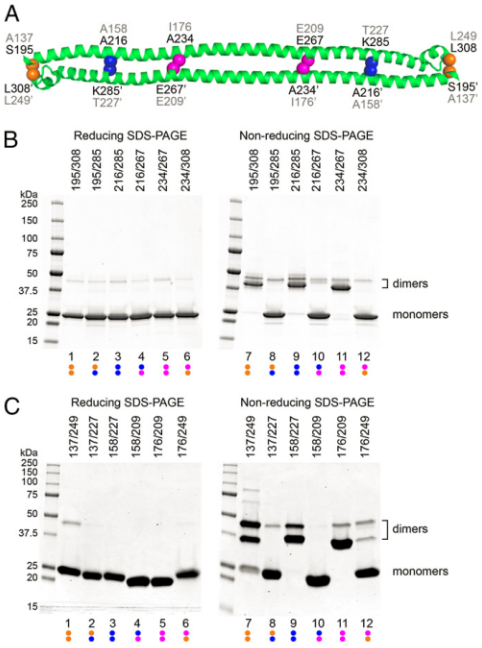


**Fig. 4.** Disulfide crosslinking of TRIM25 and TRIM5α dimers. (*A*) H1 and H2 regions of the $TRIM25_{189–379}$ structure showing positions of residue pairs chosen for cysteine mutagenesis. Equivalent TRIM25 and TRIM5α residues are labeled in black and gray, respectively. (*B*) Electrophoretic profiles of purified $TRIM25_{189–379}$ double-cysteine mutants that were dialyzed under nonreducing conditions, then denatured in SDS-PAGE buffer under reducing (*Left*) or nonreducing (*Right*) conditions. Molecular weight marker positions are labeled on the left. Positions of monomers and crosslinked dimers are labeled on the right. Note that the symmetric dimer is expected to produce two types of intermolecular disulfide-crosslinked species: one in which both cysteine pairs are oxidized (lower bands) and another in which one of the pairs is reduced (upper bands). Data are representative of 3 independent experiments. (*C*) Profiles of rhesus $TRIM5\alpha_{133–300}$ cysteine mutants that were dialyzed under mildly reducing conditions and then prepared for SDS-PAGE, as described for $TRIM25_{189–379}$. Data are representative of 3 independent experiments.

## Discussion

**Mechanistic Implications for TRIM25-Mediated Polyubiquitylation of RIG-I.** TRIM25 is an established effector of the RIG-I signaling pathway, which mediates the intracellular innate immune response to RNA viruses. TRIM25 recognizes and catalyzes Lys63-linked polyubiquitylation of the RIG-I/viral RNA recognition complex, thereby activating downstream effectors in the pathway and establishing an antiviral state (3). RIG-I/viral RNA complexes are recognized by the C-terminal B30.2 domain of TRIM25 (3, 30), and ubiquitin transfer is facilitated by the N-terminal RING domain, in cooperation with a ubiquitin E2 ligase. Our structure indicates that in the full-length TRIM25 dimer, the two catalytic RING domains will be separated by at least 17 nm at either end of the elongated dimer (Fig. S5). In this geometry, the two RING domains within one TRIM25 dimer probably could not cooperate during catalysis, at least not in the same manner as well-characterized cooperative homodimeric RING domains such as RNF4 (31) or BIRC7 (32). As illustrated in Fig. S5, the fold-back configuration of the TRIM25 subunits explains how the RING domains can approach the B30.2 domains to enable RIG-I ubiquitylation. It is likely, however, that there is a more precise positioning mechanism than we can currently describe, as TRIM25 has been shown to modify RIG-I at a specific lysine residue (3, 30). We speculate that dynamics of the L2 arm (including possibly the L2 region that is missing from

our structure) and other factors (33, 34) may make important contributions in this regard. In addition, RNA-bound RIG-I has been shown to dimerize (35). It will therefore be interesting to learn whether both subunits of the TRIM25 dimer can engage both subunits of the RIG-I dimer simultaneously.

**Implications for Dimerization of the Tripartite Motif.** Our analysis indicates that TRIM25 is likely to be an obligate dimer. Furthermore, the distinctive 7-7-7-7-11-11-11-11-7-7-7-7 pattern of heptad and hendecad repeats in the TRIM25 coiled-coil appears to be conserved, and we speculate that it may be a "signature" of the TRIM family. Studies of dimeric coiled-coils have shown that short sequence elements or "trigger sites" of 7–14 amino acids are critically important for proper folding because they are the first segments to become helical, and therefore nucleate dimerization (23–25). Once the initial dimer contact is established, the peripheral residues then "zip up" to form the fully folded coiled-coil. This general model implies that associating helices, whether homodimeric or heterodimeric, must have compatible trigger sites. Our structural and mutational analyses indicate that the center of the H1 helix is likely to be the TRIM25 coiled-coil trigger site. This element includes Tyr245 and Leu252 (hendecads 6 and 7) and is flanked by polar residues that form a buried hydrogen bond network (Fig. 3*B*). It is likely that these buried polar interactions help to define pairing specificity and helix packing registry in TRIM proteins, as has been seen in SNARE coiled-coil complexes (36). Our sequence analysis indicates that almost every human TRIM protein has a unique central sequence, although there is conservation within the same branches of the TRIM family tree (Fig. S4). This likely explains why TRIM proteins apparently do not form heterodimers promiscuously and why reports of TRIM heterodimerization generally involve closely related TRIM proteins (7, 9, 12, 13).

**Implications for Dimerization and High-Order Assembly of TRIM5α.** Our structural and biochemical data establish that the coiled-coil and L2 regions of TRIM25 and TRIM5α form similar structures. We have therefore used the TRIM25 structure to interpret the protein density seen in the 2D cryoEM reconstruction of the assembled TRIM5α hexagonal lattice (18) (Fig. 5). This analysis indicates that each edge of the TRIM5α hexagon corresponds to a single coiled-coil dimer (each 17 nm in length). This interpretation, in turn, implies that the threefold symmetric densities observed at each vertex correspond to the N-terminal RING and B-box 2 domains and that the twofold symmetric densities at the midpoint of each hexagon edge correspond to the B30.2/SPRY domains (18) (Fig. 5*A*). These assignments are consistent with the known requirement for the B-box 2 domain in high-order TRIM5α assembly (18, 37, 38) and could also explain how assembly can activate the RING domains by bringing them into close proximity, consistent with the observation that capsid binding enhances E3 ligase activity (17). We envision two possible subunit configurations for the hexagonal lattice, which differ in domain connectivity at the local threefold vertex (Fig. S6). In one configuration, the intact dimers would interact at the vertex through the RING, B-box 2, and/or ends of the coiled-coil. In the alternative configuration, the associated coiled-coil dimers would "swap" arms in a fashion reminiscent of clathrin triskelion assembly (39). We cannot yet unambiguously discriminate between these different possible assembly modes but note that domain swapping would provide a mechanism for autoinhibition, and thereby prevent unregulated assembly, and would be consistent with recent studies indicating that the L2 linker plays an important role in high-order TRIM5α assembly (40, 41).

Our domain assignments, together with the density distribution in the EM map of the TRIM5α lattice, further suggest that the B30.2 domain may interact with the coiled-coil. The sequences of TRIM5α and TRIM25 diverge considerably beyond

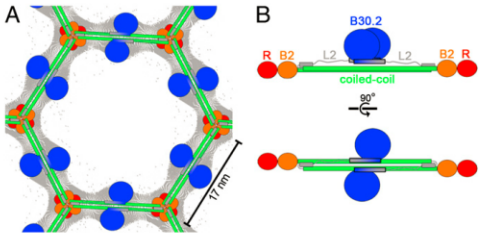


**Fig. 5.** Models of quaternary TRIM5α interactions. (*A*) Schematic model of the TRIM5α hexagonal lattice, showing the deduced positions of the different domains and overlaid with the cryoEM projection map (gray contours) (18). Domains are colored as in Fig. 1*B*. (*B*) Schematic model of the full-length TRIM5α dimer. The C-terminal B30.2 domains (blue) are shown packed against one side of the coiled-coil domain via a putative extended H3 helix (colored in gray to blue gradient and outlined in black) that spans both L2 and B30.2 sequences and forms a 4-helix bundle with the coiled-coil, as seen in the TRIM25 structure.

the short-arm H2 helix, but secondary structure algorithms predict an α-helix at the TRIM5α L2/B30.2 boundary (residues 283–300) that is equivalent in position to TRIM25 H3 (asterisks in Fig. 1*B* and Fig. S7). Interestingly, residues 291–300 of rhesus TRIM5α (colored in blue and boxed in Fig. S7) do indeed form a helix in two independent crystal structures of the isolated B30.2 domain (42, 43), although the immediately preceding residues (287–290) adopt a nonhelical loop configuration with high temperature factors in one of the structures (43). These observations lead us to speculate that the N-terminal helix of the TRIM5α B30.2 domain (or the longer, predicted helix) may pack against the center of the upstream coiled-coil to form a 4-helix bundle, as seen in the TRIM25 structure. In support of this idea, alanine substitutions of surface-exposed residues on the TRIM5α B30.2 helix (Arg297, Arg298, and Tyr299) impair both restriction activity and capsid binding. These residues are far removed from the capsid-binding surface (44) but could mediate interaction of the TRIM5α B30.2 domain against its coiled-coil. Such interactions would not only position the B30.2 domains on the same side of the dimer but also possibly define their spacing and orientation, as has been postulated to be a "minimum design feature" of retroviral capsid restriction factors (45). Consistent with this general idea, residues within the TRIM5α coiled-coil domain are under positive selection (46, 47), implying they can influence capsid recognition, and the coiled-coil itself may be a determinant of binding specificity (47).

In summary, we propose that the tripartite motif coiled-coil has a conserved structure and a conserved scaffolding function that organizes the biochemical activities of TRIM proteins, thereby facilitating selective substrate polyubiquitylation by TRIM25 and capsid pattern recognition by TRIM5α. Thus, the TRIM domains are organized spatially, consistent with the idea that they have coevolved and behave as an integrated module, rather than as a collection of independent functional elements (14, 20, 48).

## Materials and Methods

**Construct Design, Protein Purification, and Characterization.** $TRIM25_{189–379}$ and $TRIM5α_{133–300}$ protein expression constructs, purification protocols, analytical ultracentrifugation analyses, and $TRIM25_{189–379}$ crystallization and structure determination are described in *SI Materials and Methods*.

**Sequence and Structure Analysis.** Sequences aligned in Fig. 3*D* started from the last zinc-coordinating pair of the B-box 2 domain (typically His-X-X-His) and spanned the subsequent 130 residues. Sixty-seven members of the human TRIM family (table 1 in ref. 20), excluding TRIM25, were initially used to generate a multiple sequence alignment with the ClustalW2 program.

Duplicates and sequences with gaps of 3 or more residues within H1 were removed, resulting in a final alignment of 54 sequences (Fig. S4). To facilitate structure-to-sequence comparisons, a consensus sequence plot was generated using the Weblogo program (49), total buried surface areas for each residue in the TRIM25 structure were calculated using the PISA Web server (50), and the Weblogo and buried surface area plots were aligned manually.

**Differential Scanning Fluorimetry.** Thermofluor melting assays (22) were performed with a Bio-Rad CFX96 thermal cycler. Proteins in crystallization buffer were mixed with a 1:400 dilution of "10,000×" SYBR Safe dye (Invitrogen). Final protein concentrations were 2 mg/mL, except for the L252A and L348A mutants, which were 1 mg/mL and 2.6 mg/mL, respectively. Samples were held at 20 °C for 5 min, and the temperature was then raised to 100 °C in 1 °C increments every 15 s, taking fluorescence readings at each increment. Each sample was set up in 4 replicates, and melting curves for each protein were determined at least twice, with independent protein preparations. $T_m$ was determined from the maximum of the first derivative of the melting curve. The maximal variation in wild-type TRIM25$_{189–379}$ $T_m$ was <1 °C in seven independent determinations.

**Crosslinking Analysis.** Double-cysteine mutant proteins were reduced by dilution to 30 μM in reducing buffer [50 mM Tris at pH 8.0, 150 mM NaCl, 20 mM β-mercaptoethanol (βME)] and then dialyzed overnight at 4 °C into the same buffer containing 0 mM (TRIM25) or 2 mM (TRIM5α) βME to allow formation of stable disulfide crosslinks. Aliquots were then mixed with the same volume of 2× SDS-PAGE sample buffer containing either 1 M βME (reducing) or no additional βME (nonreducing), incubated for 5 min at 99 °C in a dry bath and immediately analyzed by SDS-PAGE with Coomassie blue staining.

**ACKNOWLEDGMENTS.** We thank Barbie Ganser-Pornillos, Chris Hill, and members of the O.P. and W.I.S. laboratories for critical reading of the manuscript; Ed Campbell for helpful discussions; Kate Skorupka and Peter Horanyi for technical support; Debra Eckert and Steve Alam for assistance with the equilibrium sedimentation analyses. We also thank an anonymous reviewer for helpful suggestions on the analysis of the helical repeats in the antiparallel coiled-coil. This project was supported by a Research and Development grant from the University of Virginia School of Medicine (to O.P.) and National Institutes of Health Grant P50 GM082545 (to W.I.S.). J.G.S. is supported by a predoctoral Cell and Molecular Biology Training Grant from the National Institutes of Health (T32 GM008136). K.O. participated in this study while on leave from Jagiellonian University, Krakow, Poland.

1. Han K, Lou DI, Sawyer SL (2011) Identification of a genomic reservoir for new TRIM genes in primate genomes. *PLoS Genet* 7(12):e1002388.
2. McNab FW, Rajsbaum R, Stoye JP, O'Garra A (2011) Tripartite-motif proteins and innate immune regulation. *Curr Opin Immunol* 23(1):46–56.
3. Gack MU, et al. (2007) TRIM25 RING-finger E3 ubiquitin ligase is essential for RIG-I-mediated antiviral activity. *Nature* 446(7138):916–920.
4. Oshiumi H, Matsumoto M, Seya T (2012) Ubiquitin-mediated modulation of the cytoplasmic viral RNA sensor RIG-I. *J Biochem* 151(1):5–11.
5. Stremlau M, et al. (2004) The cytoplasmic body component TRIM5α restricts HIV-1 infection in Old World monkeys. *Nature* 427(6977):848–853.
6. Grütter MG, Luban J (2012) TRIM5 structure, HIV-1 capsid recognition, and innate immune signaling. *Curr Opin Virol* 2(2):142–150.
7. Centner T, et al. (2001) Identification of muscle specific ring finger proteins as potential regulators of the titin kinase domain. *J Mol Biol* 306(4):717–726.
8. Short KM, Cox TC (2006) Subclassification of the RBCC/TRIM superfamily reveals a novel motif necessary for microtubule binding. *J Biol Chem* 281(13):8970–8980.
9. Li X, et al. (2007) Unique features of TRIM5α among closely related human TRIM family members. *Virology* 360(2):419–433.
10. Kar AK, Diaz-Griffero F, Li Y, Li X, Sodroski J (2008) Biochemical and biophysical characterization of a chimeric TRIM21-TRIM5α protein. *J Virol* 82(23):11669–11681.
11. Langelier CR, et al. (2008) Biochemical characterization of a recombinant TRIM5α protein that restricts human immunodeficiency virus type 1 replication. *J Virol* 82(23):11682–11694.
12. Herquel B, et al. (2011) Transcription cofactors TRIM24, TRIM28, and TRIM33 associate to form regulatory complexes that suppress murine hepatocellular carcinoma. *Proc Natl Acad Sci USA* 108(20):8212–8217.
13. Napolitano LM, Meroni G (2012) TRIM family: Pleiotropy and diversification through homomultimer and heteromultimer formation. *IUBMB Life* 64(1):64–71.
14. Reymond A, et al. (2001) The tripartite motif family identifies cell compartments. *EMBO J* 20(9):2140–2151.
15. Javanbakht H, Diaz-Griffero F, Stremlau M, Si Z, Sodroski J (2005) The contribution of RING and B-box 2 domains to retroviral restriction mediated by monkey TRIM5α. *J Biol Chem* 280(29):26933–26940.
16. Campbell EM, et al. (2007) TRIM5 α cytoplasmic bodies are highly dynamic structures. *Mol Biol Cell* 18(6):2102–2111.
17. Pertel T, et al. (2011) TRIM5 is an innate immune sensor for the retrovirus capsid lattice. *Nature* 472(7343):361–365.
18. Ganser-Pornillos BK, et al. (2011) Hexagonal assembly of a restricting TRIM5α protein. *Proc Natl Acad Sci USA* 108(2):534–539.
19. Javanbakht H, et al. (2006) Characterization of TRIM5α trimerization and its contribution to human immunodeficiency virus capsid binding. *Virology* 353(1):234–246.
20. Sardiello M, Cairo S, Fontanella B, Ballabio A, Meroni G (2008) Genomic analysis of the TRIM family reveals two groups of genes with distinct evolutionary properties. *BMC Evol Biol* 8:225.
21. Brown JH, Cohen C, Parry DA (1996) Heptad breaks in alpha-helical coiled coils: Stutters and stammers. *Proteins* 26(2):134–145.
22. Matulis D, Kranz JK, Salemme FR, Todd MJ (2005) Thermodynamic stability of carbonic anhydrase: Measurements of binding affinity and stoichiometry using ThermoFluor. *Biochemistry* 44(13):5258–5266.
23. Kammerer RA, et al. (1998) An autonomous folding unit mediates the assembly of two-stranded coiled coils. *Proc Natl Acad Sci USA* 95(23):13419–13424.
24. Kammerer RA, et al. (2001) An intrahelical salt bridge within the trigger site stabilizes the GCN4 leucine zipper. *J Biol Chem* 276(17):13685–13688.
25. Steinmetz MO, et al. (2007) Molecular basis of coiled-coil formation. *Proc Natl Acad Sci USA* 104(17):7062–7067.
26. Mische CC, et al. (2005) Retroviral restriction factor TRIM5α is a trimer. *J Virol* 79(22):14446–14450.
27. Perez-Caballero D, Hatziioannou T, Yang A, Cowan S, Bieniasz PD (2005) Human tripartite motif 5α domains responsible for retrovirus restriction activity and specificity. *J Virol* 79(14):8969–8978.
28. Cole C, Barber JD, Barton GJ (2008) The Jpred 3 secondary structure prediction server. *Nucleic Acids Res* 36(Web Server issue):W197–201.
29. Dombkowski AA (2003) Disulfide by Design: A computational method for the rational design of disulfide bonds in proteins. *Bioinformatics* 19(14):1852–1853.
30. Gack MU, et al. (2008) Roles of RIG-I N-terminal tandem CARD and splice variant in TRIM25-mediated antiviral signal transduction. *Proc Natl Acad Sci USA* 105(43):16743–16748.
31. Plechanovová A, Jaffray EG, Tatham MH, Naismith JH, Hay RT (2012) Structure of a RING E3 ligase and ubiquitin-loaded E2 primed for catalysis. *Nature* 489(7414):115–120.
32. Dou H, Buetow L, Sibbet GJ, Cameron K, Huang DT (2012) BIRC7-E2 ubiquitin conjugate structure reveals the mechanism of ubiquitin transfer by a RING dimer. *Nat Struct Mol Biol* 19(9):876–883.
33. Liu HM, et al. (2012) The mitochondrial targeting chaperone 14-3-3ε regulates a RIG-I translocon that mediates membrane association and innate antiviral immunity. *Cell Host Microbe* 11(5):528–537.
34. Kwon SC, et al. (2013) The RNA-binding protein repertoire of embryonic stem cells. *Nat Struct Mol Biol* 20(9):1122–1130.
35. Feng M, et al. (2013) Structural and biochemical studies of RIG-I antiviral signaling. *Protein Cell* 4(2):142–154.
36. Fasshauer D, Sutton RB, Brunger AT, Jahn R (1998) Conserved structural features of the synaptic fusion complex: SNARE proteins reclassified as Q- and R-SNAREs. *Proc Natl Acad Sci USA* 95(26):15781–15786.
37. Diaz-Griffero F, et al. (2009) A B-box 2 surface patch important for TRIM5α self-association, capsid binding avidity, and retrovirus restriction. *J Virol* 83(20):10737–10751.
38. Li X, Sodroski J (2008) The TRIM5α B-box 2 domain promotes cooperative binding to the retroviral capsid by mediating higher-order self-assodation. *J Virol* 82(23):11495–11502.
39. Fotin A, et al. (2004) Molecular model for a complete clathrin lattice from electron cryomicroscopy. *Nature* 432(7017):573–579.
40. Sastri J, et al. (2010) Identification of residues within the L2 region of rhesus TRIM5α that are required for retroviral restriction and cytoplasmic body localization. *Virology* 405(1):259–266.
41. Li X, Yeung DF, Fiegen AM, Sodroski J (2011) Determinants of the higher order association of the restriction factor TRIM5α and other tripartite motif (TRIM) proteins. *J Biol Chem* 286(32):27959–27970.
42. Biris N, et al. (2012) Structure of the rhesus monkey TRIM5α PRYSPRY domain, the HIV capsid recognition module. *Proc Natl Acad Sci USA* 109(33):13278–13283.
43. Yang H, et al. (2012) Structural insight into HIV-1 capsid recognition by rhesus TRIM5α. *Proc Natl Acad Sci USA* 109(45):18372–18377.
44. Sebastian S, et al. (2009) An invariant surface patch on the TRIM5α PRYSPRY domain is required for retroviral restriction but dispensable for capsid binding. *J Virol* 83(7):3365–3373.
45. Yap MW, Mortuza GB, Taylor IA, Stoye JP (2007) The design of artificial retroviral restriction factors. *Virology* 365(2):302–314.
46. Sawyer SL, Wu LI, Emerman M, Malik HS (2005) Positive selection of primate TRIM5α identifies a critical species-specific retroviral restriction domain. *Proc Natl Acad Sci USA* 102(8):2832–2837.
47. Maillard PV, Ecco G, Ortiz M, Trono D (2010) The specificity of TRIM5 α-mediated restriction is influenced by its coiled-coil domain. *J Virol* 84(11):5790–5801.
48. Meroni G, Diez-Roux G (2005) TRIM/RBCC, a novel class of 'single protein RING finger' E3 ubiquitin ligases. *Bioessays* 27(11):1147–1157.
49. Crooks GE, Hon G, Chandonia JM, Brenner SE (2004) WebLogo: A sequence logo generator. *Genome Res* 14(6):1188–1190.
50. Krissinel E, Henrick K (2007) Inference of macromolecular assemblies from crystalline state. *J Mol Biol* 372(3):774–797.

BIOCHEMISTRY

# Supporting Information

Sanchez et al. 10.1073/pnas.1318962111

## SI Materials and Methods

**Construct Design and Protein Expression.** Human tripartite motif 25 (TRIM25) was subcloned from a plasmid kindly provided by Dong-Er Zhang (University of California, San Diego, La Jolla, CA) (Addgene plasmid 12449) (1). Rhesus TRIM5α (GI: 44890114) was subcloned from a pLPCX/TRIM5α-HA plasmid kindly provided by Joseph Sodroski (Harvard University, Cambridge, MA) (2). $TRIM25_{189\ 379}$ and $TRIM5\alpha_{133\ 300}$ were expressed from pET24a-derived vectors (3) with $His_6$-tagged SUMO leader sequences (Table S2). Asp85 in the SUMO coding region of the TRIM5α vectors was mutated to serine to destroy a Shine-Dalgarno-like sequence that caused a nearby Ile to be used as an alternative start site for translation. Residue pairs for cysteine mutagenesis were selected with the program Disulfide-by-Design (4). The cysteine mutants were generated by PCR-based mutagenesis (Table S2). Proteins were expressed in *Escherichia coli* BL21(DE3) (TRIM25) or Rosetta(DE3) pLysS (TRIM5α), using the autoinduction method as described (5), except that the cultures were grown at 37 °C until saturation and then at 18–19 °C for 16 h.

**Purification of $TRIM25_{189–379}$.** Cells expressing $TRIM25_{189\ 379}$ from 1 L of culture were resuspended in 30 mL lysis buffer [50 mM Tris at pH 9.0, 0.3 M NaCl, 20 mM β-mercaptoethanol (βME)] supplemented with 2 mM phenylmethylsulfonylfluoride. Cells were lysed using a microfluidizer (Microfluidics model M110P) at 20,000 psi chamber pressure. Cell debris was removed by centrifugation (45,000 × *g* for 45 min at 4 °C). Filtered supernatant was incubated in a gravity flow chromatography column with 10 mL Ni-NTA resin (Qiagen) for 1 h on a rocker at 4 °C. The resin was washed with 150 mL lysis buffer, followed by 500 mL wash buffer (25 mM Tris at pH 8.0, 0.1 M NaCl, 10 mM βME, 20 mM imidazole). Bound protein was eluted in wash buffer containing 400 mM imidazole. Ulp1 protease was added to the pooled fractions (~1:100 mass ratio), and the sample was dialyzed overnight at 4 °C against cleavage buffer (25 mM Hepes at pH 7.0, 20 mM NaCl, 10 mM βME). The sample was applied to a 5-mL HiTrap SP FF column (GE Healthcare) and eluted with a linear salt gradient (0.02–1 M NaCl) in cleavage buffer. Pooled fractions were concentrated to ~3 mL and purified to homogeneity on a HiLoad 16/600 Superdex 75 gel filtration column (GE Healthcare) in crystallization buffer (10 mM Tris at pH 8.0, 0.1 M NaCl). Selenomethionine-labeled protein was purified in the same manner except that the final buffer contained 10 mM βME. The pure proteins were concentrated to ~18 mg/mL, flash-frozen in liquid nitrogen, and stored at −80 °C. The mass of freshly purified wild-type protein was determined by electrospray ionization mass spectrometry to be 21,832 Da (expected mass from sequence, 21,835 Da). Typical yields for the wild-type protein were ~5 mg/L culture. Flash-freezing or long-term incubation in solution induced a minor fraction of the protein to form an SDS-resistant 40-kDa (dimer) species (e.g., see Fig. 4*B*, lanes 1–12). Cysteine mutants were purified in the same manner as wild-type, except that 20 mM βME was added to all buffers. All cysteine mutants displayed the same elution behavior as wild-type during size-exclusion chromatography.

**Purification of $TRIM5\alpha_{133–300}$.** Cells expressing $TRIM5\alpha_{133\ 300}$ from 1 L of culture were collected and resuspended in 100 mL lysis buffer (100 mM Hepes at pH 8, 1 M LiCl, 300 mM NaCl, 30 mM imidazole) supplemented with 0.5% Triton X-100, 5% glycerol, 1 tablet cOmplete EDTA-free protease inhibitors (Roche), and 10 μg/mL DNase I (Roche). Cells were lysed by freeze-thaw and sonication (Qsonica; 2 min at 80% amplitude on ice). The lysate was clarified by centrifugation (37,000 × *g* for 45 min at 4 °C), and the 0.45-μm-filtered supernatant was incubated with 4 mL cOmplete His-tag purification resin (Roche) for 1 h with rocking. The resin was washed with 200 mL lysis buffer and 200 mL protease cleavage buffer (50 mM Tris at pH 8, 500 mM NaCl, 5% glycerol), eluted in 50 mL elution buffer (50 mM Tris at pH 8, 500 mM NaCl, 5% glycerol, 1.125 M imidazole), and dialyzed for 12 h against two changes of 2 L each of protease cleavage buffer supplemented with 0.5 mM EDTA. The sample was diluted fivefold in 50 mM Tris at pH 8, 0.5 mM EDTA, 1 mM TCEP, and the $His_6$-SUMO tag was removed by incubating with 3 mg Ulp1 protease for 6 h at 23 °C. The sample was loaded onto two 5 mL HiTrap Q HP columns (GE Healthcare) connected in series and eluted with a 100-mL linear NaCl gradient (0.05–1 M). The protein eluted in two distinct peaks, which we speculate correspond to dimers and monomers, as previously observed for longer TRIM5 constructs (6). Both peaks were pooled, concentrated, loaded on a HiLoad 16/600 Superdex 75 gel filtration column (GE Healthcare), and eluted in size-exclusion buffer (50 mM Tris at pH 8, 150 mM NaCl, 1 mM TCEP). Fractions from the major peak (corresponding to the protein dimer) were pooled and concentrated to 1 mg/mL. The average mass of the purified protein was determined by electrospray ionization mass spectrometry to be 20,236 Da (expected mass from sequence, 20,238 Da). Typical yields for the wild-type protein were ~15 mg/L culture. Cysteine mutants were purified in the same way as wild-type except that 1 mM TCEP was added to all buffers. All mutants displayed the same elution behavior as wild-type during size-exclusion chromatography.

**Analytical Ultracentrifugation.** Equilibrium sedimentation experiments were performed at 4 °C, using a Beckman Optima XL-I centrifuge, at rotor speeds of 12,000, 17,000, and 23,000 rpm. For each speed, three protein concentrations were tested (16.8, 42, and 84 μM for $TRIM25_{189\ 379}$ and 4.4, 11.1, and 22.3 μM for $TRIM5\alpha_{133\ 300}$), and each centrifugation run was performed for 24 h to reach equilibrium. TRIM25 samples were in 10 mM Hepes at pH 7.4, 40 mM NaCl, 0.5 mM TCEP. TRIM5α samples were in 50 mM Tris at pH 8, 150 mM NaCl, 1 mM TCEP. Nonlinear least-squares data fitting was performed using the Heteroanalysis software (7). Solvent density and protein partial-specific volumes were calculated with the program SEDNTERP (8). The same analyses were also performed with a TRIM25 construct that contained two additional tryptophan residues to access lower loading concentrations (6.5, 16.2, and 32.3 μM), and the results were the same.

**Crystallization and Data Collection.** Crystals of native $TRIM25_{189\ 379}$ were obtained at 17 °C in sitting drops that were set up as a 1:1:1 mix of protein solution, water, and precipitant (6–12% PEG 4,000 at pH 5.3–6.6, 10 mM sodium acetate). Selenomethionine-labeled crystals were obtained in the same manner except that the precipitant solution was 16% PEG 3,350, 80 mM Bis-Tris propane at pH 8.8, and 20 mM citric acid. Crystals were cryoprotected in mother liquor containing 25% PEG 400. The protein crystallized in at least 4 distinct space groups within the same drop, and the diffraction quality was highly variable, with most crystals diffracting poorly. After extensive screening, a native data set extending to 2.6 Å resolution ($I/\sigma \geq 2$ criterion) and anomalous Se data extending to 3.2 Å were collected at Advanced Photon Source beamline 22-ID. Diffraction data were

processed using HKL2000 (9). Data statistics are reported in Table S1.

**Structure Determination.** $TRIM25_{189\text{–}379}$ structure determination, model building, and initial refinement were performed with the AutoSol, AutoMR, and AutoBuild Wizards of the PHENIX suite (version 1.8.2–1309) (10). The Se and native data both indexed as $P2_12_12_1$, but with different unit cell dimensions (Table S1). Each had one dimer in the asymmetric unit, which packed in different ways. The initial structure was determined by single-wavelength anomalous dispersion from the Se derivative. The coiled-coil region of this structure was partially built and refined mostly as a polyalanine model (Fig. S2*A*). Further refinement of this crystal form was not continued because one of the L2 arms had extremely poor density, likely because it had dissociated from the coiled-coil (Fig. S3*B*). The partially built structure was used as a molecular replacement search model to phase the native data (Fig. S2B). Automated model building/rebuilding and refinement against the 2.6 Å native data resulted in a model that was about 80% complete. The rest of the model was built manually using the program Coot (11). To take advantage of the twofold improvement in data-to-parameter ratio afforded by noncrystallographic symmetry while taking into account the flexibility of the subunits, residues were binned into 16 noncrystallographic symmetry segments and equivalent sections were restrained to match each other [approach adapted from ref. 12; see Protein Data Bank (PDB) file header for details on the binned segments]. Multiple rounds of refinement (phenix.refine; version 1.8.2-dev-1427) and manual model building resulted in good geometry and $R/R_{\text{free}}$ of 0.20/0.26 (Table S1). The final model consists of amino acid residues 190–360 for both chains in the dimer. Density was lacking for residues 189 and 361–379, which were not included in the final model. Model validation with Molprobity (13) was performed throughout the structure refinement process. Coordinates and structure factors have been deposited in the PDB under accession code 4LTB.


1. Zou W, Zhang DE (2006) The interferon-inducible ubiquitin-protein isopeptide ligase (E3) EFP also functions as an ISG15 E3 ligase. *J Biol Chem* 281(7):3989–3994.
2. Javanbakht H, Diaz-Griffero F, Stremlau M, Si Z, Sodroski J (2005) The contribution of RING and B-box 2 domains to retroviral restriction mediated by monkey TRIM5α. *J Biol Chem* 280(29):26933–26940.
3. Andréasson C, Fiaux J, Rampelt H, Mayer MP, Bukau B (2008) Hsp110 is a nucleotide-activated exchange factor for Hsp70. *J Biol Chem* 283(14):8877–8884.
4. Dombkowski AA (2003) Disulfide by Design: A computational method for the rational design of disulfide bonds in proteins. *Bioinformatics* 19(14):1852–1853.
5. Studier FW (2005) Protein production by auto-induction in high density shaking cultures. *Protein Expr Purif* 41(1):207–234.
6. Langelier CR, et al. (2008) Biochemical characterization of a recombinant TRIM5α protein that restricts human immunodeficiency virus type 1 replication. *J Virol* 82(23):11682–11694.
7. Cole JL (2004) Analysis of heterogeneous interactions. *Methods Enzymol* 384:212–232.
8. Laue TM, Shah BD, Ridgeway TM, Pelletier SL (1992) Computer-aided interpretation of analytical sedimentation data for proteins. *Ultracentrifugation in Biochemistry and Polymer Science*, eds Rowe AJ, Horton JC (Royal Society of Chemistry, Cambridge, United Kingdom), pp 90–125.
9. Otwinowski Z, Minor W (1997) Processing of X-ray diffraction data collected in oscillation mode. *Methods Enzymol* 276:307–326.
10. Adams PD, et al. (2010) PHENIX: A comprehensive Python-based system for macromolecular structure solution. *Acta Crystallogr D Biol Crystallogr* 66(Pt 2):213–221.
11. Emsley P, Lohkamp B, Scott WG, Cowtan K (2010) Features and development of Coot. *Acta Crystallogr D Biol Crystallogr* 66(Pt 4):486–501.
12. ter Haar E, Musacchio A, Harrison SC, Kirchhausen T (1998) Atomic structure of clathrin: A β propeller terminal domain joins an α zigzag linker. *Cell* 95(4):563–573.
13. Chen VB, et al. (2010) MolProbity: All-atom structure validation for macromolecular crystallography. *Acta Crystallogr D Biol Crystallogr* 66(Pt 1):12–21.
14. Maesaki R, et al. (1999) The structural basis of Rho effector recognition revealed by the crystal structure of human RhoA complexed with the effector domain of PKN/PRK1. *Mol Cell* 4(5):793–803.
15. Nishimura T, et al. (2012) Structural basis of transcriptional gene silencing mediated by *Arabidopsis* MOM1. *PLoS Genet* 8(2):e1002484.
16. Sardiello M, Cairo S, Fontanella B, Ballabio A, Meroni G (2008) Genomic analysis of the TRIM family reveals two groups of genes with distinct evolutionary properties. *BMC Evol Biol* 8:225.
17. Tao H, et al. (2008) Structure of the MID1 tandem B-boxes reveals an interaction reminiscent of intermolecular ring heterodimers. *Biochemistry* 47(8):2450–2457.
18. D'Cruz AA, et al. (2013) Crystal structure of the TRIM25 B30.2 (PRYSPRY) domain: A key component of antiviral signalling. *Biochem J* 456(2):231–240.
19. Gack MU, et al. (2007) TRIM25 RING-finger E3 ubiquitin ligase is essential for RIG-I-mediated antiviral activity. *Nature* 446(7138):916–920.
20. Gack MU, et al. (2008) Roles of RIG-I N-terminal tandem CARD and splice variant in TRIM25-mediated antiviral signal transduction. *Proc Natl Acad Sci USA* 105(43):16743–16748.
21. Cole C, Barber JD, Barton GJ (2008) The Jpred 3 secondary structure prediction server. *Nucleic Acids Res* 36(Web Server issue):W197–201.

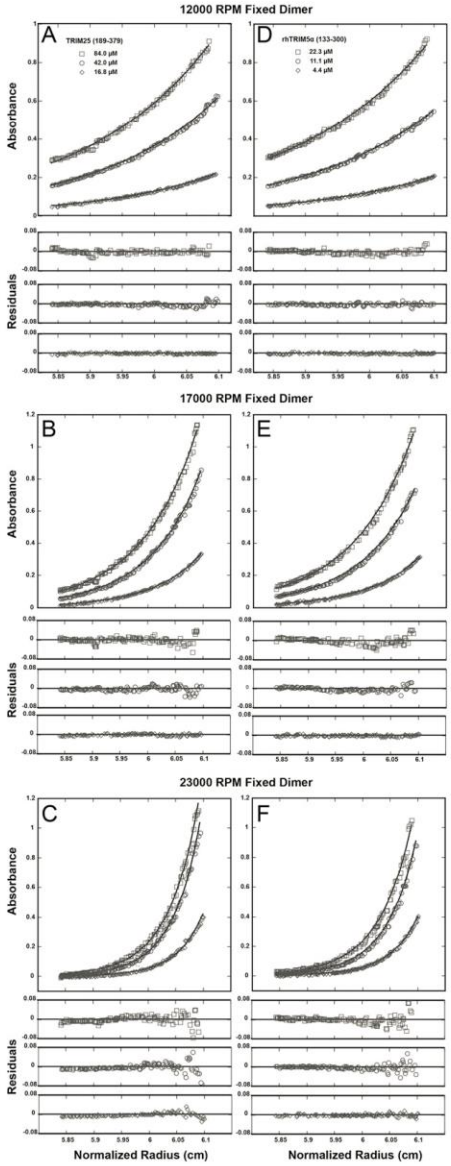


**Fig. S1.** TRIM25$_{189-379}$ and TRIM5$\alpha_{133-300}$ proteins form stable dimers. (*A–C*) Equilibrium distributions of the indicated protein concentrations were measured at rotor speeds of 12,000, 17,000, and 23,000 rpm. (*Upper*) Absorbance measurements (open symbols) and best-fit curves (solid lines). (*Lower*) Residual differences. All data were globally fit to a single-species model in which the molecular weight was constrained to that of a dimer ($M = 2 \times 21{,}835$ Da = 43,670 Da). (*D–F*) Equilibrium distributions for TRIM5$\alpha_{133-300}$ also fit a single-species dimer model ($M = 2 \times 20{,}238$ Da = 40,476 Da).

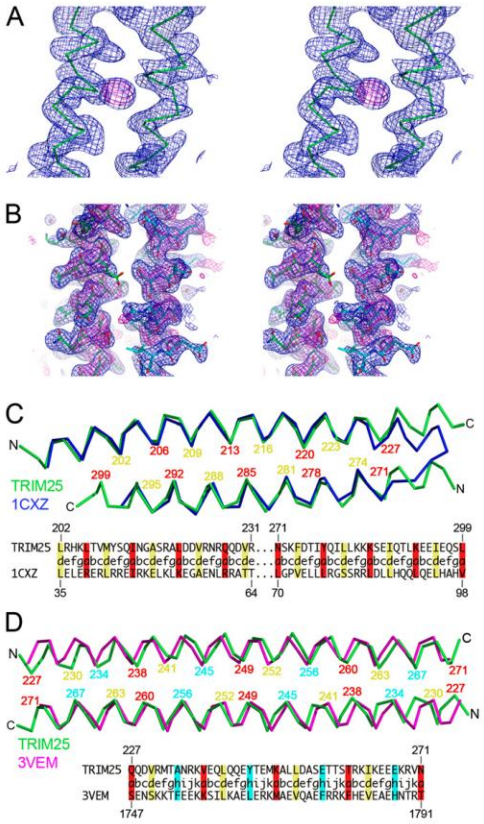


**Fig. S2.** Structure of TRIM25$_{189–379}$. (*A*) Stereoview showing a section of the experimental 2mFo-DFc density modified map (blue mesh, 1.5 σ) and anomalous Se difference map (magenta mesh, 8 σ) overlaid with a Cα trace of the partially refined model for the selenomethionine data set. Residues shown are in the area surrounding Met209. (*B*) Stereoview showing unbiased 2mFo-DFc density (magenta mesh, 1.5 σ) after a round of rigid body and real space refinement ($R$ = 0.45) of the molecular replacement solution (residues 195–200 for each subunit). Blue mesh shows 2mFo-DFc density (1 σ) calculated with phases from the final, full model. Residues shown are in helix H3, which was not present in the initial molecular replacement model. (*C*) Superposition of the TRIM25$_{189–379}$ heptad repeat regions with PDB accession no. 1CXZ chain B, which is a canonical left-handed antiparallel coiled-coil hairpin (14). The average root mean square deviation over 61 equivalent Cα atoms was 0.75 Å. The structure-based alignment with corresponding heptad assignments is indicated below. (*D*) Superposition of the TRIM25$_{189–379}$ hendecad repeat regions with PDB accession no. 3VEM, which is an antiparallel dimer containing 4 hendecads (15). The average root mean square deviation over 90 equivalent Cα atoms was 1.42 Å. The structure-based alignment with corresponding hendecad assignments is indicated below.

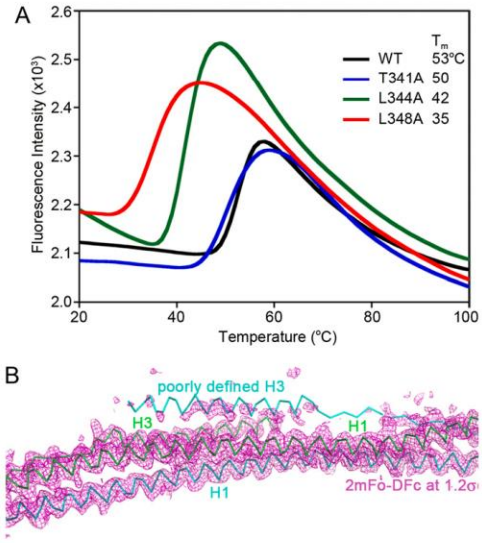


**Fig. S3.** Analysis of L2 packing against the coiled-coil. (*A*) Differential scanning fluorimetry melting profiles of H3 mutants: T341A (blue), L344A (green), and L348A (red). The wild-type curve is in black. (*B*) Electron density (magenta mesh, 1.2 σ) for the selenomethionine-labeled crystal after multiple rounds of model building and refinement. Note the poor density for one of the H3 helices (*Upper*, labeled in cyan).

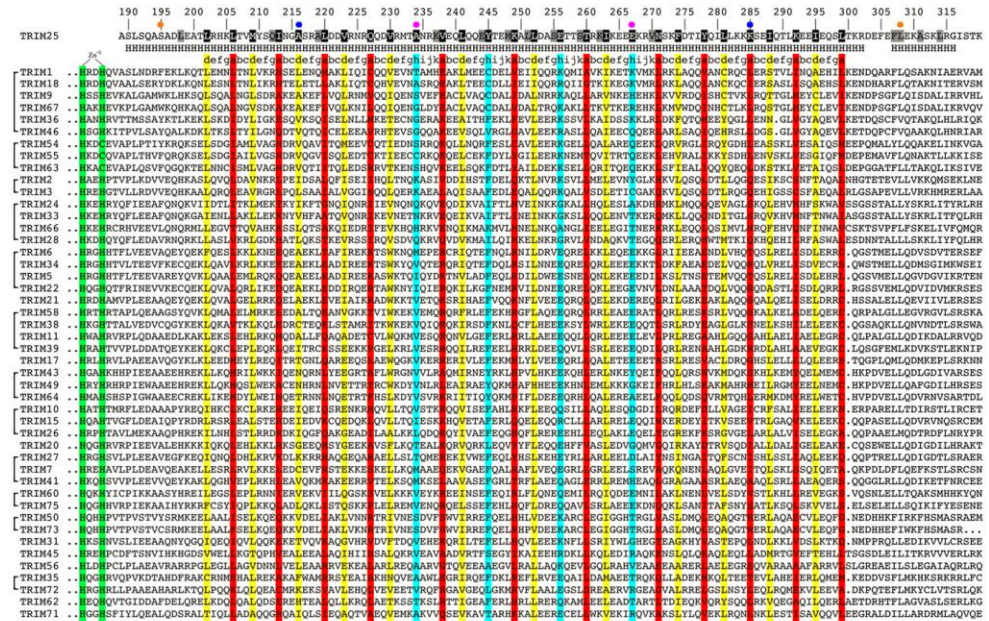

**Fig. S4.** Multiple sequence alignment of the coiled-coil domains from 54 human TRIM family members, corresponding to the H1 and H2 helices in the TRIM25 structure. The corresponding TRIM25 sequence, secondary structure, H1 heptad/hendecad assignments, and residue numbers are shown at the top for reference. Residues shaded in black indicate side-chains in the TRIM25 structure that bury 60% or more of their available surface area within the H1–H1′ dimer interface (corresponding to dark gray bars in Fig. 3*D*). Residues shaded in gray are at least 60% buried within the entire TRIM25$_{189–379}$ structure (light gray bars in Fig. 3*D*) and also mediate packing of L2 against H1. The *a*, *d*, and *h* positions are shaded as in Fig. 3 and Fig. S2. The last zinc-coordinating His/Cys pairs of the B-box 2 domains are shaded in green for reference. Colored dots indicate cysteine substitution sites in Fig. 4. TRIM family branch groupings (16) are indicated by square brackets on the left.

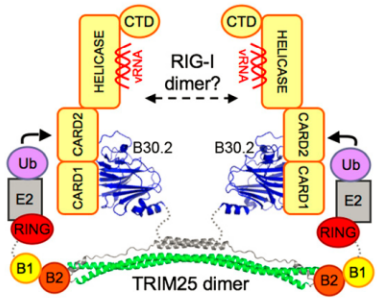


**Fig. S5.** Model for coiled-coil mediated coupling of the TRIM25 RING and B30.2 domains to facilitate RIG-I polyubiquitylation. The tandem B-boxes are likely to form an integrated unit by analogy to the structure of homologous domains from MID1/TRIM18 (17). We assume that the B-box 2 domain is closely associated with the coiled-coil on the basis of their sequence connectivity. The connecting linker (L1) between the RING domain and the B-box domain is shown as dashes because its configuration is unknown. For the same reason, the C-terminal portion of L2 (about 60 residues) that connects the last ordered residue in our structure and the first ordered residue in the recently published structure of the B30.2 domain (blue) (18) is also shown as dashes. The B30.2 domain of TRIM25 binds to the first CARD of RIG-I, and the RING domain ubiquitylates Lys172 in the second CARD (19, 20). CARD, caspase activation and recruitment domain; CTD, C-terminal domain; B1, B-box 1; B2, B-box 2; E2, E2 ubiquitin ligase; Ub, ubiquitin; vRNA, viral RNA.

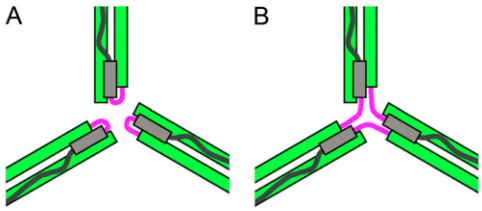


**Fig. S6.** Two possible configurations of domain connectivity at the threefold symmetry axes of the TRIM5α hexagonal lattice. The RING and B-box domains are not shown. (*A*) Three dimers with loops (magenta) connecting the coiled-coil helices (green) and L2 (gray) in the "fold-back" configuration, as observed in the TRIM25 crystal structure. (*B*) Three dimers in which the adjacent subunits have "swapped" their short arms. Note that this will also result in a domain swapping of downstream L2 and B30.2 elements.


**Fig. S7.** Secondary structure predictions for rhesus TRIM5$\alpha_{133-300}$ performed with the program JPRED (21) (H, helix; E, strand). Residues that fold into an α-helix in X-ray structures of the isolated B30.2 domain are colored in blue and boxed. The "domain" boundaries are indicated at the bottom, following the color scheme of Fig. 1*B*. Black rectangles depict the deduced helix H1 and H2 positions and the predicted H3 helix.

**Table S1. Diffraction data and refinement statistics for TRIM25$_{189–379}$**

| | Se | Native |
|---|---|---|
| Diffraction | | |
| Beamline | Advanced Photon Source 22-ID | Advanced Photon Source 22-ID |
| Wavelength, Å | 0.9791 | 1.000 |
| Space group | $P2_12_12_1$ | $P2_12_12_1$ |
| Cell dimensions | $a$ = 52.8 Å | $a$ = 57.7 Å |
| | $b$ = 69.6 Å | $b$ = 83.2 Å |
| | $c$ = 108.5 Å | $c$ = 92.8 Å |
| | $\alpha = \beta = \gamma = 90°$ | $\alpha = \beta = \gamma = 90°$ |
| Resolution range, Å | 50–3.2 (3.31–3.2) | 50–2.59 (2.69–2.59) |
| $R_{sym}$ | 0.12 (0.43) | 0.14 (0.78) |
| Mean I/σ<I> | 14.8 (2.3) | 17.3 (2.2) |
| Completeness, % | 86.8 (46.7) | 96.9 (81.4) |
| Average redundancy | 11.0 (4.6) | 13.1 (9.1) |
| Mosaicity range, degree | 0.49–1.4 | 0.72–1.22 |
| Wilson B-factor, Å$^2$ | 65.5 | 43.6 |
| Phasing | | |
| Number of sites, expected/found | 6/6 | |
| Figure of merit | 0.31 | |
| Refinement | | |
| Resolution range | | 42.2–2.59 (2.75–2.59) |
| No. of unique reflections | | 13,042 (892) |
| Reflections in free set | | 1,296 (94) |
| $R_{work}$ | | 0.20 (0.30) |
| $R_{free}$ | | 0.26 (0.38) |
| Number of nonhydrogen atoms | | |
| Protein | | 2,778 |
| Solvent | | 55 |
| Average B-factor, Å$^2$ | | |
| Protein | | 53.1 |
| Solvent | | 47.7 |
| Coordinate deviations | | |
| Bond lengths, Å | | 0.009 |
| Bond angles, degree | | 1.17 |
| Ramachandran plot | | |
| Favored, % | | 97 |
| Outliers, % | | 0 |
| Molprobity clash score | | 4.07 |
| Protein Data Bank ID | | 4LTB |

Values in parenthesis are for the highest-resolution shell.

**Table S2. Expression constructs used in this study**

| Human TRIM25$_{189–379}$ | | Rhesus TRIM5α$_{133–300}$ | |
|---|---|---|---|
| Mutation | Plasmid designation | Mutation | Plasmid designation |
| Wild-type | RBCC-297 | Wild-type | WISP13-167 |
| S195C/L308C | RBCC-381 | A137C/L249C | WISP13-168 |
| S195C/K285C | RBCC-436 | A137C/T227C | WISP13-169 |
| A216C/K285C | RBCC-384 | A158C/T227C | WISP13-170 |
| A216C/E267C | RBCC-437 | A158C/E209C | WISP13-171 |
| A234C/E267C | RBCC-387 | I176C/E209C | WISP13-172 |
| A234C/L308C | RBCC-438 | I176C/L249C | WISP13-173 |
| M209A | RBCC-434 | | |
| V223A | RBCC-422 | | |
| Y245A | RBCC-402 | | |
| L252A | RBCC-399 | | |
| T341A | RBCC-421 | | |
| L344A | RBCC-439 | | |
| L348A | RBCC-440 | | |

# CHAPTER 4

# PRIMATE TRIM5 PROTEINS FORM HEXAGONAL NETS ON HIV-1 CAPSIDS

## 4.1 Introduction

Mammalian hosts have evolved a series of different innate immune strategies to combat retroviruses (reviewed in (1-3)). TRIM5α and the related TRIMCyp protein (collectively TRIM5) are restriction factors that recognize incoming retroviral core particles, induce their dissociation and inhibit reverse transcription (4-6). The mechanistic basis for core inactivation is not yet well established, but current models invoke the involvement of proteasomes (7-12), autophagosomes (13) and/or the establishment of a general antiviral state (14). Like other members of the tripartite motif (TRIM) family (15), TRIM5 proteins comprise a RING E3 ubiquitin (Ub) ligase domain (16, 17), an L1 linker, a B-box 2 self-assembly domain (18), an antiparallel dimeric coiled-coil and an L2 linker that folds back on the coiled-coil (19-21) (Figure 4.1A). TRIM5 proteins also contain one of two different C-terminal viral recognition domains: a PRYSPRY (B30.2) domain in TRIM5α and a cyclophilin A (CypA) domain in TRIMCyp (5, 6, 22).

TRIM5 proteins act by binding the outer capsid shell of the viral core replication particle. The capsid protects and organizes the internal nucleocapsid, which comprises the viral NC protein, the RNA genome and associated replicative enzymes. Retroviral capsids

Figure 4.1 ECT analysis of TRIM5-21R 2D crystals. (A) Schematic of the TRIM5 dimer. The two RING (yellow) and B-box 2 (red) domains are separated by a ~17 nm, antiparallel dimeric coiled-coil (blue). The two L2 linkers (green) fold back towards the two-fold axis of the coiled-coil to orient two capsid-binding SPRY domains (orange). (B and C) Tomographic slice (top) of (B) full-length and (C) ΔSPRY lattices. Scale bars represent 100 nm. In both cases, the computed Fourier transform (bottom, left) and subtomogram average without imposed rotational symmetry (bottom, middle) exhibits six-fold symmetry. Isosurface representations of the densities are also shown (bottom, right). (D) A density difference map of the subtomogram averages of full-length and TRIM5-21R$_{\Delta SPRY}$ lattices reveals positive density (red) at the center of each hexagon edge, corresponding to the SPRY domain position, confirming the TRIM5α dimer model shown in (A). (E) Heat maps (bottom) of lattice arm lengths and angles measured from refined lattice points (top) selected from the TRIM5-21R tomogram in (B). (F) Histograms showing the distributions of measured arm lengths and angles. The most abundant arm length (18.5-19 nm) and arm angle (120°) are consistent with the structure model in (A) and the p6 plane group symmetry of TRIM5-21R 2D crystals (23), respectively.

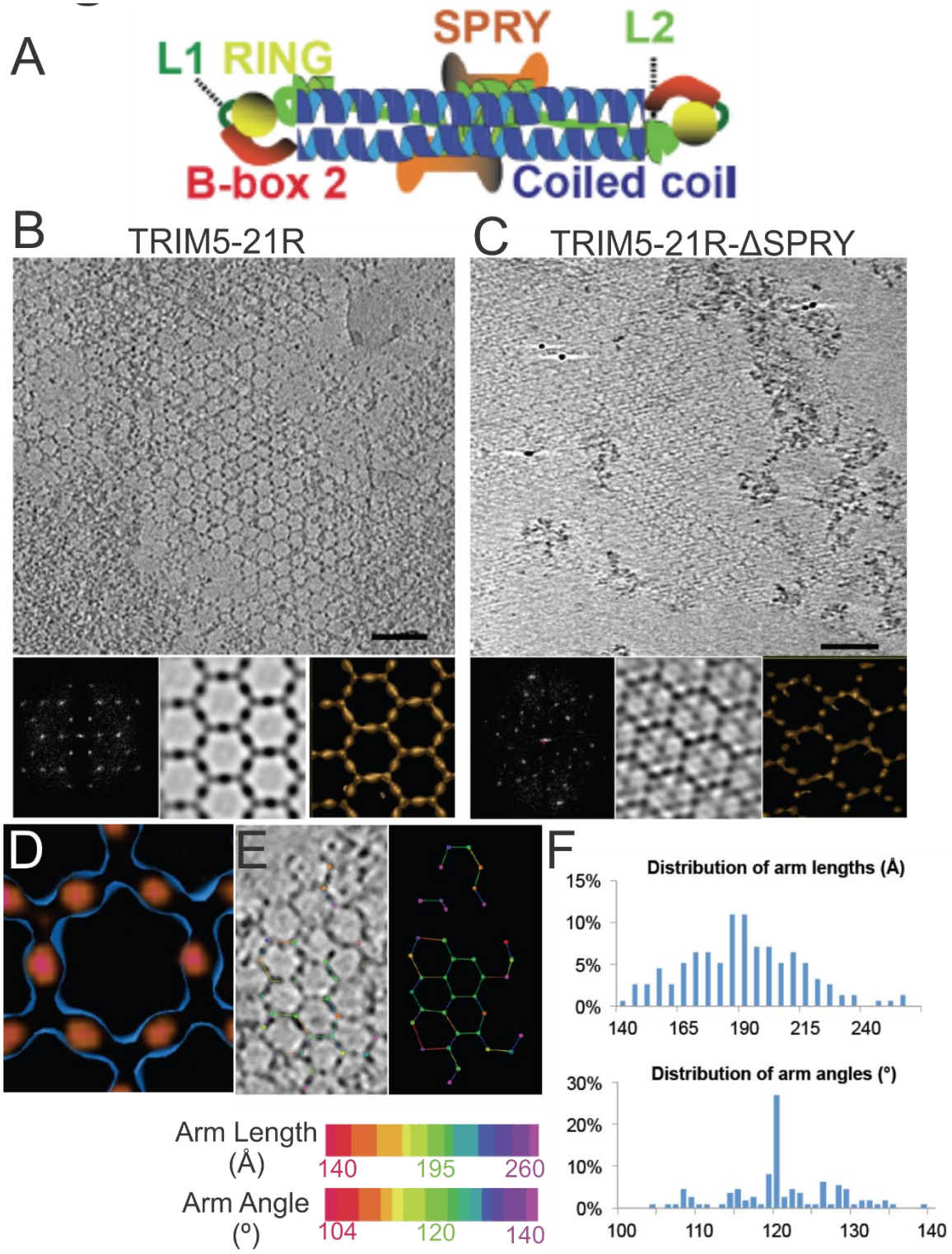
A
L1 RING
SPRY
L2
B-box 2
Coiled coil
B
TRIM5-21R
C
TRIM5-21R-ΔSPRY
D
E
F
Distribution of arm lengths (Å)
15%
10%
5%
0%
140
165
190
215
240
Distribution of arm angles (°)
30%
20%
10%
0%
100
110
120
130
140
Arm Length (Å)
140
195
260
Arm Angle (°)
104
120
140

are constructed from several hundred CA protein hexamers and exactly 12 CA pentamers (24-30). Although all retroviral capsids are organized following these principles, individual capsids are unique, asymmetric objects that can differ in hexamer numbers and pentamer distributions. For example, HIV-1 capsids are typically conical, but their sizes and cone angles can vary, and cylindrical and spherical capsids also form (31, 32). Indeed, spherical and cylindrical capsids predominate in other retroviral genera, and capsid surface properties can vary considerably because CA proteins from different genera can share <10% sequence identity (24).

To function effectively, individual TRIM5 proteins must overcome these variations in retroviral capsid shape and sequence (33). We, and others, have proposed that TRIM5 proteins accomplish this by recognizing repeating patterns on the capsid surface (20, 23, 34, 35). This model supposes that flexible loops on the PRYSPRY and CypA domains can adopt multiple different conformations and can bind weakly, but promiscuously, to conserved elements on the capsid surface (22, 35-40). These weak interactions are then amplified by TRIM5 assembly into a higher-order hexagonal lattice, which positions arrays of PRYSPRY/CypA domains to interact with repeating epitopes on the capsid surface (23, 41).

This "pattern recognition" model has been supported by biochemical and structural analyses of a TRIM5 protein construct called TRIM5-21R, which is an artificial chimera in which the RING domain from human TRIM21 replaced the RING domain of rhesus TRIM5α (42-44). This construct retains HIV-1 restriction activity, and was studied owing to its unusually favorable stability, solubility and assembly properties. Consistent with the pattern recognition model, TRIM5-21R was shown to assemble into open hexagonal

lattices, both alone and on the surface of 2D CA crystals that mimic the surface of the HIV-1 capsid (23). Structural details were limited, however, because the hexagonal TRIM5-21R assemblies were reconstructed as 2D projections rather than 3D objects, domain positions were not identified experimentally, and the reconstructions were interpreted in the absence of any high resolution information on the structure of the TRIM5 protein core. The technical challenge of purifying authentic HIV-1 cores has also been another significant experimental limitation, and all published biochemical and structural studies of TRIM5α-capsid interactions have therefore either employed crude viral core preparations or artificial mimics of the capsid surface (5, 23, 44-46). Thus, the interactions between authentic viral capsids and TRIM5 proteins have yet to be investigated biochemically or structurally. To address these shortcomings, we have developed methods for preparing authentic recombinant TRIM5 proteins and stable HIV-1 cores, and used these reagents to characterize how TRIM5 proteins recognize and assemble on HIV-1 capsids.

## 4.2 Results

### 4.2.1 Structure-based models for TRIM5-21R assembly

We began our studies by defining the domain organization within the hexagonal TRIM5-21R lattice. TRIM5-21R spontaneously assembles into flat hexagonal lattices comprising open hexameric rings that are ~19 nm along each edge (corresponding to an inter-ring spacing of ~33 nm). Recently, several high resolution crystal structures have revealed that the TRIM coiled-coil has an antiparallel orientation and is ~17 nm long, suggesting that each hexamer edge is likely to be composed of a single TRIM5α dimer (19-21). The ensuing L2 linker folds back against the coiled-coil and can form a four helix

bundle at the center of the coiled-coil, which could, in principle, serve as a "platform" that supports and orients the TRIM5α SPRY domains. However, direct structural information on the location of the SPRY domains within the hexagonal lattice has been lacking.

To visualize TRIM5-21R assemblies in three dimensions and locate the positions of the SPRY domains, we generated electron cryotomograms (ECT) from tilt series of vitrified 2D crystals of both full length TRIM5-21R (Figure 4.1B) and a construct that lacked the SPRY domain (TRIM5-21R$_{\Delta SPRY}$, residues 1-300, Figure 4.1C). The 3D reconstructions were then refined and improved by subtomogram averaging of densities centered at equivalent lattice vertices (see Figure 4.1 caption, and Experimental Methods). As expected, TRIM5-21R and TRIM5-21R$_{\Delta SPRY}$ both assembled into similar planar lattices of hexagonal rings, whose inter-ring spacings and protein densities matched those of the previous 2D projection structures (23). As shown in Figure 4.1D, difference density maps clearly revealed that the SPRY domains reside at the center of each hexagon edge. We therefore conclude that the edge of each TRIM5-21R ring is a dimer, with the overall domain organization shown in Figure 4.1A.

### 4.2.2 The TRIM5-21R lattice is hexagonal net with variable arm lengths and angles

Although the paracrystalline arrays of TRIM5-21R exhibited long-range order, individual hexamers within the lattice appeared to vary in shape and size. This variability was quantified by a nearest neighbor analysis of the refined positions of lattice vertices used for subtomogram averaging. The relative positions of 153 vertices in the 2D crystals of TRIM5-21R were used to define individual hexamer edge lengths and angles (see Figure

4.1E). The length distribution of hexamer edges was centered about a mean of 19 nm, but individual edge lengths varied by up to ±5 nm (Figure 4.1F, upper panel). Similarly, the distribution of hexamer vertex angles was centered about 120°, but varied by up to ±20°. These ranges likely underestimate the actual range of hexamer variability owing to the initial selection of well-ordered lattice points. Thus, the hexagonal TRIM5-21R lattice is neither highly regular nor rigid, but is rather best described as a paracrystalline "net", within which individual rings can exhibit considerable conformational variability.

### 4.2.3 Expression and purification of authentic primate TRIM5α and TRIMCyp proteins

Recombinant TRIM5α proteins are difficult to express and purify owing to their propensity to self-assemble, both in cells and *in vitro*. All previous biochemical and structural studies of TRIM5α proteins have therefore been performed with impure proteins or with protein fragments or nonnative chimeric constructs. To overcome this limitation, we tested a variety of different expression and purification conditions, with the goal of developing a general method for preparing multimilligram quantities of authentic, full-length primate TRIM5α and TRIMCyp proteins.

The strategy that was ultimately successful entailed expressing TRIM5 proteins in insect cells using a baculoviral expression system. As described in the Experimental Methods, expressed TRIM5 proteins formed cytoplasmic bodies that could be solubilized by lysing the cells in a low ionic strength, alkali buffer that contained the nonionic detergent, Triton X-100, as well as a nondetergent small molecule, sulfobetaine-256 (NDSB-256) that has previously been shown to inhibit protein aggregation (47, 48). Once

solubilized, primate TRIM5 proteins typically remained dimeric and soluble under low salt, alkaline conditions in the absence of Triton X-100 and NDSB-256, even at concentrations greater than 1 mg/ml. The proteins could therefore be purified, provided they were maintained at high pH, low salt and/or low protein concentrations.

Our stepwise protein purification protocol is illustrated for rhesus TRIM5α in Figure 4.2A. Briefly, N-terminal OneSTrEP-FLAG- (OSF-) or C-terminal FLAG-OneSTrEP- (FOS-) tagged TRIM5 proteins were initially purified using Strep-Tactin affinity chromatography, the affinity tag was removed by PreScission protease treatment and the proteins were then purified to homogeneity by anion exchange and gel filtration chromatography. Analogous approaches were used to express and purify wild type and mutant TRIM5α proteins from rhesus macaques (*Macaca mulatta*, here abbreviated TRIM5$\alpha_{rh}$), African green pygerythrus monkeys (*C. pygerythrus*, TRIM5$\alpha_{AGMpyg}$), chimpanzees (*P. troglodytes*, TRIM5$\alpha_{CPZ}$), humans (*H. sapiens*, TRIM5$\alpha_{hu}$) and the TRIMCyp protein from owl monkeys (*A. trivirgatus*, TRIMCyp). Yields ranged between 1.3 and 9.6 mg/L of insect cell cultures, and all of the proteins eluted with similar retention times during the final gel filtration chromatography step, indicating that they were all dimers of similar shape. All of the proteins could be purified to >95% purity (Figure 4.2B) with the exception of TRIMCyp, where our preparations also contained breakdown contaminants that mapped to proteoytic cleavage at residues Lys283 and Gln287 (not shown). These breakdown contaminants were eliminated by creating a mutant construct that expressed TRIMCyp$_{K283D,Q287D}$ (lane 10). These mutations are not expected to affect other relevant properties of the protein because TRIMCyp$_{K283D,Q287D}$ retains potent HIV-1 restriction activity (see Figure 4.3).

Figure 4.2. Purification and characterization of recombinant TRIM5 proteins. (A) Coomassie-stained SDS-PAGE showing the stepwise purification of rhesus TRIM5α (TRIM5$\alpha_{rh}$). Samples correspond to: soluble lysate from control SF9 cells (Uninfected, lane 1); soluble lysate from SF9 cells expressing OSF-TRIM5$\alpha_{rhesus}$ (Infected, lane 2); StrepTactin affinity-purified OSF-TRIM5$\alpha_{rhesus}$ (Affinity, lane 3); ΔOSF-TRIM5$\alpha_{rhesus}$ after PreScission protease treatment (Tag Cleavage, lane 4); dimeric TRIM5$\alpha_{rhesus}$ purified by Q anion exchange chromatography (Anion Exchange, lane 5); dimeric TRIM5$\alpha_{rhesus}$ purified by Superdex 200 gel filtration chromatography (Gel Filtration, lane 6). (B) Coomassie-stained SDS-PAGE showing 1.5 µg of purified dimers of rhesus, African green monkey pygerythrus (AGMpyg), chimpanzee TRIM5α, proteolysis resistant owl monkey TRIMCyp$_{K283D,Q287D}$, human TRIM5α, HIV-1-restrictive human TRIM5$\alpha_{R332P}$. (C, D) TRIM5 hexagonal assembly is a conserved feature. Negatively-stained EM image of a hexagonal array formed by (C) dimeric TRIM5$\alpha_{AGMpyg}$ and (D) TRIMCyp. Computed Fourier transforms (top right insets) show obvious hexagonal order. Projection density maps (with no imposed symmetry) of two-dimensional crystals preserved in vitreous ice (bottom left insets) also reveal hexagonal rings and density distributions reminiscent of TRIM5-21R lattices (23). The unit cell parameters are a = 345 Å, b = 345 Å, γ = 120° (TRIM5$\alpha_{AGMpyg}$); and a = 345 Å, b = 344 Å, γ = 119° (TRIMCyp). Note that the TRIMCyp samples contained a mixture of full-length TRIMCyp and fragments that were proteolyzed to the C-terminus of residues K283 or Q287 (see Results and Materials and Methods for details). The relatively thinner two-fold density in the TRIMCyp projection map could either be caused by low crystal occupancy of the CypA domain (due to proteolysis) or by inherently flexible CypA domains in TRIMCyp as has been proposed by (20).

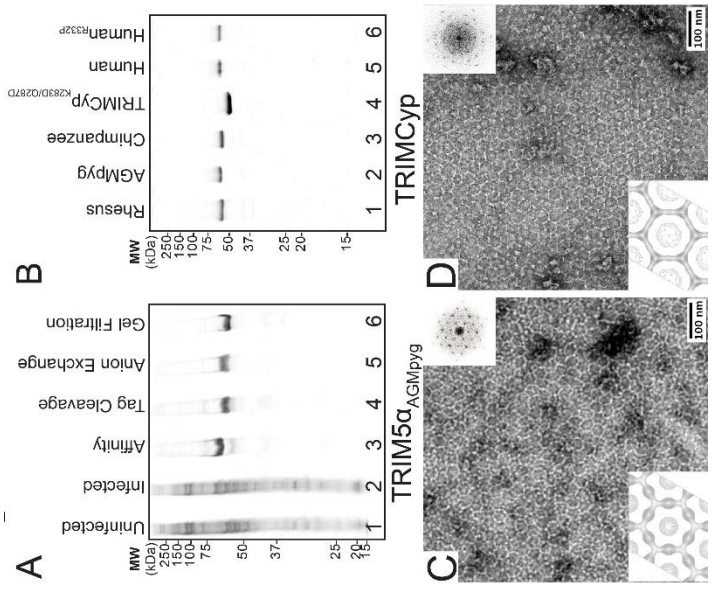
A
MW (kDa)
250
150
100
75
50
37
25
20
15
1 2 3 4 5 6
Uninfected
Infected
Affinity
Tag Cleavage
Anion Exchange
Gel Filtration
B
MW (kDa)
1 2 3 4 5 6
Rhesus
AGMpyg
Chimpanzee
TRIMCyp K283D/Q287D
Human
Human R332P
C
TRIM5α AGMpyg
100 nm
D
TRIMCyp
100 nm

Figure 4.3 HIV-1 CA restriction activity of different alleles of TRIM5 proteins.

HeLa-M cells were transiently transfected with vectors expressing TRIM5$\alpha_{human}$, TRIM5$\alpha_{CPZ}$, TRIM5$\alpha_{AGMpyg}$, TRIM5$\alpha_{rhesus}$, TRIMCyp, TRIMCyp$_{K283D,Q287D}$ and empty vector control. Cells expressed TRIM5 proteins at approximate similar levels as verified by western blotting with α-TRIM5α antibody (right) and were transduced with VSV-G pseudotyped HIV-GFP reporter virions (left). The percentage of infected cells (GFP positive cells) was determined by FACS. As expected, TRIM5 proteins from AGMpyg, rhesus, owl monkey restricted HIV-1 whereas human and chimpanzee TRIM5 did not. The proteolysis-resistance mutations (K283D, Q287D) in TRIMCyp did not affect restriction ability of TRIMCyp.

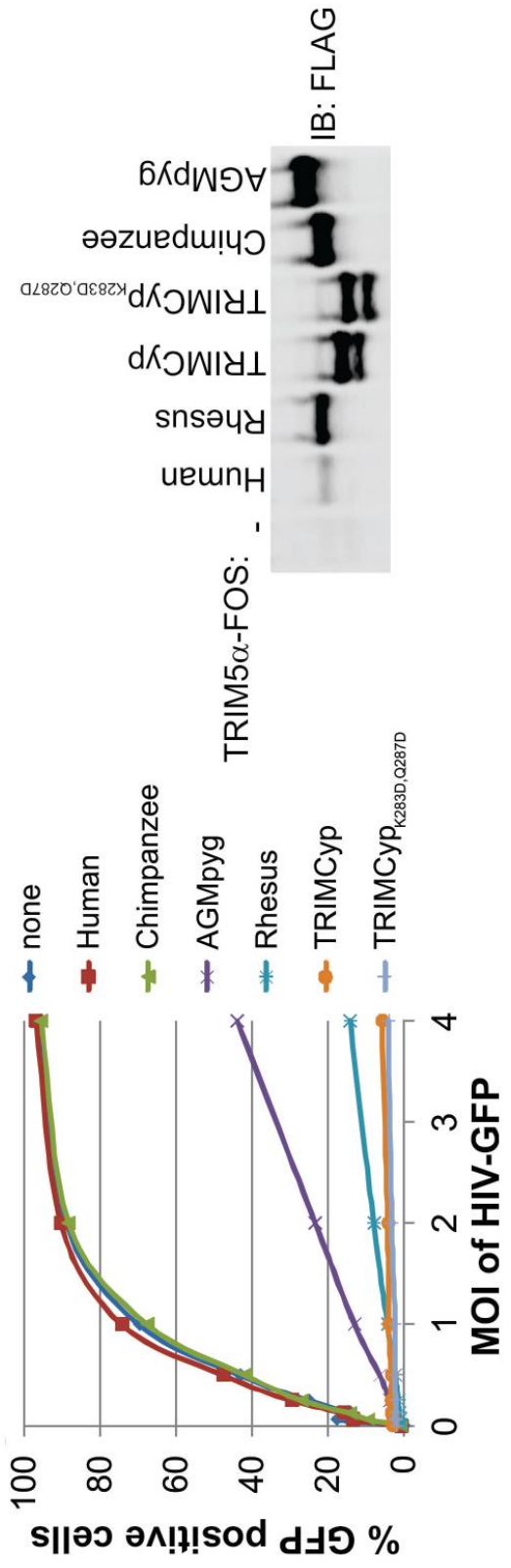
% GFP positive cells
100
80
60
40
20
0
0
1
2
3
4
MOI of HIV-GFP
none
Human
Chimpanzee
AGMpyg
Rhesus
TRIMCyp
TRIMCyp$_{K283D,Q287D}$
TRIM5α-FOS:
-
Human
Rhesus
TRIMCyp
TRIMCyp$_{K283D,Q287D}$
Chimpanzee
AGMpyg
IB: FLAG

### 4.2.4 Conservation of hexagonal TRIM5 protein assembly

To determine whether the ability to assemble hexagonal nets is conserved, we screened for conditions that promoted assembly of the different primate TRIM5 proteins, using negative stain EM imaging to assay assembly states. These screens identified conditions under which two of the proteins, TRIM5$\alpha_{AGMpyg}$ (Figure 4.2C) and TRIMCyp (Figure 4.2D) spontaneously formed 2D hexagonal assemblies that were similar in appearance to those formed by TRIM5-21R. Unstained, vitrified 2D crystals of TRIM5$\alpha_{AGMpyg}$ and TRIMCyp were imaged and processed to generate Fourier-filtered 2D projection reconstructions without any imposed symmetry (Figure 4.2C, D; bottom). Both proteins formed lattices comprising open hexameric protein rings that were similar in appearance and size to the TRIM5-21R rings, demonstrating that native TRIM5 proteins from highly diverged primates (with ~74% pairwise identities across the B-box 2, coiled-coil and L2 linker regions) share the ability to assemble into analogous hexagonal nets.

### 4.2.5 Templated hexagonal TRIM5 protein assembly on HIV-1 CA surfaces

The pattern recognition model for retroviral restriction predicts that binding to the surface of the viral capsid will promote hexagonal TRIM5 assembly. We therefore tested whether 2D crystals of HIV-1 CA, which mimic the capsid surface, could promote the assembly of three different TRIM5 proteins that can restrict HIV-1; TRIM5$\alpha_{rh}$, TRIMCyp and TRIM5$\alpha_{hu,R332P}$, and two different TRIM5 proteins that cannot restrict HIV-1; wild type TRIM5$\alpha_{hu}$ and TRIM5$\alpha_{cpz}$. To test for templated assembly, soluble dimeric TRIM5 proteins were incubated together with preassembled 2D CA crystals under solution

conditions that were sufficiently stringent to prevent untemplated assembly. TRIM5$\alpha_{AGMpyg}$ was not used in these studies because it assembled very robustly even in the absence of a template.

As shown in Figure 4.4, the three TRIM5 proteins assembled into visible hexagonal nets on the surfaces of preformed HIV-1 CA crystals, whereas template assembly was not observed for either of the nonrestricting TRIM5 proteins. Templated assembly therefore correlated well with restriction activity, emphasizing the coupling of CA binding and TRIM5 assembly. Computed Fourier transforms of the images of decorated crystals (Figure 4.4, insets) revealed well-defined first- and second-order reflections from the smaller underlying CA lattice (red and blue), as well as more diffuse peaks (TRIM5$\alpha_{rhesus}$ and TRIMCyp, green) or a powder diffraction ring (TRIM5$\alpha_{hu,R332P}$) that corresponded to the first-order reflections of the hexagonal TRIM5 lattices. Thus, all three restricting TRIM5 proteins bound the CA surface and assembled into hexagonal nets that were clearly visible, but lacked extensive long-range order.

### 4.2.6 Generation of hyperstable, disulfide-crosslinked HIV-1 core particles

The helical tubes formed by pure recombinant HIV-1 CA provide another regularized model for the curved, but less symmetrical arrays of CA hexagons displayed on the viral capsid surface [REF]. We employed a previously described sucrose cosedimentation assay to test whether the restricting TRIM5$\alpha_{AGMpyg}$ and TRIMCyp$_{K283D,Q287D}$ proteins bound the disulfide-crosslinked helical tubes formed by the HIV-1 CA$_{A14C,E45C}$ protein. As shown in Figure 4.5A, both proteins bound the mutant CA tubes, as judged by their sedimentation

Figure 4.4 Assembly of restricting TRIM5 proteins on 2D crystals of HIV-1 CA. Negative stained EM image of CA co-crystals with (A) TRIM5$\alpha_{rhesus}$, (B) TRIM5$\alpha_{human,R332P}$, (C) TRIMCyp$_{K283D,Q287D}$. Scale bars represent 100 nm. Computed Fourier transform (inset) and indexing (second inset) show the first- and second-order reflections of two CA lattices and their unit cell parameters (red and blue) as well as diffraction spots (A, C) or rings (B) corresponding to the first-order reflections of the TRIM5 lattices (green).

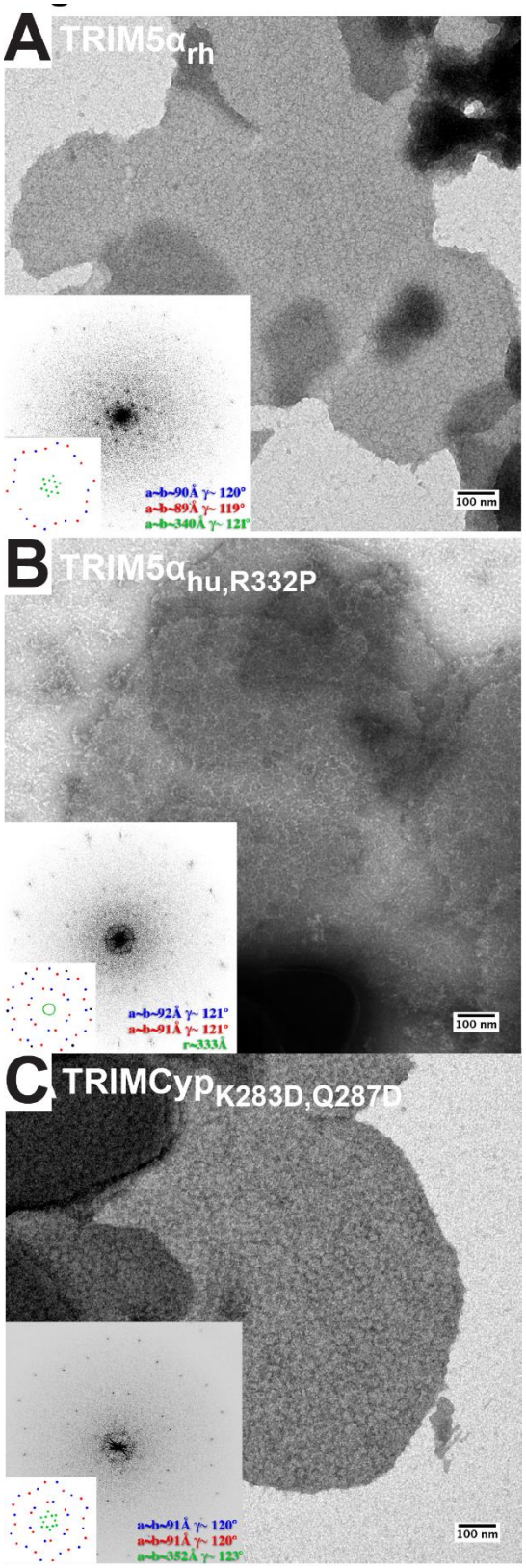
A
TRIM5α rh
a~b~90Å γ~ 120°
a~b~89Å γ~ 119°
a~b~340Å γ~ 121°
100 nm
B
TRIM5α hu,R332P
a~b~92Å γ~ 121°
a~b~91Å γ~ 121°
r~333Å
100 nm
C
TRIMCyp K283D,Q287D
a~b~91Å γ~ 120°
a~b~91Å γ~ 120°
a~b~352Å γ~ 123°
100 nm

Figure 4.5 TRIM5 protein binding to hyperstable HIV-1 CA tubes. (A) (left) Binding experiments were performed using either wild type, full-length TRIM5$\alpha_{AGMpyg}$ (Wild Type, lanes 1, 2) or truncated TRIM5$\alpha_{AGMpyg}$ that lacked the SPRY domain (ΔSPRY, lanes 3, 4), in the absence of CA tubes (lanes 1, 3) or in the presence of CA tubes (lanes 2, 4) . Pelletable CA and associated TRIM5$\alpha_{AGMpyg}$ (Pellet, 30% in total), were separated from unassembled and soluble CA proteins and unbound TRIM5$\alpha_{AGMpyg}$ (Supernatant, 3% in total) by centrifugation, and analyzed by Western blotting, with the input levels of both proteins shown for reference (Input, 3% in total). (right) Similar experiments were performed using proteolysis-resistant TRIMCyp$_{K283D,Q287D}$ in the absence (lane 5) or presence (lanes 6, 7) of helical CA tubes, without (lanes 5, 6) or with added CsA (lane 7), a specific inhibitor of the CypA-CA interaction. Lane 8 is a CA tube control, with no added TRIMCyp$_{K283D,Q287D}$ or CsA. (B) Representative electron micrographs of control CA tubes, TRIM5$\alpha_{AGMpyg}$ and TRIMCyp$_{K283D,Q287D}$ decorated tubes negatively stained with uranyl acetate (UA) or phosphotungstic acids (PTA). Scale bar represents 50 nm. (C) Histograms showing the distributions of measured inter-ring spacings (n=180). The most abundant inter-ring spacing (30-35 nm) is consistent with the spacing of TRIM5-21R 2D crystals, indicating the observed rings are correct size. (D) Deep-etch electron micrographs of control tube (top) and TRIM5α decorated CA tubes (bottom) with a blow-up view of boxed region to the right. TRIM5 hexagons were highlighted in yellow. Scale bar represents 50 nm.

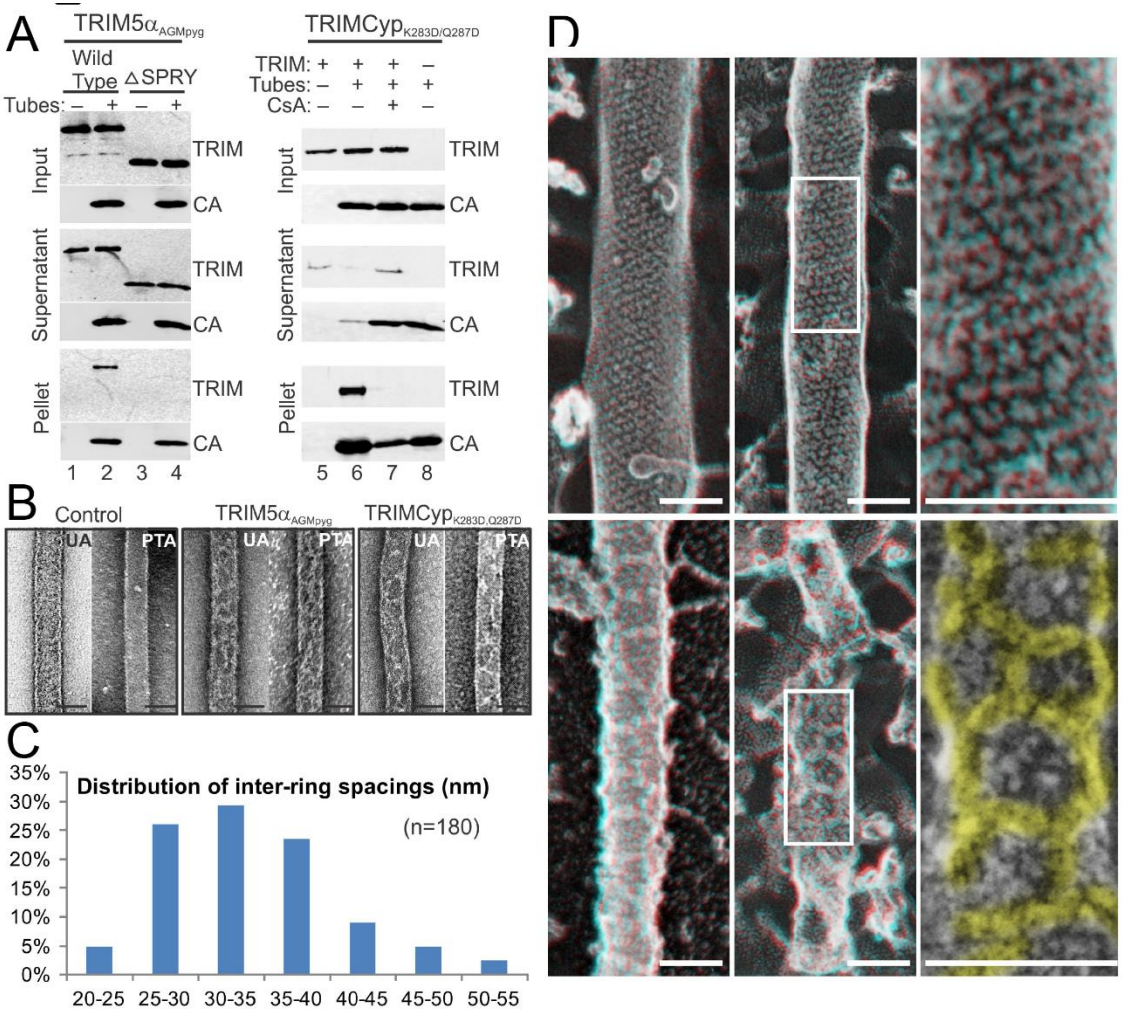
A
TRIM5α AGMpyg
TRIMCyp K283D/Q287D
Wild Type
ΔSPRY
Tubes: – + – +
TRIM: + + + –
Tubes: – + + +
CsA: – – + –
Input
Supernatant
Pellet
TRIM
CA
1 2 3 4
5 6 7 8
B
Control
TRIM5α AGMpyg
TRIMCyp K283D,Q287D
UA
PTA
C
Distribution of inter-ring spacings (nm)
(n=180)
35%
30%
25%
20%
15%
10%
5%
0%
20-25 25-30 30-35 35-40 40-45 45-50 50-55
D

through the gradient when the CA tubes were present, but not when they were absent (compare the "pellet" fractions in lanes 1 and 2 and lanes 5 and 6). Binding was specific because TRIM5$\alpha_{AGMpyg}$ did not cosediment with CA tubes when the SPRY domain was removed (compare lanes 2 and 4) and because TRIMCyp binding to CA tubes was abolished in the presence of cyclosporine A, which competitively inhibits the CypA-CA interaction (compare lanes 6 and 8). Thus, these pure recombinant TRIM5 proteins also bind the curved hexagonal lattices of helical CA tubes.

Negative stain and deep etch electron microscopy approaches were used to image the TRIM5-decorated HIV-1 CA tubes. TRIM5 proteins formed thin ring-like decorations on the surfaces of CA tubes (Figure 4.5B). These decorations appeared as light, string-like nets against the darker underlying CA tubes when either uranyl acetate (UA) or phosphotungstate was used as the stain. No equivalent decorations of control CA tubes alone were seen in either case. The most common inter-ring spacing in the TRIM5$\alpha_{AGMpyg}$ samples was 30-35 nm, in excellent agreement with the other measurements of the TRIM5 hexagonal lattice, although the rings were again irregular and inter-ring spacings varied between 20 and 55 nm (Figure 4.5C).

Deep etch EM images can often exhibit even greater contrast than negative stained transmission EM images, and this was evident even in deep etch images of undecorated HIV-1 CA tubes, where rows of invididual CA hexamers were readily visible (Figure 4.5D, upper row). Strings and rings of TRIM5$\alpha_{AGMpyg}$ were often also more visible on the decorated CA tube surfaces, and networks of rings were clearly observable in some cases (Figure 4.5D, lower panel). We therefore conclude that TRIM5 proteins can also form hexagonal nets on the surfaces of helical HIV-1 CA tubes.

### 4.2.7 Generation of hyperstable, disulfide-crosslinked HIV-1 core particles

A central goal of our studies was to analyze TRIM5 binding to authentic viral capsids, both biochemically and by direct imaging. This goal is technically challenging owing to the inherent instability of viral core particles. We reasoned that this challenge might be overcome by disulfide crosslinking the capsid shell to increase stability. This strategy was particularly attractive because our previous studies have shown that Cys residues substituted at CA positions Ala14 and Glu45 crosslink efficiently when CA hexamers are assembled *in vitro* (28, 49). We therefore tested the effect of introducing these substitution mutations into HIV-1 virions.

Normal levels of viral particles were produced from 293T cells that expressed an HIV-$1_{NL4\text{-}3}$ΔR8.2 proviral expression vector encoding the mutant $CA_{A14C,E45C}$ protein (not shown). Wild type and mutant viral cores were isolated by spinning virions through a detergent layer to remove the outer viral membrane and then directly into a 30-70% sucrose gradient, where viral cores concentrated at a density of 1.22-1.27 g/ml (fractions 10-12, highlighted in pink in Figure 4.6A, left panel) (50). As reported previously (50, 51), wild type cores can be isolated using this procedure (see Figure 4.6B), but the yields of recovered cores were consistently low in our hands (0.2±0.1% based upon total virion CA). This was apparently because most of the CA molecules dissociated from the core and migrated to the top of the gradient during purification (Figure 4.6A, left panel). In contrast, nearly all of the $CA_{A14C,E45C}$ protein migrated toward the bottom of the gradient when cores were isolated from mutant virions (Figure 4.6A, right panel). The bulk of this CA protein was present within small incomplete/broken or spherical assemblies that concentrated at

Figure 4.6 Purification of wild type and hyperstable HIV-1 cores. (A) Wild type (left) and hyperstable A14C/E45C (right) HIV-1 cores were purified using a sucrose-gradient "spin-through" method (50). Sucrose gradient profiles showing α-CA western blots of sucrose gradient fractions (top) as well as quantified CA levels (bottom) and density (bottom blue line; g/ml) of each gradient fraction. The migration of the CA peak to denser fractions clearly demonstrated the higher stability of crosslinked HIV-1 cores (compare the amounts of wild type and A14C/E45C CA in fractions 10-12). Fractions corresponding to the expected core densities (10-12) are highlighted in pink and were pooled, washed and concentrated for the analyses in B and C. (B) Negatively stained electron micrograph of wild type (left) and A14C/E45C (right) cores shows apparently normal conical, cylindrical and spherical cores. Note the presence of contaminating detritus in the background (introduced by commercial sucrose stocks). Pie charts (inset) of observed morphologies of wild type (left; n = 143 cores) and A14C/E45C cores (right; n=353 cores) show that the introduced Cys crosslinks do not alter HIV-1 core morphologies significantly. (C) Nonreducing α-CA western blots showing that A14C/E45C cores are crosslinked (compare % hexamer as a function of [β-ME]). Asterisks indicate Gag fragments (p55 and p37) that copurifed with mature cores during purification. (D, E) Representative negatively stained electron micrographs showing the relative abundance and purity of (D) A14C/E45C crosslinked cores and (E) A14C/E45C crosslinked cores with an additional A92E mutation that reduces core clustering (right) (31, 52). Scale bar represents 100 nm. The higher yield of crosslinked cores and the absence of contaminants or core clustering in the affinity purified core samples makes them ideal for ECT studies.

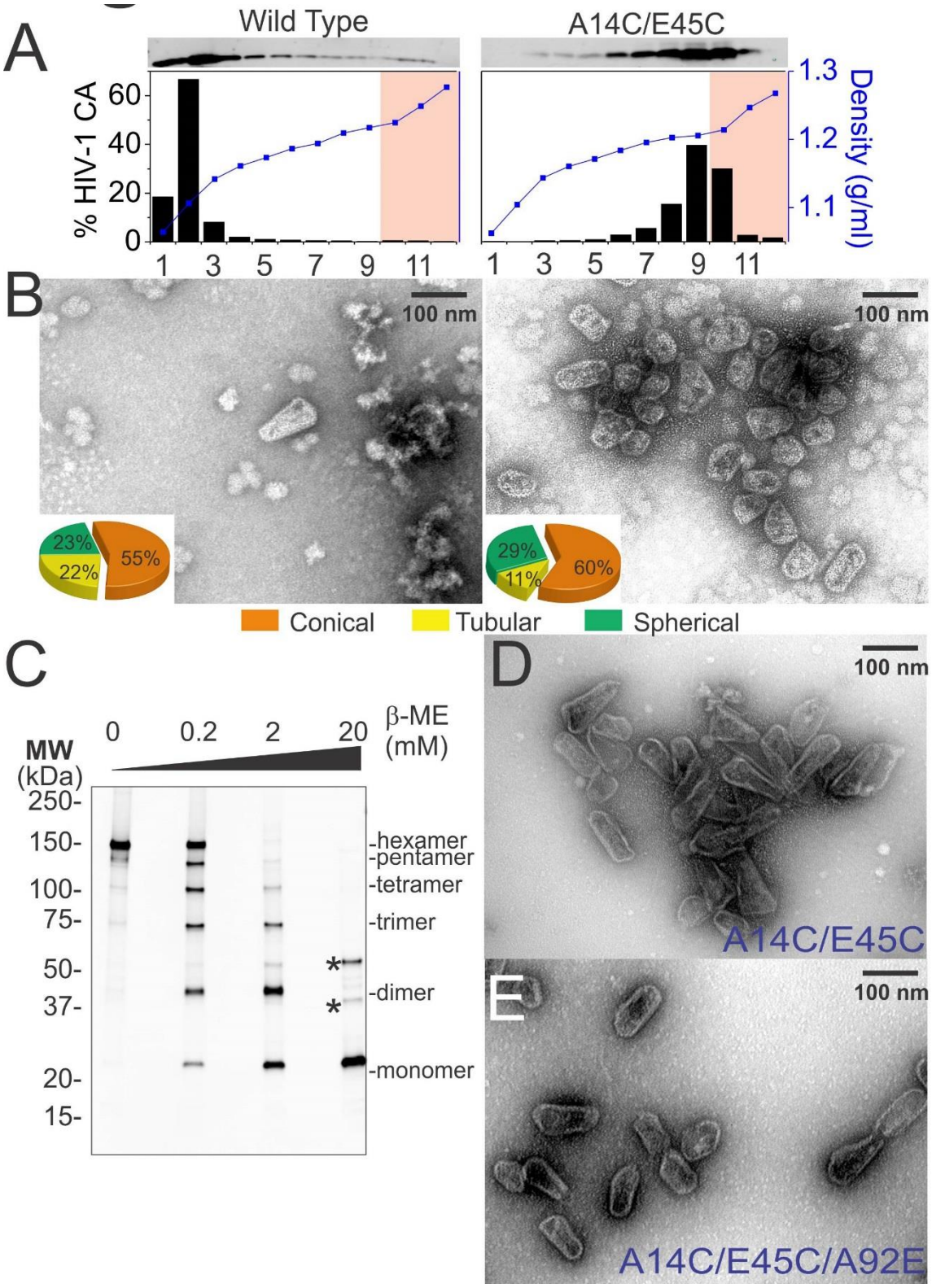
A
Wild Type
A14C/E45C
% HIV-1 CA
Density (g/ml)
B
100 nm
23%
22%
55%
29%
11%
60%
Conical
Tubular
Spherical
C
MW
(kDa)
0
0.2
2
20
β-ME
(mM)
250-
150-
100-
75-
50-
37-
20-
15-
-hexamer
-pentamer
-tetramer
-trimer
-dimer
-monomer
D
A14C/E45C
E
A14C/E45C/A92E

densities of 1.18-1.21 g/ml (gradient fractions 6-9, Figure 4.6A, right panel and see Figure 4.7). These nonnative assemblies probably arise from spurious crosslinking of CA hexamers in the free intraviral pool of CA molecules that are excluded from the mature HIV-1 capsid (53-55). Nevertheless, a substantial fraction of the CA protein also concentrated at the density expected for native core particles (fractions 10-12, highlighted in pink in Figure 4.6A, right panel). These "hyperstable" cores were reproducibly recovered in higher yields than wild type cores (0.8±1%) and their distribution of morphologies was similar to that of wild type cores (Figure 4.6B, right panel). Consistent with the experimental design, nearly all of the CA molecules within these fractions were crosslinked within stable hexamers, as analyzed by nonreducing SDS-PAGE and western blotting (Figure 4.6C). These experiments indicate that disulfide crosslinks form spontaneously in otherwise native and untreated HIV-1 capsids, and that the crosslinks stabilize the capsids without introducing any major morphological defects.

### 4.2.8 Isolation of HIV-1 core particles for cryoEM imaging

Sucrose gradient-purified hyperstable HIV-1 cores were suboptimal for imaging studies because they copurified with vesicles and other impurities and because they clustered together. To produce purer cores, we designed an alternative core affinity purification method that exploited the interaction between cyclophilin A (CypA) and HIV-1 CA (outlined in Figure 4.7) (56-58). Briefly, viral membranes were stripped using a brief Triton X-100 treatment and the liberated cores were then captured on magnetic Strep-Tactin beads derivatized with OSF-CypA. The immobilized cores were washed rigorously and then eluted using the small molecule cyclosporine A (CsA), which competitively

Figure 4.7 CA assemblies in fractions 7-9 are also composed of crosslinked hexamers. (A) Nonreducing α-CA western blots of CA assemblies in fractions 7-9. (B) Representative negative stain electron micrograph of fractions 7-9. (C) Pie chart of the observed morphological distribution of particles in fractions 7-9. (D) Purification schematic (refer to figure legend on the right.) Pure, recombinant OneSTrEP-FLAG-CypA (OSF-CypA) is added to HIV-1 virions and their limiting membrane is dissolved by detergent treatment. OSF-CypA-HIV-1 core complexes are captured using Strep-Tactin sepharose magnetic beads. The beads are restrained using a magnet and vesicles and other bound contaminants are removed by rigorous washing. Cores (but not CypA) are eluted by addition of cyclosporine A. (E) α-CA (top) and α-FLAG (CypA; bottom) western blot of samples from different steps in HIV-1 core affinity purification (see Experimental Procedures for details). Note that the eluate, which contains purified cores, is free from bound CypA and therefore suited for TRIM5α binding studies. (F) Silver-stained SDS-PAGE reveals that the expected components of HIV-1 cores are all present in our hyperstable cores.

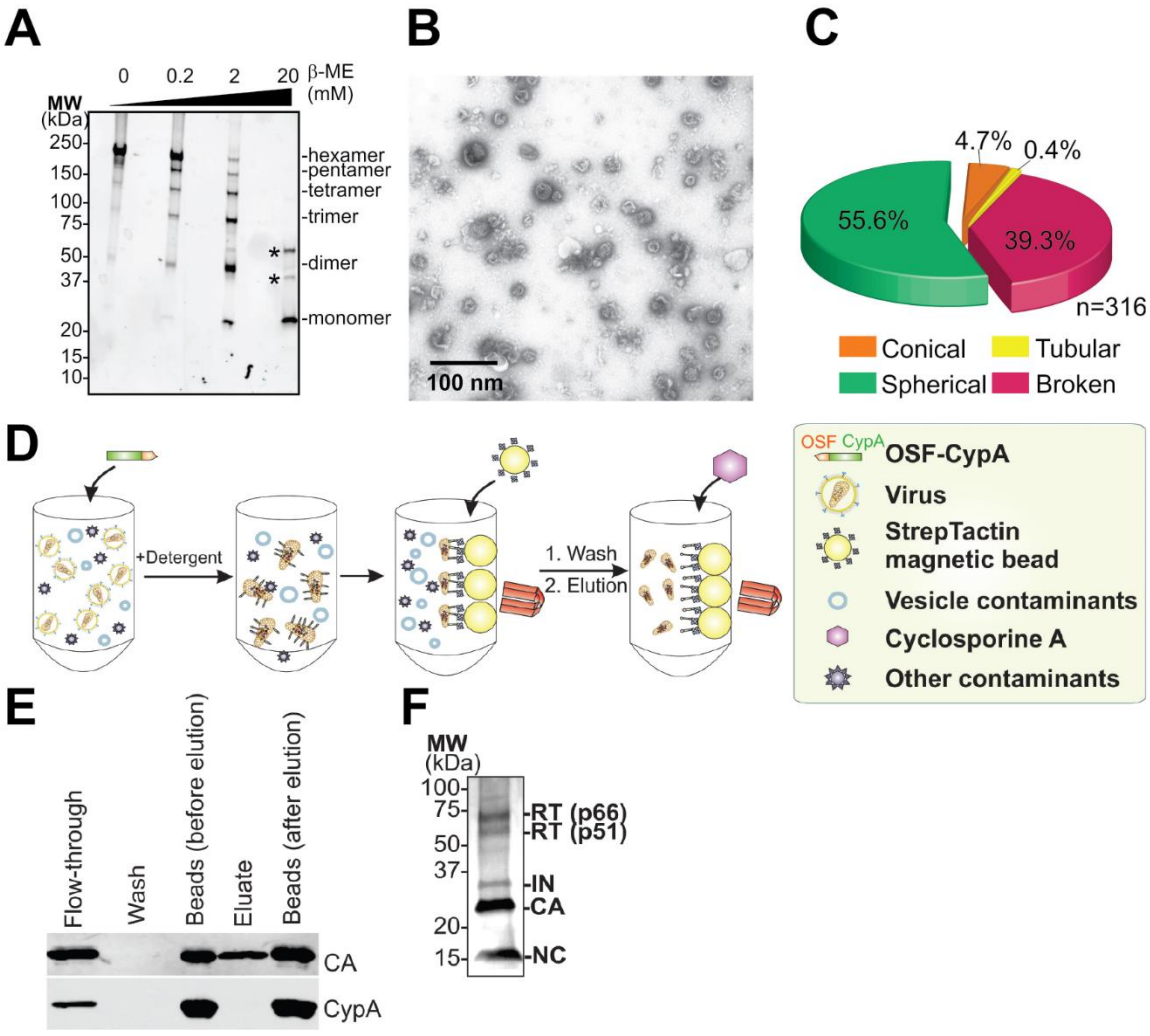
A
0
0.2
2
20
β-ME (mM)
MW (kDa)
250
150
100
75
50
37
20
15
10
hexamer
pentamer
tetramer
trimer
dimer
monomer
B
100 nm
C
4.7%
0.4%
55.6%
39.3%
n=316
Conical
Tubular
Spherical
Broken
D
+Detergent
1. Wash
2. Elution
OSF CypA
OSF-CypA
Virus
StrepTactin magnetic bead
Vesicle contaminants
Cyclosporine A
Other contaminants
E
Flow-through
Wash
Beads (before elution)
Eluate
Beads (after elution)
CA
CypA
F
MW (kDa)
100
75
50
37
20
15
RT (p66)
RT (p51)
IN
CA
NC

inhibits the CypA-CA interaction and binds CypA ~700-fold more tightly than does CA (Figure 4.6D) (59-63). This method increased core yields an additional four-fold (3±2% core recovery) and dramatically increased their purity (compare Figure 4.6D to Figure 4.6B, right panel).

To reduce core clustering, we introduced a CA Ala92Glu substitution within the exposed loop of HIV-1 CA. This mutation does not affect TRIM5α restriction (64), and it was previously shown to reduce the clustering of helical CA tubes, presumably by reducing the overall surface hydrophobicity (31, 52). As shown in Figure 4.6E, the substitution also reduced the clustering of viral cores (compare Figures 4.6D and 4.6E), and did so without altering core morphology or reducing core yields (3±1% core recovery).

In summary, hyperstable $CA_{A14C,E45C,A92E}$ cores could be purified by affinity chromatography and isolated in high yields. The purified cores contained the expected viral proteins as analyzed by silver staining (Figure 4.7), were hyperstable and fully disulfide crosslinked, exhibited normal capsid morphologies and spread diffusely on EM grids.

### 4.2.9 TRIM5 binding to HIV-1 capsids

The susceptibility of different retroviruses to restriction by different TRIM5 alleles can vary dramatically and appears to be determined at the level of capsid recognition (5, 22, 64, 65). Consistent with previous reports (4, 6, 66), we found that TRIM5 proteins restricted the transduction of HeLa cells with an HIV-1 reporter vector following the order: TRIMCyp and $TRIMCyp_{K283D,Q287D}$>$TRIM5\alpha_{rh}$>$TRIM5\alpha_{AGMpyg}$>$TRIM5\alpha_{CPZ}$ and $TRIM5\alpha_{hu}$ (Figure 4.3). A sucrose cushion cosedimentation assay was again used to test whether our pure recombinant TRIM5α proteins bound directly to hyperstable HIV-1

cores, and whether core binding correlated with restriction activity. These experiments were performed with two proteins that restrict HIV-1; TRIM5$\alpha_{AGMpyg}$ and TRIM5$\alpha_{rh}$, and one protein that does not restrict HIV-1; TRIM5$\alpha_{CPZ}$. Human TRIM5α proteins were not used in these assays because they tended to aggregate and pellet, even in the absence of HIV-1 cores. TRIMCyp was also not used, owing to the presence of low levels of residual cyclosporine A in the core preparations.

As shown in Figure 4.8, the restricting TRIM5$\alpha_{AGMpyg}$ and TRIM5$\alpha_{rh}$ proteins both bound hyperstable HIV-1 cores as evidenced by the fact that these proteins copelleted with cores through the sucrose cushion, but did not pellet in the absence of cores (compare lanes 1 and 2 and lanes 3 and 4). In contrast, the nonrestricting TRIM5$\alpha_{CPZ}$ protein did not bind cores under similar conditions (compare lanes 5 and 6). The core binding experiments were performed in the presence of excess TRIM5α proteins, and the stoichiometry of the pelleted core-TRIM5$\alpha_{AGMpyg}$ complexes was estimated by comparing the levels of CA and TRIM5$\alpha_{AGMpyg}$ to standard curves of known protein concentrations. The measured TRIM5$\alpha_{AGMpyg}$:CA ratio in these experiments was 1:7±2 (n=4). Based upon the relative sizes, we estimate that each TRIM5 ring will cover ~14 CA hexamers (23). Based upon the known stoichiometries of each ring (CA=6, TRIM5α=6), we therefore estimate that a fully saturated capsid would have a TRIM5:CA ratio of approximately 1:14. Our experiments therefore indicate that two different restricting TRIM5α proteins can bind directly to hyperstable HIV-1 cores *in vitro* at near-saturating levels, whereas the nonrestricting TRIM5$\alpha_{CPZ}$ protein does not bind cores.

Figure 4.8 TRIM5α proteins bind directly to HIV-1 cores and binding correlates with HIV-1 restriction susceptibility. TRIM5 proteins were incubated in the absence of cores (lanes 1, 3, 5) or in the presence of stable HIV-1 cores (lanes 2, 4, 6). Sucrose cushion centrifugation binding experiments were performed and pelletable cores and bound TRIM5α (Pellet, 30% of total) and unbound TRIM5α (Supernatant, 2% of total) were analyzed by western blotting for TRIM5 and CA proteins. The input levels of both proteins are also shown for reference (Input, 2% of total). Representative results from one of three independent experiments are shown.

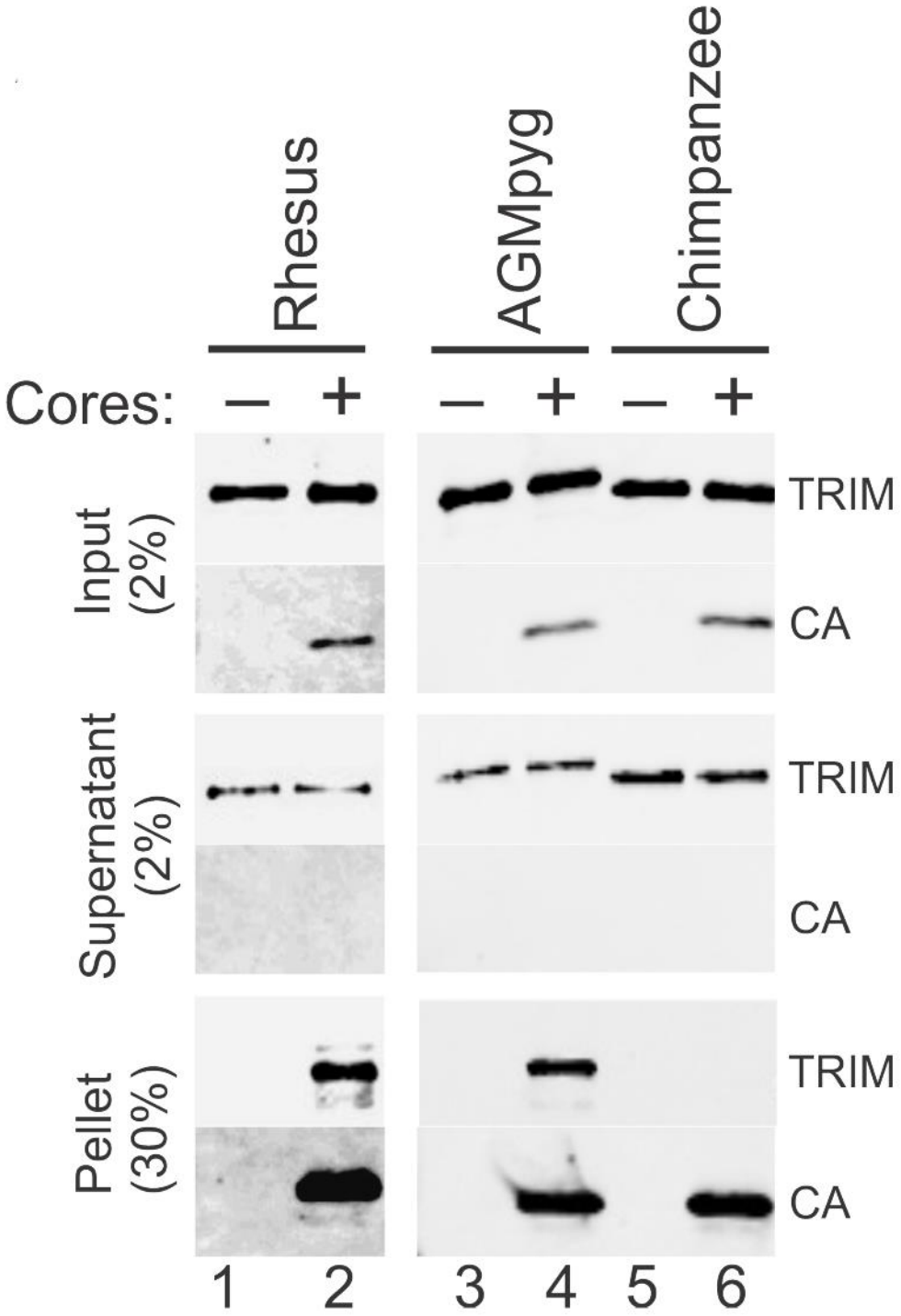
Rhesus
AGMpyg
Chimpanzee
Cores:
–
+
–
+
–
+
Input (2%)
Supernatant (2%)
Pellet (30%)
TRIM
CA
TRIM
CA
TRIM
CA
1
2
3
4
5
6

4.2.10 EM Imaging of TRIM5 decorated HIV-1 cores

Hyperstable cores were visualized in three dimensions (Figure 4.9) by electron cryotomography (ECT). Spherical, cylindrical and conical cores were observed displaying the same general size and lattice features expected of authentic HIV-1 cores (Figure 4.9). Holes in the tips of conical cores were also seen, supporting previous results suggesting that cores are frequently unclosed (67).

We next imaged cores decorated with TRIM5$\alpha_{rh}$. In addition to the cores, the most prominent feature in the images was a network of densities at the air/water interface. The network exhibited three-fold vertices (Supplemental Movie 1) in the plane of the interface that were strikingly similar to 2D hexagonal TRIM5α lattices. Approximately 12% of cores imaged were also decorated on their outer capsid surfaces with TRIM5$\alpha_{AGMpyg}$ densities. Multiple extended density "arms" approximately 19 nm in length were seen arranged in an approximately hexameric pattern (Figure 4.10, and Supplemental Movie 1).

Because there was so much TRIM5$\alpha_{AGMpyg}$ at the air/water interface, but only a small fraction of the cores were decorated with TRIM5α, we suspected that previously core-bound TRIM5α was being lost to the air/water interface during plunge-freezing. To address this issue, we crosslinked the core/TRIM5α complexes with ethylene glycol bis(sulfosuccinimidylsuccinate) (Sulfo-EGS) prior to plunge freezing. There was still a substantial amount of TRIM5α at the air/water interface under these conditions, but now the majority of cores, including spherical, cylindrical and conical shaped ones, were decorated with TRIM5$\alpha_{AGMpyg}$. Analysis of the volume surrounding these cores revealed broken, but extensive TRIM5a hexagonal nets and in some cases these nets enveloped the entire capsid (Figure 4.10B-D and Supplemental Movies 2 and 3).

Figure 4.9 ECT of stable HIV-1 cores reveals structural features expected of HIV-1 cores. (A, B) Tomographic slices of two conical HIV-1 capsids, displaying no densities above background noise around their exterior. (C, D) Tomographic slices of NAD-filtered cores display side- and front-facing views of individual CA hexamers. Boxed in black and blown-up are densities with dimensions similar to those of the crystal structure of the HIV-1 capsid. (E) Crystal structure of the HIV-1 capsid hexamer, the dimensions match those of the density highlighted in (C) and (D).

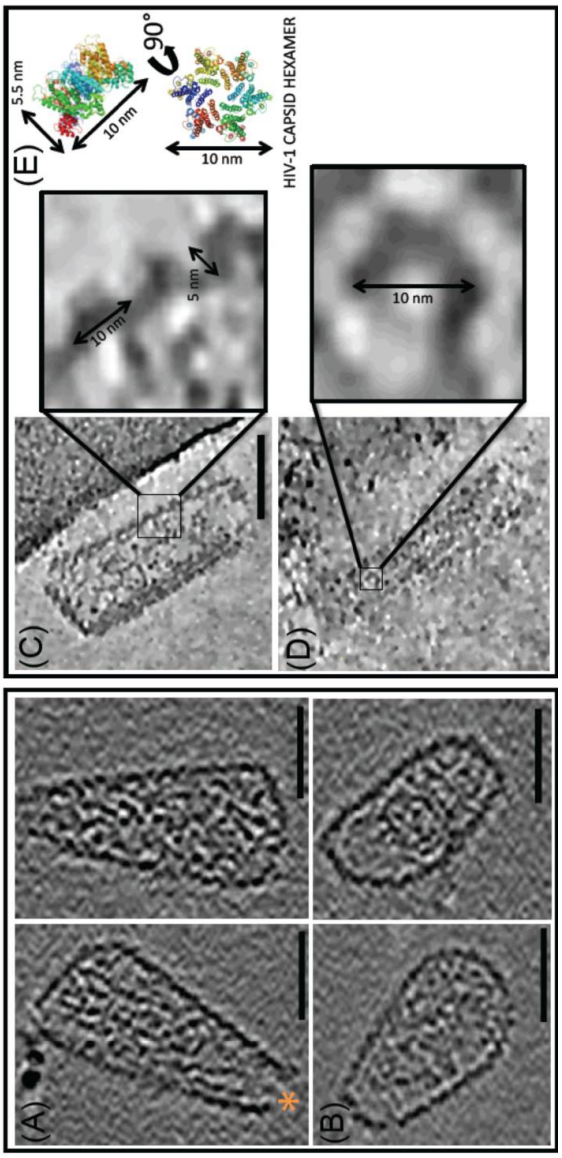
(E)
5.5 nm
10 nm
90°
10 nm
HIV-1 CAPSID HEXAMER
10 nm
5 nm
10 nm
10 nm
(C)
(D)
(A)
(B)

Figure 4.10 ECT reveals that TRIM5α forms flexible hexagonal nets on hyperstable HIV-1 cores. (A) Segmentation of a spherical HIV-1 core (yellow) decorated with TRIM5α (blue). (B) Two views of segmentation of a cylindrical HIV-1 core decorated with TRIM5α and subjected to mild sulfo-EGS crosslinking prior to vitrification. (C) segmentation of a conical HIV-1 core decorated with TRIM5α (sulfo-EGS crosslinked). (D) The same core as in (C) with the TRIM5α omitted. (E) Schematic model of an HIV-1 fullerene cone bound by a TRIM5α hexagonal net.

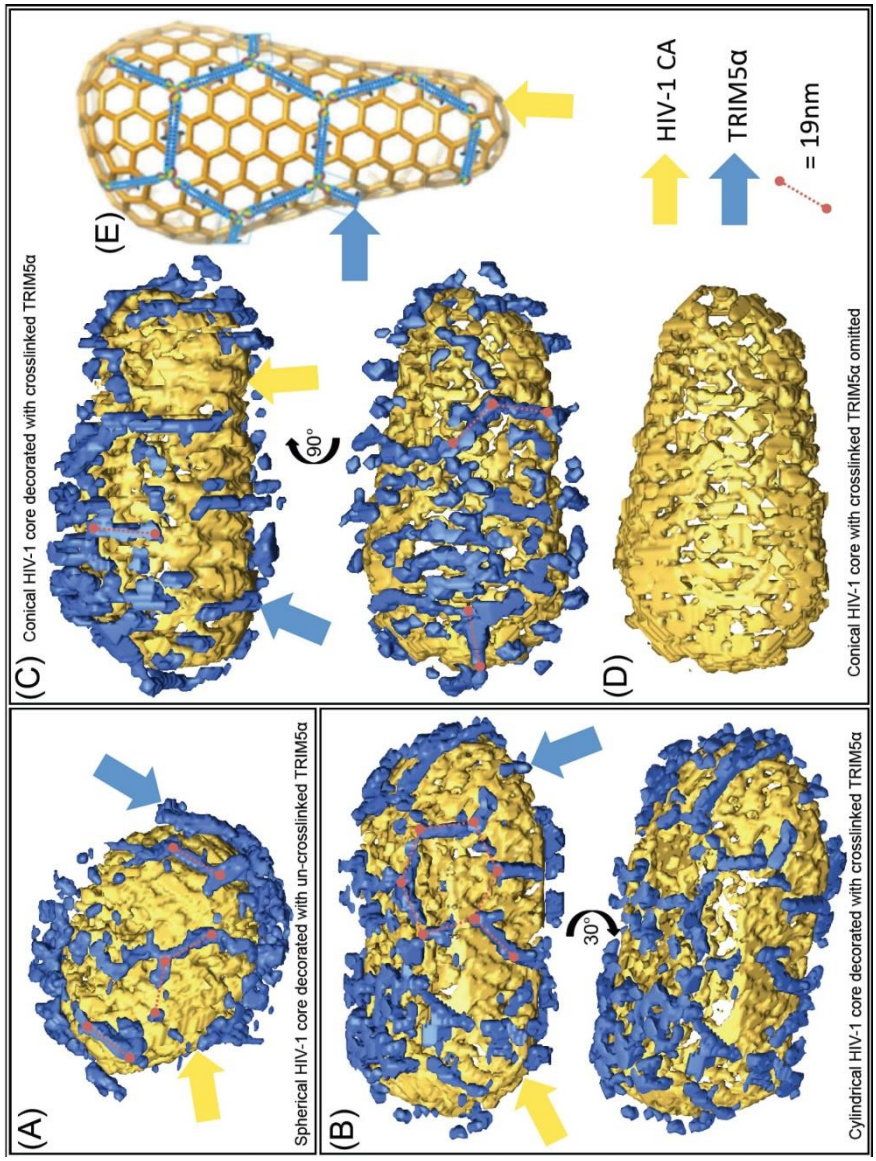
(A)
Spherical HIV-1 core decorated with un-crosslinked TRIM5α
(B)
30°
Cylindrical HIV-1 core decorated with crosslinked TRIM5α
(C)
Conical HIV-1 core decorated with crosslinked TRIM5α
90°
(E)
(D)
Conical HIV-1 core with crosslinked TRIM5α omitted
HIV-1 CA
TRIM5α
= 19nm

## 4.3 Discussion

Our studies strongly support the prevailing models that TRIM5 restriction factors bind directly to the surfaces of incoming retroviral capsids and that restriction susceptibility is dictated at the level of capsid recognition (4, 22, 37, 68, 69). We further find that the ability to assemble into hexagonal nets comprising open, six-sided rings is a conserved feature of multiple different primate TRIM5 proteins. Our EM analyses, together with recent crystal structures of fragments of nonassembling TRIM5 protein that span the core coiled-coil and L2 linker regions (20), indicate that each ring edge is formed by a TRIM5 dimer that displays two PRYSPRY (or CypA) recognition domains at its center. Most importantly, we find that capsid binding and TRIM5 assembly are coupled processes that collaborate to promote the recognition of pleomorphic retroviral cores with high affinity and specificity.

### 4.3.1 Reagent development

Through the course of our studies, we developed and characterized two new sets of reagents for studying retroviral replication and restriction: hyperstable, disulfide-crosslinked HIV-1 capsids and pure recombinant primate TRIM5 proteins. The generation of hyperstable capsids was enabled by previous studies showing that Cys residues at CA positions 14 and 45 form disulfide bonds efficiently *in vitro* when these residues are closely juxtaposed within the CA hexamer (28, 49). Our experiments demonstrate that these disulfides also form efficiently in the context of the intact HIV-1 capsid. A similar disulfide crosslinking strategy was used to link CA trimers at cysteine positions 207 and 216 across the local three-fold axes of the HIV-1 capsid (70). We have compared these two different systems, as well as an alternative strategy in which CA hexamers were crosslinked by

disulfide bonds between Cys residues at CA positions 42 and 54 (49). Disulfide bonds form readily within viral capsids in all three cases (28, 49, 70) (and data not shown), and we anticipate that the different crosslinking strategies will have distinct advantages depending upon the application. For example, we have confirmed the report that HIV-1 cores with trimerized CA proteins retain modest infectivity (70), whereas infectivity is almost completely abolished when cores are crosslinked at either site in the CA hexamer. We also find, however, that viral core yields and stabilities are greater for the two hexamer crosslinking systems, and are highest for the Cys14/Cys45 system described here. Thus, these hyperstable capsids should be optimal for analyzing the binding of proteins and drugs, and we note that a series of HIV-1 capsid binding proteins have recently been described, including CPSF6 (71, 72), Nup153 (73-75) and Nup358 (75, 76), as have several capsid binding inhibitors, including PF-74 (77) and BI-1 and BI-2 (78). Hyperstable capsids may also represent a useful starting point for the development of *in vitro* viral replication assays, particularly if the capsid disulfides can be reduced without inactivating the internal reverse transcriptase and integrase enzymes.

The development of systems for producing multimilligram quantities of pure recombinant primate TRIM5 proteins should similarly facilitate studies of restriction by enhancing methods for protein detection and enabling new mechanistic and structural analyses. For example, our recombinant TRIM5$\alpha_{rh}$ proteins have already been used successfully as antigens to generate monoclonal antibodies that can detect endogenous TRIM5α proteins (NIH AIDS Reagent Program, and Tom Hope, personal communication). Moreover, although structural studies of TRIM5 protein domains and fragments have made valuable contributions to our understanding of TRIM5 structure and enzymology, there are

a number of indications that the different domains work together as an integrated machine. It will therefore also be important to study intact TRIM5 proteins, particularly to determine how capsid recognition is coupled to ubiquitin signaling (14).

### 4.3.2 TRIM5 recognition of retroviral capsids and its implications for restriction

Antiviral innate immune factors that function by recognizing retroviral capsids must overcome considerable sequence and structural variability. Primate TRIM5 proteins accomplish this task by coupling weak recognition of conserved capsid epitopes with hexagonal net assembly, thereby amplifying intrinsically weak binding affinities through avidity effects. Our studies confirm the conservation of hexagonal net assembly, but also reveal that TRIM5 hexagonal nets are not highly regular. The lack of strict regularity in the TRIM5 net may be an adaptation to the opposing lack of regularity in retroviral capsids, where every CA hexagon occupies a slightly different local environment and pentagons and other kinds of lattice "defects" are also prevalent (67).

Consistent with a lattice assembly model, imaging studies have provided direct evidence that multiple TRIM5 molecules can bind continuously to incoming capsids, (10). The stoichiometry of TRIM5-capsid interactions within cells is not yet known, but we find that TRIM5 molecules can cover most of the capsid surface *in vitro*. However, a patch of just 4-6 TRIM5 rings covers about half of the capsid surface (see Figure 4.10), and would present ~40 recognition domains for avid capsid binding. Thus, there is no reason to believe that the entire capsid must be completely enveloped within a surrounding TRIM5 lattice for restriction to occur. Indeed, CA mixing studies have shown that efficient TRIM5

restriction can occur even when only 25% of the capsid subunits are competent for TRIM5 binding (79).

TRIM5-mediated restriction appears to proceed via a multistep pathway in which capsid recognition is followed by steps that lead to capsid dissociation and inhibition of reverse transcription (5, 14). In cells, the later processes can be decoupled from the initial binding event by treatment with proteasome inhibitors or by mutations in the RING domain (8, 80). These treatments do not block TRIM5 binding, but presumably do interfere with ubiquitin-mediated signaling events. Thus, although TRIM5 binding can destabilize helical CA tubes *in vitro* (45, 46), capsid destabilization and inhibition of reverse transcription appear to require ubiquitin-dependent signaling in cells. Capsid binding can activate TRIM5 ubiquitin E3 ligase activity *in vitro* (14), and the structure of the hexagonal TRIM5 lattice suggests how this could occur. Recent structural studies of the RING domains from TRIM37 (PDB ID: 3LRQ) and TRIM5α (D. Ivanov, personal communication) have demonstrated that the RING domains function as dimers. However, the antiparallel structure of the TRIM5 coiled-coil precludes close contact of the two RING domains within a single TRIM5 dimer (19, 20). Thus, RING domains from multiple different TRIM5 dimers must presumably come together to transfer ubiquitin, and our lattice structure predicts that just such an association of three TRIM5 RING domains will occur at local three-fold axes in the hexagonal net. Hence, formation of the hexagonal TRIM5 lattice may not only enhance binding avidity, but also activate the ubiquitin signaling cascade that ultimately results in capsid dissociation and inhibition of reverse transcription.

## 4.4 Experimental procedures

### 4.4.1 Plasmids, cells and antibodies

HEK 293T and HeLa-M cells were grown in DMEM media (Gibco) supplemented with 10% heat-inactivated FCS and 2 mM L-Glutamine, at 37°C with 5% $CO_2$. Plasmid constructs for virus production and for expressing TRIM5, CA and OSF-CypA in mammalian, insect and bacterial cells were created by standard cloning and mutagenesis methods.

### 4.4.2 Expression and purification of TRIM5 proteins

Recombinant baculoviruses expressing TRIM5 proteins with either N-terminal One-STrEP-FLAG (OSF) or C-terminal FLAG-One-STrEP (FOS) PreScission protease-cleavable tags were generated using the Bac-to-Bac baculovirus expression system (Life Technologies). Suspension SF9 insect cells (2 L at 2 x $10^6$ cells/ml) grown in ESF-921 medium (Expression Systems) were infected with recombinant baculoviruses at multiplicities of infection of 10, and harvested by centrifugation 48 hours later. All purification steps were performed at 4°C. Cell pellets were resuspended in 5 times the pellet volume of lysis buffer (70 mM N-Cyclohexyl-2-aminoethanesulfonic acid (CHES), 100 mM NDSB-256, 1.5% Triton X-100, 100 nM $ZnCl_2$, 1 mM Tris(2-carboxyethyl)phosphine (TCEP), 0.7% protease inhibitor cocktail (v/v, Sigma), 100 U avidin, pH 10) and lysed by freeze-thaw and sonication (3 x 30 seconds on ice; Branson sonifier 450, 50% duty cycle, 50% output). Cell lysates were clarified by ultracentrifugation at 184,000xg (Beckman Ti 50.2 rotor) for 1 hour. The supernatants were filtered (0.45 μm) and loaded onto a 5 ml StrepTrap HP column (GE Healthcare) pre-equilibrated in binding buffer (20 mM CHES,

100 nM $ZnCl_2$, 1 mM TCEP, pH 10). The column was washed with 20 column volumes (CV) of binding buffer supplemented with 1 M NaCl and 100 U avidin (VWR), followed by 5 CV of binding buffer, and the protein was eluted in 6 CV binding buffer supplemented with 2.5 mM D-desthiobiotin (Sigma). The eluate was diluted to 0.3 mg/ml protein in binding buffer to minimize protein loss due to self-assembly, and dialyzed overnight against 1L cleavage buffer (25 mM Tris, 1 mM TCEP, pH 8) supplemented with ~ 1:100 (by mass, enzyme:substrate) $His_6$-HRV14-3C and $His_6$-Usp2 enzymes to remove the OSF tag and any ubiquitin chains added during insect cell expression. TRIM5$\alpha_{hu}$ and TRIMCyp formed soluble/insoluble aggregates at pH 8 and were therefore dialyzed against 20 mM CHES, 1 mM TCEP, pH 9. Most TRIM5 proteins were sensitive to nonspecific internal proteolysis by HRV14-3C protease. We therefore used the minimal amount (which differed between constructs) required to completely cleave the OSF tag overnight. When cleavage was complete, the pH of protein solution was adjusted to 10 by direct addition of 1M CHES, pH 10, to a final concentration of 100 mM. The sample was applied onto two tandem 5 ml HiTrap Q HP columns (GE Healthcare) pre-equilibrated with binding buffer, and eluted with a 12 CV linear NaCl gradient (0-1 M) in binding buffer. Fractions containing TRIM5 proteins were pooled, dialyzed against 1 L binding buffer for at least 4 hours, loaded onto a HiLoad 16/600 Superdex 200 gel filtration column (GE Healthcare) pre-equilibrated with binding buffer and eluted in 1 CV of binding buffer. Fractions corresponding to TRIM5 dimers were pooled and concentrated to 1 mg/ml using Vivaspin 20 concentrator (10,000 MWCO PES for TRIM5$\alpha_{AGMpyg}$ ΔSPRY and 30,000 MWCO PES for full-length TRIM5α and TRIMCyp, Sartorius Stedim). Average yields were 4 mg (1.3-

9.6 mg) per 1L insect cell culture. The protein identities were confirmed by electrospray ionization mass spectrometry.

4.4.3 TRIM5 2D crystallization

TRIM5-21R proteins were expressed, purified and crystallized as previously described (23), except that the TRIM5-21R$_{1-300}$ assembly was modified from the original publication as follows. Spontaneous assembly was promoted by addition of an equal volume of 0.1M Sodium chloride, 0.1M Bicine pH-9.0, 20% PEG MME to the concentrated protein solution.

Freshly purified TRIM5$\alpha_{AGMpyg}$ protein was concentrated to 1-3 mg/ml and assembled by incubating at room temperature for 1 hour at 4°C for 1-2 days. For EM analyses, 5 µl sample aliquots were incubated on carbon-coated EM grids for 5 minutes. The grids were washed by placing each grid on a single 40 µL drop of 0.1M KCl for 3 minutes, briefly blotted and then stained on a single 20 µL drop of 2% uranyl acetate for an additional 3 minutes.

Unlike TRIM5$\alpha_{AGMpyg}$, TRIMCyp did not spontaneously assemble into hexagonal lattices following concentration. However, rare crystals could be observed when an equal volume of 0.01M Cobalt chloride hexahydrate, 0.1 M MES monohydrate pH 6.5 and 1.8 M ammonium sulfate was added to freshly concentrated protein at ~1 mg/ml.

4.4.4 Templated assembly of TRIM5 on hexagonal arrays of HIV-1 CA-NC

As previously described (23), 2-dimensional crystals composed of crosslinked, hexagonal HIV-1 CA were prepared by incubating the HIV-1 CA-NC$_{A14C/E45C/W184A}$ (232

μM) protein with a small 25-TG oligo (143 μM). TRIM5 proteins were then added in 1- to 10-fold molar excess, and the pH was immediately adjusted to 9 by direct addition of Tris buffer to a final concentration of 100 mM. Samples were incubated for 1-96 hours, applied to carbon-coated EM grids for 60 seconds, and washed and stained as described above, and visualized by EM. 10-fold lower amounts were sufficient for $TRIMCyp_{K283D,Q287D}$ templated assembly.

### 4.4.5 Bacterial protein expression and purification

#### *4.4.5.1 OSF-Cyclophilin A (OSF-CypA)*

OSF-CypA was expressed in *E. coli* Rosetta (λDE3) pLysS cells (Stratagene) grown in ZYP-5052 media using an autoinduction system (81). Cells were lysed on ice by sonication in lysis buffer (50 mM Tris, pH 8, 50 mM NaCl, 10 mM β-mercaptoethanol (β-ME), 0.2% (w/v) deoxycholate, 2.5 nmol avidin, 20 μg/ml DNAse) supplemented with protease inhibitors (20 μg/ml PMSF, 0.4 μg/ml pepstatin, 0.8 μg/ml leupeptin and 1.6 μg/ml aprotinin). All purification steps were performed at 4°C. Cell lysates were clarified by centrifugation at 15,000 rpm (Beckman JA-20 rotor) for 45 minutes, filtered (0.45 μm) and loaded onto two 5 ml tandem StrepTrap HP columns (GE Healthcare) pre-equilibrated in binding buffer (100 mM Tris, 150 mM NaCl, 10 mM β-ME, pH 8). The column was washed with 10 CV of binding buffer and OSF-CypA was eluted in 3CV of the same buffer supplemented with 2.5mM D-desthiobiotin. The protein was dialyzed against Q buffer (50 mM Tris, 50 mM NaCl, 10 mM β-ME, pH 8) and loaded onto two connected 5 ml HiTrap HP Q-Sepharose anion exchange columns (GE Healthcare) pre-equilbrated in the same buffer. The OSF-CypA-containing flowthrough was collected and concentrated using

Amicon Stirred Ultrafiltration Cells (Millipore). OSF-CypA (>99% pure) was obtained in high yields (～100 mg per 1L bacterial culture) and its identity was confirmed by ESI-MS ($MW_{exp}$ =23,806 Da, $MW_{calc, -Met1}$=23,807 Da).

*4.4.5.2 HIV-1 $CA_{A14C/E45C/A92E}$*

The plasmid for expressing HIV-1 CA A14C/E45C/A92E was kindly provided by Dr. Owen Pornillos. *E.coli* Rosetta (λDE3) pLysS cells (Stratagene) were grown to an $OD_{600\ nm}$ of 0.6 in LB medium at 37°C, cooled to 19°C and protein expression was induced with 1 mM isopropyl-β-D-thiogalactopyranoside (IPTG) and incubated overnight with shaking. HIV-1 CA proteins were purified and assembled into tubes as previously described (49), except that a higher concentration of DTT (100 mM) was used during protein purification to improve solubility and increase yields. Cells were lysed as described above and proteins were purified from clarified lysates by ammonium sulfate precipitation, dialyzed against 25 mM KMOPS, 100 mM DTT, pH 6.5 and loaded onto a 5 ml HiTrap Q HP column (GE Healthcare) pre-equilibrated with the same buffer. The flowthrough was applied onto a 5 ml Hi-Load SP Sepharose High Performance column (GE Lifesciences) and eluted with a linear NaCl gradient (0-500 mM) in the same buffer. Fractions containing CA proteins were pooled and dialyzed overnight against storage buffer (20 mM Tris, 40 mM NaCl and 100 mM DTT, pH 8). The CA proteins were then concentrated to a stock of 3 mg/ml using Vivaspin 20 concentrator (10,000 MWCO PES, Sartorius Stedim) and stored at -80°C. Yields were ~20 mg per 1L of culture and the protein identity was confirmed by ESI-MS ($MW_{exp}$=25,667 Da, $MW_{calc}$=25,667 Da).

4.4.6 Assembly of hyperstable CA tubes

CA tubes were assembled at 1 mg/ml by dialysis against dialysis buffer (20 mM Tris pH 8.0, 1M NaCl and 100 mM DTT) at 4°C overnight, followed by dialysis against the same buffer lacking DTT overnight to allow the formation of disulfide crosslinks within the CA hexamers. Disulfide-crosslinked CA tubes were then dialyzed against 20 mM Tris, 40 mM NaCl, pH 8.0 and stored at 4°C.

4.4.7 Preparation of HIV-1 virions

HEK 293T cells (29 x 10 cm plates) were cotransfected (polyethylenimine, PEI, Polysciences) at 70-80% confluency with pLOX-GFP (5 μg DNA/plate) (82) and pCMV-ΔR8.2 vectors (5 μg DNA/plate) (83) that expressed HIV structural proteins encoding the wild type or mutant CA sequences (A14C/E45C or A14C/E45C/A92E). 40 hours later, the virus-containing media was pooled, filtered (0.45 μm) and pelleted by ultracentrifugation through a 4 ml, 20% sucrose/PBS cushion in 25x89 mm polyallomer centrifuge tubes (Beckman Coulter) at 28,000 rpm (Beckman SW 32 Ti rotor) for 2 hours at 4°C. Subsequent core purification steps were performed at 4°C.

4.4.8 Sucrose gradient purification of HIV-1 cores

Wild type HIV-1 cores and hyperstable HIV-1 A14C/E45C cores were isolated from virions using an adaptation of a sucrose gradient spin-through method (44, 50). Virion pellets were resuspended with 2.4 ml ST buffer (20 mM Tris, 75 mM NaCl, pH 7.4). 6 x 11.5 ml 30-70% (w/v) continuous sucrose gradients in ST buffer were made in 14x89 mm polyallomer centrifuge tubes (Beckman Coulter) using a gradient maker (Biocomp). The

gradients were overlaid with a 300 µl 15% (w/v) sucrose cushion in ST buffer containing 0.5% Triton X-100 (to delipidate the virions as they migrated through the cushion) and then with a 300 µl nondetergent barrier layer (7.5% sucrose in ST buffer), which protected virions from premature detergent exposure. Concentrated virions were applied to the top of the gradient and centrifuged through the cushion and gradient at 35,000 rpm (Beckman SW41Ti rotor) for 16 hours. 12 x 1 ml fractions were collected from the bottom of each tube and the density of each fraction was determined from the refractive index using a digital refractometer (Leica). The CA content in each fraction was analyzed by western blotting using rabbit anti-HIV-1 CA polyclonal antibodies (made in-house, 1:3000 dilution). Fractions 10-12 (density = 1.22-1.27 g/ml), which contained intact HIV-1 cores, were pooled, diluted with ST buffer to 14 ml and subjected to ultracentrifugation at 35,000 rpm (Beckman SW41Ti rotor) for 2 hours. The pelleted cores were resuspended in ST buffer.

4.4.9 Affinity purification of HIV-1 cores

2.4 ml of concentrated virions in PBS were mixed gently with an equal volume of lysis buffer (1% Triton X-100, 100 mM Tris, 2M NaCl, pH 8) in the presence of 35 µM OSF-CypA and incubated for 3 minutes. 8 mg of MagStrep”type2HC” beads (IBA GmbH) were added to the lysed virions and mixed gently by inversion for 7 minutes to allow OSF-CypA to bind the membrane-stripped cores. The sample was then placed on a PolyATtract system 1000 magnet separation stand (Promega) for 3 minutes, and the supernatant (‘Flow-through’ Figure 4.7D) was removed. Captured cores were washed 10 times with high salt buffer (50 mM Tris, 1M NaCl, pH 8) to remove unbound CA proteins and contaminating

vesicles and the final wash sample was saved for western blot analysis ('Wash' in Figure 4.7D). Cores were eluted in 150 µl of 50 mM Tris (pH 8), 75 mM NaCl supplemented with 40 µM Cyclosporine A (Sigma-Aldrich) buffer and incubated with inversion for 40 minutes. The sample was briefly centrifuged in a tabletop ultracentrifuge at 2000 rpm for 5 seconds and placed on a Magnesphere Technology Magnetic Separation Stand (Promega) for 5 minutes. The supernatant containing the purified cores ('Eluate' in Figure 4.7D) was collected and used in the experiments shown in Figures 4.6, 4.7, 4.8, 4.9 and 4.10. Beads before and after CsA elution were also saved for western blot analyses (Figure 4.7).

### 4.4.10 Characterization of purified hyperstable cores

#### *4.4.10.1 Core yields*

Virus inputs and core yields were quantified by western blot densitometry against a standard curve of recombinant CA proteins for reference. The recovery of cores from virions was calculated by normalizing core yields to corresponding virus inputs, which were set to 100%. As illustrated in Figure 4.6, disulfide crosslinks apparently stabilized HIV-1 cores, resulting in a ~four-fold increase in the core recovery (0.8±1%; core yields: 0.6±0.5 µg CA; virus inputs: 100±80 µg CA, n=10) compared to wild type cores (0.2±0.1%; core yields: 0.08±0.05 µg CA; virus inputs: 40±30 µg CA, n=7). The affinity purification method consistently produced ~four-fold higher recoveries still of hyperstable HIV-1 A14C/E45C cores (3±2%; core yields: 1±0.6 µg CA; virus input: 40±8 µg CA, n=3) than the sucrose gradient spin-through method. Core recovery was not affected by the A92E mutation (3±1%; core yields: 3±1 µg CA; virus inputs: 100±60 µg CA, n=7).

*4.4.10.2 Analyses of HIV-1 core morphologies*

Particles were imaged by negative stain EM and scored as "tubular" if their edges appeared parallel, as "spherical" if they were spherical or elliptical or as "conical" if they lacked the above properties. The final class included conical, triangular, bullet-shaped and coffin-shaped cores. Particles were not scored if they were obscured by other cores.

*4.4.10.3 Disulfide crosslinks*

To examine the extents of disulfide crosslinks within purified cores, sucrose gradient fractions 7-9 and 10-12 were pooled separately, mixed with SDS-PAGE sample loading buffer lacking β-ME (or containing the concentrations designated in Figure 4.6C), heated at 95°C for 10 minutes, and electrophoresed on 4-15% gradient SDS polyacrylamide gels (Bio-Rad) and analyzed by western blotting.

4.4.11 CA tube binding experiments

CA tube binding experiments were performed as previously described, with minor modifications (5, 23, 44). Recombinant TRIM5α and TRIMCyp proteins (0.25 μM) were incubated alone or with $CA_{A14C/E45C/A92E}$ tubes (2 μM) in binding buffer (20 mM HEPES, 25 mM NaCl, 1mM TCEP, pH 7.2) in a final volume of 225 μl at 4 °C for 1 hour. Aliquots (10 μl) of the incubation mixtures were mixed with 2X SDS-PAGE sample loading buffer for assessment of protein amounts in the inputs. Aliquots (200 μl) of the mixtures were layered onto a 60% (w/v) sucrose/PBS cushion (4 ml, prepared in binding buffer lacking TCEP) and centrifuged at 34,000 rpm for 30 minutes in a Beckman SW50.1 rotor at 4°C to separate free TRIM5α or TRIMCyp and unassembled CA proteins from CA tube-bound

TRIM5 proteins and pelletable CA tubes. Following centrifugation, aliquots (45 µl) of supernatant (500 µl in total) were mixed with 4X SDS-PAGE sample loading buffer, and the pellets were resuspended in 25 µl 1X SDS-PAGE sample loading buffer. The TRIM5 and CA proteins in the input (3%), supernatant (3%) and pellet (30%) were separated by 12% SDS-PAGE and analyzed by western blotting as described above.

4.4.12 Core binding experiments

Recombinant TRIM5$\alpha_{AGMpyg}$ (0.5 µM) and TRIM5$\alpha_{CPZ}$ (0.5 µM) were incubated at 4 °C for 1 hour alone or with hyperstable HIV-1 cores (0.5-1 µM) in binding buffer (40 mM HEPES, 50 mM NaCl, 1 mM TCEP, pH 7.2) in a final volume of 75 µl. Rhesus TRIM5$\alpha_{rh}$ (0.25 µM) was incubated alone or with hyperstable cores under slightly more alkali conditions (40 mM Tris, 50 mM NaCl, 1 mM TCEP, pH 8) to minimize untemplated assembly of TRIM5α during sedimentation. Aliquots (5 µl) of the mixtures were mixed with 2X SDS-PAGE sample loading buffer ('Input' in Figure 4.8). The mixtures were layered onto a 30% (w/v) sucrose/PBS cushion (4 ml, prepared in binding buffer lacking TCEP) and centrifuged at 40,000 rpm for 2.5 hours in a Beckman SW50.1 rotor to separate free TRIM5α and unassembled CA proteins from capsid-bound TRIM5 proteins and pelletable cores. Following centrifugation, aliquots (45 µl) of supernatant (500 µl in total) were mixed with 4X SDS-PAGE sample loading buffer, and the pellets were resuspended in 25 µl 1X SDS-PAGE sample loading buffer. The TRIM5 and CA proteins in the input (2%), supernatant (2%) and pellet (30%) were separated by 12% SDS-PAGE, electrophoretically transferred onto nitrocellulose membranes (Bio-Rad) and analyzed by western blotting with mouse anti-TRIM5α monoclonal (clone 5D5-1-1, NIH AIDS

Research and Reference Reagent Program, 1:1000 dilution) and rabbit anti-HIV-1 CA polyclonal (made in-house, 1:3000 dilution) antibodies. Secondary IRDye800cw-conjugated Donkey anti-mouse IgG (1:10,000, Rockland) or IRDye700DX-conjugated Donkey anti-rabbit IgG (1:10,000, Rockland) antibodies were visualized using an Odyssey infrared imaging system (LI-COR Bioscience). The integrated intensities of protein bands on the western blots were measured using the Odyssey software (LI-COR Bioscience). The molar ratios of TRIM5$\alpha_{AGMpyg}$ to CA in the pellets were estimated from standard curves constructed from known amounts of TRIM5$\alpha_{AGMpyg}$ and CA loaded on the same gel.

### 4.4.13 TRIM5-21R ECT

TRIM5-21R and TRIM5-21R$_{\Delta SPRY}$ 2D crystals were prepared as described previously (Ganser-Pornillos etal 2011). To prepare samples for ECT, 3 µl of polymerized lattice was mixed with 10 nm Au fiducials and applied to a 2/2 holey carbon-coated Cu EM grid (Quantifoil). The sample was then transferred with forceps to the environment chamber of a Vitrobot Mark III (FEI) maintained at 25 °C and 80% relative humidity. Excess liquid was manually blotted from the grids on one side before plunging into liquid ethane. Cryo-preserved grids were then imaged in a 300-kV FEI G2 Polara equipped with a field emission gun and energy filter (slit width set at 20 eV), and fitted with a K2 Summit direct detector. Tilt-series were collected over a series of angles ranging from -60 to +60 degrees using a step size of 1°; 22,500x magnification (effective pixel size of raw data is 5 Å), a total dose of 150 e/Å$^2$ and a defocus of -6 µm. UCSF Tomo (84) was used to collect the tilt series and 3D reconstructions were carried out using a weighted back-projection algorithm tracking 10 nm fiducials in IMOD (85). Pixel size in the final reconstruction was 20 Å.

Subtomogram averages of the TRIM5-21R and TRIM5-21R$_{\Delta SPRY}$ lattices were generated using PEET in IMOD (86). 153 and 75 vertices were selected in the TRIM5-21R and TRIM5-21R$_{\Delta SPRY}$ 2D lattices, respectively, and a volume of 60 nm x 60 nm x 20 nm (x,y,z) centered on the refined positions of the selected vertices was used to generate the averaged volume. To localize the SPRY domain in the full length TRIM-21R lattice, the density values of the averaged lattice volumes were rescaled to reflect a mean value of zero and standard deviation of 10. The volumes were then aligned in Chimera (87) and the TRIM5-21R$_{\Delta SPRY}$ density values were subtracted from the TRIM5-21R volume. The resulting density difference map was contoured and displayed at 3 sigma above the mean.

To quantify the variability in the TRIM5-21R hexagonal lattice, the refined positions of each vertex were used to calculate: 1) the distance between neighboring vertices, and 2) the average angle of hexamer edges extending from the 3-fold vertices. These values were entered into the *imodsetvalues* program in IMOD and a pseudo-colored model was generated to reflect length (colored lines) and average angles (colored spheres).

### 4.4.14 Negative stain transmission electron microscopy

3.5 µl sample solutions of undecorated or TRIM5-decorated CA tubes were spread onto the carbon side of freshly glow-discharged Formvar carbon-coated 200-mesh copper grids (Electron Microscopy Science). The samples were incubated for 4 minutes, rinsed briefly by flotation on a drop of 100 mM KCl, blotted dry, stained for 2 minutes in filtered, saturated uranyl acetate (or 1 minute of phosphotungstic acid (PTA)), blotted dry and allowed to air-dry. Samples were viewed on a JEOL JEM-1400 Plus transmission electron microscope operated at 120 kV accelerating voltage, and images were acquired as Gatan

Digital Micrograph 3 (DM3) files with a Gatan Ultrascan CCD camera or on a Hitachi 7100 TEM at 75 kV accelerating voltage with a Gatan ORIUS CCD camera, and converted into JPEG images using ImageJ software (NIH Bethesda, MD, USA).

### 4.4.15 ECT of TRIM5α-decorated HIV-1 cores

#### *4.4.15.1 Cryo-grid preparation*

TRIM5α-decorated HIV-1 cores were made by incubating 0.25 μM TRIM5$\alpha_{AGMpyg}$ with 1 μM CA equivalents of hyperstable HIV-1 cores in 20 mM HEPES (pH 7.2), 25 mM NaCl and 1 mM TCEP at 4°C for 1 hour, a condition that permits saturated binding in the cosedimentation assay (data not shown). Cores or TRIM5α-core complexes were mixed with BSA-coated colloidal gold particles (10 nm, SPI Supplies), which served as fiducials required for aligning the tilt stacked images. For crosslinked complexes, samples were incubated with 1 mM Sulfo-EGS before freezing. Samples (3.5 μl) were placed on the carbon side of freshly glow-discharged Quantifoil R2/2, 300 mesh holey carbon grids (SPI Supplies) for 1 minute, thinned by automatic blotting using FEI Vitrobot (-1.5 mm offset, 6-8 seconds, with filter papers from both sides at 80-85% relative humidity) and vitrified by plunge-freezing into liquid ethane. The cryo-grid was transferred to the microscope using a cryo-transfer holder.

#### *4.4.15.2 Electron cryo-tomography (ECT)*

Images were collected using a FEI Polara 300kV FEG transmission electron microscope equipped with an energy filter (slit width 20 eV; Gatan) and a 4k x 4k x 4k K2 Summit using the direct electron counting mode (Gatan). Pixels on the detector represented

0.26 nm (41,000x) at the specimen level. The tilt series were recorded from -60° to +60° with an increment of 1° and 4 μm underfocus. The cumulative dose of a tilt-series was 80-100 e-/Å$^2$. UCSF Tomo (84) was used for automatic acquisition of the tilt series and 2D projection images. The tilt series were aligned and binned by 4 into 1k x 1k using the IMOD software package (85) and 3D reconstructions were calculated using the simultaneous reconstruction technique (SIRT) using the TOMO3D software package (88), or weighted back projection using IMOD. Noise reduction was performed using the nonlinear anisotropic diffusion (NAD) method in IMOD (89), typically using a K value of 0.03 – 0.04 with 10 iterations.

*4.4.15.3 Segmentation and isosurface generation*

Segmentation and isosurface rendering was performed in Amira (FEI). Firstly the outer boundary of the HIV-1 core was manually identified and a material mask was generated inside the boundary. A second region of interest surrounding the core that typically extended 9 nm from the exterior surface was generated (densities inside this region correspond to TRIM5α protein). The area inside the second region was segmented and an isosurface generated for the densities inside. Those islands containing six voxels or less in 3D were deleted. The exterior layer of capsid protein within the HIV-1 core of the first material was also segmented using a similar threshold value and an isosurface was generated. Movie image sequences were generated in .jpg format in Amira (FEI) and converted into movies using QuickTime Player 7. Photoshop CS6 (Adobe) was then used to produce the finalized versions of the movies.

4.4.16 Screening for TRIM5 decoration on CA tubes

TRIM5-tube complexes were prepared by incubating TRIM5α or TRIMCyp$_{K283D, Q287D}$ with hyperstable CA tubes in 50 mM Tris, 7.7 mM NaCl buffer at 4°C. Decoration conditions were surveyed over a range of TRIM5 concentrations (0.6-22.5 μM) at a constant CA concentration (7.5 μM) (corresponding to molar ratios of TRIM5 to CA of 1:6, 1:1 and 3:1), pH values (8.0 and 9.0) and incubation times (4-32 hours). Conditions that gave the best TRIM5 decoration on CA tubes and minimal TRIM5 self-assemblies were determined by negative stain TEM. The resulting complexes were imaged on a JEOL JEM-1400 Plus transmission electron microscope as described above. Image contrast was adjusted to enhance the decoration patterns of TRIM5 proteins on CA tubes using Adobe Photoshop CS5. The spacings of hexagonal TRIM5 rings were measured using ImageJ.

4.4.17 Deep-etch electron microscopy

Deep etch EM of TRIM5-bound helical CA arrays were performed as described in (90).

4.4.18 TRIM5 restriction assays

HEK 293T cells were used to generate lentiviral vectors for transduction of HeLa cells for expression of TRIM5 proteins with a C-terminal Flag One-Strep tag. pCMV-ΔR8.2 (structural genes), pCMV-VSVG (envelope) and CSII-IDR2 (contains a packaging signal and genes for TRIM5 and DsRed) were cotransfected in 293T cells. After 3 days, virion-containing media was removed from the cells, passed through a 0.45 μm filter (Nalgene SFCA syringe filters), layered on top of a 20% sucrose cushion in HS buffer (10 mM HEPES pH 7.2 and 140 mM NaCl) and spun in an Optima L-90K Ultracentrifuge using a

SW 32 Ti rotor at 28,000 rpms for 2 hours. Virion containing pellets were resuspended in HS buffer, aliquoted, and frozen at -80°C. Thawed aliquots were titrated on HeLa cells to determine viral titers by monitoring the number of DsRed positive cells using fluorescence-activated cell sorting (FACS).

HeLa cells ($1 \times 10^5$ cells per well of 6-well plate) were transduced with lentiviral vectors expressing different TRIM5 proteins at an MOI of 1. Three days after transduction, cells were split and reseeded at $5 \times 10^4$ cells per well of a 24-well plate and infected with increasing amounts of HIV-GFP per well. The remaining cells were used for western blot analysis to determine TRIM5 expression levels. Three days after infection with HIV-GFP, cells were trypsinized and GFP and DsRed positive cells were counted using FACS. Only DsRed positive cells (which also express TRIM5) were used for statistical analysis of HIV-GFP restriction.

## 4.5 Contributions

Yen-Li Li purified and characterized HIV-1 cores and CA tubes and performed all binding assays and negative stain EM imaging. Dr. Barbie Ganser-Pornillos performed the TRIM5-CA 2D electron crystallography. Dr. Stephen Carter and Dr. Cora Woodward performed the ECT analyses. Dr. Devin Christensen performed the TRIM5 restriction assay and Robyn Roth performed the deep-etch electron microscopy. These authors prepared all figures except Figure 4.2.

## 4.6 References


1. **Bieniasz PD.** 2003. Restriction factors: a defense against retroviral infection. Trends in microbiology **11:**286-291.

2. **Bieniasz PD.** 2004. Intrinsic immunity: a front-line defense against viral attack. Nat Immunol **5:**1109-1115.

3. **Harris RS, Hultquist JF, Evans DT.** 2012. The restriction factors of human immunodeficiency virus. J Biol Chem **287:**40875-40883.

4. **Stremlau M, Owens CM, Perron MJ, Kiessling M, Autissier P, Sodroski J.** 2004. The cytoplasmic body component TRIM5alpha restricts HIV-1 infection in Old World monkeys. Nature **427:**848-853.

5. **Stremlau M, Perron M, Lee M, Li Y, Song B, Javanbakht H, Diaz-Griffero F, Anderson DJ, Sundquist WI, Sodroski J.** 2006. Specific recognition and accelerated uncoating of retroviral capsids by the TRIM5alpha restriction factor. Proc Natl Acad Sci U S A **103:**5514-5519.

6. **Sayah DM, Sokolskaja E, Berthoux L, Luban J.** 2004. Cyclophilin A retrotransposition into TRIM5 explains owl monkey resistance to HIV-1. Nature **430:**569-573.

7. **Anderson JL, Campbell EM, Wu X, Vandegraaff N, Engelman A, Hope TJ.** 2006. Proteasome inhibition reveals that a functional preintegration complex intermediate can be generated during restriction by diverse TRIM5 proteins. J Virol **80:**9754-9760.

8. **Wu X, Anderson JL, Campbell EM, Joseph AM, Hope TJ.** 2006. Proteasome inhibitors uncouple rhesus TRIM5alpha restriction of HIV-1 reverse transcription and infection. Proc Natl Acad Sci U S A **103:**7465-7470.

9. **Diaz-Griffero F, Kar A, Lee M, Stremlau M, Poeschla E, Sodroski J.** 2007. Comparative requirements for the restriction of retrovirus infection by TRIM5alpha and TRIMCyp. Virology **369:**400-410.

10. **Campbell EM, Perez O, Anderson JL, Hope TJ.** 2008. Visualization of a proteasome-independent intermediate during restriction of HIV-1 by rhesus TRIM5alpha. J Cell Biol **180:**549-561.

11. **Rold CJ, Aiken C.** 2008. Proteasomal degradation of TRIM5alpha during retrovirus restriction. PLoS Pathog **4:**e1000074.

12. **Lukic Z, Hausmann S, Sebastian S, Rucci J, Sastri J, Robia SL, Luban J, Campbell EM.** 2011. TRIM5alpha associates with proteasomal subunits in cells while in complex with HIV-1 virions. Retrovirology **8:**93.

13. **Mandell MA, Jain A, Arko-Mensah J, Chauhan S, Kimura T, Dinkins C, Silvestri G, Munch J, Kirchhoff F, Simonsen A, Wei Y, Levine B, Johansen T, Deretic V.** 2014. TRIM Proteins Regulate Autophagy and Can Target Autophagic Substrates by Direct Recognition. Developmental cell **30:**394-409.

14. **Pertel T, Hausmann S, Morger D, Zuger S, Guerra J, Lascano J, Reinhard C, Santoni FA, Uchil PD, Chatel L, Bisiaux A, Albert ML, Strambio-De-Castillia C, Mothes W, Pizzato M, Grutter MG, Luban J.** 2011. TRIM5 is an innate immune sensor for the retrovirus capsid lattice. Nature **472:**361-365.

15. **Reymond A, Meroni G, Fantozzi A, Merla G, Cairo S, Luzi L, Riganelli D, Zanaria E, Messali S, Cainarca S, Guffanti A, Minucci S, Pelicci PG, Ballabio A.** 2001. The tripartite motif family identifies cell compartments. EMBO J **20:**2140-2151.

16. **Yamauchi K, Wada K, Tanji K, Tanaka M, Kamitani T.** 2008. Ubiquitination of E3 ubiquitin ligase TRIM5 alpha and its potential role. FEBS J **275:**1540-1555.

17. **Meroni G, Diez-Roux G.** 2005. TRIM/RBCC, a novel class of 'single protein RING finger' E3 ubiquitin ligases. Bioessays **27:**1147-1157.

18. **Li X, Sodroski J.** 2008. The TRIM5alpha B-box 2 domain promotes cooperative binding to the retroviral capsid by mediating higher-order self-association. J Virol **82:**11495-11502.

19. **Sanchez JG, Okreglicka K, Chandrasekaran V, Welker JM, Sundquist WI, Pornillos O.** 2014. The tripartite motif coiled-coil is an elongated antiparallel hairpin dimer. Proc Natl Acad Sci U S A **111:**2494-2499.

20. **Goldstone DC, Walker PA, Calder LJ, Coombs PJ, Kirkpatrick J, Ball NJ, Hilditch L, Yap MW, Rosenthal PB, Stoye JP, Taylor IA.** 2014. Structural studies of postentry restriction factors reveal antiparallel dimers that enable avid binding to the HIV-1 capsid lattice. Proc Natl Acad Sci U S A **111:**9609-9614.

21. **Li Y, Wu H, Wu W, Zhuo W, Liu W, Zhang Y, Cheng M, Chen YG, Gao N, Yu H, Wang L, Li W, Yang M.** 2014. Structural insights into the TRIM family of ubiquitin E3 ligases. Cell research **24:**762-765.

22. **Stremlau M, Perron M, Welikala S, Sodroski J.** 2005. Species-specific variation in the B30.2(SPRY) domain of TRIM5alpha determines the potency of human immunodeficiency virus restriction. J Virol **79:**3139-3145.

23. **Ganser-Pornillos BK, Chandrasekaran V, Pornillos O, Sodroski JG, Sundquist WI, Yeager M.** 2011. Hexagonal assembly of a restricting TRIM5alpha protein. Proc Natl Acad Sci U S A **108:**534-539.

24. **Ganser BK, Li S, Klishko VY, Finch JT, Sundquist WI.** 1999. Assembly and analysis of conical models for the HIV-1 core. Science **283:**80-83.

25. **Ganser BK, Cheng A, Sundquist WI, Yeager M.** 2003. Three-dimensional structure of the M-MuLV CA protein on a lipid monolayer: a general model for retroviral capsid assembly. EMBO J **22:**2886-2892.

26. **Mortuza GB, Haire LF, Stevens A, Smerdon SJ, Stoye JP, Taylor IA.** 2004. High-resolution structure of a retroviral capsid hexameric amino-terminal domain. Nature **431:**481-485.

27. **Campos-Olivas R, Newman JL, Summers MF.** 2000. Solution structure and dynamics of the Rous sarcoma virus capsid protein and comparison with capsid proteins of other retroviruses. J Mol Biol **296:**633-649.

28. **Pornillos O, Ganser-Pornillos BK, Kelly BN, Hua Y, Whitby FG, Stout CD, Sundquist WI, Hill CP, Yeager M.** 2009. X-ray structures of the hexameric building block of the HIV capsid. Cell **137:**1282-1292.

29. **Pornillos O, Ganser-Pornillos BK, Yeager M.** 2011. Atomic-level modelling of the HIV capsid. Nature **469:**424-427.

30. **Cardone G, Purdy JG, Cheng N, Craven RC, Steven AC.** 2009. Visualization of a missing link in retrovirus capsid assembly. Nature **457:**694-698.

31. **Ganser-Pornillos BK, von Schwedler UK, Stray KM, Aiken C, Sundquist WI.** 2004. Assembly properties of the human immunodeficiency virus type 1 CA protein. J Virol **78:**2545-2552.

32. **Heymann JB, Butan C, Winkler DC, Craven RC, Steven AC.** 2008. Irregular and Semi-Regular Polyhedral Models for Rous Sarcoma Virus Cores. Computational and mathematical methods in medicine **9:**197-210.

33. **Hatziioannou T, Cowan S, Goff SP, Bieniasz PD, Towers GJ.** 2003. Restriction of multiple divergent retroviruses by Lv1 and Ref1. EMBO J **22:**385-394.

34. **Yang H, Ji X, Zhao G, Ning J, Zhao Q, Aiken C, Gronenborn AM, Zhang P, Xiong Y.** 2012. Structural insight into HIV-1 capsid recognition by rhesus TRIM5alpha. Proc Natl Acad Sci U S A **109:**18372-18377.

35. **Biris N, Yang Y, Taylor AB, Tomashevski A, Guo M, Hart PJ, Diaz-Griffero F, Ivanov DN.** 2012. Structure of the rhesus monkey TRIM5alpha PRYSPRY domain, the HIV capsid recognition module. Proc Natl Acad Sci U S A **109:**13278-13283.

36. **Caines ME, Bichel K, Price AJ, McEwan WA, Towers GJ, Willett BJ, Freund SM, James LC.** 2012. Diverse HIV viruses are targeted by a conformationally dynamic antiviral. Nature structural & molecular biology **19:**411-416.

37. **Song B, Gold B, O'Huigin C, Javanbakht H, Li X, Stremlau M, Winkler C, Dean M, Sodroski J.** 2005. The B30.2(SPRY) domain of the retroviral restriction

factor TRIM5alpha exhibits lineage-specific length and sequence variation in primates. J Virol **79:**6111-6121.

38. **Price AJ, Marzetta F, Lammers M, Ylinen LM, Schaller T, Wilson SJ, Towers GJ, James LC.** 2009. Active site remodeling switches HIV specificity of antiretroviral TRIMCyp. Nature structural & molecular biology **16:**1036-1042.

39. **Ylinen LM, Price AJ, Rasaiyaah J, Hue S, Rose NJ, Marzetta F, James LC, Towers GJ.** 2010. Conformational adaptation of Asian macaque TRIMCyp directs lineage specific antiviral activity. PLoS Pathog **6:**e1001062.

40. **Kovalskyy DB, Ivanov DN.** 2014. Recognition of the HIV capsid by the TRIM5alpha restriction factor is mediated by a subset of pre-existing conformations of the TRIM5alpha SPRY domain. Biochemistry **53:**1466-1476.

41. **Li X, Sodroski J.** 2008. The TRIM5{alpha} B-box 2 Domain Promotes Cooperative Binding to the Retroviral Capsid by Mediating Higher-order Self-association. J Virol.

42. **Li X, Li Y, Stremlau M, Yuan W, Song B, Perron M, Sodroski J.** 2006. Functional replacement of the RING, B-box 2, and coiled-coil domains of tripartite motif 5alpha (TRIM5alpha) by heterologous TRIM domains. J Virol **80:**6198-6206.

43. **Kar AK, Diaz-Griffero F, Li Y, Li X, Sodroski J.** 2008. Biochemical and biophysical characterization of a chimeric TRIM21-TRIM5alpha protein. J Virol **82:**11669-11681.

44. **Langelier CR, Sandrin V, Eckert DM, Christensen DE, Chandrasekaran V, Alam SL, Aiken C, Olsen JC, Kar AK, Sodroski JG, Sundquist WI.** 2008. Biochemical characterization of a recombinant TRIM5alpha protein that restricts human immunodeficiency virus type 1 replication. J Virol **82:**11682-11694.

45. **Black LR, Aiken C.** 2010. TRIM5alpha disrupts the structure of assembled HIV-1 capsid complexes in vitro. J Virol **84:**6564-6569.

46. **Zhao G, Ke D, Vu T, Ahn J, Shah VB, Yang R, Aiken C, Charlton LM, Gronenborn AM, Zhang P.** 2011. Rhesus TRIM5alpha disrupts the HIV-1 capsid at the inter-hexamer interfaces. PLoS Pathog **7:**e1002009.

47. **Vuillard L, Braun-Breton C, Rabilloud T.** 1995. Non-detergent sulphobetaines: a new class of mild solubilization agents for protein purification. The Biochemical journal **305 ( Pt 1):**337-343.

48. **Sainsbury S, Ren J, Saunders NJ, Stuart DI, Owens RJ.** 2008. Crystallization and preliminary X-ray analysis of CrgA, a LysR-type transcriptional regulator from pathogenic Neisseria meningitidis MC58. Acta crystallographica. Section F, Structural biology and crystallization communications **64:**797-801.

49. **Pornillos O, Ganser-Pornillos BK, Banumathi S, Hua Y, Yeager M.** 2010. Disulfide bond stabilization of the hexameric capsomer of human immunodeficiency virus. J Mol Biol **401:**985-995.

50. **Kotov A, Zhou J, Flicker P, Aiken C.** 1999. Association of Nef with the human immunodeficiency virus type 1 core. J Virol **73:**8824-8830.

51. **Forshey BM, von Schwedler U, Sundquist WI, Aiken C.** 2002. Formation of a human immunodeficiency virus type 1 core of optimal stability is crucial for viral replication. J Virol **76:**5667-5677.

52. **Li S, Hill CP, Sundquist WI, Finch JT.** 2000. Image reconstructions of helical assemblies of the HIV-1 CA protein. Nature **407:**409-413.

53. **Briggs JA, Simon MN, Gross I, Krausslich HG, Fuller SD, Vogt VM, Johnson MC.** 2004. The stoichiometry of Gag protein in HIV-1. Nature structural & molecular biology **11:**672-675.

54. **Lanman J, Lam TT, Emmett MR, Marshall AG, Sakalian M, Prevelige PE, Jr.** 2004. Key interactions in HIV-1 maturation identified by hydrogen-deuterium exchange. Nature structural & molecular biology **11:**676-677.

55. **Benjamin J, Ganser-Pornillos BK, Tivol WF, Sundquist WI, Jensen GJ.** 2005. Three-dimensional structure of HIV-1 virus-like particles by electron cryotomography. J Mol Biol **346:**577-588.

56. **Franke EK, Yuan HE, Luban J.** 1994. Specific incorporation of cyclophilin A into HIV-1 virions. Nature **372:**359-362.

57. **Thali M, Bukovsky A, Kondo E, Rosenwirth B, Walsh CT, Sodroski J, Gottlinger HG.** 1994. Functional association of cyclophilin A with HIV-1 virions. Nature **372:**363-365.

58. **Luban J, Bossolt KL, Franke EK, Kalpana GV, Goff SP.** 1993. Human immunodeficiency virus type 1 Gag protein binds to cyclophilins A and B. Cell **73:**1067-1078.

59. **Wear MA, Patterson A, Malone K, Dunsmore C, Turner NJ, Walkinshaw MD.** 2005. A surface plasmon resonance-based assay for small molecule inhibitors of human cyclophilin A. Anal Biochem **345:**214-226.

60. **Franke EK, Luban J.** 1996. Inhibition of HIV-1 replication by cyclosporine A or related compounds correlates with the ability to disrupt the Gag-cyclophilin A interaction. Virology **222:**279-282.

61. **Gamble TR, Vajdos FF, Yoo S, Worthylake DK, Houseweart M, Sundquist WI, Hill CP.** 1996. Crystal structure of human cyclophilin A bound to the amino-terminal domain of HIV-1 capsid. Cell **87:**1285-1294.

62. **Yoo S, Myszka DG, Yeh C, McMurray M, Hill CP, Sundquist WI.** 1997. Molecular recognition in the HIV-1 capsid/cyclophilin A complex. J Mol Biol **269:**780-795.

63. **Braaten D, Franke EK, Luban J.** 1996. Cyclophilin A is required for an early step in the life cycle of human immunodeficiency virus type 1 before the initiation of reverse transcription. J Virol **70:**3551-3560.

64. **Li Y, Li X, Stremlau M, Lee M, Sodroski J.** 2006. Removal of arginine 332 allows human TRIM5alpha to bind human immunodeficiency virus capsids and to restrict infection. J Virol **80:**6738-6744.

65. **Sebastian S, Luban J.** 2005. TRIM5alpha selectively binds a restriction-sensitive retroviral capsid. Retrovirology **2:**40.

66. **Song B, Javanbakht H, Perron M, Park DH, Stremlau M, Sodroski J.** 2005. Retrovirus restriction by TRIM5alpha variants from Old World and New World primates. J Virol **79:**3930-3937.

67. **Yu Z, Dobro MJ, Woodward CL, Levandovsky A, Danielson CM, Sandrin V, Shi J, Aiken C, Zandi R, Hope TJ, Jensen GJ.** 2013. Unclosed HIV-1 capsids suggest a curled sheet model of assembly. J Mol Biol **425:**112-123.

68. **Ohkura S, Yap MW, Sheldon T, Stoye JP.** 2006. All three variable regions of the TRIM5alpha B30.2 domain can contribute to the specificity of retrovirus restriction. J Virol **80:**8554-8565.

69. **Perez-Caballero D, Hatziioannou T, Yang A, Cowan S, Bieniasz PD.** 2005. Human tripartite motif 5alpha domains responsible for retrovirus restriction activity and specificity. J Virol **79:**8969-8978.

70. **Byeon IJ, Meng X, Jung J, Zhao G, Yang R, Ahn J, Shi J, Concel J, Aiken C, Zhang P, Gronenborn AM.** 2009. Structural convergence between Cryo-EM and NMR reveals intersubunit interactions critical for HIV-1 capsid function. Cell **139:**780-790.

71. **Price AJ, Fletcher AJ, Schaller T, Elliott T, Lee K, KewalRamani VN, Chin JW, Towers GJ, James LC.** 2012. CPSF6 defines a conserved capsid interface that modulates HIV-1 replication. PLoS Pathog **8:**e1002896.

72. **Lee K, Ambrose Z, Martin TD, Oztop I, Mulky A, Julias JG, Vandegraaff N, Baumann JG, Wang R, Yuen W, Takemura T, Shelton K, Taniuchi I, Li Y, Sodroski J, Littman DR, Coffin JM, Hughes SH, Unutmaz D, Engelman A, KewalRamani VN.** 2010. Flexible use of nuclear import pathways by HIV-1. Cell Host Microbe **7:**221-233.

73. **Schaller T, Ocwieja KE, Rasaiyaah J, Price AJ, Brady TL, Roth SL, Hue S, Fletcher AJ, Lee K, KewalRamani VN, Noursadeghi M, Jenner RG, James**

**LC, Bushman FD, Towers GJ.** 2011. HIV-1 capsid-cyclophilin interactions determine nuclear import pathway, integration targeting and replication efficiency. PLoS Pathog **7:**e1002439.

74. **Matreyek KA, Yucel SS, Li X, Engelman A.** 2013. Nucleoporin NUP153 phenylalanine-glycine motifs engage a common binding pocket within the HIV-1 capsid protein to mediate lentiviral infectivity. PLoS Pathog **9:**e1003693.

75. **Di Nunzio F, Danckaert A, Fricke T, Perez P, Fernandez J, Perret E, Roux P, Shorte S, Charneau P, Diaz-Griffero F, Arhel NJ.** 2012. Human nucleoporins promote HIV-1 docking at the nuclear pore, nuclear import and integration. PloS one **7:**e46037.

76. **Bichel K, Price AJ, Schaller T, Towers GJ, Freund SM, James LC.** 2013. HIV-1 capsid undergoes coupled binding and isomerization by the nuclear pore protein NUP358. Retrovirology **10:**81.

77. **Blair WS, Pickford C, Irving SL, Brown DG, Anderson M, Bazin R, Cao J, Ciaramella G, Isaacson J, Jackson L, Hunt R, Kjerrstrom A, Nieman JA, Patick AK, Perros M, Scott AD, Whitby K, Wu H, Butler SL.** 2010. HIV capsid is a tractable target for small molecule therapeutic intervention. PLoS Pathog **6:**e1001220.

78. **Lamorte L, Titolo S, Lemke CT, Goudreau N, Mercier JF, Wardrop E, Shah VB, von Schwedler UK, Langelier C, Banik SS, Aiken C, Sundquist WI, Mason SW.** 2013. Discovery of novel small-molecule HIV-1 replication inhibitors that stabilize capsid complexes. Antimicrob Agents Chemother **57:**4622-4631.

79. **Shi J, Friedman DB, Aiken C.** 2013. Retrovirus restriction by TRIM5 proteins requires recognition of only a small fraction of viral capsid subunits. J Virol **87:**9271-9278.

80. **Roa A, Hayashi F, Yang Y, Lienlaf M, Zhou J, Shi J, Watanabe S, Kigawa T, Yokoyama S, Aiken C, Diaz-Griffero F.** 2012. RING domain mutations uncouple TRIM5alpha restriction of HIV-1 from inhibition of reverse transcription and acceleration of uncoating. J Virol **86:**1717-1727.

81. **Studier FW.** 2005. Protein production by auto-induction in high density shaking cultures. Protein expression and purification **41:**207-234.

82. **Salmon P, Oberholzer J, Occhiodoro T, Morel P, Lou J, Trono D.** 2000. Reversible immortalization of human primary cells by lentivector-mediated transfer of specific genes. Mol Ther **2:**404-414.

83. **Naldini L, Blomer U, Gage FH, Trono D, Verma IM.** 1996. Efficient transfer, integration, and sustained long-term expression of the transgene in adult rat brains injected with a lentiviral vector. Proc Natl Acad Sci U S A **93:**11382-11388.

84. **Zheng SQ, Keszthelyi B, Branlund E, Lyle JM, Braunfeld MB, Sedat JW, Agard DA.** 2007. UCSF tomography: an integrated software suite for real-time electron microscopic tomographic data collection, alignment, and reconstruction. Journal of structural biology **157:**138-147.

85. **Kremer JR, Mastronarde DN, McIntosh JR.** 1996. Computer visualization of three-dimensional image data using IMOD. Journal of structural biology **116:**71-76.

86. **Nicastro D, Schwartz C, Pierson J, Gaudette R, Porter ME, McIntosh JR.** 2006. The molecular architecture of axonemes revealed by cryoelectron tomography. Science **313:**944-948.

87. **Pettersen EF, Goddard TD, Huang CC, Couch GS, Greenblatt DM, Meng EC, Ferrin TE.** 2004. UCSF Chimera--a visualization system for exploratory research and analysis. Journal of computational chemistry **25:**1605-1612.

88. **Agulleiro JI, Fernandez JJ.** 2011. Fast tomographic reconstruction on multicore computers. Bioinformatics **27:**582-583.

89. **Kremer JR, Mastronarde DN, McIntosh JR.** 1996. Computer Visualization of Three-Dimensional Image Data Using Imod. J Struct Biol **116:**71-76.

90. **Cashikar AG, Shim S, Roth R, Maldazys MR, Heuser JE, Hanson PI.** 2014. Structure of cellular ESCRT-III spirals and their relationship to HIV budding. eLife **3**.

# CHAPTER 5

# X-RAY CRYSTALLOGRAPHY OF TRIM5 HEXAGONAL ASSEMBLIES

## 5.1 Introduction

Mammalian TRIM5α and TRIMCyp restriction factors are E3 ubiquitin ligases that block reverse transcription of susceptible retroviruses by binding and accelerating capsid dissociation (1, 2). TRIM5 restriction is an active area of research, yet the central question of how capsid binding by TRIM5 proteins leads to capsid dissociation and/or degradation is still poorly understood. In one model for restriction, capsid binding triggers TRIM5α E3 Ub ligase activity, which in turn leads to proteasome recruitment, capsid disassembly and inhibition of reverse transcription (3-8). A recent study showed, however, that TRIM5α can also regulate selective autophagy by binding p62/Sequestosome-1 and Beclin-1, which recruit autophagosomes to degrade capsids (9). It is not yet clear how to reconcile the proteasomal and autophagic models. Capsid-bound TRIM5α also helps establish a cellular antiviral state by recruiting the heterodimeric ubiquitin conjugating enzyme, Ubc13/Uev1B, to synthesize K63-linked poly-Ub chains that recruit TAK1/TAB2 kinase complexes and activate AP-1 and NF-κB signaling ((10) and Dr. Devin Christensen, personal communication).

Retroviral capsids are curved hexagonal shells comprising a few hundred CA protein hexamers and exactly 12 CA pentamers (reviewed in (11)). Capsid recognition is a challenging task for host restriction systems because capsids from different retroviruses vary greatly in shape, hexameric spacing and distribution, and CA sequence. (12-14). Even individual capsids from a single retrovirus, such as HIV-1, can differ in interhexameric CA spacings (~90-110 Å) and can be conical, cylindrical or spherical (15-18).

TRIM5 proteins have evolved a remarkable "pattern recognition" mechanism to bind structurally diverse capsids with high affinity (Chapters 2 and 4, (10, 19)). As illustrated in Figure 5.1A, TRIM5α comprises RING, B-box 2 and coiled-coiled domains (collectively known as RBCC or tripartite motif domains), followed by a C-terminal capsid-binding B30.2 (PRYSPRY) domain (or a cyclophilin A domain, in the case of TRIMCyp). The RING/B-box 2 and the coiled-coil/PRYSPRY domains are separated by L1 and L2 linker regions, respectively. The PRYSPRY and CypA domains of individual TRIM5 alleles can bind directly to different retroviral capsids, albeit with weak intrinsic affinities (20, 21). This weak affinity is amplified by powerful avidity effects that arise from coiled-coil-mediated TRIM5α dimerization and B-box 2-mediated higher-order self-assembly into flexible hexagonal nets (Figure 5.1B; Chapters 2 and 4). Thus, TRIM5 proteins can tolerate capsid structural variability because they cooperatively assemble flexible hexagonal nets that can adapt to the symmetry, spacing and curvature of the capsid surface.

Figure 5.1 Model for the TRIM5α dimer. (A) TRIM5α domain architecture. Positions of structures used for modeling are highlighted by dashed boxes. Structures of human TRIM5α RING-L1 (black; PDB ID: 2ECV), assembly-incompetent rhesus TRIMCyp$_{E120K,\ R121D}$ B-box 2-coiled-coil-L2 (red; PDB ID: 4TN3), and rhesus TRIM5α SPRY (blue; PDB IDs: 4B3N, 3UV9 and 2LM3). (B) Two-dimensional projection density map of TRIM5α$_{AGMpyg}$ reproduced from Chapter 4, Figure 4.2C. The unit cell parameters are a = b = 343, γ = 120°. (C) (top) The core of a TRIM5α dimer comprises two B-box 2 domains (red) packed against a 17 nm, antiparallel dimeric coiled-coil (blue). The L2 linker (green, disordered regions marked by dashed lines) folds back towards the center of the coiled-coil to present two capsid binding SPRY domains (orange) on one face of the coiled coil. Two RING domains (yellow) are modeled as mobile elements connected to B-box 2 domains by flexible L1 linkers. (bottom) Top view of the TRIM5α dimer (with the RING domains omitted for clarity).

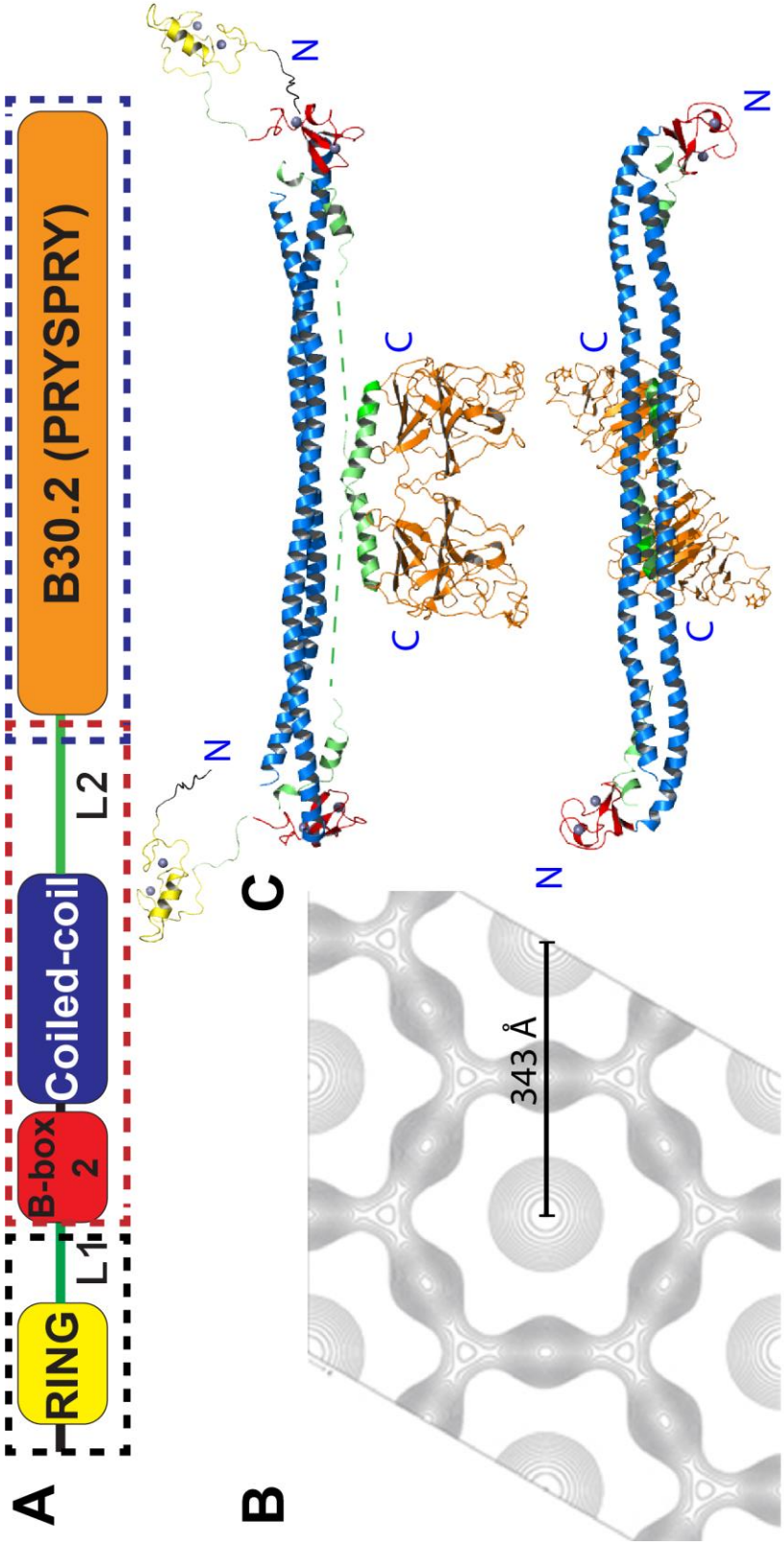
A
RING
L1
B-box 2
Coiled-coil
L2
B30.2 (PRYSPRY)
B
343 Å
C
N
C
N
C
N

Atomic structures of assembled TRIM5α are not yet available, but NMR and X-ray structures of individual TRIM5 domains and the recent crystal structure of the rhesus TRIMCyp B-box 2-coiled-coil-L2 dimer (highlighted schematically by dashed boxes in Figure 5.1A) overlap sufficiently to permit modeling of the TRIM5α tertiary structure (Figure 5.1C) (22-26). The coiled-coil forms a ~17 nm-long antiparallel dimer (blue), and two B-box 2 domains (red) are attached to its N-terminal ends in a fixed orientation. The two L2 linker elements (green) at the C-terminus of the coiled-coil fold back towards the central two-fold axis to display two PRYSPRY domains (orange) that can presumably contact a capsid surface simultaneously. Finally, the two RING domains (yellow) are modeled as mobile domains that are connected to the B-box 2 domains via flexible L1 linkers, although it is alternatively possible that they are also held in a fixed orientation.

We aimed to learn the molecular basis of TRIM5 hexagonal assembly and capsid recognition by determining crystal structures of assembled TRIM5 and TRIM5-CA complexes. To this end, we discovered how to solubilize and purify dimeric TRIM5 alleles in quantities and concentrations sufficient for 3D crystallization trials (Chapter 4) and performed crystal trials on constructs from 10 different mammalian TRIM5α alleles.

## 5.2 Results

### 5.2.1 Primate TRIM5 dimers can be purified in quantities sufficient for 3D crystallography

Protein homologs often differ in crystallizability and provide a naturally occurring source of sequence variation for crystal screening (27). We therefore selected TRIM5α alleles from Old World monkeys, New World monkeys, great apes and cattle (as well as

owl monkey TRIMCyp) for expression, purification and crystal screening (Figure 5.2A). Three crystallization constructs were designed for each TRIM5α allele (Figure 5.2A): (a) full-length TRIM5α, (b) a ΔV1 mutant that lacked the functionally important, but disordered V1 loop in the SPRY domain (see Figure 1.5 and refs. (25, 26)), and (c) a ΔSPRY variant that lacked the entire SPRY domain, but could nevertheless assemble into hexagonal lattices (Chapter 2; (19)). OneSTrEP-FLAG-tagged (OSF-tagged) TRIM5 proteins were expressed using insect cell/baculovirus expression systems and purified by sequential Strep-Tactin affinity, Q anion exchange and Superdex-200 size exclusion chromatography (Figure 5.2B). Figure 5.2C shows the stepwise purification of a representative construct, chimpanzee TRIM5α ΔSPRY (residues 1-296). Figure 5.2D shows SDS-PAGE gels of Strep-Tactin affinity-purified full-length (left), ΔV1 (middle) and ΔSPRY (right) proteins for all TRIM5α alleles. The resulting dimers were stable in solution at pH 10 in the absence of added salt and could typically be concentrated to ~10 mg/ml for crystal trials. Thus, TRIM5 solubility and self-assembly could be controlled using pH and ionic strength, with higher pH and low ionic strength favoring solubility (and conversely).

### 5.2.2 Crystallization of African green monkey and chimpanzee TRIM5α ΔSPRY constructs

Crystal trials were performed in collaboration with Prof. Chris Hill's laboratory using a Phoenix crystallization robot (Art Robbins Scientific). We succeeded in crystallizing two constructs: African green monkey pygerythrus (AGMpyg) TRIM5α ΔSPRY (residues 1-298) and chimpanzee (CPZ) TRIM5α ΔSPRY (residues 1-296). Both

Figure 5.2 Summary of strategies used for TRIM5 purification and 3D crystallization. (A) Full-length, ΔV1 constructs lacking the flexible V1 hypervariable loop in the SPRY domain and ΔSPRY constructs lacking the entire SPRY domain were designed for all of the listed TRIM5 alleles. (B) Insect cell lysates expressing TRIM5 proteins were purified using the following stepwise protocol: (a) Strep-Tactin affinity chromatography, (b) removal of the OSF tag and any attached Ub chains by Prescission protease and Usp2 deubiquitylase treatment, (c) Q anion exchange chromatography and (d) Superdex 200 gel filtration chromatography. (C) Coomassie-stained SDS-PAGE showing the step-wise purification of a representative construct, CPZ TRIM5α ΔSPRY (1-296). (D) Coomassie-stained SDS-PAGE analysis of eluates from Strep-Tactin affinity chromatography of full-length (left), ΔV1 (middle) and ΔSPRY constructs, showing partially-purified TRIM5 proteins. Note that all TRIM5α ΔSPRY proteins contain intact N-terminal OSF tags, except for African green monkey tantalus TRIM5α ΔSPRY (AGMtan) and squirrel monkey (sq. m.) TRIM5α ΔSPRY, which were eluted by PreScission protease cleavage. These two constructs therefore migrate more rapidly than the others.

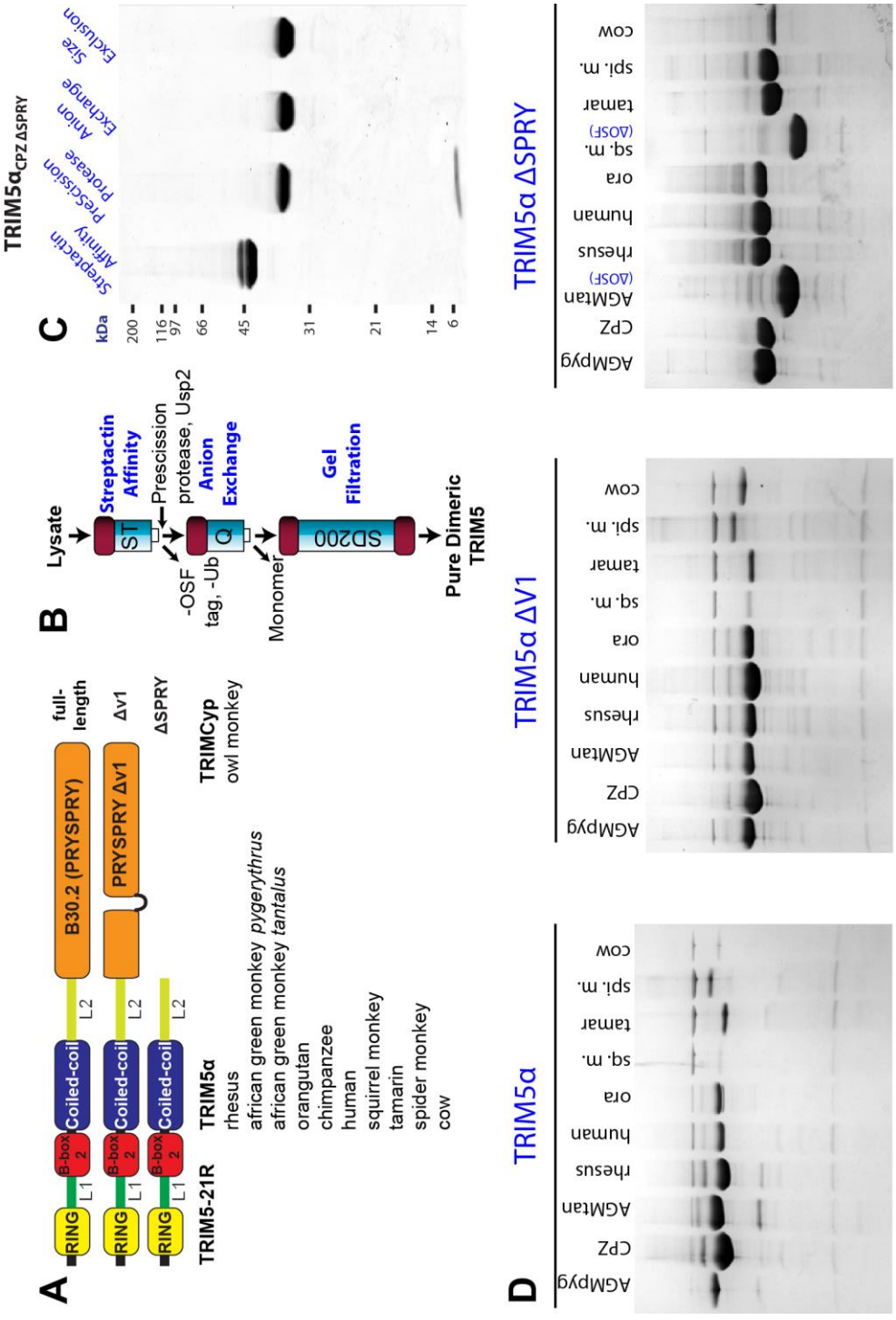
A
RING
L1
B-box 2
Coiled-coil
L2
B30.2 (PRYSPRY)
full-length
PRYSPRY Δv1
Δv1
ΔSPRY
TRIM5-21R
TRIM5α
rhesus
african green monkey pygerythrus
african green monkey tantalus
orangutan
chimpanzee
human
squirrel monkey
tamarin
spider monkey
cow
TRIMCyp
owl monkey
B
Lysate
ST
Streptactin Affinity
Prescission protease, Usp2
-OSF tag, -Ub
Q
Anion Exchange
Monomer
SD200
Gel Filtration
Pure Dimeric TRIM5
C
TRIM5α CPZ ΔSPRY
kDa
200
116
97
66
45
31
21
14
6
Streptactin Affinity
PreScission protease
Anion Exchange
Size Exclusion
D
TRIM5α
TRIM5α ΔV1
TRIM5α ΔSPRY
AGMpyg
CPZ
AGMtan
(AOSF)
rhesus
human
ora
sq. m.
(AOSF)
tamar
spi. m.
cow

constructs crystallized in 100 mM HEPES pH 7.5, 500 mM Magnesium Formate at 20 °C. The AGMpyg TRIM5α ΔSPRY crystals had a hexagonal tabular crystal habit (Figure 5.3A, top), diffracted (anisotropically) only to ~12 Å resolution, and were highly sensitive to radiation damage. In spite of the limited diffraction order, we were able to collect datasets with >80% completeness and ~14 Å resolution at beamline 12-2 of the Stanford Synchrotron Radiation Lightsource (SSRL). The crystals were indexed to the space group P622 with unit cell dimensions of 686 Å x 686 Å x 135 Å. Our attempts to determine phases by experimental and molecular replacement approaches failed, but the unit cell dimensions and symmetry indicated that the crystals likely comprised stacks of dimeric TRIM5α hexagonal assemblies. The unit cell a and b dimensions (686 Å) were exactly twice those observed in 2D projection maps of full-length AGMpyg TRIM5α 2D crystals (343 Å; see Figure 4.2C). This observation suggests the presence of translational pseudosymmetry, which is the presence of two or more copies of TRIM5α in the unit cell that are related to each other by a simple translation. It must be stressed, however, that translational pseudosymmetry can often result in misindexing of the data and/or obsure the presence of any twinning (28).

The CPZ TRIM5α ΔSPRY crystals (Figure 5.3A, bottom) had trigonal pyramidal or triangular prismatic habits and diffracted to 5.1 Å resolution. ~90% complete, 6.8 Å-resolution datasets were collected at SSRL beamline 12-2 and indexed in space group R32:H, with cell dimensions of 303 Å x 303 Å x 59 Å. Unfortunately, anomalous diffraction from the TRIM5α Zn atoms did not provide sufficient phasing power and the crystals were extremely sensitive to heavy metal soaks. Molecular replacement using the B-box 2-coiled-coil of TRIMCyp (24) also failed, perhaps due to low data completeness

Figure 5.3 TRIM5α 3D crystallization. Crystals, unit cell parameters and representative X-ray diffraction patterns obtained from crystallization trials of (A) TRIM5$\alpha_{AGMpyg}$ ΔSPRY (1-298) and (B) TRIM5$\alpha_{CPZ}$ ΔSPRY (1-296). (B) (left) Coomassie-stained SDS-PAGE of TRIM5$\alpha_{AGMpyg}$ ΔSPRY (1-298) (Input) proteolyzed by Zymit in solution (+Zymit) and in crystals (Crystals). "REVKL" were the five N-terminal residues of the major band identified by N-terminal sequencing. (right) Compiled ESI mass spectrum of TRIM5$\alpha_{AGMpyg}$ ΔSPRY (1-298) (calculated intact mass: 35131 Da) demonstrates that the major species (experimental mass: 25926.3 Da) is TRIM5$\alpha_{AGMpyg}$ (82-298) (calculated mass: 25929 Da). (C) Schematic showing the site of proteolysis in the L1 linker. The "second generation" ΔRING, ΔRING/ΔSPRY and ΔRING/ ΔV1 constructs are also illustrated. (D) Image showing that the purified ΔRING/ΔSPRY construct, GP-TRIM5$\alpha_{AGMpyg}$ (82-298), can crystallize into similar hexagonal tabular crystals from both robotic- and hand-poured vapor diffusion trials. (E) NMR structure of the human TRIM5α B-box 2 domain (PDB ID: 2YRG), with structured residues in red, unstructured residues in green and the conserved Arg121 sidechain in purple. (F) Image showing that GP-TRIM5$\alpha_{AGMpyg}$ (94-298), a ΔRING/ΔSPRY that lacks the unstructured residues shown in (E), crystallizes into a new habit of clusters of needles.

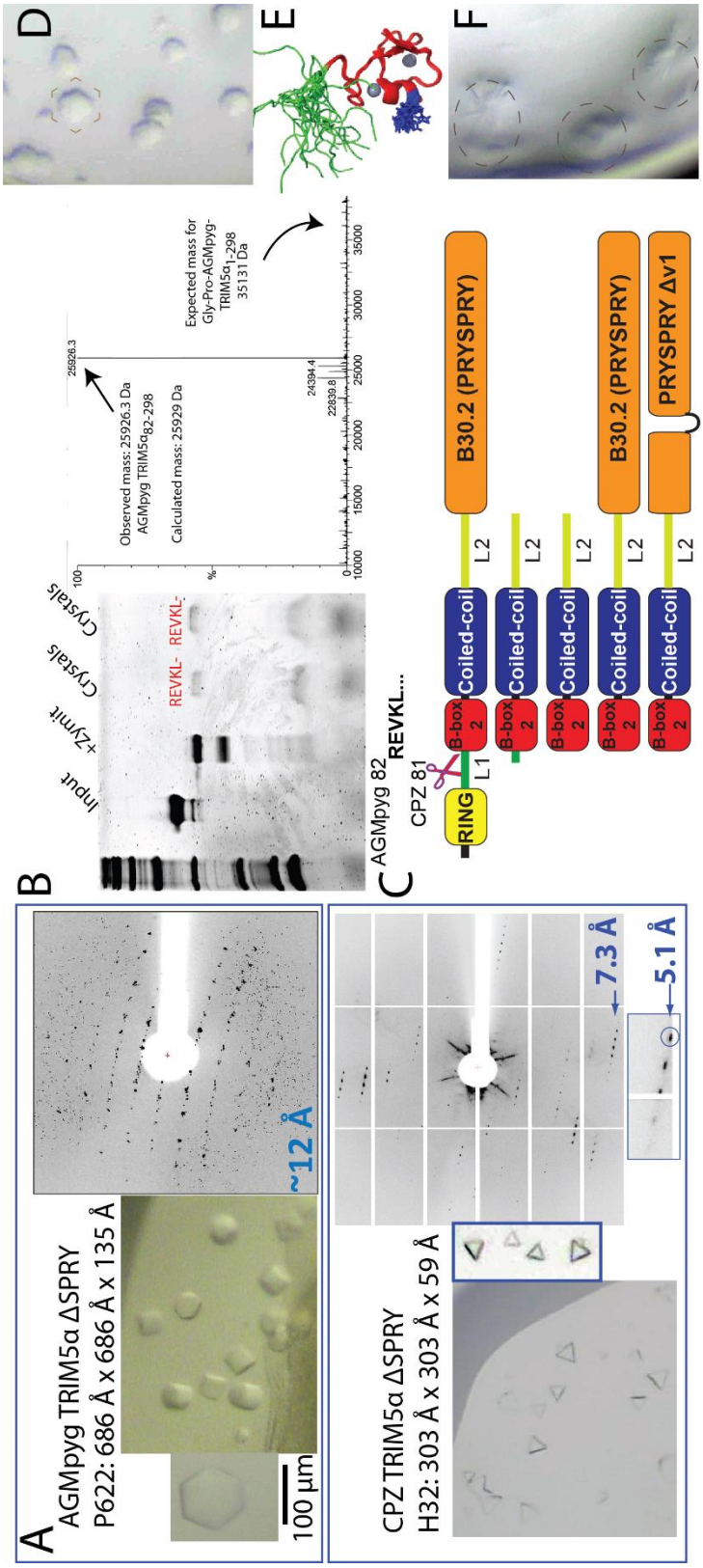
A
AGMpyg TRIM5α ΔSPRY
P622: 686 Å x 686 Å x 135 Å
100 µm
~12 Å
CPZ TRIM5α ΔSPRY
H32: 303 Å x 303 Å x 59 Å
7.3 Å
5.1 Å
B
Input
+ZYmit
Crystals
Crystals
Crystals
REVKL-
REVKL-
Observed mass: 25926.3 Da
AGMpyg TRIM5α82-298
Calculated mass: 25929 Da
Expected mass for
Gly-Pro-AGMpyg-
TRIM5α1-298
35131 Da
C
AGMpyg 82
REVKL...
CPZ 81
RING
L1
B-box 2
Coiled-coil
L2
B30.2 (PRYSPRY)
PRYSPRY Δv1
D
E
F

as well as the inherent difficulty of performing molecular replacement at low resolution on elongated molecules such as coiled-coils (and α-helices in general).

### 5.2.3 Proteolytic removal of the RING domain *in situ* promoted crystal growth

The symmetry and cell dimensions of the CPZ TRIM5α ΔSPRY crystals were inconsistent with the hexagonal symmetry and dimensions expected from 2D crystallographic studies of TRIM5α (Chapters 2 and 4). Furthermore, crystals of both constructs were recalcitrant to all optimization attempts, such as pH, precipitant and temperature variation, micro- and macro-seeding, random matrix microseeding (rMMS) and additive screening. Indeed, the crystals only grew in 96-well robot trays despite repeated attempts to reproduce them by hand pipetting. The explanation for these unusual observations was clear when we analyzed the crystals by SDS-PAGE. This analysis revealed that both the AGMpyg and CPZ TRIM5α ΔSPRY proteins had been proteolyzed *in situ* by Zymit®, a proprietary mixture of a protease, amylase and detergent that was used to clean the sample dispensing needle of the Phoenix crystallization robot (Figure 5.3B, compare lanes marked ‘Input’ and ‘Crystals’). The site of proteolysis was identified using N-terminal protein sequencing and electrospray ionization-mass spectrometry (ESI-MS) (Figure 5.3B). These analyses revealed that both constructs were cleaved at equivalent sites in the L1 linker: Leu81/Arg82 (AGMpyg) and Leu80/Arg81 (CPZ). This local region appears to be particularly sensitive to proteolysis because an earlier study had also reported proteolysis at the C-terminus of this Arg residue when the chimeric TRIM5 construct, TRIM5-21R, was incubated with trypsin (29). These results suggest

that residues in the L1 linker may be unstructured or accessible in solution. In any event, we conclude that serendipitous proteolysis during crystal trials led to RING-L1 removal and facilitated crystallization of the B-box 2-coiled-coil-L2 fragments, AGMpyg TRIM5α (82-298) and CPZ TRIM5α (81-296).

### 5.2.4 Insect cell-expressed ΔRING constructs form similar crystals

To test whether constructs that comprised only the B-box 2-coiled-coil-L2 region (i.e., ΔRING, ΔSPRY) could yield improved crystals, I cloned, expressed and purified N-terminal OSF-tagged AGMpyg TRIM5α (82-298) and CPZ TRIM5α (81-296) (Figure 5.3C and data not shown). Unlike the fragments generated by Zymit-proteolysis, these constructs contained an N-terminal Gly-Pro dipeptide that remained after the N-terminal OSF tag was removed by PreScission protease treatment. As shown in Figure 5.3D, Gly-Pro-AGMpyg TRIM5α (82-298) also crystallized into hexagonal tabular crystals, both in robotic and hand trays. However, the X-ray diffraction properties of these crystals remain to be studied.

A recent NMR structure of the human TRIM5α B-box 2 domain (PDB ID: 2YRG) reveals additional information on the protein's domain architecture. In this structure, the region from Arg82 (the first residue in the ΔRING fragments) to Leu93 of the L1 linker is unstructured (i.e., Val94 is the first ordered residue) (Figure 5.3E, disordered residues are depicted in green, and ordered residues in red) (23). We therefore purified a new construct, Gly-Pro-AGMpyg TRIM5α (94-298), that lacked the unstructured residues. Interestingly, this construct crystallized in a new crystal habit (Figure 5.3F; thin needle-like showers), suggesting that removing the disordered residues somehow altered, and

perhaps improved its assembly properties. We now plan to optimize these crystals further and conduct X-ray diffraction studies. We are also concerned that the non-native Gly-Pro overhang at the N-terminus of the ΔRING constructs may disrupt crystal growth by interfering with B-box 2 assembly interactions at the three-fold interface of the TRIM5 hexagonal lattice. We have therefore designed constructs that express N-terminal OSF-SUMOstar tags that can be completely removed by SUMOstar protease (LifeSensors, Malvern, PA) without any overhanging residues (30). We have also designed longer constructs that include the SPRY domain but lack the RING domain (Figure 5.3C). These constructs will be used in future 3D crystallization trials with hexameric CA assemblies. Taken together, our results suggest that the RING domain may not be absolutely required for hexagonal lattice formation and that trimeric B-box 2 and dimeric coiled-coil interactions may suffice to support TRIM5α hexagonal lattice formation (Figure 5.4).

## 5.3 Discussion and future directions

TRIM5 proteins spontaneously self-assemble under physiological conditions *in vitro*, making them difficult to purify and concentrate for crystallization studies (19). In this study, we overcame these technical hurdles and have crystallized the B-box 2-coiled-coil-L2 linker of African green monkey and chimpanzee TRIM5α. Although we have thus far failed to determine the structure of an assembled TRIM5α construct, we recently discovered that standard techniques to optimize our crystals in hand trays failed owing to serendipitous proteolysis of the RING domain during robotic crystal trials of RING-containing constructs. This observation prompted us to go back and redesign new constructs that lacked RING domains and we found that these constructs crystallize into

Figure 5.4 A model for the TRIM5α hexagonal lattice (A) surface representation with a close-up of the putative B-box 2 domain-mediated three-fold interface, inset. Domains are colored following the scheme in Figure 5.1A. (B) RING domain dimerization. The N-terminal residues (black) and the C-terminal L1 linker (green) form a four-helix bundle that stabilizes RING domain core interactions (D. Ivanov, personal communication). The analogous dimer formed by the RING domain of TRIM37 (PDB ID: 3LRQ) has been used in the figure because coordinates for the structure of the TRIM5α RING dimer are not yet available.

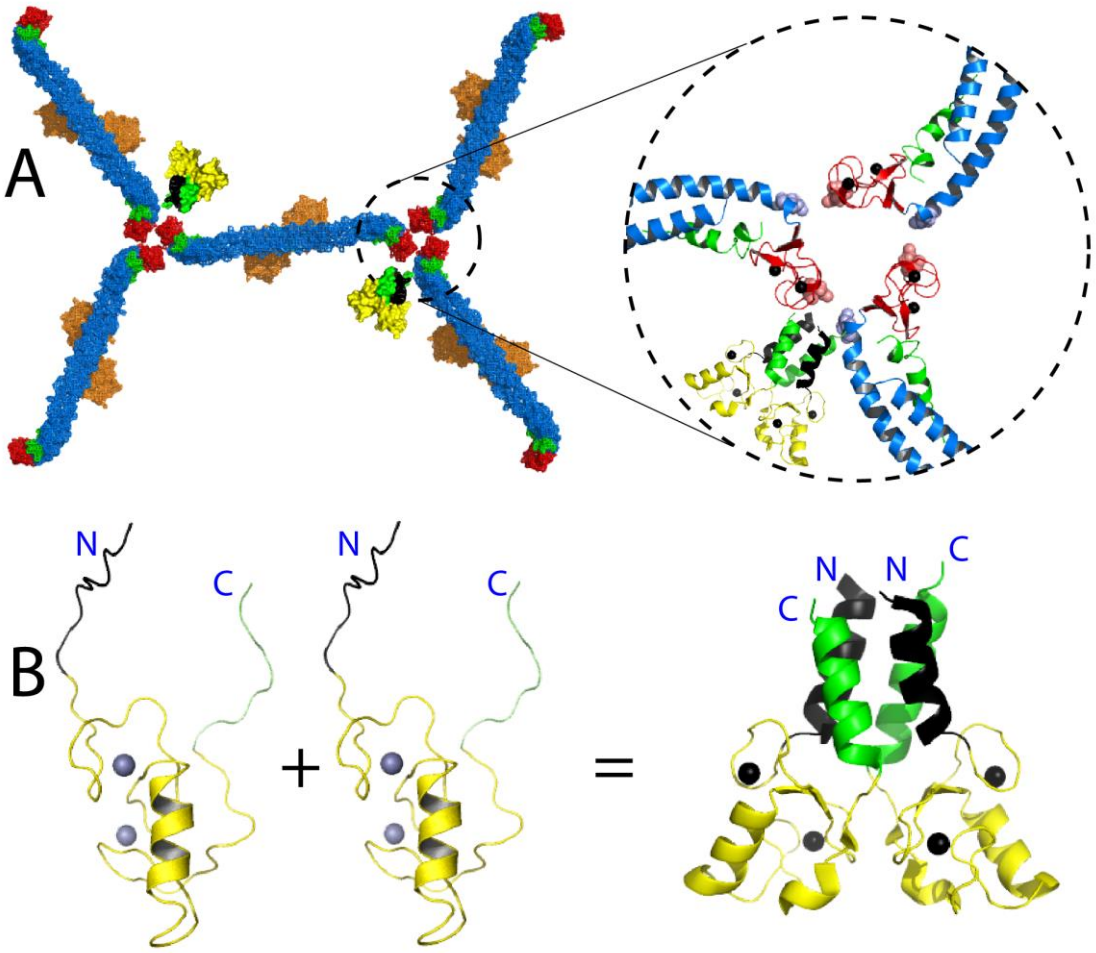
A
B
N
C
N
C
+
=
N
N
C
C

presumably equivalent lattices, but the X-ray diffraction properties of these new crystals are yet to be studied. The hexagonal symmetry and a=b=686 Å unit cell dimensions of the AGMpyg TRIM5α (82-298) crystals are consistent with independent electron crystallographic analyses of full-length AGMpyg TRIM5α (Chapter 4) and indicate that our 3D crystals may comprise stacked sheets of TRIM5α hexagonal lattices. Hexagonal assembly therefore apparently does not absolutely require the N-terminal RING-L1 and C-terminal SPRY regions and the B-box 2-coiled-coil-L2 region therefore appears to constitute the TRIM5 "self-assembly core", as others have previously suggested (24, 31). If this is correct, then the B-box 2 domain must trimerize at the three-fold interface of the hexagonal lattice (Figure 5.1B). B-box 2 trimerization and coiled-coil dimerization (24, 32) alone could, in principle, then combine to generate TRIM5 hexagonal rings, provided the two symmetry axes are parallel.

Based on this idea, we have produced a tentative model for the TRIM5 hexagonal lattice (Figure 5.4A), by (a) positioning a monomer of rhesus TRIMCyp B-box 2-coiled-coil-L2 (24), so that the noncrystallographic two-fold symmetry axis of the coiled-coil coincides exactly with the crystallographic two-fold axis of a theoretical P6 lattice with a=b=343 Å (experimentally determined by 2D electron crystallography; Chapter 4, see Figure 4.2) and c=100 Å (chosen to be large enough to prevent atomic clashes between successive layers); and (b) rotating the molecule about the two-fold axis by an arbitrary angle (14° clockwise) until application of the P6 space group symmetry operations results in a continuous hexagonal lattice. This model predicts that the functionally important Arg121 residue of the B-box 2 domain (33, 34) could stabilize the three-fold interface by forming a salt bridge with Glu135 in the coiled-coil domain (Figure 5.4A, inset;

sidechain atoms of both residues are shown as spheres). Mutating either residue to one of opposite charge should therefore diminish TRIM5α restriction activity and the R121E/E135R double mutation should rescue restriction. Consistent with this model, TRIM5α$_{R121E}$ indeed lacks self-assembly, capsid binding and restriction abilities (19, 33). Dr. Devin Christensen, a postdoc in our laboratory, is currently testing the activities of the single E135R and double R121E/E135R mutants in a restriction assay.

Recent unpublished studies from the Ivanov laboratory have demonstrated that the TRIM5α RING domain must dimerize to function (D. Ivanov, personal communication). The Zn-bound cores of individual RING monomers interact to form the dimer interface, which is further stabilized by a four-helix bundle formed by flexible loops that flank the RING domain (Figure 5.4B). RING dimerization will result in a symmetry mismatch between the dimeric RING domains and (putative) trimeric B-box 2 domains, which is depicted in Figure 5.4 using the dimeric structure of the TRIM37 RING (PDB ID: 3LRQ). Two of the local RING domains may therefore dimerize to leave an unpaired third RING domain (not shown for clarity). An intriguing alternative explanation is that the 2D projection structures of assembled TRIM5α (Figure 5.1B) are actually composed of *two* hexagonal layers stacked face-to-face and that the 6 resulting RING domains, 3 from each layer, form a trimer of dimers between the two layers, as observed in the crystal structure of the RING domain from cIAP2 (PDB ID: 3EB6) (35). 2D projection maps obtained by electron crystallography cannot typically distinguish multilayered from monolayered 2D crystals. This explanation would eliminate the symmetry mismatch between the RING and B-box 2 domains, but lacks any supporting experimental evidence. Regardless of the structural details at the three-fold interface, juxtaposition of

the RING domains when TRIM5 assembles on capsids apparently underlies activation of RING E3 ubiquitin ligase activity to initiate antiviral signaling and trigger accelerated capsid dissociation (6, 10).

In summary, we are continuing our TRIM5 crystallographic studies because we anticipate that these studies, if successful, will help reveal the structural basis of TRIM5 assembly and thereby provide mechanistic insights into retroviral restriction. Our ultimate goal is to understand the molecular basis of capsid recognition by determining structures of TRIM5 proteins in complex with mimics of the capsid surface. Toward this end, we plan to conduct co-crystallization trials with stable hexameric assemblies of HIV-1 CA (36, 37).

## 5.4 Materials and methods

### 5.4.1 Construction, expression and purification of recombinant TRIM5

pLPCX vectors encoding TRIM5 cDNA from all species used in this study were kind gifts from Dr. Joseph Sodroski (Dana Farber Cancer Institute, Boston, MA). N-terminal OneSTrEP-FLAG-tagged, full-length, ΔV1 and ΔSPRY TRIM5 cDNAs were subcloned into pFastBac1 baculovirus entry vectors using standard sequence and ligation independent cloning (SLIC) methods (38). Recombinant *Bac-to-bac* baculoviruses expressing these proteins were generated using manufacturer-recommended procedures (Life technologies) in a high-throughput format developed by the Joint Center for Innovative Membrane Protein Technologies (JCIMPT) (39). All proteins were expressed and purified as described in Chapter 4.

5.4 2 Crystallization

Sitting drop, vapor diffusion trials were performed in 96-well Intelliplates (Art Robbins Scientific) using a Phoenix crystallization robot (Art Robbins Scientific) and incubated at 4, 13, 20 or 28 °C in constant temperature rooms. Crystals of AGMpyg and CPZ TRIM5α ΔSPRY were obtained by serendipitous *in situ* proteolysis (see Section 4-2, Results). The crystals grew at 20 °C after 3 days (AGMpyg) or 2 weeks (CPZ) in 100 mM HEPES pH 7.0-8.0, 300-800 mM Magnesium Formate, 1 µM Zinc Chloride. Crystals were cryoprotected in 20% ethylene glycol or in a mixture of 10% PEG200 and 15% ethylene glycol. Data were collected remotely at SSRL beamline 12-2. Data reduction was carried out using HKL2000 or XDS (using the autoxds script available at SSRL). Crystallographic statistics for the best datasets from both constructs are given in Table 5.1.

Electrospray ionization mass spectrometry was performed by Dr. Chad Nelson and Dr. Krishna Parsawar at the University of Utah mass spectrometry core facility. N-terminal sequencing was performed by Dr. John Schulze at the University of California at Davis proteomics core facility.

Table 5.1 Data processing statistics

| Construct | AGMpyg TRIM5$\alpha_{82-298}$ | CPZ TRIM5$\alpha_{81-296}$ |
|---|---|---|
| Space group | P622 | R32:H |
| Cell dimensions | a = b = 686 Å, c = 158 Å<br>$\alpha = \beta = 90^o, \gamma = 120^o$ | a = b = 298.3 Å, c = 58.8 Å<br>$\alpha = \beta = 90^o, \gamma = 120^o$ |
| Resolution range, Å | 80-14 | 38.8-6.48 |
| Wavelength, Å | 1.2825 | 0.9795 |
| Rsym, % | 11.8 | 10.4 |
| Mean <I>/σ<I> | 25.06 | 3.6 |
| Completeness, % | 83.7 | 90.6 |
| Average redundancy | 10.6 | 4.1 |
| Mosaicity | 1.6 | 0.31 |

## 5.5 References


1. **Stremlau M, Owens CM, Perron MJ, Kiessling M, Autissier P, Sodroski J.** 2004. The cytoplasmic body component TRIM5alpha restricts HIV-1 infection in Old World monkeys. Nature **427:**848-853.

2. **Stremlau M, Perron M, Lee M, Li Y, Song B, Javanbakht H, Diaz-Griffero F, Anderson DJ, Sundquist WI, Sodroski J.** 2006. Specific recognition and accelerated uncoating of retroviral capsids by the TRIM5alpha restriction factor. Proc Natl Acad Sci U S A **103:**5514-5519.

3. **Anderson JL, Campbell EM, Wu X, Vandegraaff N, Engelman A, Hope TJ.** 2006. Proteasome inhibition reveals that a functional preintegration complex intermediate can be generated during restriction by diverse TRIM5 proteins. J Virol **80:**9754-9760.

4. **Diaz-Griffero F, Li X, Javanbakht H, Song B, Welikala S, Stremlau M, Sodroski J.** 2006. Rapid turnover and polyubiquitylation of the retroviral restriction factor TRIM5. Virology **349:**300-315.

5. **Campbell EM, Perez O, Anderson JL, Hope TJ.** 2008. Visualization of a proteasome-independent intermediate during restriction of HIV-1 by rhesus TRIM5alpha. J Cell Biol **180:**549-561.

6. **Roa A, Hayashi F, Yang Y, Lienlaf M, Zhou J, Shi J, Watanabe S, Kigawa T, Yokoyama S, Aiken C, Diaz-Griffero F.** 2012. RING domain mutations uncouple TRIM5alpha restriction of HIV-1 from inhibition of reverse transcription and acceleration of uncoating. J Virol **86:**1717-1727.

7. **Rold CJ, Aiken C.** 2008. Proteasomal degradation of TRIM5alpha during retrovirus restriction. PLoS Pathog **4:**e1000074.

8. **Wu X, Anderson JL, Campbell EM, Joseph AM, Hope TJ.** 2006. Proteasome inhibitors uncouple rhesus TRIM5alpha restriction of HIV-1 reverse transcription and infection. Proc Natl Acad Sci U S A **103:**7465-7470.

9. **Mandell MA, Jain A, Arko-Mensah J, Chauhan S, Kimura T, Dinkins C, Silvestri G, Munch J, Kirchhoff F, Simonsen A, Wei Y, Levine B, Johansen T, Deretic V.** 2014. TRIM Proteins Regulate Autophagy and Can Target Autophagic Substrates by Direct Recognition. Developmental cell **30:**394-409.

10. **Pertel T, Hausmann S, Morger D, Zuger S, Guerra J, Lascano J, Reinhard C, Santoni FA, Uchil PD, Chatel L, Bisiaux A, Albert ML, Strambio-De-Castillia C, Mothes W, Pizzato M, Grutter MG, Luban J.** 2011. TRIM5 is an innate immune sensor for the retrovirus capsid lattice. Nature **472:**361-365.

11. **Ganser-Pornillos BK, Yeager M, Sundquist WI.** 2008. The structural biology of HIV assembly. Curr Opin Struct Biol **18:**203-217.

12. **Ganser BK, Cheng A, Sundquist WI, Yeager M.** 2003. Three-dimensional structure of the M-MuLV CA protein on a lipid monolayer: a general model for retroviral capsid assembly. EMBO J **22:**2886-2892.

13. **Mortuza GB, Haire LF, Stevens A, Smerdon SJ, Stoye JP, Taylor IA.** 2004. High-resolution structure of a retroviral capsid hexameric amino-terminal domain. Nature **431:**481-485.

14. **Campos-Olivas R, Newman JL, Summers MF.** 2000. Solution structure and dynamics of the Rous sarcoma virus capsid protein and comparison with capsid proteins of other retroviruses. J Mol Biol **296:**633-649.

15. **Ganser BK, Li S, Klishko VY, Finch JT, Sundquist WI.** 1999. Assembly and analysis of conical models for the HIV-1 core. Science **283:**80-83.

16. **Benjamin J, Ganser-Pornillos BK, Tivol WF, Sundquist WI, Jensen GJ.** 2005. Three-dimensional structure of HIV-1 virus-like particles by electron cryotomography. J Mol Biol **346:**577-588.

17. **Briggs JA, Grunewald K, Glass B, Forster F, Krausslich HG, Fuller SD.** 2006. The mechanism of HIV-1 core assembly: insights from three-dimensional reconstructions of authentic virions. Structure **14:**15-20.

18. **Briggs JA, Wilk T, Welker R, Krausslich HG, Fuller SD.** 2003. Structural organization of authentic, mature HIV-1 virions and cores. EMBO J **22:**1707-1715.

19. **Ganser-Pornillos BK, Chandrasekaran V, Pornillos O, Sodroski JG, Sundquist WI, Yeager M.** 2011. Hexagonal assembly of a restricting TRIM5alpha protein. Proc Natl Acad Sci U S A **108:**534-539.

20. **Sebastian S, Luban J.** 2005. TRIM5alpha selectively binds a restriction-sensitive retroviral capsid. Retrovirology **2:**40.

21. **Caines ME, Bichel K, Price AJ, McEwan WA, Towers GJ, Willett BJ, Freund SM, James LC.** 2012. Diverse HIV viruses are targeted by a conformationally dynamic antiviral. Nature structural & molecular biology **19:**411-416.

22. **Lienlaf M, Hayashi F, Di Nunzio F, Tochio N, Kigawa T, Yokoyama S, Diaz-Griffero F.** 2011. Contribution of E3-ubiquitin ligase activity to HIV-1 restriction by TRIM5alpha(rh): structure of the RING domain of TRIM5alpha. J Virol **85:**8725-8737.

23. **Diaz-Griffero F, Qin XR, Hayashi F, Kigawa T, Finzi A, Sarnak Z, Lienlaf M, Yokoyama S, Sodroski J.** 2009. A B-box 2 surface patch important for TRIM5alpha self-association, capsid binding avidity, and retrovirus restriction. J Virol **83:**10737-10751.

24. **Goldstone DC, Walker PA, Calder LJ, Coombs PJ, Kirkpatrick J, Ball NJ, Hilditch L, Yap MW, Rosenthal PB, Stoye JP, Taylor IA.** 2014. Structural studies of postentry restriction factors reveal antiparallel dimers that enable avid binding to the HIV-1 capsid lattice. Proc Natl Acad Sci U S A **111:**9609-9614.

25. **Biris N, Yang Y, Taylor AB, Tomashevski A, Guo M, Hart PJ, Diaz-Griffero F, Ivanov DN.** 2012. Structure of the rhesus monkey TRIM5alpha PRYSPRY domain, the HIV capsid recognition module. Proc Natl Acad Sci U S A **109:**13278-13283.

26. **Yang H, Ji X, Zhao G, Ning J, Zhao Q, Aiken C, Gronenborn AM, Zhang P, Xiong Y.** 2012. Structural insight into HIV-1 capsid recognition by rhesus TRIM5alpha. Proc Natl Acad Sci U S A **109:**18372-18377.

27. **Campbell JW, Duee E, Hodgson G, Mercer WD, Stammers DK, Wendell PL, Muirhead H, Watson HC.** 1972. X-ray diffraction studies on enzymes in the glycolytic pathway. Cold Spring Harbor symposia on quantitative biology **36:**165-170.

28. **Zwart PH, Grosse-Kunstleve RW, Lebedev AA, Murshudov GN, Adams PD.** 2008. Surprises and pitfalls arising from (pseudo)symmetry. Acta crystallographica. Section D, Biological crystallography **64:**99-107.

29. **Kar AK, Diaz-Griffero F, Li Y, Li X, Sodroski J.** 2008. Biochemical and Biophysical Characterization of a Chimeric TRIM21-TRIM5alpha Protein. J Virol.

30. **Liu L, Spurrier J, Butt TR, Strickler JE.** 2008. Enhanced protein expression in the baculovirus/insect cell system using engineered SUMO fusions. Protein expression and purification **62:**21-28.

31. **Kar AK, Mao Y, Bird G, Walensky L, Sodroski J.** 2011. Characterization of a core fragment of the rhesus monkey TRIM5alpha protein. BMC biochemistry **12:**1.

32. **Sanchez JG, Okreglicka K, Chandrasekaran V, Welker JM, Sundquist WI, Pornillos O.** 2014. The tripartite motif coiled-coil is an elongated antiparallel hairpin dimer. Proc Natl Acad Sci U S A **111:**2494-2499.

33. **Li X, Sodroski J.** 2008. The TRIM5{alpha} B-box 2 Domain Promotes Cooperative Binding to the Retroviral Capsid by Mediating Higher-order Self-association. J Virol.

34. **Li X, Song B, Xiang SH, Sodroski J.** 2007. Functional interplay between the B-box 2 and the B30.2(SPRY) domains of TRIM5alpha. Virology **366:**234-244.

35. **Mace PD, Linke K, Feltham R, Schumacher FR, Smith CA, Vaux DL, Silke J, Day CL.** 2008. Structures of the cIAP2 RING domain reveal conformational changes associated with ubiquitin-conjugating enzyme (E2) recruitment. J Biol Chem **283:**31633-31640.

36. **Pornillos O, Ganser-Pornillos BK, Kelly BN, Hua Y, Whitby FG, Stout CD, Sundquist WI, Hill CP, Yeager M.** 2009. X-Ray Structures of the Hexameric Building Block of the HIV Capsid. Cell.

37. **Pornillos O, Ganser-Pornillos BK, Banumathi S, Hua Y, Yeager M.** 2010. Disulfide bond stabilization of the hexameric capsomer of human immunodeficiency virus. J Mol Biol **401:**985-995.

38. **Li MZ, Elledge SJ.** 2012. SLIC: a method for sequence- and ligation-independent cloning. Methods Mol Biol **852:**51-59.

39. **Hanson MA, Brooun A, Baker KA, Jaakola VP, Roth C, Chien EY, Alexandrov A, Velasquez J, Davis L, Griffith M, Moy K, Ganser-Pornillos BK, Hua Y, Kuhn P, Ellis S, Yeager M, Stevens RC.** 2007. Profiling of membrane protein variants in a baculovirus system by coupling cell-surface detection with small-scale parallel expression. Protein expression and purification **56:**85-92.

# APPENDIX

## BIOCHEMICAL CHARACTERIZATION OF A RECOMBINANT TRIM5α PROTEIN THAT RESTRICTS HUMAN IMMUNODEFICIENCY VIRUS TYPE 1 REPLICATION

Charles R. Langelier, Virginie Sandrin, Debra M. Eckert, Devin E. Christensen, Viswanathan Chandrasekaran, Steven L. Alam, Christopher Aiken, John C. Olsen, Alak Kanti Kar, Joseph G. Sodroski, and Wesley I. Sundquist

Reprinted with permission from Journal of Virology 82(23), 11682-11694.

JOURNAL OF VIROLOGY, Dec. 2008, p. 11682–11694 Vol. 82, No. 23
0022-538X/08/$08.00+0 doi:10.1128/JVI.01562-08


# Biochemical Characterization of a Recombinant TRIM5α Protein That Restricts Human Immunodeficiency Virus Type 1 Replication▽†

Charles R. Langelier,[1] Virginie Sandrin,[1] Debra M. Eckert,[1] Devin E. Christensen,[1] Viswanathan Chandrasekaran,[1] Steven L. Alam,[1] Christopher Aiken,[2] John C. Olsen,[3] Alak Kanti Kar,[4] Joseph G. Sodroski,[4] and Wesley I. Sundquist[1]*

*Department of Biochemistry, University of Utah, Salt Lake City, Utah 84112-5650[1]; Department of Microbiology and Immunology, Vanderbilt University School of Medicine, A-5301 Medical Center North, Nashville, Tennessee 37232-2363[2]; Department of Medicine, Cystic Fibrosis/Pulmonary Research and Treatment Center, University of North Carolina at Chapel Hill, Chapel Hill, North Carolina 27599[3]; and Department of Cancer Immunology and AIDS, Dana-Farber Cancer Institute, Division of AIDS, Harvard Medical School, Boston, Massachusetts 02115[4]*

Received 23 July 2008/Accepted 5 September 2008

**The rhesus monkey intrinsic immunity factor TRIM5α$_{rh}$ recognizes incoming capsids from a variety of retroviruses, including human immunodeficiency virus type 1 (HIV-1) and equine infectious anemia virus (EIAV), and inhibits the accumulation of viral reverse transcripts. However, direct interactions between restricting TRIM5α proteins and retroviral capsids have not previously been demonstrated using pure recombinant proteins. To facilitate structural and mechanistic studies of retroviral restriction, we have developed methods for expressing and purifying an active chimeric TRIM5α$_{rh}$ protein containing the RING domain from the related human TRIM21 protein. This recombinant TRIM5-21R protein was expressed in SF-21 insect cells and purified through three chromatographic steps. Two distinct TRIM5-21R species were purified and shown to correspond to monomers and dimers, as analyzed by analytical ultracentrifugation. Chemically cross-linked recombinant TRIM5-21R dimers and mammalian-expressed TRIM5-21R and TRIM5α proteins exhibited similar sodium dodecyl sulfate-polyacrylamide gel electrophoresis mobilities, indicating that mammalian TRIM5α proteins are predominantly dimeric. Purified TRIM5-21R had ubiquitin ligase activity and could autoubquitylate with different E2 ubiquitin conjugating enzymes in vitro. TRIM5-21R bound directly to synthetic capsids composed of recombinant HIV-1 CA-NC proteins and to authentic EIAV core particles. HIV-1 CA-NC assemblies bound dimeric TRIM5-21R better than either monomeric TRIM5-21R or TRIM5-21R constructs that lacked the SPRY domain or its V1 loop. Thus, our studies indicate that TRIM5α proteins are dimeric ubiquitin E3 ligases that recognize retroviral capsids through direct interactions mediated by the SPRY domain and demonstrate that these activities can be recapitulated in vitro using pure recombinant proteins.**

Susceptibility to retroviral infections influences species survival and has driven the evolution of cellular restriction factors that inhibit retroviral replication. One important antiretroviral intrinsic immune response is mediated by TRIM5α, which can block early postentry steps in the replication of certain retroviruses in specific primate lineages (3, 37, 55, 58). Under normal restrictive conditions, TRIM5α proteins block accumulation of retroviral reverse transcripts (55) and accelerate the rate at which viral capsids dissociate from high-molecular-weight complexes into lower-molecular-weight subunits (42, 56). The allelic specificity of TRIM5α restriction is illustrated by the fact that rhesus macaque TRIM5α potently inhibits human immunodeficiency virus type 1 (HIV-1) replication, whereas human TRIM5α instead exhibits restriction activity against N-tropic murine leukemia virus but not HIV-1 (23, 29, 43, 55, 67). These differences can be attributed to the differential abilities of TRIM5α proteins to interact with retroviral capsids after viral entry (34, 42, 56).

Like other tripartite (TRIM) family members, TRIM5α contains RING, B-box, coiled-coil, and B30.2/SPRY domains, and each of these domains contributes to restriction activity. The RING domain of TRIM5α has intrinsic E3 ubiquitin ligase activity (63, 64), which is important both for autoubiquitylation and for protein turnover in vivo (12, 26). The E3 ubiquitin ligase activity also contributes to restriction but is not absolutely required (26, 41, 55), and the precise functions of ubiquitylation and the role of the ubiquitin/proteasome system in retroviral restriction are not yet fully understood. Specifically, proteasome activity is not required for TRIM5α antiviral activity per se (12, 41), but proteasome inhibitors do alter the normal progression of TRIM5α restriction, allowing reverse transcripts to accumulate and impairing the ability of TRIM5α to accelerate the dissociation of intact viral capsids (2, 10, 62). Moreover, the restriction of incoming capsids results in proteasome-dependent degradation of TRIM5α (47), again suggesting possible involvement of the proteasome in the normal stepwise progression of restriction.

The B-box domain of TRIM5α plays an essential, but still

* Corresponding author. Mailing address: Department of Biochemistry, University of Utah, Salt Lake City, UT 84112-5650. Phone: (801) 585-5402. Fax: (801) 581-7959. E-mail: wes@biochem.utah.edu.

† Supplemental material for this article may be found at http://jvi.asm.org/.

▽ Published ahead of print on 17 September 2008.

undefined role in restriction activity, and mutations in this domain can influence protein turnover, intracellular localization, and restriction activity (11). The coiled-coil and ensuing linker 2 (L2) regions of TRIM5α also contribute to efficient capsid binding and restriction, and these elements appear to function primarily in protein oligomerization (27, 36). Cross-linking studies have suggested that TRIM5α may function as a trimer, but trimerization has not been rigorously demonstrated by biophysical studies of pure TRIM5 proteins (36). Finally, the C-terminal B30.2/SPRY domain of TRIM5α is essential for viral capsid recognition and is the key determinant of antiviral specificity (38, 41, 54–56, 68). Several motifs within the SPRY domain have been subject to significant positive selection and exhibit pronounced variability between species (35, 38, 49, 50, 54, 57). In particular, variable region 1 (V1, residues 323 to 350 in rhesus TRIM5α) is critical both for efficient restriction and for capsid binding, and a single amino acid alteration at position 332 of the V1 loop allows human TRIM5α to bind HIV-1 capsids and inhibit HIV-1 replication (34, 54, 68). These and other observations show that the SPRY domain dictates retroviral capsid recognition, although direct binding interactions have not yet been demonstrated and characterized using pure TRIM5α proteins.

TRIM5α proteins appear to recognize the outer shell of the retroviral core particle, which is called the capsid. Lentiviruses such as HIV-1 and equine infectious anemia virus (EIAV) have conical capsids composed of CA protein hexamers that form hexagonal assemblies called fullerene cones (4, 19–21, 28, 32). Intact retroviral core particles can be isolated from membrane-stripped retroviruses and purified by using sucrose-gradient centrifugation, but these assemblies are rather unstable and typically disassemble spontaneously in buffer (1, 17, 30, 46, 60). Structural and biochemical studies of the HIV-1 capsid have therefore frequently used synthetic assemblies created from pure recombinant CA proteins (20). The assemblies formed by pure HIV-1 CA-NC proteins on DNA templates are particularly stable and can be formed under near physiological conditions (7, 21). These CA-NC/DNA assemblies are a mixture of cylindrical and conical structures that recapitulate the hexagonal lattice of CA hexamers found in authentic viral capsids (4, 21, 32). Synthetic HIV-1 CA-NC/DNA assemblies, like membrane-stripped viral capsids, also bind exogenously expressed TRIM5α proteins present in crude cell lysates (51, 56), indicating that the CA-NC/DNA assemblies recapitulate the key elements required for TRIM5α recognition.

In summary, it is now well established that capsid recognition dictates the allelic specificity of TRIM5α restriction. However, direct interactions between pure TRIM5 proteins and retroviral capsids have not yet been demonstrated in vitro, largely owing to the technical challenges of creating suitable capsid targets and of expressing and purifying recombinant TRIM5α proteins. To date, soluble full-length TRIM5α proteins have not been expressed successfully in *Escherichia coli*, and TRIM5α proteins tend to turnover rapidly and aggregate into cytoplasmic bodies when overexpressed in mammalian systems (6, 12, 53). However, replacing the TRIM5α RING domain with the RING domain from the homologous TRIM21 protein reduces protein turnover without compromising HIV-1 restriction substantially (12, 33). We have taken advantage of this observation to develop systems for expressing and purifying chimeric TRIM5-21R proteins in quantities suitable for biochemical and biophysical characterization.

## MATERIALS AND METHODS

**Cell cultures.** Human 293T and HeLa cells were maintained in Dulbecco modified Eagle medium supplemented with 10% fetal calf serum. HeLa cells stably expressing rhesus TRIM5α (TRIM5$\alpha_{rh}$) (55) were maintained with an additional supplement of 1 μg of puromycin/ml.

**Expression vectors.** The pLPCX TRIM5-21R expression vector, encoding a hemagglutinin (HA)-tagged TRIM5-21R (12), was used as a PCR template to create a DNA fragment containing the TRIM5-21R gene with KpnI and XhoI restriction sites. This fragment was ligated into the pCAG.OSFT (WISP-08-189) backbone, which itself was modified from the pCAG vector backbone (Addgene) to encode an N-terminal OneStrep and Flag (OSF) epitope tag followed by a TEV protease cleavage site. The resulting vector, pCAG.OSFT-TRIM5-21R (WISP-08-176), was used as a PCR template to amplify a DNA fragment with terminal attB sites to allow for recombination into the pDONR221 Gateway Entry Vector (Invitrogen) to create the pDONR221.OSFT-TRIM5-21R Entry Vector (WISP-08-177). This vector was used as a template for QuikChange site-directed mutagenesis (Stratagene) to create pDONR221.OSFT-TRIM5-21RΔV1 (WISP-08-178) (deletion in the V1 variable loop of the SPRY domain corresponding to TRIM5$\alpha_{rh}$ residues 332 to 344) and pDONR221.OSFT-TRIM5-21RΔSPRY (WISP-08-179) (deletion of the entire SPRY domain and L2 element, TRIM5$\alpha_{rh}$ residues 233 to 497). The pCAG.OSFT-TRIM5$\alpha_{rh}$ and pDONR221.OSFT-TRIM5$_{rh}$ vectors (WISP-08-197 and -08-198) were constructed in an analogous fashion. Recombinant baculoviruses expressing TRIM5-21R, TRIM5-21RΔV1, and TRIM5-21RΔSPRY were prepared in situ by using the BaculoDirect system (Invitrogen). Equivalent mammalian cell expression constructs were generated in the Gateway pcDNA-DEST40 vector (WISP-08-180, -181, -182, and -199, respectively). pET28-based plasmids for bacterial expression of UbcH5 (WISP-08-190), UbcH6 (WISP-08-191), UbcH7 (WISP08-192), and Uba1 (WISP-08-192) were generous gifts from Rachel Klevit (University of Washington) (5, 8), and the Uba1 gene was originally a gift from Richard Vierstra (University of Wisconsin) (22).

**Expression and purification of recombinant proteins. (i) TRIM5-21R.** Two liters of SF-21 insect cells were grown to a density of $2 \times 10^6$ cells/ml in SF-900 II media (Invitrogen), infected at a multiplicity of infection of 1.0 with recombinant baculoviruses encoding TRIM5-21R and variants, and the expressed proteins were allowed to accumulate for 36 to 44 h (100 rpm shaking, 27°C). All subsequent steps were carried out at 4°C, except where noted. Cells were collected by centrifugation at 500 × *g* for 8 min, resuspended in 1:25 (vol/vol) of lysis buffer (50 mM NaCl, 50 mM Tris [pH 8.0], 1.5% Triton X-100, 1 mM TCEP, and mammalian protease inhibitor cocktail [Sigma] at 1:150 [vol/vol]), and lysed in a 100-ml Dounce homogenizer (15 strokes). The lysate was clarified by ultracentrifugation (Beckman Ti 50.2 rotor; 45,000 rpm, 184,000 × *g*, 40 min), filtered (0.45 μm), and loaded at 2 ml/min onto a 10-ml StrepTactin Superflow affinity column (IBA). The bound protein was washed with 50 ml of buffer (50 mM NaCl, 50 mM Tris [pH 8.0], 1 mM TCEP) and eluted with wash buffer supplemented with 2.5 mM D-desthiobiotin. The eluate was loaded directly onto two 5-ml HiTrap Q-Sepharose anion-exchange columns connected in series (GE Healthcare) and eluted with a NaCl gradient from 50 mM to 1 M over 200 ml of buffer (50 mM Tris [pH 8.0], 1 mM TCEP). Purified TRIM5-21R eluted in two peaks (see Fig. 1B). Fractions containing the early eluting peak were pooled, concentrated to 2 ml (Vivaspin concentrator; Sartorius), and loaded onto a 120-ml Superose-6 gel filtration column. The later eluting protein fraction peak tended to aggregate under high-ionic-strength conditions and was therefore loaded directly onto a Superose-6 column without concentration (4-ml fractions). Gel filtration chromatography was performed at 1 ml/min in 25 mM NaCl, 50 mM Tris (pH 8.0), 1 mM TCEP. The gel filtration column was calibrated by using the HMW standard gel filtration calibration kit (GE Healthcare), and the two TRIM5-21R species eluted with apparent molecular masses of 232 kDa (dimer, second anion exchange peak) and 70 kDa (monomer, first anion exchange peak). The purified monomer could be concentrated to 10 mg/ml, whereas the dimer tended to precipitate at concentrations above 3 mg/ml. Concentrated proteins were stored at 4°C for short-term use but tended to precipitate when stored for multiple days. Alternatively, proteins were flash frozen in liquid nitrogen and retained CA-NC binding and autoubiquitylation activities when thawed.

**(ii) Ubiquitin-related proteins.** Recombinant E1 and E2 proteins were expressed in BL21-Codon Plus (DE3)-RIPL bacteria (Stratagene) grown in LB media and purified as described previously (8). Briefly, human UbcH5c, UbcH6, and UbcH7 were purified by cation-exchange chromatography (SP Sepharose) and eluted with a 0 to 0.5 M NaCl gradient in 30 mM MES (morpholineethane-

TABLE 1. Posttranslational modifications of TRIM5-21R and TRIM5$\alpha_{rh}$ proteins

| Cell type | Protein | No. of peptides identified[a] | % Coverage | MASCOT score (total protein score) |
|---|---|---|---|---|
| SF-21 | TRIM5-21R | 77* | 54 | 7365 |
| | Ubiquitin | 7† | 79 | 138 |
| 293T | TRIM5$\alpha_{rh}$-HA | 42* | 47 | 2162 |
| | Ubiquitin | 2 | 23 | 63 |

[a] *, Two nested TRIM5-21R phosphopeptides were identified: $^{81}$LREVKLSP EEGQK$^{93}$ and $^{83}$EVKLSPEEGQK$^{93}$. †, One ubiquitylated ubiquitin peptide was identified: $^{43}$LIFAGKQLEDGR$^{54}$.

sulfonic acid)–1 mM EDTA (pH 6.0). E2-rich fractions were pooled and purified further by size exclusion chromatography in 25 mM sodium phosphate (pH 7.0)–150 mM NaCl. Wheat His$_6$-Uba1 (E1) was purified by $Ni^{2+}$-affinity chromatography, followed by size exclusion chromatography. Ubiquitin was purified as described previously (44).

**Mass spectrometry.** Monomeric and dimeric TRIM5-21R proteins were desalted for electrospray ionization mass spectrometry using a C18 Ziptip (Millipore) and analyzed on a Quattro-II mass spectrometer (Micromass, Inc.). The data were acquired with a cone voltage of 50 eV, a spray voltage of 2.8 kV, and scanning from 800 to 1,400 $m/z$ in 4 s. Spectra were combined, and the multiply charged molecular ions were deconvoluted into a molecular-mass spectrum by using MaxEnt software (Micromass, Inc.).

Liquid chromatography tandem mass spectrometry experiments were used to examine posttranslational modifications of both TRIM5$\alpha_{rh}$ expressed in 293T cells and TRIM5-21R expressed in SF-21 cells. TRIM5$\alpha_{rh}$ contained a C-terminal HA tag (55) and was affinity purified from 293T cells by using α-HA-conjugated Sepharose matrices as described below for cross-linking experiments. Dimeric TRIM5-21R was purified by anion-exchange chromatography, concentrated, and mixed with an equal volume of 2× sodium dodecyl sulfate (SDS) loading buffer. In both cases, samples were boiled, separated by SDS-4 to 20%polyacrylamide gel electrophoresis (PAGE), and visualized using Coomassie blue staining. Major bands corresponding to each TRIM5 protein, as well as minor bands corresponding to higher-molecular-mass (modified) TRIM5 proteins were excised, digested with TPCK (tolylsulfonyl phenylalanyl chloromethyl ketone)-modified trypsin (Promega) and introduced by nanoLC (Eksigent, Inc.) with nano-electrospray ionization (ThermoElectron Corp) into a LTQ-FT hybrid mass spectrometer (ThermoElectron Corp). Peptide molecular masses were measured by Fourier transform ion cyclotron resonance, and peptide sequencing was performed by collision-induced dissociation in the linear ion trap of the instrument. Protein identification and posttranslational modifications (phosphorylation and ubiquitylation) of peptides in tryptic digests were determined by using the MASCOT search engine (Matrix Science) and the NCBI$_{nr}$ mammalian taxonomy database using a significance threshold of $P < 0.05$ and an ion score cutoff value of 20 (Table 1).

**Equilibrium sedimentation analyses.** Equilibrium sedimentation of purified TRIM5-21R proteins was performed using Optima XL-I and XL-A centrifuges (Beckman) at protein subunit concentrations of 6.09, 3.05, and 1.53 μM (monomer) or 6.0, 3.0, and 1.5 μM (dimer) in 50 mM Tris-HCl (pH 8.0)–50 mM NaCl–1 mM β-mercaptoethanol (monomer) or in 25 mM NaCl–50 mM Tris-HCl (pH 8.0)–1 mM TCEP (dimer). Centrifugation (4°C) was performed at two speeds: 14,000 and 18,000 rpm (monomer) and 14,000 and 16,000 rpm (dimer). The resulting six data sets for each oligomeric species were globally fit to single ideal species models with fixed or floating molecular masses using the nonlinear least-squares algorithms in the Heteroanalysis software (9). Solvent density and the partial specific volume of TRIM5-21R were calculated by using the program SEDNTERP (version 1.09) (31).

**Autoubiquitylation activity assays.** TRIM5-21R-directed ubiquitylation assays were carried out in 50-μl reaction mixtures containing 1.0 μM TRIM5-21R, 1.0 μM concentrations of the specified E2 enzyme, 20 μM ubiquitin, and 0.5 μM wheat Uba1. Reactions were incubated for 60 min with or without addition of 5 mM ATP–10 mM $MgCl_2$, and reaction products were analyzed by SDS–7.5% PAGE and Western blotting as described below.

**Cross-linking reactions. (i) Cross-linking of recombinant TRIM5-21R proteins.** Pure recombinant TRIM5-21R proteins were dialyzed overnight into phosphate-buffered saline (PBS; 1 mM $KH_2PO_4$, 5.6 mM $Na_2HPO_4$, 154 mM NaCl) plus 1 mM TCEP. Cross-linking reactions were then performed for 10 min at 25°C in 30-μl reaction volumes at final protein concentrations of 0.5 μM, along with 0, 0.1, 0.5, or 1 mM fresh EGS [ethylene glycol-bis(succinimidyl succinate)] cross-linker. Reactions were quenched by addition of 30 μl of 0.1 M Tris-HCl (pH 7.5), and samples were mixed with SDS loading buffer plus 1.2% β-mercaptoethanol, and analyzed by SDS–7.5% PAGE and Western blotting. For reactions performed in the presence of mammalian cell lysate, recombinant TRIM5-21R proteins in PBS plus 1 mM TCEP buffer were incubated in 30-μl reactions containing final concentrations of 50% clarified lysate prepared from 293T cells (see below), 0.25 μM TRIM5-21R, and EGS at 0, 0.1, 0.5, or 1 mM (20 min, 25°C). Reactions were quenched by the addition of 30 μl of 0.1 M Tris-HCl (pH 7.5), diluted to 400 μl with PBS plus 1 mM EDTA, and incubated with 30 μl of StrepTactin Sepharose (IBA) at 4°C for 2 h. The matrix was washed four times with PBS plus 0.5% NP-40 and resuspended in 30 μl of SDS loading buffer plus 1.2% β-mercaptoethanol for Western blot analysis.

**(ii) Cross-linking of TRIM proteins expressed in mammalian cells.** For each cross-linking series (four samples), a 10-cm plate of confluent 293T cells expressing OSF-tagged TRIM5-21R or HA-tagged TRIM5$\alpha_{rh}$ was lysed in 300 μl of PBS plus 0.5% NP-40 supplemented 1:150 with protease inhibitor cocktail (Sigma) for 15 min on ice. Lysates were clarified by centrifugation at 16,100 × $g$ for 30 min, and the resulting supernatant was diluted to a final volume of 1.7 ml with PBS plus 1 mM EDTA. Then, 400-μl aliquots of diluted lysate were incubated with 0, 0.1, 0.5, or 1.0 mM EGS (20 min at 25°C). Reactions were quenched by the addition of 400 μl of 0.1 M Tris-HCl (pH 7.5), mixed with 30 μl of pre-equilibrated StrepTactin Sepharose (TRIM21-5R; IBA) or α-HA-conjugated Sepharose (TRIM5$\alpha_{rh}$; Sigma), and incubated for 2 h at 4°C. Matrices were washed four times with PBS plus 0.5% NP-40 and resuspended in 30 μl of SDS loading buffer plus 1.2% β-mercaptoethanol for Western blot analysis using SDS–7.5% PAGE.

**Western blotting.** Proteins were separated by SDS-PAGE, transferred to PVDF-FL membranes (Millipore) in Tris-glycine–10% methanol buffer, blocked in 5% milk–Tris-buffered saline (20 min), and incubated with primary antibodies diluted in 5% nonfat milk–Tris-buffered saline plus 0.1% Tween 20 (16 h, 4°C). Blots were visualized by using an Odyssey infrared imaging system (Li-Cor, Inc.) to detect Alexa 680-nm (Molecular Probes; 1:10,000) or IRDye 800-nm (Rockland; 1:10,000) secondary antibodies. The primary antibodies and dilutions used were as follows: mouse anti-FLAG (Sigma) at 1:3,000 for OSF-TRIM5-21R (Fig. 1, 3 to 5, and 7), mouse anti-HA.11 (Sigma) at 1:1,000 for TRIM5α-HA (Fig. 3), rabbit anti-HIV-1 CA (UT415 made against purified NL4-3 CA protein and affinity purified) at 1:15,000 (Fig. 5), and rabbit anti-EIAV CA (UT418 made against purified EIAV CA protein and affinity-purified) at 1:5,000 (Fig. 7).

**Restriction assays. (i) HIV-1 restriction assays.** The HIV-1 vector pCMVΔR8.2, which expresses a lacZ reporter, was packaged into vesicular stomatitis virus G-pseudotyped HIV-1 as described previously (48a, 59a). For restriction assays, $3 \times 10^4$ HeLa-M cells were seeded in 24-well plates and transfected (Lipofectamine 2000) 24 h later with 1 μg of the control pcDNA-DEST40 vector or with vectors expressing OSFT-TRIM5$\alpha_{rh}$, OSFT-TRIM5-21R, OSFT-TRIM5-21RΔV1, or OSFT-TRIM5-21RΔSPRY. Cells were incubated for 24 h, washed with media, transduced for 24 h with various quantities of the HIV-1 vector, washed again, and the percentage of infected cells was determined by assaying for lacZ expression at 48 h post infection. Equivalent expression levels of the different TRIM5 constructs were verified by Western blotting.

**(ii) EIAV restriction assay.** To assay for restriction, 293T cells were transfected in a 10-cm plate with the CeGFPW EIAV vector system as described below, and infectivity was subsequently assayed as previously described (48). Briefly, dilutions of vector preparations were added to target cells (HeLa or HeLa-TRIM5$\alpha_{rh}$, $2.0 \times 10^5$ cells/well, six-well plate) and incubated for 72 h at 37°C. Transduction efficiencies were determined from the percentage of GFP-positive cells measured by fluorescence-activated cell sorting.

**EIAV core isolation.** EIAV cores were prepared by using an adaptation of a method described previously (30). Briefly, EIAV virions were produced by co-transfection of 293T cells (16 × 10-cm plates) with an EIAV vector system. Each 10-cm plate of cells was transfected (CalPhos mammalian transfection kit; Clontech) with 8.1 μg of pEV53 (EIAV structural proteins), 7.5 μg of pSIN6.1CeGFPW (packaged GFP expression vector), and 2.7 μg of phCMV-VSV-G (VSV-G envelope) (39, 69). After 36 h, the supernatants were removed, pooled (four plates/pool), filtered (0.45-μm pore size), and pelleted through a 4-ml 20% sucrose cushion in a Beckman SW-32Ti rotor (134,000 × $g$, 2 h, 4°C). Each set of pelleted virions was resuspended by gentle pipetting (4 h at 4°C) in 400 μl of ST buffer (10 mM Tris-HCl [pH 7.4], 50 mM NaCl). Four 11.5-ml sucrose gradients (30 and 70% [wt/vol] sucrose in ST buffer) were prepared in 14-by-89-mm tubes using a gradient mixer (Biocomp). The gradients were overlaid with a 0.3-ml cushion of 15% sucrose containing 1% Triton X-100 and then with a 0.3-ml barrier layer of 7.5% sucrose in ST buffer. Each tube of concen-

trated EIAV particles was carefully layered on top of a gradient and centrifuged in a Beckman SW-41 rotor (210,000 × *g*, 16 h, 4°C). Twelve 1-ml fractions were collected from the bottom of each tube, and fraction densities were measured by using a digital refractometer (Leica), and EIAV CA was assayed by Western blotting. Three 1-ml fractions of the correct density (1.22 to 1.26 g/ml) contained intact EIAV core particles and were pooled, repelleted by centrifugation in a Beckman SW-41 rotor (2,000 × *g*, 2 h, 4°C), and resuspended in 40 μl of ST buffer for binding assays.

**Capsid binding assays.** Recombinant HIV-1 CA-NC was expressed and purified as described previously (21). Cylindrical and conical assemblies were created by coincubating 10 μM CA-NC and 2 μM $d(TG)_{50}$ oligonucleotide (15) in 1 ml of assembly buffer (50 mM Tris-HCl [pH 8.0], 500 mM NaCl) for 16 h at 4°C. Assembled complexes were enriched by centrifugation at 10,000 rpm in a microcentrifuge (~9,000 × *g*) for 5 min, and pelleted assemblies were resuspended in 200 μl of supernatant. TRIM5-21R proteins were used at final concentrations of 5.0 μM (for the experiments described in Fig. 5B and 6B comparing different TRIM5-21R constructs), 0.5 or 0.15 μM (0.3×) (for the more stringent binding assays described in Fig. 5C), or 0.36 μM (for the EIAV core binding assays described in Fig. 7B). TRIM5-21R proteins were mixed with 20 μl of concentrated CA-NC particles (see the figure legends for quantities) or with purified EIAV cores (~100 ng, ~20 nM CA) in reaction volumes of 200 μl, with a final buffer composition of 10 mM Tris, 2 mM $KH_2PO_4$, 11 mM $Na_2HPO_4$, and 280 mM NaCl (Fig. 5B), 308 mM NaCl (Fig. 5C, 1×), 316 mM NaCl (Fig. 5C, 0.3×), or 250 mM NaCl (Fig. 7B). Reactions were incubated for 45 min at 25°C (CA-NC binding assays) or 4°C (EIAV core assays) with gentle mixing at 10-min intervals. Prior to centrifugation, a 10-μl sample was removed and mixed with SDS loading buffer (input). Binding reactions were layered onto a 4.2-ml cushion of 70% (CA-NC) or 57% (EIAV cores) sucrose (wt/vol; sucrose-PBS plus 1 mM TCEP) in 13-by-51-mm tubes and centrifuged in a Beckman SW-50.1 rotor (110,000 × *g*, 1 h, 4°C). Samples of the supernatant remaining above the sucrose cushion were saved (supernatant), the sucrose cushions were removed by aspiration, and the pellet was resuspended in 40 μl of 1× SDS loading buffer. Input, supernatant, and pellet samples were analyzed by Western blotting at concentrations in which the supernatant samples corresponded to 1.25% (CA-NC) and 2% (EIAV cores) of the total supernatant, and pellet samples corresponded to 80% of the total pellet. Under these conditions, ~2.5% of the input EIAV cores pelleted, and ~1.6% (5.0 μM input TRIM5-21R), 1.6% (0.5 μM input TRIM5-21R), and 2.4% (0.15 μM input TRIM5-21R) of the CA-NC assemblies pelleted.

**Transmission electron microscopy analyses of TRIM-bound CA-NC tubes.** For transmission electron microscopy analyses, binding reactions containing 5-μl suspensions of CA-NC particles (prepared as described above) were incubated with final TRIM5-21R concentrations of 20 to 50 μM (15-μl total volumes, 25°C, 45 min, with gentle mixing every 10 min). Carbon-coated grids were placed on aliquots of each reaction mixture (7 μl, 90 s), washed with 3 to 4 drops of 0.1 M KCl, stained with 3 or 4 drops of 4% uranyl acetate, and air dried. Samples were imaged on Hitachi 7100 and Philips Tecnai 12 transmission electron microscopes at magnifications between ×25,000 and ×100,000. Each electron microscopic analysis was repeated at least three times with proteins from at least three separate purifications.

## RESULTS

**TRIM5-21R expression and purification.** Wild-type rhesus TRIM5α accumulates at low levels and tends to aggregate when overexpressed in mammalian and insect cells (12; data not shown). These properties have made it difficult to obtain sufficient quantities of pure recombinant TRIM5α proteins for biophysical and structural studies. Substitution of the $TRIM5\alpha_{rh}$ RING domain with the RING domain of the homologous human TRIM21 protein (58% identity), however, generates a fusion protein (designated TRIM5-21R) that has a longer half-life and accumulates to higher levels in mammalian cells than does wild-type TRIM5α (12). Importantly, TRIM5-21R restricts HIV-1 replication, although its activity is slightly reduced relative to wild-type TRIM5α (12; see also Fig. S1A in the supplemental material). TRIM5-21R was therefore an attractive candidate for large-scale expression in insect cells.

TRIM5-21R constructs with N-terminal OSF epitope tags were expressed in SF-21 cells using baculoviral expression systems. TRIM5-21R expression was detectable in Western blots of soluble lysates of infected SF-21 cells but not in control lysates (Fig. 1A, upper panel, compare lanes 1 and 2). The soluble TRIM5-21R protein was affinity purified on a Strep-Tactin matrix, and elution with D-desthiobiotin yielded TRIM5-21R as essentially the only protein detectable by either Western blotting (upper panel, lane 3) or Coomassie blue staining (lower panel). The protein was further purified by anion-exchange chromatography, where it separated into two distinct species, both of which corresponded to TRIM5-21R (Fig. 1B, upper panel, and Fig. 1A, lanes 4 and 5). The ratios of the two species varied between preparations, but it was common for the late-eluting species to predominate, as shown in Fig. 1B.

Gel filtration chromatography was used as a final step to purify the two distinct TRIM5-21R species. The two species again exhibited different chromatographic behavior, eluting with apparent molecular weights of 232 kDa (late-eluting anion-exchange peak) and 77 kDa (early-eluting anion-exchange peak). The apparent size of the smaller protein suggested that it was likely to be a TRIM5-21R monomer, whereas the apparent size of the larger protein suggested that it was probably either a trimer or a dimer with an extended Stokes radius. Typical yields were 150 μg (larger species) and 200 μg (smaller species) per liter of infected SF-21 cells.

The identities of the two purified recombinant TRIM5-21R proteins were confirmed by electrospray mass spectrometric (ESI/MS) analyses of the intact proteins, and by liquid chromatography tandem mass spectrometric analyses of tryptic digests. The mass of the intact smaller species corresponded to a TRIM5-21R protein that was missing the N-terminal methionine and was acetylated at the N terminus ($MW_{actual}$ = 62,518 g/mol, $MW_{calculated}$ = 62,520 g/mol), and the mass spectra revealed no evidence for posttranslational modifications. In contrast, the oligomeric species showed a protein of the same mass ($MW_{actual}$ = 62,517 g/mol), as well as a second protein with a mass that corresponded to a singly phosphorylated protein ($MW_{actual}$ = 62,596 g/mol, $MW_{calc}$ = 62,595; ~30% of protein). Peptide mapping experiments were therefore performed on TRIM5-21R proteins produced in both SF-21 (insect) and 293T (mammalian) cells. These studies identified a single phosphoserine residue at position 87 within the L1 linker between the RING and B-box domains in TRIM5-21R proteins isolated from both insect and human cells (Table 1, $TRIM5\alpha_{rh}$ numbering). Given its location, this phosphorylation site could, in principle, modulate a postulated interaction between the RING and adjacent L1 elements (24). Ubiquitin-derived peptides were also detected in trypsin digests of purified TRIM5-21R expressed in both insect and mammalian cells, indicating that the protein was also ubiquitylated at low levels. Interestingly, ubiquitin peptides with Lys-48 isopeptide linkages were also detected, indicating that TRIM5-21R could be polyubiquitylated with Lys-48 chains.

In summary, we have developed methods that can be used to express and purify up to milligram quantities of two different TRIM5-21R oligomers, and the larger species can be phosphorylated and ubiquitylated in human and in insect cells.

**Recombinant TRIM5-21R proteins are monomers and dimers.** Equilibrium sedimentation centrifugation experiments can provide shape-independent measures of protein solution mass,

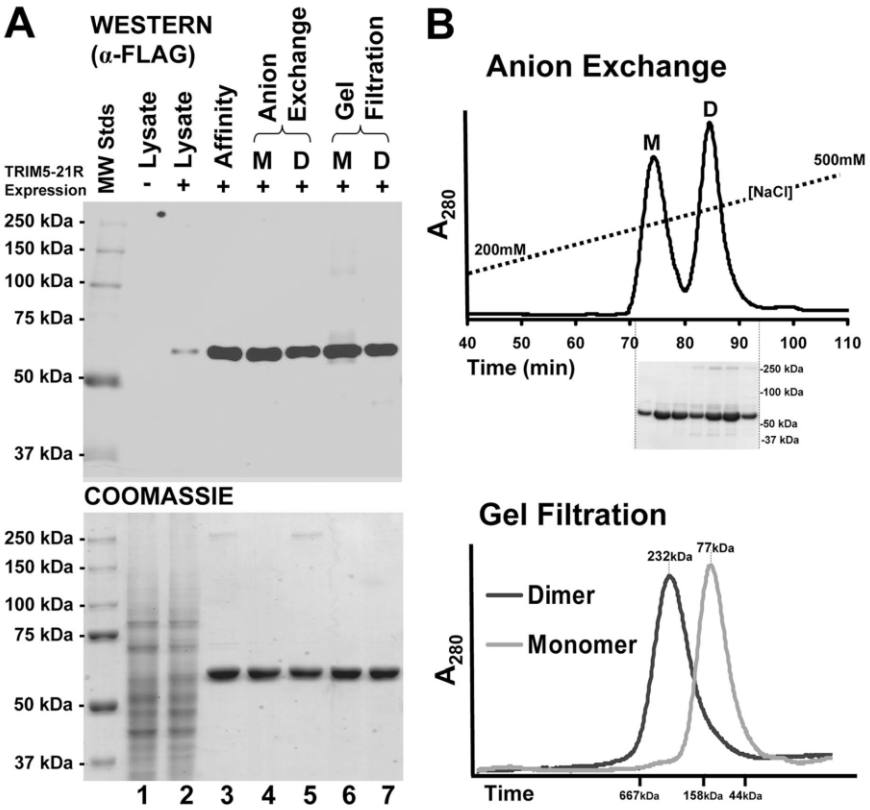


FIG. 1. TRIM5-21R expression and purification. (A) Western blot (upper, anti-FLAG) and Coomassie blue-stained SDS-PAGE gel (lower) showing the stepwise purification of recombinant TRIM5-21R proteins. Lane 1, soluble lysate from control SF-21 cells; lane 2, lysate from SF-21 cells infected with baculovirus expressing TRIM5-21R; lane 3, StrepTactin affinity-purified TRIM5-21R; lanes 4 and 5, monomeric (M, early eluting peak) and dimeric (D, late eluting peak) TRIM5-21R proteins purified by anion-exchange chromatography; lanes 6 and 7, monomeric (M, late eluting peak) and dimeric (D, early eluting peak) TRIM5-21R proteins purified by gel filtration chromatography. (B) Anion-exchange (upper) and gel filtration (lower) chromatographs showing the elution profiles of monomeric (M) and dimeric (D) TRIM5-21R proteins. Inset (upper panel) shows a Coomassie blue-stained SDS-PAGE analysis of the designated fractions. Elution positions of control molecular mass standards are shown below the gel filtration chromatograph for reference, and estimated molecular masses are given above the peaks of monomeric and dimeric TRIM5-21R.

and this approach was therefore used to determine the oligomeric state of each TRIM5-21R species. Sedimentation data were collected at three different protein concentrations and two rotor speeds, yielding a total of six data sets for each TRIM5-21R species. These six data sets were globally fit to single species models in which the molecular weight was allowed to float and also to monomer, dimer, and trimer models with fixed molecular weights. As illustrated in Fig. 2A, the distribution of the smaller TRIM5-21R species fit a protein with a predicted mass of 59,305 g/mol, which matched the mass expected for a TRIM5-21R monomer (62,520 g/mol, $M_{obs}/M_{calc} = 0.95$). The data for three initial concentrations of TRIM5-21R centrifuged at 14,000 rpm are shown together with the global fits (Fig. 2A, upper panel), and the small, random residuals indicate that the data were satisfactorily fit by a simple single species model (lower panels). Global fits to the three data sets collected at 18,000 rpm were also satisfactory (data not shown). Similarly, when fixed monomer, dimer, or trimer molecular weights were used during the global fitting procedure, the monomer model was clearly the best fit to the data (see Fig. S2A in the supplemental material).

In contrast, equilibrium distributions of the larger TRIM5-21R species indicated that this TRIM5-21R protein was a dimer. As shown in Fig. 2B, data fit with a floating molecular

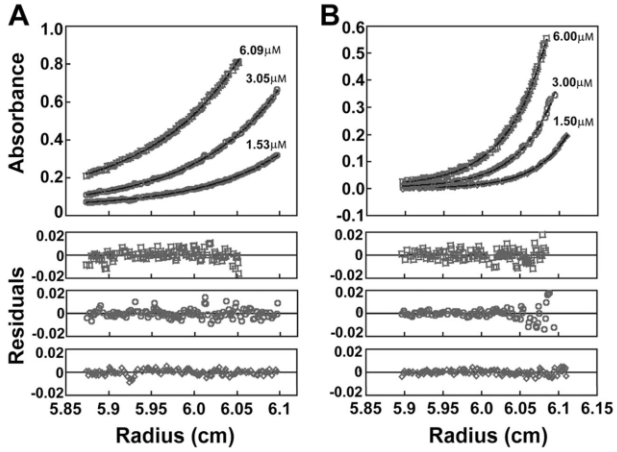


FIG. 2. Recombinant TRIM5-21R proteins are monomers and dimers. Equilibrium sedimentation distributions of purified monomeric (A) and dimeric (B) TRIM5-21R proteins (upper panels), and residual differences between the data and the single species models (lower panels). The data are shown for initial subunit protein concentrations of 6.09, 3.05, and 1.53 μM (monomer), and 6.0, 3.0, and 1.5 μM (dimer) at rotor speeds of 14,000 rpm. The data sets were also collected at 18,000 rpm (monomer) and 16,000 (dimer), and all of the data were globally fit to a single species model in which the molecular weight was allowed to float during the refinement. The data points are shown in open symbols, and the best-fit curves are shown as solid lines. Estimated molecular weights were as follows: TRIM5-21R monomer, 59,305 g/mol ($MW_{monomer}$ = 62,520 g/mol, $M_{obs}/M_{calc}$ = 0.95); and TRIM5-21R dimer, 123,825 g/mol ($MW_{dimer}$ = 125,040 g/mol, $M_{obs}/M_{monomer}$ = 1.98).

weight gave an estimated mass of 123,825 g/mol, which matched the molecular weight expected for a TRIM5-21R dimer (125,040 g/mol, $M_{obs}/M_{monomer}$ = 1.98), and the global fits again exhibited small, random residuals (Fig. 2B and data not shown). The dimer model was also clearly best when the data were globally fit to fixed TRIM5-21R monomer, dimer, or trimer models (see Fig. S2B in the supplemental material). We therefore conclude that the smaller TRIM5-21R species is a monomer and that the larger species is a dimer.

**Recombinant TRIM5-21R dimers and mammalian TRIM5-21R and TRIM5α proteins exhibit similar cross-linking patterns.** The observation that recombinant TRIM5-21R formed monomers and dimers was somewhat surprising because previous studies had suggested that TRIM5α proteins might be trimers (36). This conclusion was based upon the SDS-PAGE electrophoretic mobilities of chemically cross-linked, mammalian-expressed TRIM5α proteins, whose mobilities appeared to correspond to trimers (~150 kDa). To reconcile these observations, we tested whether chemically cross-linked TRIM5 dimers exhibited anomalously slow SDS-PAGE electrophoretic mobilities. Our first set of experiments examined the mobilities of pure recombinant monomeric and dimeric TRIM5-21R proteins cross-linked with EGS. The monomeric protein was used as a control to ensure that protein and cross-linker concentrations were sufficiently low to prevent nonspecific intermolecular cross-linking of nonassociated proteins. As shown in Fig. 3A, TRIM5-21R dimers formed intermolecular cross-links efficiently, whereas TRIM5-21R monomers did not. The major cross-linked species for the TRIM5-21R dimer migrated at an apparent molecular mass of ~160 kDa on a SDS–7.5% PAGE gel, and a species migrating at ~125 kDa was also observed at trace levels. Thus, the major cross-linked form of the TRIM5-21R dimer exhibits anomalously slow SDS-PAGE mobility.

In a second set of experiments, we tested whether the oligomeric state or cross-linking properties of TRIM5α proteins could be altered by cross-linking in crude lysates, by expression in human versus insect cells, or by the non-native N-terminal OSF tag or RING domain of the TRIM5-21R construct. As shown in the first panel of Fig. 3B, the cross-linking pattern did not change significantly when the pure recombinant TRIM5-21R dimers were cross-linked either in a buffer solution or in a soluble mammalian cell extract, indicating that TRIM5-21R dimer does not appreciably cross-link with extract proteins under these conditions (compare the first panel of Fig. 3B to Fig. 3A). A very similar cross-linking pattern was also seen when TRIM5-21R proteins were expressed in human 293T cells and cross-linked directly in their soluble extracts (compare Fig. 3B, second and third panels), although in this case the minor, faster-migrating cross-linked species was more evident. This experiment indicates that TRIM5-21R forms similar dimers when expressed in human or insect cells. Finally, we examined the cross-linking of an authentic TRIM5α protein expressed in 293T cells. Although the C-terminally HA-tagged TRIM5α had a slightly lower molecular weight than TRIM5-21R, the cross-linking pattern of the authentic TRIM5α-HA protein expressed in human 293T cells was again very similar to those seen for the various TRIM5-21R proteins. Thus, TRIM5-21R and TRIM5α proteins are predominantly dimeric when ex-

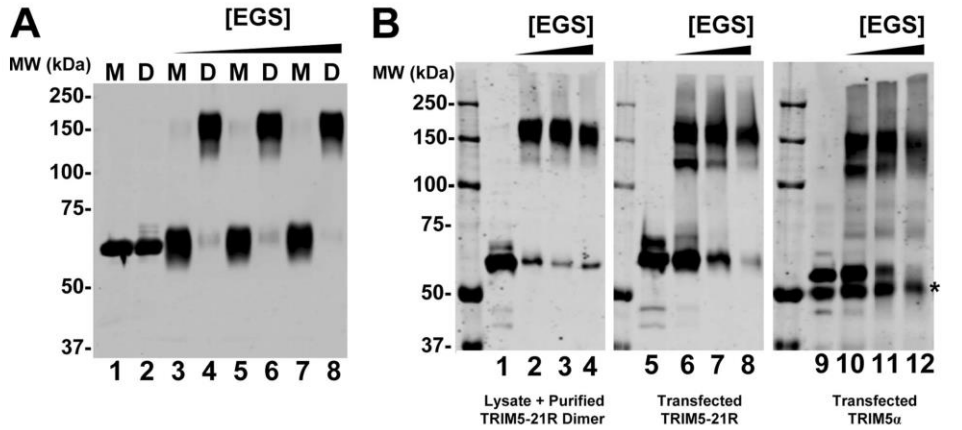


FIG. 3. Recombinant TRIM5-21R dimers and mammalian-expressed TRIM5-21R and TRIM5α proteins exhibit similar cross-linking patterns. (A) Western blot (anti-FLAG) showing purified monomeric (M) and dimeric (D) proteins cross-linked with increasing concentrations of EGS (lanes 3 to 8) or controls without EGS (lanes 1 and 2). (B) Western blots (anti-FLAG) showing purified recombinant TRIM5-21R dimer added to 293T cell lysate and cross-linked in the presence of increasing concentrations of EGS (first panel); TRIM5-21R expressed in 293T cells, cross-linked directly in the lysate, and concentrated by StrepTactin affinity purification (second panel); and TRIM5α expressed in 293T cells, cross-linked directly in the lysate, and concentrated by α-HA affinity purification (third panel). Lanes 1, 5, and 9 show controls in the absence of EGS, and the asterisk denotes contaminating immunoglobulin G heavy chain eluted from the HA-Sepharose beads. Note that all of the samples were run on the same gel, and migration positions can therefore be compared directly.

pressed in human or insect cells, but the cross-linked dimers exhibit anomalously slow electrophoretic mobilities.

**Autoubiquitylation of recombinant TRIM5-21R proteins.** TRIM5α exhibits ubiquitin E3 ligase activity (63, 64), and a recent study showed that a partially purified, recombinant MBP-TRIM5α fusion protein could pair with the UbcH5b E2 enzyme and exhibit ubiquitin E3 ligase activity in vitro (64). We also tested whether our purified TRIM5-21R proteins were active for autoubiquitylation in vitro, using three different pure E2 enzymes. As shown in Fig. 4, both monomeric and dimeric TRIM5-21R proteins paired successfully with UbcH5c and UbcH6, but not with UbcH7 in our in vitro autoubiquitylation assays. Ubiquitylation was particularly efficient in the UbcH5 reactions, where most of the TRIM5-21R dimer was modified with ubiquitin (compare lanes 8 and 9). Control reactions behaved as expected in that ubiquitylated products were not observed in the absence of ATP (compare even and odd lanes).

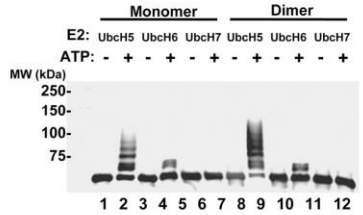


FIG. 4. TRIM5-21R proteins can be autoubiquitylated in vitro. Purified monomeric (lanes 1 to 6) and dimeric (lanes 7 to 12) TRIM5-21R proteins were incubated with the wheat Uba1 E1 enzyme, ubiquitin, and one of three ubiquitin E2-conjugating enzymes—UbcH5c, UbcH6, or UbcH7—in the presence or absence of ATP. Reactions were terminated after 60 min, and TRIM5-21R reaction products were analyzed by Western blotting (α-FLAG).

Interestingly, UbcH5 and UbcH6 produced dramatically different product distributions, with UbcH5 catalyzing polyubiquitylation (or possibly multimonoubiquitylation) and UbcH6 catalyzing only monoubiquitylation of TRIM5-21R. These results demonstrate that the purified TRIM5-21R protein is an active ubiquitin E3 ligase and are in good agreement with the report of Yamauchi et al. (64), who found that MBP-TRIM5α was active with UbcH5B but not with UbcH7 (UbcH6 was not tested). Our results are also consistent with the observations that TRIM5α, TRIM21, and TRIM5-21R can self-ubiquitylate to form polyubiquitin chains in vivo, which can contain Lys-48 linkages (64; the present study). Finally, our experiments raise the possibility that TRIM5α and TRIM21 may exhibit different product distributions when paired with different E2 ubiquitin-conjugating enzymes in vivo. Such behavior has been seen previously for other RING and U-box E3 ligases (e.g., BRCA1 and CHIP, respectively) (8, 72) but remains to be confirmed with in vivo studies of nonchimeric TRIM5α and TRIM21 proteins.

**Recombinant TRIM5-21R proteins bind HIV-1 CA-NC assemblies.** Although numerous studies have established that the B30.2/SPRY domains of TRIM5α proteins dictate the specificity of retroviral capsid recognition (34, 38, 41, 54–56, 68), direct binding of TRIM5α proteins to retroviral CA protein assemblies has not yet been demonstrated. We therefore tested whether pure recombinant TRIM5-21R proteins could bind

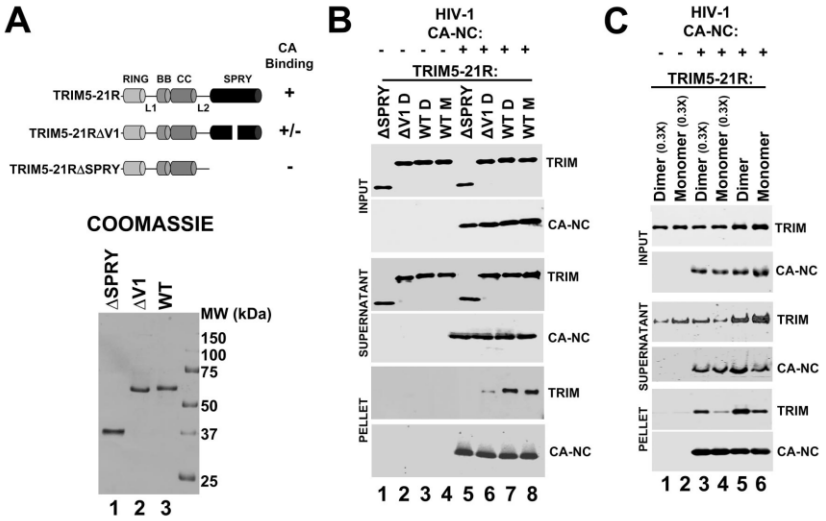


FIG. 5. TRIM5-21R binds CA-NC assemblies. (A) Schematic summary (above) and SDS-PAGE/Coomassie blue analyses (below) of purified full-length dimeric TRIM5-21R (lane 3, denoted WT), a dimeric TRIM5-21R construct missing part of the V1 loop (lane 2, denoted ΔV1), and a monomeric TRIM5-21R construct missing the entire SPRY domain (lane 1, denoted ΔSPRY). (B) TRIM5-21R protein binding to CA-NC/DNA assemblies. Monomeric (M) or dimeric (D) TRIM5-21R (WT, lanes 3 and 4 and lanes 7 and 8), TRIM5-21RΔV1 (ΔV1, lanes 2 and 6), or TRIM5-21RΔSPRY (ΔSPRY, lanes 1 and 5) proteins were incubated alone (lanes 1 to 4) or with CA-NC/DNA assemblies (lanes 5 to 8) and then centrifuged through a 70% sucrose cushion to separate CA-NC assemblies and bound proteins (pellet) from unbound and lower-molecular-weight proteins (supernatant). Western blots show the distribution of TRIM (α-FLAG, first, third, and fifth panels) and CA-NC (α-CA, second, fourth, and sixth panels). Note that CA-NC assemblies bound full-length TRIM5-21R constructs better than either TRIM5-21RΔV1 or TRIM5-21RΔSPRY. Ratios of bound CA-NC and TRIM5-21R proteins were obtained by combining known input protein concentrations, quantification of bound CA-NC levels using a standard curve of known CA-NC protein concentrations, and quantification of Western blot band intensities. Estimated bound ratios were as follows: CA-NC/TRIM5-21R dimer = 1.1, CA-NC/TRIM5-21R monomer = 0.8, and CA-NC/TRIM5-21RΔV = 0.18. (C) CA-NC/DNA assemblies bind better to dimeric TRIM5-21R proteins than to monomeric proteins under stringent conditions. Monomeric (lanes 2, 4, and 6) or dimeric (lanes 1, 3, and 5) proteins were incubated alone (lanes 1 and 2) or with CA-NC/DNA assemblies (lanes 3 to 6) and then centrifuged through a 70% sucrose cushion to separate CA-NC assemblies and bound proteins (pellet) from unbound and lower molecular weight proteins (supernatant). Western blots show the distribution of TRIM5-21R (α-FLAG, TRIM panels) and CA-NC (α-CA, CA-NC panels). The concentrations of TRIM5-21R proteins in lanes 5 and 6 were 3.33-fold higher than in lanes 3 and 4, and all binding assays were performed at lower protein concentrations than those shown in part (B) (see Materials and Methods). Note that under these conditions, CA-NC assemblies bound dimeric TRIM5-21R better than monomeric TRIM5-21R. The estimated ratios of bound proteins were as follows: CA-NC/TRIM5-21R dimer (0.15 μM input) = 0.025; CA-NC/TRIM5-21R monomer (0.15 μM input) = 0.01, CA-NC/TRIM5-21R dimer (0.5 μM input) = 0.068; and CA-NC/TRIM5-21R monomer (0.5 μM input) = 0.028.

the tubular and conical assemblies formed in vitro by pure recombinant HIV-1 CA-NC proteins on DNA templates. Previous studies have shown that these CA-NC/DNA assemblies form the same hexagonal surface lattices as authentic HIV-1 capsids and should therefore present native-like capsid surfaces for TRIM5-21R recognition. Our binding studies took advantage of the observation that CA-NC/DNA assemblies can be separated from free proteins by centrifugation through sucrose cushions (56). TRIM5-21R proteins therefore remained in the supernatants above the cushion, unless they bound and copelleted with the CA-NC/DNA assemblies.

Our studies used both monomeric and dimeric wild-type TRIM5-21R proteins, as well as two mutant TRIM5-21R proteins used as specificity controls (Fig. 5A). The first specificity control (denoted TRIM5-21RΔV1) lacked 13 residues from the middle of the V1 recognition loop of the SPRY domain (10). This loop is required for efficient HIV-1 capsid binding and restriction, although the TRIM5-21RΔV1 protein does retain modest residual HIV-1 restriction activity (10; see Fig. S1A in the supplemental material). The recombinant TRIM5-21RΔV1 protein behaved like wild-type TRIM5-21R in that it formed both monomers and dimers, and the purified TRIM5-21RΔV1 dimer was used in our studies. The second specificity control (denoted TRIM5-21RΔSPRY) lacked the entire SPRY domain and the preceding L2 linker. This control was used because TRIM5 constructs lacking SPRY domains cannot bind HIV-1 capsid in extracts or restrict HIV-1 replication in vivo (56). This construct differed from wild-type TRIM5-21R in that it was exclusively monomeric (data not shown), and the purified monomer was therefore used in our studies.

As shown in Fig. 5B, CA-NC/DNA proteins formed a mixture of assembled tubes and cones, which pelleted to the bottom of the sucrose cushion, and disassembled proteins, which remained in the supernatant (lanes 5 to 8). As expected, all

TRIM5-21R proteins remained exclusively in the supernatant in the absence of CA-NC/DNA assemblies (lanes 1 to 4, compare panels 3 and 5). In the presence of CA-NC/DNA assemblies, however, both monomeric and dimeric wild-type TRIM5-21R proteins partitioned between the supernatant and pellet fractions, indicating that both TRIM5-21R proteins could bind CA-NC/DNA assemblies (compare lanes 7 and 8 to lanes 3 and 4 in the sixth panel). The TRIM5-21RΔV1 protein also bound detectably to CA-NC/DNA assemblies (compare lane 6 to lane 3), but at much lower levels than either of the two wild-type TRIM5-21R proteins (compare lane 6 to lanes 7 and 8). A deletion in the SPRY domain V1 loop therefore reduced, but did not entirely eliminate, CA-NC/DNA binding. The TRIM5-21RΔSPRY protein did not bind CA-NC/DNA assemblies detectably in this assay, indicating that the SPRY domain was required for CA-NC/DNA binding (compare lane 5 to lanes 7 and 8). These experiments demonstrate that pure recombinant TRIM5-21R proteins bind directly to CA-NC/DNA assemblies and show that efficient binding requires the SPRY domain and its V1 loop.

Although our binding experiments were not performed under equilibrium conditions, we have nevertheless estimated the concentrations and stoichiometries of the binding reaction components in an initial effort to define the parameters that govern the TRIM5-CA interaction. CA-NC tubes and cones can assemble and disassemble reversibly, and we therefore estimated the concentration of CA-NC protein in the pelletable assemblies by quantifying Western blot band intensities and comparing them to a standard curve of known CA-NC concentrations. Analyzed in this fashion, the pelletable CA-NC protein in each experiment shown in Fig. 5B corresponded to 11 pmol (corresponding to an initial concentration of 55 nM). The initial concentration of TRIM5-21R subunits in each reaction mixture was 5 μM, and the quantity of pelleted TRIM5-21R dimer corresponded to 12 pmol of protein. Thus, in this experiment, the binding reaction was performed with substantial excess of TRIM5-21R dimer over assembled CA-NC protein (~100-fold), and under these conditions the ratio of bound TRIM5-21 to CA-NC was approximately 1:1. The TRIM5-21RΔV1 protein bound less well in this experiment, at a TRIM5-21ΔV1/CA-NC ratio of 0.18:1. Although these estimated values neglect several potential complications, including possible incomplete CA-NC tube pelleting efficiency and dissociation of CA-NC assemblies during the assay, the data nevertheless imply that TRIM5-21R can bind assembled CA-NC lattices at nearly stoichiometric levels.

**CA-NC/DNA assemblies bind TRIM5-21R dimers more efficiently than monomers.** TRIM5α protein oligomerization has been shown to enhance retroviral capsid binding owing to avidity effects (27), and it was therefore surprising that CA-NC/DNA assemblies bound equivalent levels of TRIM5-21R monomers and dimers in the previous assay. We therefore tested whether more stringent binding conditions might reveal differential CA-NC binding of TRIM5-21R monomers and dimers. The stringency was increased by reducing the TRIM5-21R concentration, and under these conditions CA-NC/DNA assemblies bound TRIM5-21R dimers better than monomers. This effect is illustrated in Fig. 5C, which shows that TRIM5-21R dimers bound better at two different initial TRIM5-21R concentrations (0.5 and 0.15 μM, compare lanes 3 and 4 to lanes 5 and 6 in the bottom panel). Under these more stringent conditions, the quantity of pelletable CA-NC protein did not change, but the ratios of pelletable CA-NC to bound TRIM5-21R proteins were substantially lower, demonstrating that the binding conditions were indeed more stringent (see the caption to Fig. 5C). These data suggest that although TRIM5-21R monomers and dimers can both bind CA-NC/DNA assemblies, TRIM5-21R dimerization enhances the efficiency of binding under more stringent conditions, in agreement with the observation that disruption of the coiled-coil oligomerization motif of TRIM5α inhibits restriction (27).

**Electron microscopic analyses of TRIM5-21R-decorated CA-NC tubes.** The effects of TRIM5-21R binding to CA-NC tubes were visualized by using transmission electron microscopy of negatively stained CA-NC/DNA assemblies incubated with a 10- to 50-fold excess of TRIM5-21R prior to imaging. As shown in Fig. 6, TRIM5-21R binding did not dramatically alter the appearance of CA-NC/DNA tubes, but two effects were evident. First, CA-NC/DNA tubes incubated with excess TRIM5-21R consistently exhibited increased exterior stain deposition compared to tubes incubated with control TRIM5-21RΔV1 or TRIM5-21RΔSPRY proteins. The simplest explanation for this effect is that it reflects formation of TRIM5-21R coats on the CA-NC/DNA tube exteriors. This effect was sometimes subtle and difficult to discern, but in extreme cases resulted in a thick, dark irregular coat on tube exteriors, as though the TRIM5-21R were aggregating about the tube (Fig. 6, panel 8). Second, CA-NC/DNA tubes decorated with TRIM5-21R frequently appeared more broken and irregular than their counterparts incubated with control TRIM5-21RΔV1 or TRIM5-21RΔSPRY proteins (tube breaks are highlighted by arrows in Fig. 6, panels 5 to 8). This observation suggests that high levels of TRIM5-21R destabilized the tubes and increased their fragmentation, although the effect was modest, and most tubes remained intact. Overall, our electron microscopic data indicate that TRIM5-21R can coat and destabilize CA-NC/DNA assemblies, but both effects were subtle. Higher-resolution cryo-electron microscopic analyses will be required to determine the density and location of TRIM5-21 binding sites on the CA-NC/DNA assemblies.

**EIAV core binding assays.** Retroviral cores are the actual targets of TRIM5α restriction, and we therefore tested whether TRIM5-21R could bind authentic, purified core particles. Cores isolated from EIAV vectors were used in these experiments because TRIM5$\alpha_{rh}$ restricts EIAV (10, 23, 71; see Fig. S1B in the supplemental material) and because we are able to purify cores from membrane-stripped EIAV virions more reproducibly and in higher yields than HIV-1 cores. EIAV cores were membrane stripped with a brief Triton X-100 detergent treatment (30) and then purified on a sucrose gradient where they concentrated at the expected density of ~1.24 g/ml (Fig. 7A).

Purified EIAV cores were incubated with a ~16-fold excess of pure recombinant TRIM5-21R or control ΔV1 or ΔSPRY variants. As in the CA-NC/DNA binding assay, high-molecular-weight EIAV cores were pelleted by centrifugation through a sucrose cushion (Fig. 7B, lanes 4 to 6 in the sixth panel). Wild-type dimeric TRIM5-21R protein bound and copelleted with the EIAV cores but did not pellet in the absence of cores (compare lanes 3 and 6, fifth panel). In contrast, much lower

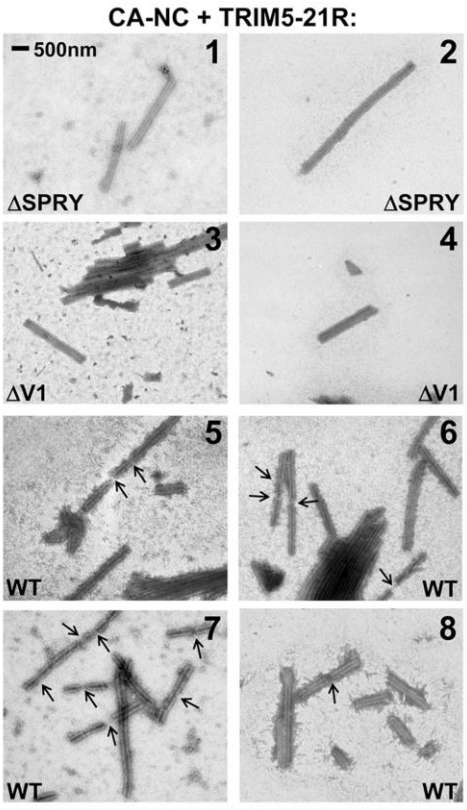


FIG. 6. Electron microscopic images of CA-NC assemblies incubated with full-length TRIM5-21R or deletion mutants. Negatively stained, transmission electron microscopic images of CA-NC assemblies incubated with monomeric TRIM5-21RΔSPRY (panels 1 and 2), dimeric TRIM5-21RΔV1 (panels 3 and 4), or full-length dimeric TRIM5-21R (panels 5 to 8). Note that CA-NC/DNA assemblies incubated with TRIM5-21R show enhanced exterior staining and more frequent breaks (arrows) compared to the TRIM5-21RΔV1 or TRIM5-21RΔSPRY controls. TRIM5-21R-induced breaks were quantified by scoring randomly selected electron microscopic images of CA-NC/DNA tubes for the presence of discontinuities (see arrows), with the following results: TRIM5-21RΔSPRY-treated tubes (0% broken, 0 total breaks, $n = 26$ tubes), TRIM5-21RΔV1-treated tubes (4% broken, 2 total breaks, $n = 50$), and TRIM5-21R-treated tubes (42% broken, 55 total breaks, $n = 50$).

levels of the control TRIM5-21R ΔV1 protein copelleted with the EIAV cores (compare lanes 5 and 6), and no detectable TRIM5-21R ΔSPRY protein copelleted with the cores (compare lanes 4 and 6). We therefore conclude that TRIM5-21R binds and copellets with authentic EIAV core particles and that this interaction is specific because the wild-type TRIM5-21R protein binds much better than control proteins lacking part of the V1 loop or the entire SPRY domain.

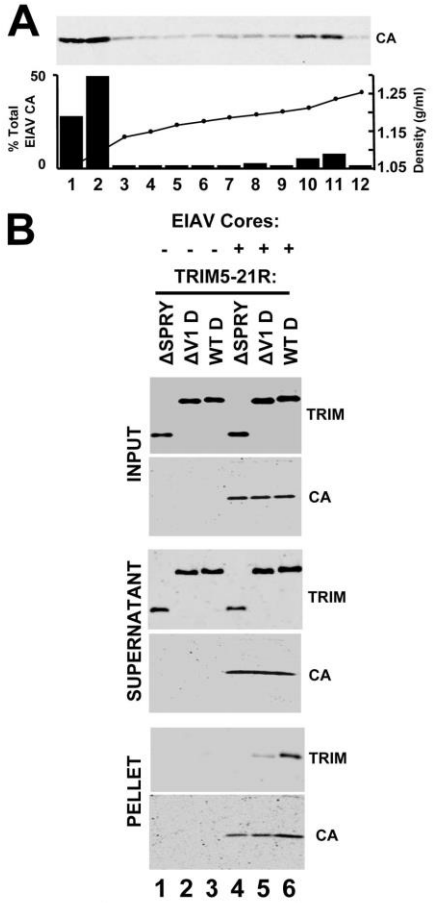


FIG. 7. TRIM5-21R binds EIAV cores. (A) Sucrose gradient purification of membrane-stripped cores produced by an EIAV vector. The Western blot (α-CA) shows the distribution of EIAV CA protein across a sucrose density gradient (with fraction densities shown). The CA distribution is quantified below, and the CA protein in fractions 10 to 12 corresponds to core particles. (B) TRIM5-21R protein binding to purified EIAV cores. Dimeric TRIM5-21R (WT, lanes 3 and 6), dimeric TRIM5-21RΔV1 (ΔV1, lanes 2 and 5), or monomeric TRIM5-21RΔSPRY (ΔSPRY, lanes 1 and 4) proteins were incubated alone (lanes 1 to 3) or with purified EIAV cores (lanes 4 to 6) and then centrifuged through a 57% sucrose cushion to separate EIAV cores and bound proteins (pellet) from unbound and lower-molecular-weight proteins (supernatant). Western blots show the distribution of TRIM (α-FLAG, TRIM panels) and EIAV CA (α-CA, CA panels). Note that the pelleted EIAV cores bound full-length TRIM5-21R better than either TRIM5-21RΔV1 or TRIM5-21RΔSPRY.

## DISCUSSION

We have described the expression, purification, and characterization of TRIM5-21R, which represents the first study of a pure recombinant TRIM5α protein capable of restricting HIV-1 replication. Our experiments provide direct experimental support for the importance of both TRIM5α protein oligomerization and the B30.2/SPRY domain in retroviral capsid recognition. Specifically, we found that deletion of the SPRY domain eliminates binding to both HIV-1 CA-NC assemblies and EIAV cores, that a deletion in the V1 loop reduces binding significantly, and that TRIM5-21R dimerization enhances binding to HIV-1 CA-NC assemblies under stringent binding conditions. These in vitro binding activities correlate well with restriction activities in vivo, indicating that our in vitro experiments accurately recapitulate interactions between capsids and TRIM5 proteins during retroviral restriction.

Our experiments indicate that restricting TRIM5α proteins, including TRIM5α itself, are dimers. Previous studies had established that TRIM5α proteins oligomerize and that the oligomeric state might be trimeric (27, 36). We now show, however, that TRIM5-21R forms dimers but that chemically cross-linked TRIM5-21R dimers exhibit anomalously slow electrophoretic mobility, causing them to appear trimeric. Cross-linked TRIM5α proteins expressed in mammalian cells exhibit very similar mobilities, implying that authentic TRIM5α proteins are also dimeric. It will be of interest to determine whether other members of the TRIM protein family are also dimers. In this regard, we note that others have reported that the related TRIM21 protein forms trimers (45). This conclusion was again based upon the electrophoretic mobility of chemically cross-linked TRIM21 proteins, however, which may be subject to the same uncertainties as cross-linked TRIM5α proteins. Moreover, another group has reported that the TRIM21/SS-A/Ro52 protein may instead be dimeric, based on its gel filtration mobility (59), and two groups have reported that the isolated coiled-coil region of TRIM21 forms dimers rather than trimers (27, 40). We therefore speculate that dimerization may be a common property of many members of the tripartite motif protein family. If so, there are several intriguing similarities between TRIM proteins and immunoglobulin G proteins, since both types of protein can dimerize to display a pair of terminal immunoglobulin-like domains that can recognize antigens, including repeating motifs on viral capsid surfaces.

Once formed, TRIM5-21R dimers are stable and can be purified without appreciable dissociation. Similarly, we saw no evidence of monomer accumulation in equilibrium distributions of TRIM5-21R dimers across a range of micromolar concentrations, again indicating that assembled TRIM5-21R dimers are highly stable (or kinetically inert). Nevertheless, monomeric TRIM5-21R proteins were produced in our baculoviral expression system. These TRIM5-21R monomers did not exhibit a propensity to dimerize, suggesting that they may be kinetically "trapped," perhaps owing to misfolding of the coiled-coil motif. Not surprisingly, a TRIM5-21R construct missing the SPRY domain and preceding L2 linker was exclusively monomeric, a finding consistent with previous experiments showing that the TRIM5α L2 region is required for oligomerization (40).

SPRY domains of TRIM proteins, presumably including TRIM5α, adopt immunoglobulin-like folds consisting of two antiparallel β-sheets. The ligand binding surface is located at one end of the β-sandwich and is composed of six extended loops and two pockets (25, 61). The loops, which are hypervariable in both amino acid composition and length, share homology with the complementarity-determining region loops of immunoglobulins and account for the species specificity of restriction. In particular, the variable region 1 loop of $TRIM5\alpha_{rh}$ is a critical determinant of capsid binding and antiviral activity, and a deletion within the V1 loop also reduced capsid recognition by TRIM5-21R in our in vitro binding assays. Our results are therefore in good agreement with the prevailing model that retroviral capsid recognition is mediated by the variable loops of the SPRY domain of TRIM5α (34, 54, 68). Furthermore, our experiments demonstrate that this interaction is direct and can be highly efficient. Indeed, under some conditions we observed essentially stoichiometric binding of TRIM5-21R to CA-NC assemblies. Electron microscopic images of CA-NC tubes decorated with TRIM5-21R proteins also suggest that TRIM5-21R can "coat" the CA-NC surface, although higher-resolution studies will be necessary to confirm and extend this finding.

TRIM5α restriction represents a very intriguing problem in molecular recognition because specific TRIM5α alleles are able to recognize a remarkable variety of different retroviral capsids, despite their substantial variation in amino acid sequence and surface topology. This attribute is exemplified by $TRIM5\alpha_{rh}$, which is able to recognize both EIAV and HIV-1 capsids even though the HIV-1 and EIAV CA proteins share only ~25% sequence identity. Retroviral capsids do share a common organization, however, since all capsids are assembled on a hexagonal surface lattice composed of CA hexamers. It is therefore likely that both reading heads of the dimeric TRIM5α protein engage similar sites on the capsid surface, and this is most easily accomplished by binding across a local twofold symmetry axis on the capsid lattice (although asymmetric binding is also a formal possibility). Hexagonal HIV-1 CA arrays exhibit two distinct types of local twofold symmetry, one of which is colinear with the local sixfold axes and the other of which connects adjacent hexamers. These two sites have different subunit orientations and spacing, and it is therefore likely that only one of these sites is the preferred TRIM5α binding site.

In solution, HIV-1 CA forms dimers that correspond to the twofold symmetric interactions between adjacent hexamers in the assembled hexagonal lattice. Expression of HIV-1 CA alone does not abrogate restriction, however, indicating that the CA dimer alone probably does not create a high-affinity TRIM5α binding site (14, 16, 51, 52). It is possible that CA alone cannot abrogate restriction because the CA solution dimer is not the preferred TRIM5α binding site or because this CA dimer is weak and/or inherently flexible. However, an interesting alternative is that isolated SPRY domains, and even isolated TRIM5α dimers, may have weak intrinsic capsid binding energies and that high-affinity binding is achieved through the cooperative formation of even higher-order TRIM5α assemblies. This model would be consistent with the observation that TRIM5α proteins are highly susceptible to aggregation or assembly in vitro and in vivo. Indeed, fluorescence images

indicate that at least in some cases, large numbers of TRIM5α proteins can assemble on HIV-1 capsids in vivo (6). This model could also help explain how individual TRIM5 alleles can bind such a variety of different retroviral capsid surfaces because direct TRIM5α-CA interfaces would not need to form a large number of favorable interactions but rather could utilize just a few specific interactions and then be stabilized by the cooperative formation of multiple TRIM5α-CA and TRIM5α-TRIM5α interfaces. In contrast, isolated TRIM-Cyp proteins, in which a cyclophilin A domain replaces the SPRY domain, may bind specific retroviral capsids with higher affinities because the cyclophilin A domain can make specific interactions with individual HIV-1 CA subunits (18, 70). This "high-affinity" recognition mechanism could explain why the upstream RING and B-box domains play less important roles in TRIM-Cyp restriction activity (10, 13, 65, 66) but may come at the cost of reducing the ability of TRIM-Cyp restriction factors to recognize as broad a variety of different retroviral capsids as canonical TRIM5α alleles.

Our electron microscopic analyses also indicated that high-level TRIM5-21R binding destabilizes the CA-NC lattice to some degree because TRIM5-21R induced many more breaks in CA-NC/DNA tubes than did nonbinding control TRIM5-21R constructs. Destabilization of the CA-NC lattice could reflect steric hindrance upon saturation binding of TRIM5-21R and/or mismatches in the symmetry or spacing between the CA-NC lattice and putative higher-order TRIM5-21R assemblies. We emphasize, however, that the capsid destabilization induced by TRIM5-21R binding was a relatively minor effect because most CA-NC assemblies remained largely intact, even in the presence of a large excess of TRIM5-21R. Similarly, EIAV cores remained pelletable in the presence of excess TRIM5-21R. Thus, the dramatic destabilization of retroviral capsids observed under restrictive conditions in vivo does not appear to be a direct consequence of TRIM5α binding. Rather, it appears that capsid recognition by TRIM5α and subsequent destabilization/restriction are largely separable events. This idea is consistent with a series of other observations, including the fact that mutations in the B-box region of TRIM5α can abrogate restriction without apparently affecting capsid recognition (11), and that capsid destabilization is abrogated upon inhibition of the proteasome (6, 10).

In summary, our biochemical and biophysical studies have established that purified recombinant TRIM5-21R forms stable dimers that can bind specifically to higher-order HIV-1 CA-NC assemblies and to authentic EIAV core particles. It will be important to ascertain precisely how TRIM5α binds the capsid lattice and to determine the minimal CA assembly required for high-affinity binding, and we anticipate that the availability of recombinant TRIM5-21R protein will facilitate such studies.

## ACKNOWLEDGMENTS

We are grateful to Chad Nelson and the University of Utah Mass Spectrometry facility for ESI and LC mass spectral analyses, Rachel Klevit for the gift of expression vectors for E1 and E2 enzymes, and Chris Hill for critical review of the manuscript.

This research was supported by National Institutes of Health grants AI076121 (to C.A.), AI063978 and AI076094 (to J.G.S.), and AI045405 and GM082545 (to W.I.S.).

## REFERENCES

1. **Accola, M. A., A. Ohagen, and H. G. Gottlinger.** 2000. Isolation of human immunodeficiency virus type 1 cores: retention of Vpr in the absence of p6(gag). J. Virol. **74:**6198–6202.
2. **Anderson, J. L., E. M. Campbell, X. Wu, N. Vandegraaff, A. Engelman, and T. J. Hope.** 2006. Proteasome inhibition reveals that a functional preintegration complex intermediate can be generated during restriction by diverse TRIM5 proteins. J. Virol. **80:**9754–9760.
3. **Bieniasz, P. D.** 2004. Intrinsic immunity: a front-line defense against viral attack. Nat. Immunol. **5:**1109–1115.
4. **Briggs, J. A., T. Wilk, R. Welker, H. G. Krausslich, and S. D. Fuller.** 2003. Structural organization of authentic, mature HIV-1 virions and cores. EMBO J. **22:**1707–1715.
5. **Brzovic, P. S., A. Lissounov, D. E. Christensen, D. W. Hoyt, and R. E. Klevit.** 2006. A UbcH5/ubiquitin noncovalent complex is required for processive BRCA1-directed ubiquitination. Mol. Cell **21:**873–880.
6. **Campbell, E. M., O. Perez, J. L. Anderson, and T. J. Hope.** 2008. Visualization of a proteasome-independent intermediate during restriction of HIV-1 by rhesus TRIM5α. J. Cell Biol. **180:**549–561.
7. **Campbell, S., and V. M. Vogt.** 1995. Self-assembly in vitro of purified CA-NC proteins from Rous sarcoma virus and human immunodeficiency virus type 1. J. Virol. **69:**6487–6497.
8. **Christensen, D. E., P. S. Brzovic, and R. E. Klevit.** 2007. E2-BRCA1 RING interactions dictate synthesis of mono- or specific polyubiquitin chain linkages. Nat. Struct. Mol. Biol. **14:**941–948.
9. **Cole, J. L.** 2004. Analysis of heterogeneous interactions. Methods Enzymol. **384:**212–232.
10. **Diaz-Griffero, F., A. Kar, M. Lee, M. Stremlau, E. Poeschla, and J. Sodroski.** 2007. Comparative requirements for the restriction of retrovirus infection by TRIM5α and TRIMCyp. Virology **369:**400–410.
11. **Diaz-Griffero, F., A. Kar, M. Perron, S. H. Xiang, H. Javanbakht, X. Li, and J. Sodroski.** 2007. Modulation of retroviral restriction and proteasome inhibitor-resistant turnover by changes in the TRIM5α B-box 2 domain. J. Virol. **81:**10362–10378.
12. **Diaz-Griffero, F., X. Li, H. Javanbakht, B. Song, S. Welikala, M. Stremlau, and J. Sodroski.** 2006. Rapid turnover and polyubiquitylation of the retroviral restriction factor TRIM5. Virology **349:**300–315.
13. **Diaz-Griffero, F., N. Vandegraaff, Y. Li, K. McGee-Estrada, M. Stremlau, S. Welikala, Z. Si, A. Engelman, and J. Sodroski.** 2006. Requirements for capsid-binding and an effector function in TRIMCyp-mediated restriction of HIV-1. Virology **351:**404–419.
14. **Dodding, M. P., M. Bock, M. W. Yap, and J. P. Stoye.** 2005. Capsid processing requirements for abrogation of fv1 and ref1 restriction. J. Virol. **79:**10571–10577.
15. **Fisher, R. J., A. Rein, M. Fivash, M. A. Urbaneja, J. R. Casas-Finet, M. Medaglia, and L. E. Henderson.** 1998. Sequence-specific binding of human immunodeficiency virus type 1 nucleocapsid protein to short oligonucleotides. J. Virol. **72:**1902–1909.
16. **Forshey, B. M., J. Shi, and C. Aiken.** 2005. Structural requirements for recognition of the human immunodeficiency virus type 1 core during host restriction in owl monkey cells. J. Virol. **79:**869–875.
17. **Forshey, B. M., U. von Schwedler, W. I. Sundquist, and C. Aiken.** 2002. Formation of a human immunodeficiency virus type 1 core of optimal stability is crucial for viral replication. J. Virol. **76:**5667–5677.
18. **Gamble, T. R., F. F. Vajdos, S. Yoo, D. K. Worthylake, M. Houseweart, W. I. Sundquist, and C. P. Hill.** 1996. Crystal structure of human cyclophilin A bound to the amino-terminal domain of HIV-1 capsid. Cell **87:**1285–1294.
19. **Ganser-Pornillos, B. K., A. Cheng, and M. Yeager.** 2007. Structure of full-length HIV-1 CA: a model for the mature capsid lattice. Cell **131:**70–79.
20. **Ganser-Pornillos, B. K., M. Yeager, and W. I. Sundquist.** 2008. The structural biology of HIV assembly. Curr. Opin. Struct. Biol. **18:**203–217.
21. **Gauser, B. K., S. Li, V. Y. Klishko, J. T. Finch, and W. I. Sundquist.** 1999. Assembly and analysis of conical models for the HIV-1 core. Science **283:**80–83.
22. **Hatfield, P. M., J. Callis, and R. D. Vierstra.** 1990. Cloning of ubiquitin activating enzyme from wheat and expression of a functional protein in *Escherichia coli*. J. Biol. Chem. **265:**15813–15817.
23. **Hatziioannou, T., S. Cowan, S. P. Goff, P. D. Bieniasz, and G. J. Towers.** 2003. Restriction of multiple divergent retroviruses by Lv1 and Ref1. EMBO J. **22:**385–394.
24. **Hennig, J., A. Bresell, M. Sandberg, K. D. Hennig, M. Wahren-Herlenius, B. Persson, and M. Sunnerhagen.** 2008. The fellowship of the RING: the RING-B-box linker region interacts with the RING in TRIM21/Ro52, contains a native autoantigenic epitope in Sjogren syndrome, and is an integral and conserved region in TRIM proteins. J. Mol. Biol. **377:**431–449.
25. **James, L. C., A. H. Keeble, Z. Khan, D. A. Rhodes, and J. Trowsdale.** 2007. Structural basis for PRYSPRY-mediated tripartite motif (TRIM) protein function. Proc. Natl. Acad. Sci. USA **104:**6200–6205.
26. **Javanbakht, H., F. Diaz-Griffero, M. Stremlau, Z. Si, and J. Sodroski.** 2005. The contribution of RING and B-box 2 domains to retroviral restriction mediated by monkey TRIM5α. J. Biol. Chem. **280:**26933–26940.

27. **Javanbakht, H., W. Yuan, D. F. Yeung, B. Song, F. Diaz-Griffero, Y. Li, X. Li, M. Stremlau, and J. Sodroski.** 2006. Characterization of TRIM5α trimerization and its contribution to human immunodeficiency virus capsid binding. Virology **353:**234–246.
28. **Jin, Z., L. Jin, D. L. Peterson, and C. L. Lawson.** 1999. Model for lentivirus capsid core assembly based on crystal dimers of EIAV p26. J. Mol. Biol. **286:**83–93.
29. **Keckesova, Z., L. M. Ylinen, and G. J. Towers.** 2004. The human and African green monkey TRIM5α genes encode Ref1 and Lv1 retroviral restriction factor activities. Proc. Natl. Acad. Sci. USA **101:**10780–10785.
30. **Kotov, A., J. Zhou, P. Flicker, and C. Aiken.** 1999. Association of Nef with the human immunodeficiency virus type 1 core. J. Virol. **73:**8824–8830.
31. **Laue, T., B. Shah, T. Ridgeway, and S. Pelletier.** 1992. Computer-aided interpretation of analytical sedimentation data for proteins, p. 90–125. *In* A. Rowe and J. Horton (ed.), Ultracentrifugation in biochemistry and polymer science. Royal Society of Chemistry, Cambridge, England.
32. **Li, S., C. P. Hill, W. I. Sundquist, and J. T. Finch.** 2000. Image reconstructions of helical assemblies of the HIV-1 CA protein. Nature **407:**409–413.
33. **Li, X., B. Gold, C. O'Huigin, F. Diaz-Griffero, B. Song, Z. Si, Y. Li, W. Yuan, M. Stremlau, C. Mische, H. Javanbakht, M. Scally, C. Winkler, M. Dean, and J. Sodroski.** 2006. Unique features of TRIM5α among closely related human TRIM family members. Virology **360:**419–433.
34. **Li, Y., X. Li, M. Stremlau, M. Lee, and J. Sodroski.** 2006. Removal of arginine 332 allows human TRIM5α to bind human immunodeficiency virus capsids and to restrict infection. J. Virol. **80:**6738–6744.
35. **Liu, H. L., Y. Q. Wang, C. H. Liao, Y. Q. Kuang, Y. T. Zheng, and B. Su.** 2005. Adaptive evolution of primate TRIM5α, a gene restricting HIV-1 infection. Gene **362:**109–116.
36. **Mische, C. C., H. Javanbakht, B. Song, F. Diaz-Griffero, M. Stremlau, B. Strack, Z. Si, and J. Sodroski.** 2005. Retroviral restriction factor TRIM5α is a trimer. J. Virol. **79:**14446–14450.
37. **Nisole, S., and A. Saib.** 2004. Early steps of retrovirus replicative cycle. Retrovirology **1:**9.
38. **Ohkura, S., M. W. Yap, T. Sheldon, and J. P. Stoye.** 2006. All three variable regions of the TRIM5α B30.2 domain can contribute to the specificity of retrovirus restriction. J. Virol. **80:**8554–8565.
39. **O'Rourke, J. P., J. C. Olsen, and B. A. Bunnell.** 2005. Optimization of equine infectious anemia derived vectors for hematopoietic cell lineage gene transfer. Gene Ther. **12:**22–29.
40. **Ottosson, L., J. Hennig, A. Espinosa, S. Brauner, M. Wahren-Herlenius, and M. Sunnerhagen.** 2006. Structural, functional, and immunologic characterization of folded subdomains in the Ro52 protein targeted in Sjogren's syndrome. Mol. Immunol. **43:**588–598.
41. **Perez-Caballero, D., T. Hatziioannou, A. Yang, S. Cowan, and P. D. Bieniasz.** 2005. Human tripartite motif 5α domains responsible for retrovirus restriction activity and specificity. J. Virol. **79:**8969–8978.
42. **Perron, M. J., M. Stremlau, M. Lee, H. Javanbakht, B. Song, and J. Sodroski.** 2007. The human TRIM5α restriction factor mediates accelerated uncoating of the N-tropic murine leukemia virus capsid. J. Virol. **81:**2138–2148.
43. **Perron, M. J., M. Stremlau, B. Song, W. Ulm, R. C. Mulligan, and J. Sodroski.** 2004. TRIM5α mediates the postentry block to N-tropic murine leukemia viruses in human cells. Proc. Natl. Acad. Sci. USA **101:**11827–11832.
44. **Pickart, C. M., and S. Raasi.** 2005. Controlled synthesis of polyubiquitin chains. Methods Enzymol. **399:**21–36.
45. **Rhodes, D. A., and J. Trowsdale.** 2007. TRIM21 is a trimeric protein that binds IgG Fc via the B30.2 domain. Mol. Immunol. **44:**2406–2414.
46. **Roberts, M. M., and S. Oroszlan.** 1989. The preparation and biochemical characterization of intact capsids of equine infectious anemia virus. Biochem. Biophys. Res. Commun. **160:**486–494.
47. **Rold, C. J., and C. Aiken.** 2008. Proteasomal degradation of TRIM5α during retrovirus restriction. PLoS Pathog. **4:**e1000074.
48. **Sandrin, V., and F. L. Cosset.** 2006. Intracellular versus cell surface assembly of retroviral pseudotypes is determined by the cellular localization of the viral glycoprotein, its capacity to interact with Gag, and the expression of the Nef protein. J. Biol. Chem. **281:**528–542.
48a. **Sanes, J. R., J. L. Rubenstein, and J. F. Nicolas.** 1986. Use of recombinant retrovirus to study post-implantation cell lineage in mouse embryos. Embo J. **5:**3133–3142.
49. **Sawyer, S. L., M. Emerman, and H. S. Malik.** 2007. Discordant evolution of the adjacent antiretroviral genes TRIM22 and TRIM5 in mammals. PLoS Pathog. **3:**e197.
50. **Sawyer, S. L., L. I. Wu, M. Emerman, and H. S. Malik.** 2005. Positive selection of primate TRIM5α identifies a critical species-specific retroviral restriction domain. Proc. Natl. Acad. Sci. USA **102:**2832–2837.
51. **Sebastian, S., and J. Luban.** 2005. TRIM5alpha selectively binds a restriction-sensitive retroviral capsid. Retrovirology **2:**40.
52. **Shi, J., and C. Aiken.** 2006. Saturation of TRIM5α-mediated restriction of HIV-1 infection depends on the stability of the incoming viral capsid. Virology **350:**493–500.
53. **Song, B., F. Diaz-Griffero, D. H. Park, T. Rogers, M. Stremlau, and J. Sodroski.** 2005. TRIM5α association with cytoplasmic bodies is not required for antiretroviral activity. Virology **343:**201–211.
54. **Song, B., B. Gold, C. O'Huigin, H. Javanbakht, X. Li, M. Stremlau, C. Winkler, M. Dean, and J. Sodroski.** 2005. The B30.2(SPRY) domain of the retroviral restriction factor TRIM5α exhibits lineage-specific length and sequence variation in primates. J. Virol. **79:**6111–6121.
55. **Stremlau, M., C. M. Owens, M. J. Perron, M. Kiessling, P. Autissier, and J. Sodroski.** 2004. The cytoplasmic body component TRIM5α restricts HIV-1 infection in Old World monkeys. Nature **427:**848–853.
56. **Stremlau, M., M. Perron, M. Lee, Y. Li, B. Song, H. Javanbakht, F. Diaz-Griffero, D. J. Anderson, W. I. Sundquist, and J. Sodroski.** 2006. Specific recognition and accelerated uncoating of retroviral capsids by the TRIM5α restriction factor. Proc. Natl. Acad. Sci. USA **103:**5514–5519.
57. **Stremlau, M., M. Perron, S. Welikala, and J. Sodroski.** 2005. Species-specific variation in the B30.2(SPRY) domain of TRIM5α determines the potency of human immunodeficiency virus restriction. J. Virol. **79:**3139–3145.
58. **Towers, G. J.** 2007. The control of viral infection by tripartite motif proteins and cyclophilin A. Retrovirology **4:**40.
59. **Wang, D., J. P. Buyon, Z. Yang, F. Di Donato, M. E. Miranda-Carus, and E. K. Chan.** 2001. Leucine zipper domain of 52 kDa SS-A/Ro promotes protein dimer formation and inhibits in vitro transcription activity. Biochim. Biophys. Acta **1568:**155–161.
59a. **Ward, D. M., M. B. Vaughn, S. L. Shiflett, P. L. White, A. L. Pollock, J. Hill, R. Schnegelberger, W. I. Sundquist, and J. Kaplan.** 2005. The role of LIP5 and CHMP5 in multivesicular body formation and HIV-1 budding in mammalian cells. J. Biol. Chem. **280:**10548–10555.
60. **Welker, R., H. Hohenberg, U. Tessmer, C. Huckhagel, and H. G. Krausslich.** 2000. Biochemical and structural analysis of isolated mature cores of human immunodeficiency virus type 1. J. Virol. **74:**1168–1177.
61. **Woo, J. S., H. Y. Suh, S. Y. Park, and B. H. Oh.** 2006. Structural basis for protein recognition by B30.2/SPRY domains. Mol. Cell **24:**967–976.
62. **Wu, X., J. L. Anderson, E. M. Campbell, A. M. Joseph, and T. J. Hope.** 2006. Proteasome inhibitors uncouple rhesus TRIM5α restriction of HIV-1 reverse transcription and infection. Proc. Natl. Acad. Sci. USA **103:**7465–7470.
63. **Xu, L., L. Yang, P. K. Moitra, K. Hashimoto, P. Rallabhandi, S. Kaul, G. Meroni, J. P. Jensen, A. M. Weissman, and P. D'Arpa.** 2003. BTBD1 and BTBD2 colocalize to cytoplasmic bodies with the RBCC/tripartite motif protein, TRIM58. Exp. Cell Res. **288:**84–93.
64. **Yamauchi, K., K. Wada, K. Tanji, M. Tanaka, and T. Kamitani.** 2008. Ubiquitination of E3 ubiquitin ligase TRIM5α and its potential role. FEBS J. **275:**1540–1555.
65. **Yap, M. W., M. P. Dodding, and J. P. Stoye.** 2006. Trim-cyclophilin A fusion proteins can restrict human immunodeficiency virus type 1 infection at two distinct phases in the viral life cycle. J. Virol. **80:**4061–4067.
66. **Yap, M. W., G. B. Mortuza, I. A. Taylor, and J. P. Stoye.** 2007. The design of artificial retroviral restriction factors. Virology **365:**302–314.
67. **Yap, M. W., S. Nisole, C. Lynch, and J. P. Stoye.** 2004. Trim5α protein restricts both HIV-1 and murine leukemia virus. Proc. Natl. Acad. Sci. USA **101:**10786–10791.
68. **Yap, M. W., S. Nisole, and J. P. Stoye.** 2005. A single amino acid change in the SPRY domain of human Trim5α leads to HIV-1 restriction. Curr. Biol. **15:**73–78.
69. **Yee, J. K., A. Miyanohara, P. LaPorte, K. Bouic, J. C. Burns, and T. Friedmann.** 1994. A general method for the generation of high-titer, pantropic retroviral vectors: highly efficient infection of primary hepatocytes. Proc. Natl. Acad. Sci. USA **91:**9564–9568.
70. **Yoo, S., D. G. Myszka, C. Yeh, M. McMurray, C. P. Hill, and W. I. Sundquist.** 1997. Molecular recognition in the HIV-1 capsid/cyclophilin A complex. J. Mol. Biol. **269:**780–795.
71. **Zhang, F., T. Hatziioannou, D. Perez-Caballero, D. Derse, and P. D. Bieniasz.** 2006. Antiretroviral potential of human tripartite motif-5 and related proteins. Virology **353:**396–409.
72. **Zhang, M., M. Windheim, S. M. Roe, M. Peggie, P. Cohen, C. Prodromou, and L. H. Pearl.** 2005. Chaperoned ubiquitylation: crystal structures of the CHIP U box E3 ubiquitin ligase and a CHIP-Ubc13-Uev1a complex. Mol. Cell **20:**525–538.